

Development of functionalized tetravalent phthalocyanines for low-cost organic photovoltaics

BY

Mario César Vebber

Thesis submitted to the University of Ottawa
in partial fulfilment of the requirements for the
Doctorate of Philosophy degree in Chemical Engineering

© Mario César Vebber, Ottawa, Canada, 2023

ABSTRACT

Organic photovoltaic (OPV) devices possess several advantages over their silicon-based counterparts, namely mechanical flexibility, inexpensive high throughput processing and lightweight modules. These characteristics have prompted the scientific community to intensify efforts to make such technology economically viable. In the past two decades, due to clever molecular engineering, the power conversion efficiency (PCE) of OPVs has increased from around 2% to almost 20%. Unfortunately, such accomplishments have come from the design and development of organic semiconducting compounds whose synthesis and purification are increasingly complex, hindering commercial deployment. Alternatively, axially substituted silicon phthalocyanines (R_2 -SiPc) are promising candidates for low-cost OPVs. SiPc dyes have been employed in organic electronics for almost 50 years, owing to their high molar extinction coefficient, high chemical and thermal stability, and ease of manufacturing. In this thesis, we aimed to explore how the physical, chemical, and electrochemical properties of R_2 -SiPc derivatives interplay with their performance in OPVs. We have demonstrated that the solubility of the derivatives plays a significant role on their performance as ternary additives in Poly(3-hexylthiophene-2,5-diyl):[6,6]-Phenyl-C61-butyric acid methyl ester (P3HT and PC₆₁BM, respectively) bulk heterojunctions. We demonstrated that when employed as stand-alone acceptors, the final morphology of P3HT/ R_2 -SiPc films, and consequently their performance, correlates to basic thermodynamic properties such as critical radius, miscibility, and crystallization enthalpy. Such properties have also been correlated with the length and branching of axial silane groups, serving as a guide for molecular design, in particular, with respect to the solubilizing alkyl groups present in many organic semiconductors. We have demonstrated that R_2 -SiPc derivatives can be paired with polymers other than P3HT, to achieve respectable metrics, namely V_{oc} , but the overall efficiency is limited due to their shallow highest occupied and lower unoccupied molecular orbitals (HOMO and LUMO) energy levels. As such, we have also explored peripherally fluorinated R_2 -F_xSiPcs derivatives and characterized how the degree of fluorination affects the electrochemical and physical properties of the R_2 -SiPcs. Through control of the degree of fluorination, it was possible to pair, in OPVs, R_2 -F_xSiPcs with polymers that unfluorinated R_2 -SiPcs was not originally compatible with, such as poly[[6,7-difluoro[(2-hexyldecyl)oxy]-5,8-quinoxalinediyl]-2,5-thiophenediyl]] (PTQ10) and even achieve air-stable electron conduction. Ultimately, we found that the degree of fluorination controls the charge carrier (electron or holes) that is preferably conducted in the R_2 -F_xSiPcs phase. The results establish novel property-performance relationships that can be used to move away from trial-and-error approaches and designing organic electronics and further establishes silicon phthalocyanines as promising cores for organic electronics.

ABSTRAIT

Les dispositifs photovoltaïques organiques (« Organic Photovoltaics» *OPV*) possèdent plusieurs avantages par rapport à leurs homologues à base de silicium, à savoir une flexibilité mécanique, un traitement à grande échelle peu coûteux et des modules légers. Ces caractéristiques ont incité la communauté scientifique à intensifier ses efforts pour rendre cette technologie économiquement viable. Au cours des deux dernières décennies, grâce aux progrès dans l'ingénierie moléculaire des dispositifs, le rendement de conversion de puissance (« Power Conversion Efficiency, » *PCE*) des *OPVs* est passé d'environ 2 % à près de 20 %. Malheureusement, ces réalisations sont issues de la conception et du développement de semi-conducteurs organiques dont la synthèse et la purification sont de plus en plus complexes, ce qui entrave leur déploiement commercial. Alternativement, les phtalocyanines de silicium avec des substituants en position axiale (R_2 -SiPc) sont des candidats prometteurs pour le développement d'*OPVs* à faible coût. Les colorants SiPc sont utilisés dans l'électronique organique depuis près de 50 ans en raison de leur coefficient d'extinction molaire et de leur stabilité chimique et thermique élevés, ainsi que leur facilité de fabrication. Dans cette thèse, nous cherchons à déterminer comment les propriétés physiques, chimiques et électrochimiques des R_2 -SiPcs interagissent avec leur performance dans des *OPVs*. Nous avons démontré que la solubilité des dérivés joue un rôle significatif sur leur performance en tant qu'additifs ternaires dans le *Poly(3-hexylthiophene-2,5-diyl):[6,6]-Phenyl-C61-butyric acid methyl ester* (P3HT :PC₆₁BM) à hétérojonctions en masse. Nous avons démontré que la morphologie finale des films composé de P3HT/ R_2 -SiPc jouant le rôle d'accepteurs individuels, et, par conséquent, leur performance, est corrélée à leurs propriétés thermodynamiques telles que le rayon critique, la miscibilité et l'enthalpie de cristallisation. Ces propriétés ont également été corrélées avec la longueur et la ramification des groupes axiaux. Cela permet de guider la conception moléculaire, particulièrement en ce qui concerne les groupes alkyles solubilisant présents dans de nombreux semi-conducteurs organiques. Nous avons démontré que les R_2 -SiPc peuvent être associés à des polymères autres que P3HT, pour obtenir des métriques de performance respectables, à savoir le *Voc*. Cependant, l'efficacité globale est limitée en raison des niveaux d'énergie peu profonds de leurs orbitales moléculaires occupées et inférieures inoccupées (« *Highest Occupied Molecular Orbital*, » HOMO et « *Lowest Unoccupied Molecular Orbital*, » LUMO). À ce titre, nous avons également exploré les dérivés de R_2 -F_xSiPcs fluorés en périphérie, et caractérisé comment le degré de fluoration affecte les propriétés électrochimiques et physiques des R_2 -SiPcs. Grâce au contrôle du degré de fluoration, il a été possible d'associer, dans des *OPVs*, les R_2 -F_xSiPcs à des polymères avec lesquels les R_2 -SiPcs non fluorés n'étaient pas compatibles, tel que le *poly[[6,7-difluoro[(2-hexyldécyl)oxy]-5, 8-quinoxalinediyl]-2,5-thiophènediyl]* (PTQ10). Cela a permis d'atteindre une conduction électronique stable à l'air. Finalement, nous avons constaté que le degré de fluoration dicte le porteur de charge (électron ou trous) de préférence conduit dans la phase des R_2 -F_xSiPcs. Ces résultats établissent de nouvelles relations propriétés-performances qui peuvent être utilisées pour s'éloigner des approches par essai et erreur et démontrent l'importance des phtalocyanines de silicium pour le développement de l'électronique organique.

ACKNOWLEDGEMENTS

I would like to firstly thank my supervisor Benoit Lessard for taking me as his student in a field I had long wished to work in and helping me with my application to the University of Ottawa, which can become challenging when you're coming from abroad. Benoit has also harboured a healthy and productive work environment and I could not have asked for a better research group to be part of.

I would like to thank all group members in the Lessard Group, past and present, for their amazing companionship and contributions to my thesis and PhD journey. Everyone is a brilliant and generous researcher. I would like to specially thank Trevor Grant and Kaitlin Wagner, who taught me how to make OPVs when I first join the group.

I am also thankful for my co-supervisor Jaclyn Brusso, who has first took me as in intern in my undergrad about 10 years ago, and introduced me to the field of organic electronics. Jaclyn has always been available to discuss any challenges I had in the chemistry I carried out during my PhD, as well as allow me to work in her laboratory for reactions we didn't have the appropriate equipment for, in the Lessard group.

We could not have achieved the results we did without the University of Ottawa staff in the chemical engineering department. Special thanks to thank Franco Ziroldo, James MacDermid, Gerard Nina and Patrick Pageau, who have always promptly supported us in the implementation and repair of the equipment in our lab. I would also like thank Francine Petrin for supporting us on the day-to-day administrative tasks that are so necessary, and at times, stressful.

Finally, I would like to thank my family, friends and boyfriend, who have supported me when I decided to move to Canada for my PhD and who have encouraged me and kept me sane during the past 4 years.

TABLE OF CONTENTS

ABSTRACT.....	ii
ABSTRAIT	iii
ACKNOWLEDGEMENTS	iv
TABLE OF CONTENTS.....	v
LIST OF FIGURES	x
LIST OF TABLES.....	xiii
LIST OF ABBREVIATIONS	xiv
1. INTRODUCTION	1
1.1 Photovoltaics vs Organic Photovoltaics	1
1.2 Organic Photovoltaic Working Principles.....	2
1.3 Characterization of the Photovoltaic Effect	4
1.4 Device Configuration and Morphology	6
1.5 OPV Materials.....	11
1.6 R ₂ -SiPcs as ternary additives.....	15
1.7 R ₂ -SiPcs as non-fullerene acceptors (NFAs).....	17
1.8 Scope of the Thesis.....	19
1.9 References	19
2. UNDERSTANDING THE ROLE OF SILICON PHTHALOCYANINE SOLUBILITY IN DEVICE PERFORMANCE AS TERNARY ADDITIVES IN ORGANIC PHOTOVOLTAICS.....	27
2.1 Context	27
2.2 Contribution.....	28
2.3 Abstract	28
2.4 Introduction	28
2.5 Experimental Section	30
2.5.1 Materials	30
2.5.2 Synthesis of silicon phthalocyanine ternary additives.....	31
2.5.3 Materials Characterizations	33
2.5.4 Device Preparation.....	33
2.6 Results and Discussion.....	34
2.6.1 Synthesis and Characterization of SiPcs.....	34
2.6.2 UV-Vis Spectroscopy and Cyclic Voltammetry.....	35

2.6.3	Solubility.....	36
2.6.4	Contact Angle.....	37
2.6.5	OPV performance.....	38
2.7	Conclusions.....	44
2.8	References.....	45
3.	THERMODYNAMIC PROPERTY-PERFORMANCE RELATIONSHIPS IN SILICON PHTHALOCYANINE-BASED ORGANIC PHOTOVOLTAICS.....	49
3.1	Context.....	49
3.2	Contribution.....	50
3.3	Abstract.....	50
3.4	Introduction.....	51
3.5	Experimental.....	53
3.5.1	Materials.....	53
3.5.2	Materials Characterization.....	53
3.5.3	Device Preparation and Characterization.....	53
3.6	Results and Discussion.....	54
3.6.1	OPV performance.....	54
3.6.2	Relationship Between Thermodynamic Properties and Photovoltaic Efficiency.....	57
3.7	Conclusions.....	64
3.8	Acknowledgements.....	65
3.9	References.....	66
4.	VARIANCE-RESISTANT PTB7 AND AXIALLY-SUBSTITUTED SILICON PHTHALOCYANINES AS ACTIVE MATERIALS FOR HIGH-VOC ORGANIC PHOTOVOLTAICS.....	71
4.1	Context.....	71
4.2	Contribution.....	72
4.3	Abstract.....	72
4.4	Introduction.....	72
4.5	Experimental section.....	74
4.5.1	Materials.....	74
4.5.2	Devices.....	74
4.6	Results and Discussion.....	75

4.7	Conclusion.....	81
4.8	Acknowledgements	81
4.9	References	81
5.	FROM P-TYPE TO N-TYPE: PERIPHERAL FLUORINATION OF AXIALLY SUBSTITUTED SILICON PHTHALOCYANINES ENABLES FINE TUNING OF CHARGE TRANSPORT.....	86
5.1	Context	86
5.2	Contributions	87
5.3	Abstract	87
5.4	Introduction	88
5.5	Experimental	89
5.5.1	Materials	89
5.5.2	Synthesis	90
5.5.3	Materials Characterizations	92
5.5.4	Device Preparation.....	92
5.5.5	Device Characterization.....	93
5.6	Results and Discussion.....	94
5.6.1	Synthesis	94
5.6.2	Material characterization	96
5.6.3	Light-absorbing devices.....	99
5.6.4	OTFT devices	101
5.7	Conclusions	105
5.8	Acknowledgements	106
5.9	References	106
6.	CONCLUSIONS AND FUTURE WORK.....	112
6.1	Summary and Main Findings	112
6.2	Recommendations for Future Work.....	114
6.2.1	Evaluate different donor/acceptor systems.....	114
6.2.2	Stability studies.....	115
6.2.3	Explore other F _x SiPc derivatives	116
6.3	References	118
7.	ADDITIONAL CONTRIBUTIONS	120

7.1	Low-Cost Silicon Phthalocyanine as a Non-Fullerene Acceptor for Flexible Large Area Organic Photovoltaics	120
7.1.1	Abstract.....	120
7.1.2	Contributions	121
7.2	High Performance Solution Processed n-Type OTFTs through Surface Engineered F–F Interactions Using Asymmetric Silicon Phthalocyanines	121
7.2.1	Abstract.....	121
7.2.2	Contributions	121
7.3	Polymeric Composites for Industrial Water Treatment: An Overview.....	122
7.3.1	Abstract.....	122
7.3.2	Contributions	123
7.4	Design of ternary additive for organic photovoltaics: a cautionary tale	123
7.4.1	Abstract.....	123
7.4.2	Contributions	123
7.5	N-Type Solution-Processed Tin versus Silicon Phthalocyanines: A Comparison of Performance in Organic Thin-Film Transistors and in Organic Photovoltaic	123
7.5.1	Abstract.....	124
7.5.2	Contributions	124
7.6	Thin-Film Engineering of Solution-Processable n-Type Silicon Phthalocyanines for Organic Thin-Film Transistors.....	124
7.6.1	Abstract.....	125
7.6.2	Contributions	125
7.7	Mechanism of formation, characterization and cytotoxicity of green synthesized zinc oxide nanoparticles obtained from <i>Ilex paraguariensis</i> leaves extract	125
7.7.1	Abstract.....	126
7.7.2	Contribution.....	126
7.8	Preparation, characterization and application of polymeric thin films containing silver and copper nanoparticles with bactericidal activity	126
7.8.1	Abstract.....	127
7.8.2	Contribution.....	127

7.9	Influence of silver nanoparticle deposition on self-assembled thin films of weak polyelectrolytes/TiO ₂ for bezafibrate photodegradation through central composite experimental design.....	127
7.9.1	Abstract.....	128
7.9.2	Contribution.....	128
APPENDIX A - Supporting information for Chapter 2.....		129
APPENDIX B – Supporting information for Chapter 3.		136
APPENDIX C – Supporting information for Chapter 5.		139
APPENDIX D – Permissions to reproduce work.		155

LIST OF FIGURES

Figure 1.1. a) Flexible polymer-fullerene solar cell; ¹¹ b) OPV solar tree modules presented at EXPO 2015 in Milan; ¹² and c) OPV bus-stop roof, fabricated with green processes. ¹³	2
Figure 1.2. Charge transfer diagram of a donor-acceptor heterojunction. I) photon absorption and exciton formation; II) Exciton dissociation and electron transfer between donor and acceptor; and III) Electron and hole drift to collectors (electrodes). ¹⁶	3
Figure 1.3. a) diagram of the circuit of a photovoltaic cell; b) Dark (dotted line) and illuminated (solid line) <i>J-V</i> curves of an operating photovoltaic cell. ¹⁷	5
Figure 1.4. a) Planar heterojunction device structure; b) bulk heterojunction device structure. ³⁴	7
Figure 1.5. a) standard direct architecture; b) inverted device architecture. ¹⁷	7
Figure 1.6. BHJ structures: a) random blend with large domains and many isolated islands; b) random blend with small domains and connected to the edges of the charge collectors; and c) interdigitated rods blend with complete connectivity to charge collectors. Effectiveness of the active layer, keep everything else the same, should increase from a) to c). ³⁷	8
Figure 1.7. Examples of BHJ morphology modifications: a) Use of high boiling-point solvents decrease the drying rate and result is higher degree of order in the film as indicated by AFM images; ⁴² b) Solvents that do not interact similarly with donor and acceptor can cause preferential precipitation/aggregation of one of the phases into undesirable, large domains, such as the case shown for toluene that causes the formation of bubble-like PC ₆₁ BM domains; ⁴³ c) Thermal annealing results in ordering of the polymeric phase, connecting adjacent chains into a cocontinuous morphology that favours charge collection; ⁴⁸ d) Modifying the alkyl chains of donor/acceptor materials have a strong effect on the final performance, leading to larger or smaller domains and degrees of crystallization. ⁴¹	9
Figure 1.8. Simulated current (<i>J</i>), exciton splitting efficiency (<i>n_{ex}</i>) and charge collection (<i>n_{cc}</i>) in BHJ with domains of different sizes when the morphology is characterized by a) impure domains; b) diffuse interfacial edges and c) pure domains with sharp edges. ⁵¹	11
Figure 1.9. Chemical structure of common donor polymers employed in OPVs. ⁶⁷	12
Figure 1.10. Absorption spectra of common small-molecule acceptors employed in OPVs. ⁶⁷	13
Figure 1.11. Comparison between average efficiencies achieved by select organic semiconductors and their synthetic complexity index.	14

Figure 1.12. a) Structure of a tetravalent phthalocyanine with a metal center (M, in red), axial groups (Ra, in green) and peripheral groups (Rp, in blue); b) Absorption spectra of selected MPcs.	15
Figure 1.13. Possible morphologies of a ternary BHJ.	16
Figure 1.14. Extension of spectral coverage when adding 4 wt% of SiPc (blue) to a P3HT/PC61BM blend (purple). ⁹³	17
Figure 2.1. Axially substituted (R ₃ SiO) ₂ -SiPc synthesized and characterized in the present study.	31
Figure 2.2. a) UV-Vis spectrum of the (R ₃ SiO) ₂ -SiPc and b) CV spectra and (R ₃ SiO) ₂ -SiPc for HOMO level estimation.	36
Figure 2.3. Solubility of different (R ₃ SiO) ₂ -SiPcs, P3HT and PCBM in DCB.	37
Figure 2.4. Contact angle and corresponding surface energy measurements of (R ₃ SiO) ₂ -SiPc films on OTS treated glass.	38
Figure 2.5. EQE spectra of all the devices produced in this work divided by (R ₃ SiO) ₂ -SiPc compounds.	40
Figure 2.6. Solubility correlation with OPV performance parameters a) PCE, b) <i>V_{oc}</i> , c) <i>J_{sc}</i> and d) Fill Factor.	42
Figure 2.7. Proposed mechanism for the relationship found between additive and device performance: a) P3HT/PCBM structure when no additive is present; b) precipitation of low solubility (R ₃ SiO) ₂ -SiPc, with low chance of interfacial coverage and possible formation of crystalline domains; and c) Preferred configuration, which happens when the additive solubility somewhat matches that of the polymer donor (P3HT).	43
Figure 3.1. Axially substituted R ₃ SiO-SiPcs applied as NFAs in the present study.....	55
Figure 3.2. Representative atomic force microscopy (AFM) height (a-f) and phase (g-l) images of the P3HT/(R ₃ SiO) ₂ -SiPc active layers fabricated with compounds (3.1) – (3.6).	59
Figure 3.3. Power conversion efficiency (PCE) of P3HT/(R ₃ SiO) ₂ -SiPc OPV devices as a function of the critical radius (<i>r_s</i>) of (R ₃ SiO) ₂ -SiPcs.	60
Figure 3.4. Device PCE as a function of (a) the Flory–Huggins’ miscibility parameter (χ_{12}) and (b) of excess crystallization enthalpy (ΔH_c^*) for blends of (R ₃ SiO) ₂ -SiPc in P3HT.	62

Figure 3.5. Relationship between $(R_3SiO)_2$ -SiPc crystallization enthalpy and device performance for (a) fast drying and (b) slow drying conditions.	63
Figure 4.1. a) Chemical structure of donor and acceptor materials; b) energy level diagram of the device components; and c) schematic representation of device architecture.	76
Figure 4.2. AFM height images of the PTB7/(3BS) ₂ -SiPc films on two different scales (10 and 2.5 μ m a) before annealing and b) after annealing (15 min at 100 °C).	78
Figure 4.3. OPV characteristics a) <i>J-V</i> curves, where line thickness corresponds to the standard deviation of 4 devices, and b) EQE spectra of the optimized device (12) and the fullerene-containing baseline (1).	80
Figure 5.1. Synthetic pathway used in the production of functionalized F_x SiPcs i) Tetraline, LiHDMS, 2 h; ii) $SiCl_4$, 200°C, 16 h; iii) Cl-Benzene, BCl_3 , 100°C, 72h; iv) Cl-Benzene, 4-Tertbutylphenol, 130°C, 16 h.	95
Figure 5.2. a) Solution UV-Vis spectra (in DCM) and b) voltammograms of $(tb-Ph)_2-F_{16}SiPc$	97
Figure 5.3. HOMO and LUMO energy levels of $(tb-Ph)_2-F_{16}SiPc$ estimated from UPS data.	98
Figure 5.4. a) Energy levels of the semiconductors and electrodes; b) OPV device structure; c) <i>J-V</i> curves for OPVs prepared from PTQ10 and $(tb-Ph)_2-F_xSiPcs$; and d) <i>J-V</i> curves for OPD devices prepared from PTQ10 and $(tb-Ph)_2-F_4SiPcs$	101
Figure 5.5. a) Energy levels of the semiconductors and electrodes; b) OTFT device configurations; and curves of evaporated $(tb-Ph)_2-F_xSiPcs$ transistors characterized at room temperature in N_2 , with Ag electrodes, operating as c) n-type ($V_{DS} = + 50V$) and d) p-type ($V_{DS} = - 50V$) semiconductors.	103
Figure 5.6. N-type and p-type mobilities of $(tb-Ph)_2-F_xSiPc$ as function of peripheral fluorination. .	105
Figure 6.1. Frontier orbital energy levels of commercial polymer donors and SiPcs with different degrees of fluorination	117
Figure 6.2. Structure of F_xSiPcs derivatives proposed for future studies.	118

LIST OF TABLES

Table 2.1 Optical and electrochemical (CV) characterization of silicon phthalocyanine derivatives ...	35
Table 2.2. Current density – voltage results for all the assembled OPVs and J_{sc} estimation from EQE measurements.....	39
Table 3.1. Current density – voltage results for all the assembled OPVs and J_{sc} estimation from EQE measurements.....	56
Table 3.2. Selected physical properties of $(R_3SiO)_2-SiPcs$, P3HT, and their blends.....	59
Table 3.3. Current density – voltage results for the OPVs containing thicker active layers.....	64
Table 4.1. Experimental conditions and resulting performance of PTB7// $(3BS)_2-SiPc$ BHJ OPV devices.	76
Table 4.2. Thickness, series and shunt resistances of the optimized devices and relevant comparative devices.....	80
Table 5.1. Ratio between the Cl_2-F_XSiPc and F_2-F_XSiPc signals in mass spectroscopy analysis and fraction of the X_2-F_XSiPc samples that can be axially functionalized by phenols (Cl-benzene, reflux, 16h).	96
Table 5.2. Optical, electrochemical and UPS characteristics of functionalized F_XSiPcs	98
Table 5.3. Current density-voltage results for all assembled OPVs, including photoconversion efficiency (PCE), open circuit voltage (V_{oc}), short circuit current (J_{sc}), fill factor (FF) and number of devices (n); and OPDs, including dark current(J_{dark}), responsivity (R) and detectivity (D^*).....	100
Table 5.4. Summary of OTFT n-type characteristics, measured at room temperature in a nitrogen atmosphere.	103
Table 5.5. Summary of OTFT p-type characteristics, measured at room temperature in a nitrogen atmosphere.	104
Table 5.6. OTFT n-type characteristics of $(tb-Ph)_2-F_{16}SiPc$ devices tested in air.....	105

LIST OF ABBREVIATIONS

$(R_3SiO)_2$ -SiPc: silicon phthalocyanines axially substituted with trialkyl silanes.

$(tb-Ph)_2-F_x$ Sipc: fluorinated silicon phthalocyanines axially substituted with tertbutylphenoxy groups.

μ_e : electron mobility.

μ_h : hole mobility.

AFM: atomic force microscopy.

BHJ: bulk heterojunction.

CB: chlorobenzene.

CF: chloroform.

CT: charge transfer state.

CV: cyclic voltammetry.

DCB: 1,2-dichlorobenzene.

DIO: 1,8-diiodooctane

DPE: diphenyl ether

DSC: differential scanning calorimetry.

E_{bg}: band gap.

E_{ox} : oxidation potential.

EQE: external quantum efficiency.

E_{red} : reduction potential.

FF: fill factor.

HOMO: highest occupied molecular orbital.

ICBA: 1',1'',4',4''-Tetrahydro-di[1,4]methanonaphthaleno[1,2:2',3',56,60:2'',3''] [5,6]fullerene-C₆₀.

ITIC: 3,9-bis(2-methylene-(3-(1,1-dicyanomethylene)-indanone))-5,5,11,11-tetrakis(4-hexylphenyl)-dithieno[2,3-d:2',3'-d']-s-indaceno[1,2-b:5,6-b']dithiophene.

ITO: indium tin oxide.

J_{dark} : current density in the dark.

J_{MP} : current density at maximum power.

J_{sc}: short-circuit current density.

J-V: current density-voltage curves.

LUMO: lowest unoccupied molecular orbital.

MPcs: metal phthalocyanine.

MS: mass spectroscopy.

NMR: nuclear magnetic resonance.

O-IDTBR: (5Z,5'Z)-5,5'-((7,7'-(4,4,9,9-tetraoctyl-4,9-dihydro-s-indaceno[1,2-b:5,6-b']dithiophene-2,7-diyl)bis(benzo[c][1,2,5]thiadiazole-7,4-diyl))bis(methanylylidene))bis(3-ethyl-2-thioxothiazolidin-4-one).

OLED: organic light-emitting diode.

OPD: organic photodetector.

OPV: organic photovoltaic.

OTFT: organic thin-film transistor.

P3HT: Poly(3-hexylthiophene-2,5-diyl).

PBDB-T: Poly[(2,6-(4,8-bis(5-(2-ethylhexyl)thiophen-2-yl)-benzo[1,2-b:4,5-b']dithiophene))-alt-(5,5-(1',3'-di-2-thienyl-5',7'-bis(2-ethylhexyl)benzo[1',2'-c:4',5'-c']dithiophene-4,8-dione))].

PBDTPD: Poly[(5,6-dihydro-5-octyl-4,6-dioxo-4H-thieno[3,4-c]pyrrole-1,3-diyl)[4,8-bis[(2-ethylhexyl)oxy]benzo[1,2-b:4,5-b']dithiophene-2,6-diyl]].

PC₆₁BM: [6,6]-Phenyl-C₆₁-butyric acid methyl ester.

PC₇₁BM: [6,6]-Phenyl-C₇₁-butyric acid methyl ester.

PCDTBT: Poly[N-9'-heptadecanyl-2,7-carbazole-alt-5,5-(4',7'-di-2-thienyl-2',1',3'-benzothiadiazole)].

PCE: power conversion efficiency.

PDI: perylene-3,4,9,10-tetracarboxylic diimide.

PHJ: planar heterojunction.

PM6: Poly[(2,6-(4,8-bis(5-(2-ethylhexyl-3-fluoro)thiophen-2-yl)-benzo[1,2-b:4,5-b']dithiophene))-alt-(5,5-(1',3'-di-2-thienyl-5',7'-bis(2-ethylhexyl)benzo[1',2'-c:4',5'-c']dithiophene-4,8-dione))].

PTB7: Poly[[4,8-bis[(2-ethylhexyl)oxy]benzo[1,2-b:4,5-b']dithiophene-2,6-diyl][3-fluoro-2-[(2-ethylhexyl)carbonyl]thieno[3,4-b]thiophenediyl]].

PTQ10: Poly [[6,7-difluoro[(2-hexyldecyl)oxy]-5,8-quinoxalinediyl]-2,5-thiophenediyl]].

PV: photovoltaics.

R₂-F_XSiPc: axially substituted fluorinated silicon phthalocyanine.

R₂-SiPc: axially substituted fluorinated silicon phthalocyanine.

r_c : critical radius.

r_m : molecular radius.

R_s : series resistance.

R_{sh} : shunt resistance.

S1: excited state.

SC: synthetic complexity index.

SC-XRD: single-crystal X-ray diffraction.

T_d : degradation temperature.

TGA: thermogravimetric analysis.

T_m : melting temperature.

UPS: ultraviolet photoelectron spectroscopy.

UV-Vis: ultraviolet-visible spectroscopy.

V_m : molecular volume.

V_{MP} : voltage at maximum power.

V_{oc} : short-circuit voltage.

V_t : threshold voltage.

χ_{12} : Flory-Huggings miscibility parameter.

XRD: X-ray diffraction.

Y6: 2,2'-((2Z,2'Z)-((12,13-bis(2-ethylhexyl)-3,9-diundecyl-12,13-dihydro-[1,2,5]thiadiazolo[3,4-e]thieno[2'',3'':4',5']thieno[2',3':4,5]pyrrolo[3,2-g]thieno[2',3':4,5]thieno[3,2-b]indole-2,10-diyl)bis(methanylylidene))bis(5,6-difluoro-3-oxo-2,3-dihydro-1H-indene-2,1-diylidene))dimalononitrile.

γ_s : surface energy.

ΔH_c : crystallization enthalpy.

1. INTRODUCTION

Yearly, the total energy received by Earth from the Sun is estimated to be 13 times larger than all fossil fuel reserves (coal, natural gas, oil) combined.¹ Therefore, taking advantage of this renewable natural source is paramount to guarantee environmental and energy security around the world in the decades to come.² Photovoltaics (PVs), which convert sun light directly into electricity, are arguably the most studied solar technology for energy production. In the following chapter, I will introduce many concepts important to the manufacture and application of such devices, with a focus on organic photovoltaics (OPVs) and silicon phthalocyanine (SiPc)-based active layers.

1.1 Photovoltaics vs Organic Photovoltaics

Crystalline silicon solar cells were the first generation PVs (1954) and still constitute over 90% of the global market, due to their high efficiency of approximately 20%, as result of the maturity of silicon technology, which is propelled by the industries of microelectronics and information technology.^{3,4} However, silicon solar cells are manufactured by energy-intensive, expensive processes, which greatly reduces their economical competitiveness towards traditional energy sources.^{2,5} In that context, complimentary research is looking towards thin-film technology that facilitate low-cost and low-energy fabrication.

In that regard, OPVs are a rapidly advancing alternative to silicon photovoltaic technology, that applies carbon-based small molecules and/or polymers in the production of solar cells.² Organic semiconductors have unique properties that have been explored in the past three decades for a wide range of applications. This is due in large part to their properties such as processability by low-cost, solution-based techniques, which facilitates high throughput printing fabrication, and their mechanical properties, which enable the fabrication of flexible, resilient devices. Another key characteristic is the chemical versatility, that permits the functionalization of materials through simple molecular-design.^{6,7} Through the development of new organic semiconductors, OPV performances reached efficiencies between 16%-19%, approaching those of commercial inorganic cells.⁸⁻¹⁰ In addition to the recently achieved competitive performances, the properties of these OPVs, namely their flexibility (**Figure 1.1a**), allows these devices to be incorporated in complex

structures (**Figure 1.1b**) and also take advantage of larger, irregular areas on the roofs of buildings, bus-stops, windows etc. (**Figure 1.1c**).^{11–13}

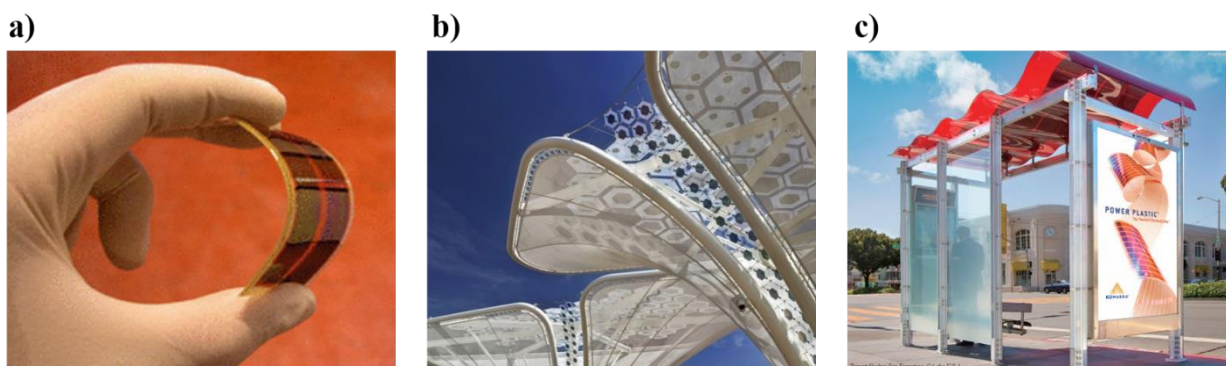


Figure 1.1. a) Flexible polymer-fullerene solar cell;¹¹ b) OPV solar tree modules presented at EXPO 2015 in Milan;¹² and c) OPV bus-stop roof, fabricated with green processes.¹³

1.2 Organic Photovoltaic Working Principles

The overall working principle of any solar cell is the conversion of photonic energy (light) into electric energy, by exciting the electrons present in a semiconductor. A difference in potential energy must exist in order for work to be extracted from the process, according to the equation $P = IV$, where P is power, I is current (or charge/electron per second) and V is the potential difference or voltage.² One of the main differences between inorganic and organic solar devices lies in the mechanics of extraction of these electrons after they are excited. In Si PVs, due to their relatively high dielectric constant, free electrons are generated directly after the excitation by light. Alternatively, organic semiconductors are excitonic, forming electron-hole pairs that are coulombically bound, following the photon absorption.^{11,14} The coulombic energy is considerably larger than the thermal energy at room temperature, therefore additional potential energy must be present in the system to split these pairs and extract useful work from the device.

The concept of acceptor/donor heterojunctions was developed by Tang *et al*¹⁵, where two materials with different frontier orbital energies are employed in order to drive exciton dissociation. Typically, the donor is a p-type semiconductor (conducts primarily positive charges, i.e. holes) and the acceptor is an n-type semiconductor (conducts primarily negative charges, i.e. electrons). This process is depicted in **Figure 1.2**. The relative positions of the lowest unoccupied molecular orbitals (LUMOs) and highest occupied molecular orbitals (HOMO) of donors and acceptors provide a difference in potential energy that drives electron transfer from the donor to

the acceptor LUMO and hole transfer from the acceptor to the donor HOMO.^{15–17} Typically, this LUMO and HOMO offset between the donor and acceptor has to be of a few hundreds of millivolts to provide enough driving force for effective dissociation of excitons (>0.25 eV).^{18,19} Once the pair is dissociated, a charge transfer state (CT) is formed, as shown in **Figure 1.2**. The energy difference between the excited state (S1) and the CT state, corresponds to the generative energy loss in acceptor/donor junctions. It becomes clear, therefore, that a much too large difference between the S1 and CT states lead to larger energy losses. Recently, several acceptor/donor pairs with very small offsets between their energy levels have been reported with high efficiencies. They take advantage of the acceptor-donor-acceptor (ADA) fused rings structure to optimize charge transfer, while finetuning a small energy offset that maximizes V_{oc} .^{20–22} However, a complete understanding of how charge transfer occurs in such near-zero energy offset blends is still elusive and may as well be system-specific.²³

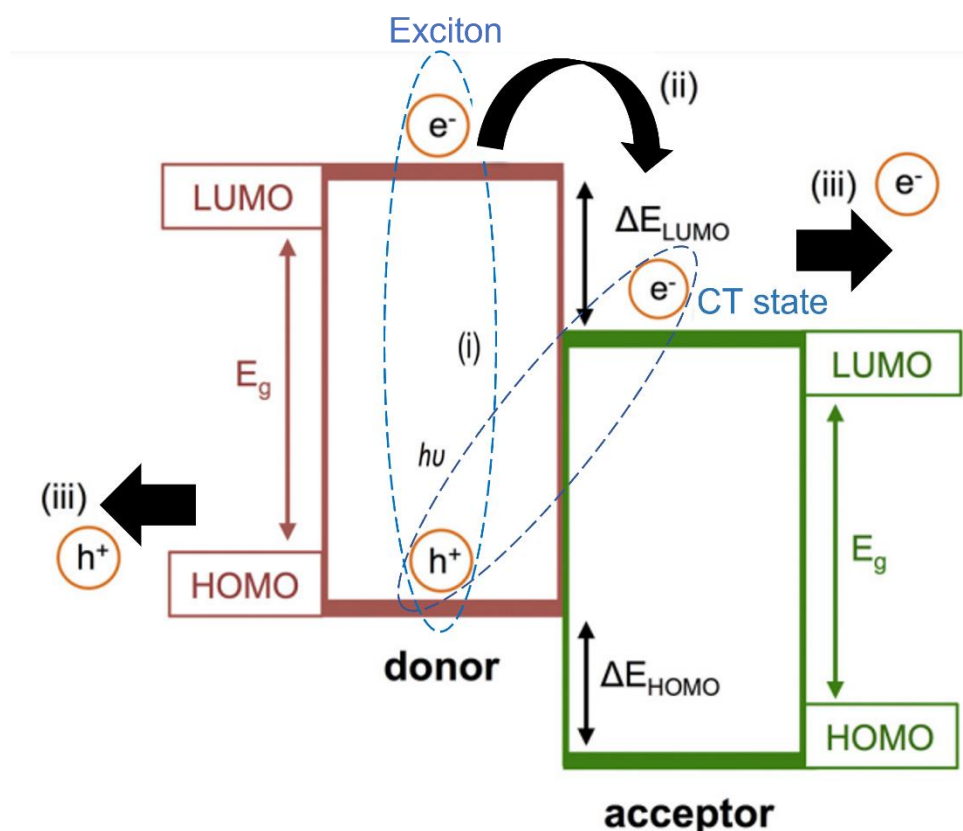


Figure 1.2. Charge transfer diagram of a donor-acceptor heterojunction. i) photon absorption and exciton formation; ii) Exciton dissociation and electron transfer between donor and acceptor; and iii) Electron and hole drift to collectors (electrodes).¹⁶

Before work can be extracted from the charge carriers within the device, they need to travel from the donor/acceptor interface to the correct electrodes. This transport is driven by the difference in the work functions of the electrodes, which generates an intrinsic electric field that propels charges to their respective collectors. Additionally, it is standard to include transport layers between the active layer and electrodes, to reduce contact resistances and improve charge injection. Ideally, positive and negative charge carriers should be balanced in the device, to avoid charge accumulation. Electrons and holes may still recombine while travelling to the electrodes, especially if they become physically isolated in island domains that are not immediately in contact with the correct electrode. Hence a direct path through either the donor or acceptor to the electrodes is necessary.^{2,24}

A semiconductor can be excited only by photons with energies equal or greater than that of its band gap (E_{bg}), defined as the difference between its HOMO and LUMO levels, therefore limiting the amount of the solar spectrum the material can absorb. Absorption of photons with higher energies than the E_{bg} rapidly undergo thermal relaxation and decay into the band edge, losing energy in the process. This limits the total possible efficiency of photovoltaics, that, through the Shockley-Queisser model,²⁵ has been calculated to be around 33% for of single-junction inorganic cells, and coincides with an E_{bg} of approximately 1.3 eV.²⁶ In OPVs, due to their excitonic nature and the additional free-energy loss that happens at the donor-acceptor interface, this maximum efficiency has been calculated to be approximately 25% (for a single junction), depending on the energy level offset.²⁷

1.3 Characterization of the Photovoltaic Effect

Photovoltaics are characterized by modelling their behaviour to that of a photodiode, which generates electric power from light when operated in reverse bias. A photovoltaic circuit and operational current density versus voltage (J - V) curves are shown in **Figure 1.3**.¹⁷ If no photons are incident to the cell, a very small saturation current forms for small biases, that can be estimated by **Equation (1.1)** for ideal conditions. When illuminated (**Figure 1.3b**), the current curves shift by a value equal that of the photogenerated current, which reaches its maximum for short-circuit conditions (J_{sc}). The J_{sc} metric depends on the efficiencies of each one of the steps depicted in **Figure 1.2**. Alternatively, the cell's point of maximum electric potential happens under open-circuit (no current) conditions (V_{oc}), whose value in OPVs is often associated to a function of the

difference between the LUMO of the acceptor and HOMO of the donor materials.¹⁷ A device provides maximum power at the curve's inflection point (denoted J_{MP} and V_{MP} in **Figure 1.3b**), where the power conversion efficiency (PCE) is measured, according to **Equation (1.2)**. Ideally, the shape of the curve should be a perfect square, as depicted by the red lined in **Figure 1.3b**, which would mean no drop in power due to resistance and charge recombination. The deviation from ideality can be assessed by the fill factor (FF), which is a measure of the “squareness” of the curve and can be calculated by **Equation (1.3)**. The FF is closely related to the series resistance (R_s) and shunt resistance (R_{sh}) of the cell. Combining these concepts, the overall OPV J - V curve can be predicted by the Kirchoff's law, presented in **Equation (1.4)**.^{2,17}

OPVs tend to present lower FF values (0.5-0.7), i.e. larger deviation from ideality, than their inorganic counterparts (0.8-0.9), which arises from low R_{sh} and/or high R_s values (see **Equation 4**). R_s aggregates all the resistances of all components and interfaces in the device, and they tend to be higher in OPVs due to their relative lower conductivities. Alternatively, R_{sh} is a result of current leakage, typically due to trap states, charge recombination and edge effects, which all become more prevalent in complex multi-component systems, such as OPVs.^{2,17,28} All these sources of efficiency loss are intimately connected to the device morphology and can be refined in order to optimize device performance.

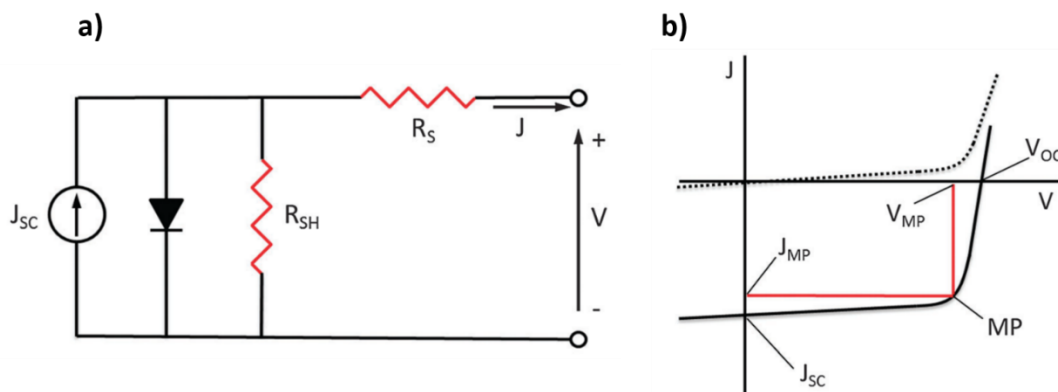


Figure 1.3. a) diagram of the circuit of a photovoltaic cell; b) Dark (dotted line) and illuminated (solid line) J - V curves of an operating photovoltaic cell.¹⁷

$$J_{dark} = J_0 \left(\frac{qV}{e^{k_b T}} - 1 \right) \quad (1.1)$$

$$PCE = \frac{J_{MP} V_{MP}}{P_{light}} \quad (1.2)$$

$$FF = \frac{J_{MP} V_{MP}}{J_{SC} V_{OC}} \quad (1.3)$$

$$J = J_{SC} - J_{dark} - J_{SH} = J_{SC} - J_0 \left(\frac{qV}{e^{k_b T}} - 1 \right) - \frac{V + JR_s}{R_{SH}} \quad (1.4)$$

Naturally, the metrics and overall efficiency measured in PV devices depends highly on the source of illumination. In the field of photovoltaics, the standard illumination employed to allow meaningful comparison between systems is the AM1.5 spectrum. It corresponds to a 1000 W m^{-2} solar light intensity, when the sun is at 48° from the horizon. Solar modules placed in different places of the world will measure different power outputs depending on their latitude, time of day, climatic conditions and so forth.²⁹ Even larger changes may occur if the source of light is artificial, namely indoor lighting photovoltaics, which is an emergent application of OPVs, where devices can achieve over 30% efficiency.³⁰

1.4 Device Configuration and Morphology

The first OPV developed by Tang *et al* was a planar heterojunction (PHJ), as the one depicted in **Figure 1.4a**. This geometry is a straightforward stack of each one of the materials that compose the device and is still being studied and optimized today due to its simple structure, ease of fabrication and compatibility with printing techniques, such as roll-to-roll.^{15,31} However, excitons can typically travel only a few nanometers before recombining, therefore, in this configuration, only excitons formed very near the interface live long enough in order to dissociate and generate power. This fact greatly limited the PCE of OPVs produced for nearly a decade. In 1995, however, a new breakthrough happened when the concept of bulk heterojunction (BHJ) was developed by Heeger *et al*, with the first report of polymer/fullerene OPV. In this type of device, the donor and acceptor blend is cast as a single interpenetrated layer composed of nanometric domains of each material, as depicted in **Figure 1.4b**. This enables a larger number of excitons to reach the interface and dissociate, greatly improving the photocurrent of such devices.^{32,33}

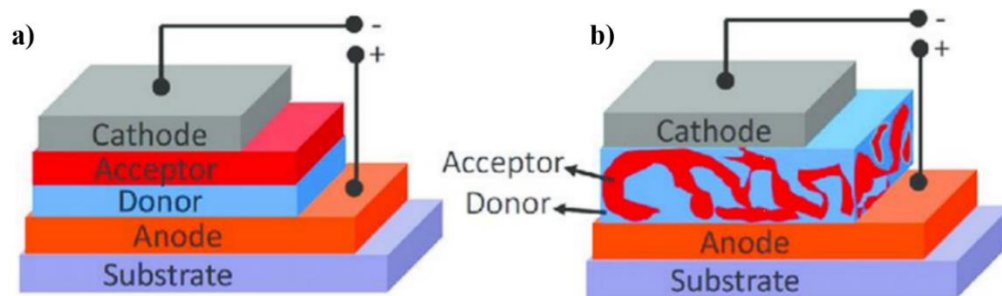


Figure 1.4. a) Planar heterojunction device structure; b) bulk heterojunction device structure. ³⁴

The BHJ configuration is arguably the most popular configuration for OPVs and is the choice for most top-performing OPV devices to date.^{8,10} The donor-acceptor pair of poly(3-hexylthiophene) (P3HT) and phenyl-C₆₁-butyric acid methyl ester (PC₆₁BM) has been the most extensively studied BHJ in OPVs, and even though its performance has been long surpassed by the use of advanced conjugated polymers and acceptors, it is a benchmark of OPV technology and often serves as reference point when assessing new materials.^{17,35} These devices can also have a direct or inverted architecture, as depicted in **Figure 1.5**. The inverted BHJ uses a transparent electrode as the cathode, often indium-tin oxide (ITO), and eliminates the need for low work-function, reactive metals as electrodes.^{17,36}

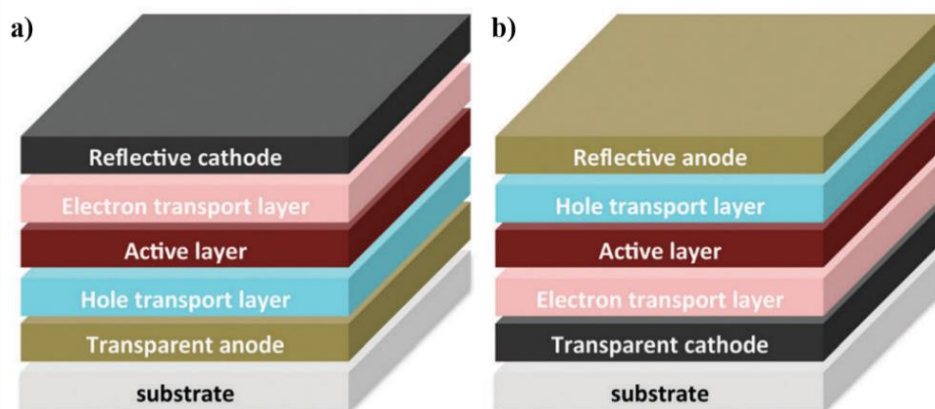


Figure 1.5. a) standard direct architecture; b) inverted device architecture. ¹⁷

The ability to be solution processed is key for the success of OPVs, as it enables the use of a number of inexpensive manufacturing techniques, such as spin-coating, blade-coating, screen-printing, roll-to-roll printing, which is precisely their edge compared to the silicon technologies.^{2,35} The resulting device performance, however, is highly dependent on the properties of the initial solution and its components, such as polarity, solubility, solvent volatility, surface energy, among

others. Typically, it is considered that an ideal BHJ morphology should have interpenetrated domains with sizes in the order of 10-20 nm. In summary, the active layer must present high interfacial area in order to dissociate the greatest possible number of excitons, while maintaining continuous paths for charges to be collected by electrodes, such as the scenarios presented on **Figure 1.6** (**Figure 1.6c** would be the ideal case). These features are, however, challenging to control via solution processes, which prompted many researchers to study how to optimize the active layer morphology, if possible, through comprehensive and robust design rules, for both process and molecular design.³⁸⁻⁴⁰

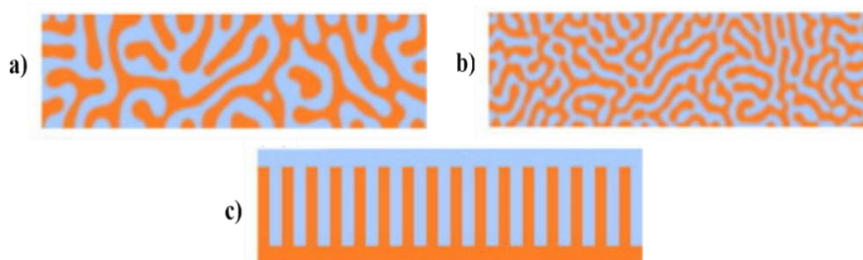


Figure 1.6. BHJ structures: a) random blend with large domains and many isolated islands; b) random blend with small domains and connected to the edges of the charge collectors; and c) interdigitated rods blend with complete connectivity to charge collectors. Effectiveness of the active layer, keep everything else the same, should increase from a) to c).³⁷

For non-patterned BHJs (**Figure 1.6a** and **b**), the morphology is typically optimized by controlling the material properties and the processing conditions. For example, by annealing the cast film and/or adjusting the polymers' characteristics, such as regioregularity and length of solubilizing alkyl chain one can tune the thin film crystallization rate.^{40,41} The crystallization rate is also highly dependent on the solvent properties, and the relative interactions of each component with the processing solvent. It has been demonstrated that the use of high boiling point solvents promotes higher crystallinity and induces order within the BHJ, due to slower drying rates (**Figure 1.7a**).⁴² Alternatively, if at least one of the components does not show strong interactions with the solvent of choice, extensive phase separation can occur with the formation of large domains, that greatly reduces the efficiency of the device (**Figure 1.7b**).^{43,44} In fact, it has been demonstrated that P3HT/fullerene active layers show the best efficiency when both components have similar

solubilities.⁴⁵ The same effect can be driven by differences in surface energy of the two solid components.^{44,46,47}

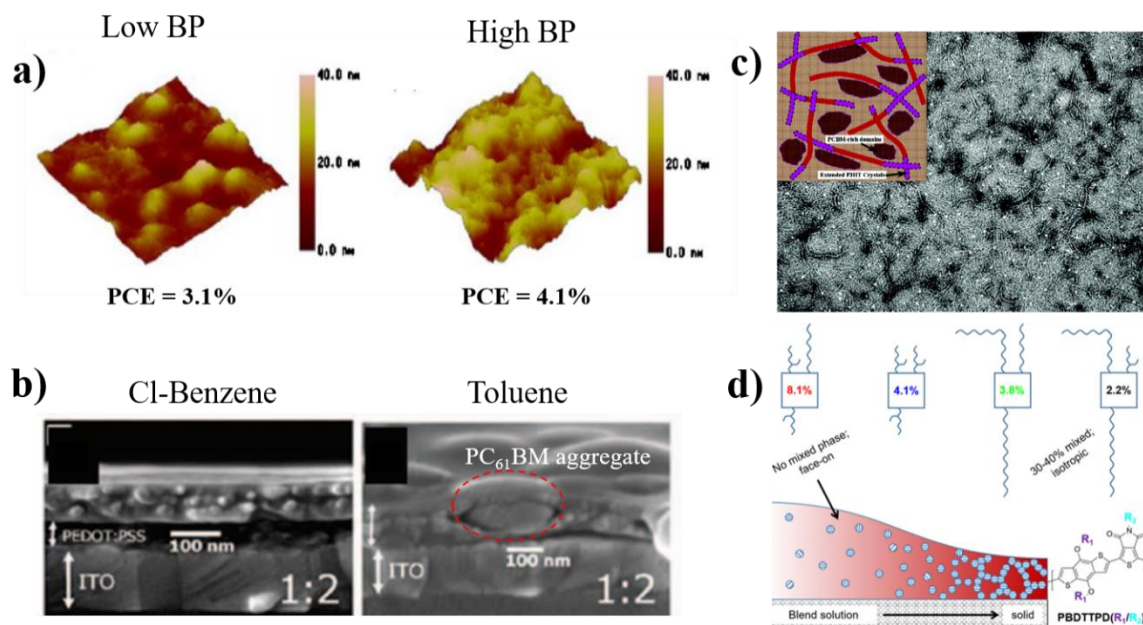


Figure 1.7. Examples of BHJ morphology modifications: a) Use of high boiling-point solvents decrease the drying rate and result is higher degree of order in the film as indicated by AFM images;⁴² b) Solvents that do not interact similarly with donor and acceptor can cause preferential precipitation/aggregation of one of the phases into undesirable, large domains, such as the case shown for toluene that causes the formation of bubble-like PC₆₁BM domains;⁴³ c) Thermal annealing results in ordering of the polymeric phase, connecting adjacent chains into a cocontinuous morphology that favours charge collection;⁴⁸ d) Modifying the alkyl chains of donor/acceptor materials have a strong effect on the final performance, leading to larger or smaller domains and degrees of crystallization.⁴¹

Because the drying of the film is a kinetically driven process in spin coating it is possible that ideal morphologies are not attained in time. Thermal and solvent annealing can be employed to drive the formation of larger, more crystalline domains and the smoothing of the interfaces. In the case of the P3HT/PC₆₁BM blend, it has been demonstrated that thermal annealing promotes a increase of crystallinity of P3HT while driving phase-separation to form co-continuous phases, which greatly improves charge transfer from the BHJ to the electrodes (**Figure 1.7c**).^{40,48} Domain growth and increase in crystallinity also happens when the BHJ is exposed to a solvent vapor, during solvent annealing. It is important to note, however, that over-annealing can have a detrimental effect if the extent of phase separation and growth is too large, when the domains get too large for effective exciton dissociation.⁴⁹ Ultimately, the morphology can be improved by

careful molecular design, which affect solubility, solvent interactions, surface energy, miscibility of phases, etc. For example, highly regioregular polymers tend to have improved performance in OPVs due to their tendency to form more organized domains. Alternatively, for some materials and processes, amorphous domains are desired, therefore a polymer with lower regioregularity can be selected.⁵⁰ The length and placing of alkyl chains on the polymer backbone also have a strong effect on device performance. Savikhin *et al* demonstrated that by simply swapping the solubilizing groups in Poly[(5,6-dihydro-5-octyl-4,6-dioxo-4H-thieno[3,4-c]pyrrole-1,3-diyl)[4,8-bis[(2-ethylhexyl)oxy]benzo[1,2-b:4,5-b']dithiophene-2,6-diyl] (PBDTTPD) donors, the PCE increased 4-fold, varying from 1.98 to 8.1%, as result of the formation of smaller, more crystalline, pure domains (**Figure 1.7d**). This effect was attributed to changes in the molecular packing which can be greatly affected by the presence of bulky alkyl groups.⁴

Lyons *et al.* have developed a model that correlates the relative effect of domain size, domain purity and domain interface to the efficiency of BHJ OPVs, more specifically, how it affects the efficiency of exciton dissociation and charge collection. The smaller domain size, the greater the exciton dissociation efficiency but the lower the charge collection efficiency, due to discontinuity of the domains. Both purity and sharpness of the domains have a positive effect on the charge collection. One of the main findings of this model is, however, that domain size has little effect on the overall performance if they are not pure, because the benefits of exciton dissociation are offset by an increase in charge trapping, as depicted in **Figure 1.8**.⁵¹ These findings underline the need to assess the solid-state interactions between donor and acceptor, as well as the individual properties of the organic semiconductors employed, in addition to solvent interactions. It is critical to study the miscibility, solubility and crystallization characteristics on the resulting thin film morphology to truly understand the effect on OPV performance. While models like the Hansen solubility parameters^{52,53} and the Flory-Huggins miscibility parameters⁵⁴ exist and can support the understanding of solvent-solid and solid-solid interactions in BHJs, their application towards optimization of OPVs is still rare.

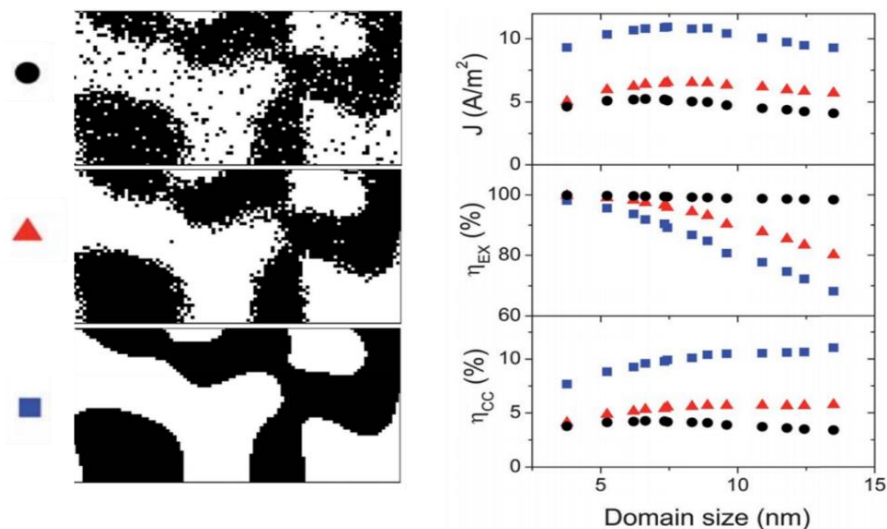


Figure 1.8. Simulated current (J), exciton splitting efficiency (η_{EX}) and charge collection (η_{CC}) in BHJ with domains of different sizes when the morphology is characterized by **a)** impure domains; **b)** diffuse interfacial edges and **c)** pure domains with sharp edges.⁵¹

1.5 OPV Materials

Between 2005 and 2015, the search for advanced OPV materials, especially low-bandgap polymers to be employed as donors, has greatly intensified, and led to important breakthroughs.²³ Before that, the vast majority of studies focused on the P3HT/PC₆₁BM pair, whose efficiency is in the 3-4% range, due to relatively low V_{oc} and small solar spectral coverage.³⁵ A variety of novel conjugated polymers with narrower bandgaps have been developed in recent years, capable of harvesting a broad range of wavelengths, leading to higher currents, and having deeper HOMO levels, which can potentially increase their V_{oc} , when paired with fullerenes. **Figure 1.9** displays the absorption the chemical structure selected donor polymers, including P3HT. Among the donor polymers shown in **Figure 1.9**, Poly[[4,8-bis[(2-ethylhexyl)oxy]benzo[1,2-b:4,5-b']dithiophene-2,6-diyl][3-fluoro-2-[(2ethylhexyl)carbonyl]thieno[3,4-b]thiophenediyl]] (PTB7) and poly[N-9'-heptadecanyl-2,7-carbazole-alt-5,5-(4',7'-di-2-thienyl-2',1',3'-benzothiadiazole)] (PCDTBT) initially stood out for being commercially available and widely used in current studies, and with PCEs that may exceed 6% when using fullerenes as acceptor.⁵⁵ More recently Poly[(2,6-(4,8-bis(5-(2-ethylhexyl-3-fluoro)thiophen-2-yl)-benzo[1,2-b:4,5-b']dithiophene))-alt-(5,5-(1',3'-di-2-thienyl-5',7'-bis(2-ethylhexyl)benzo[1',2'-c:4',5'-c']dithiophene-4,8-dione)] (PM6) has also been increasingly used in research, achieving high PCEs above 15%, when paired with high-performing acceptors.^{23,56}

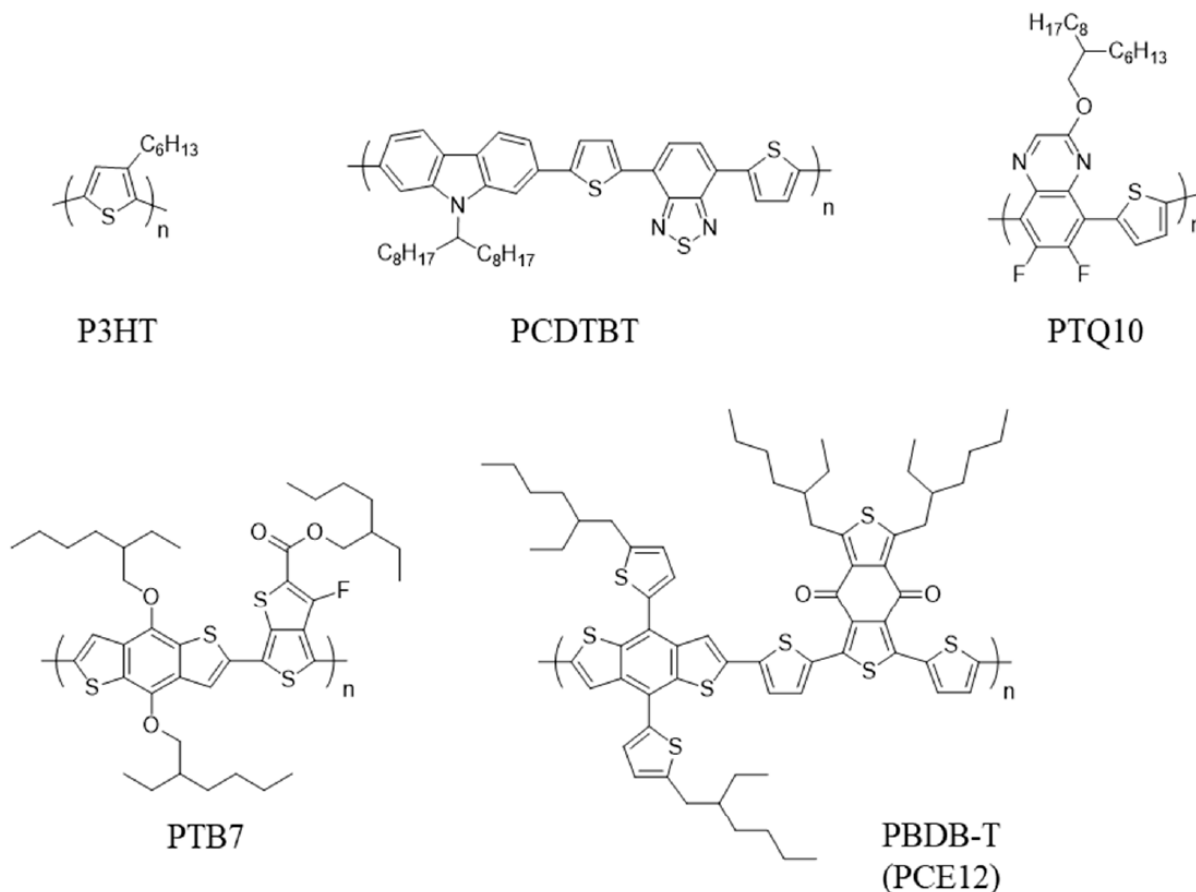


Figure 1.9. Chemical structure of common donor polymers employed in OPVs. ⁶⁷

Alternatively, in the past decade, most of the advances in OPV performance have focused on the acceptor compounds, as the field moves on from fullerene derivatives. The most prominent acceptors in OPVs are the Y6 (2,2'-((2Z,2'Z)-((12,13-bis(2-ethylhexyl)-3,9-diundecyl-12,13-dihydro-[1,2,5]thiadiazolo[3,4-e]thieno[2'',3''':4',5']thieno[2',3':4,5]pyrrolo[3,2-g]thieno[2',3':4,5]thieno[3,2-b]indole-2,10-diyl)bis(methanylylidene))bis(5,6-difluoro-3-oxo-2,3-dihydro-1H-indene-2,1-diylidene))dimalononitrile) and ITIC (3,9-bis(2-methylene-(3-(1,1-dicyanomethylene)-indanone))-5,5,11,11-tetrakis(4-hexylphenyl)-dithieno[2,3-d:2',3'-d']-s-indaceno[1,2-b:5,6-b']dithiophene) series, which are based on derivations of the A-D-A (fusing acceptor A and donor D moieties together) approach to design organic semiconductors. These acceptors achieve high efficiencies, often above 10%, ^{9,23,57} and high V_{oc} s, due to the small energy offset required for charge separation.¹⁸ Through fine-tuning these organic semiconductors' E_{bg} , it was possible to also improve charge generation by extending light absorption in the near-IR region (>750 nm). Select acceptors are shown in **Figure 1.10**.⁵⁸

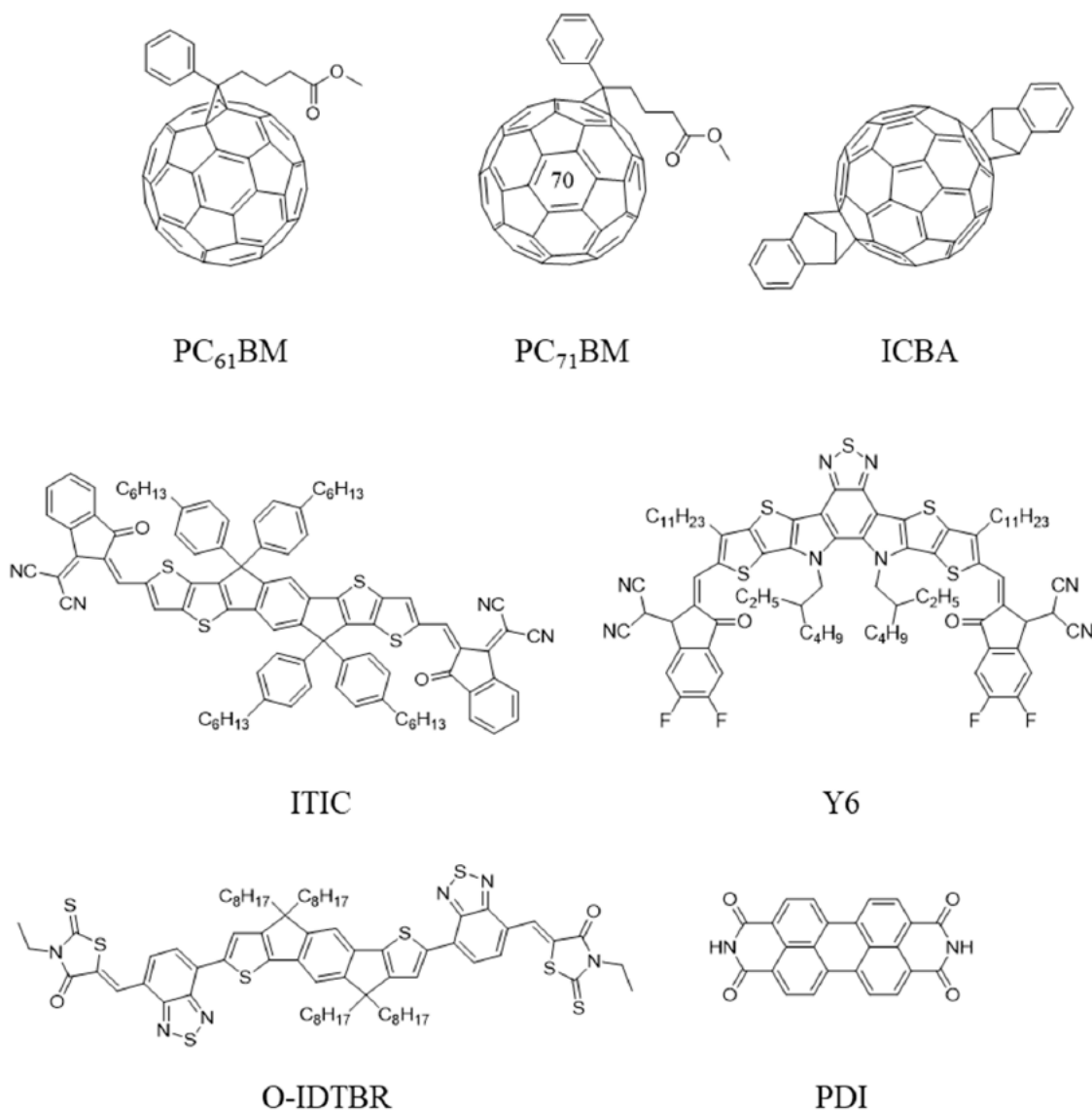


Figure 1.10. Absorption spectra of common small-molecule acceptors employed in OPVs.⁶⁷

The main drawback of such advanced semiconductors is their synthetic complexity which often leads to high costs. They require complex multi-step synthesis to be manufactured, and commercial options can be as much as 9 times more expensive than P3HT. Multi low yielding reactions associated with high-performing materials are prohibitive for large-scale production. One of the major thrusts for the development of OPVs is their low manufacturing cost so using overly expensive polymers defeats the purpose of fabricating OPVs.^{59–63} The complexity and, therefore, scalability and cost of conjugated polymers and small molecule acceptors can be categorized in terms of their synthetic complexity index (SC), coined by Po. et al.⁶⁴ This model takes into account the number of synthetic steps, the reciprocal of the cumulative synthetic yield, the number of unit operations, the number

of column chromatography purification steps, and the number of highly hazardous chemicals involved in the synthesis. It provides a comparison framework between the economical feasibility and efficiency of materials employed in OPVs. **Figure 1.11** provides a comparison of common OPV materials as to their SC. The highest performing materials have considerably larger SC, therefore, while the gains in OPVs efficiency have been remarkable, they have not resulted in commercially relevant products or applications. Hence, while the OPV field moves towards ever more complicated conjugates polymers,^{65,66} whose production is not scalable, in this thesis I propose the study and improvement of devices containing commercially viable materials.

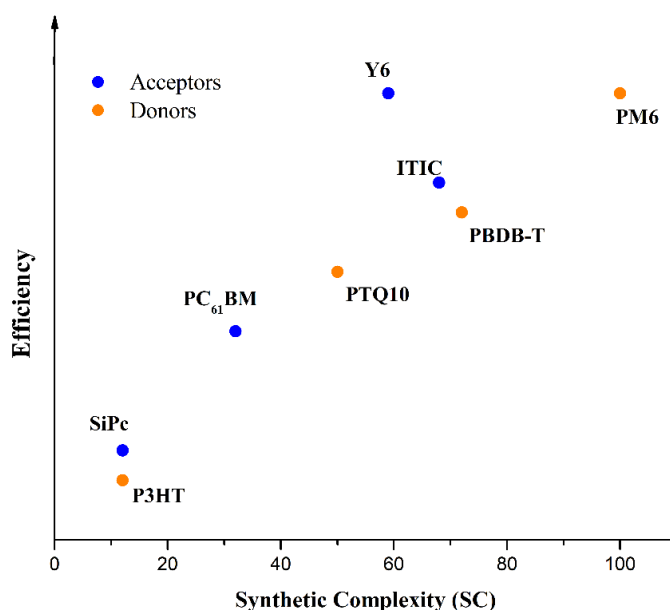


Figure 1.11. Comparison between average efficiencies achieved by select organic semiconductors and their synthetic complexity index.

One class of organic compounds that has found innumerable applications in electronics are metal and metalloid-containing phthalocyanines (MPcs), which are conjugated molecules composed of a tetramer of nitrogen-linked isoindole. The MPc structure is shown in **Figure 1.12a**. These materials have been employed as commercial photoreceptors for almost 50 years and over 100 years, as a commercial pigment.⁶⁸ The synthesis and purification of MPcs is relatively simple, high-yield and well understood, making them desirable candidates for low-cost OPV devices.^{68–71} In fact, the first ever heterojunction made by Tang¹⁵, employed copper phthalocyanine (CuPc) as electron donor. MPcs have a high molar extinction coefficient ($10^5 \text{ M}^{-1}\text{cm}^{-1}$) and absorb light in the red and near infrared region, complimenting the absorption of well-established organic

semiconductors, such as P3HT, PCDTBT and PC₆₁BM, that often show poor performance in that region of the solar spectrum.^{71–73} The absorption spectrum of typical MPcs are presented in **Figure 1.12b**.

While divalent MPcs (Zn, Cu, etc) have been widely reported as active materials and employed in many organic electronics devices, tetravalent MPcs have not been as explored. Tetravalent MPcs, such as silicon phthalocyanines (R₂-SiPcs), have two axial bonds available for chemical modification (**Figure 1.12a**), imparting broader chemical versatility and facilitating the tuning of not only their electrochemical properties, but also physical properties, such as solid-state packing, solubility, melting point, surface energy, etc.^{68–71} R₂-SiPcs have inherent n-type conductivity and have been employed in organic light-emitting diodes (OLED)^{74–76}, and organic thin film transistors (OTFTs)^{77–81}, with respectable mobilities, of up to 0.1 cm² V⁻¹ s⁻¹. In OPVs, R₂-SiPcs have been studied as additives, to improve the efficiency of benchmark BHJ (such as P3HT/PC₆₁BM), and, to a lesser extent, as electron acceptors.^{46,82–85} Axially functionalized R₂-SiPcs are especially suited for low-cost applications, as their synthetic complexity is relatively low (**Figure 1.11**).⁸⁶

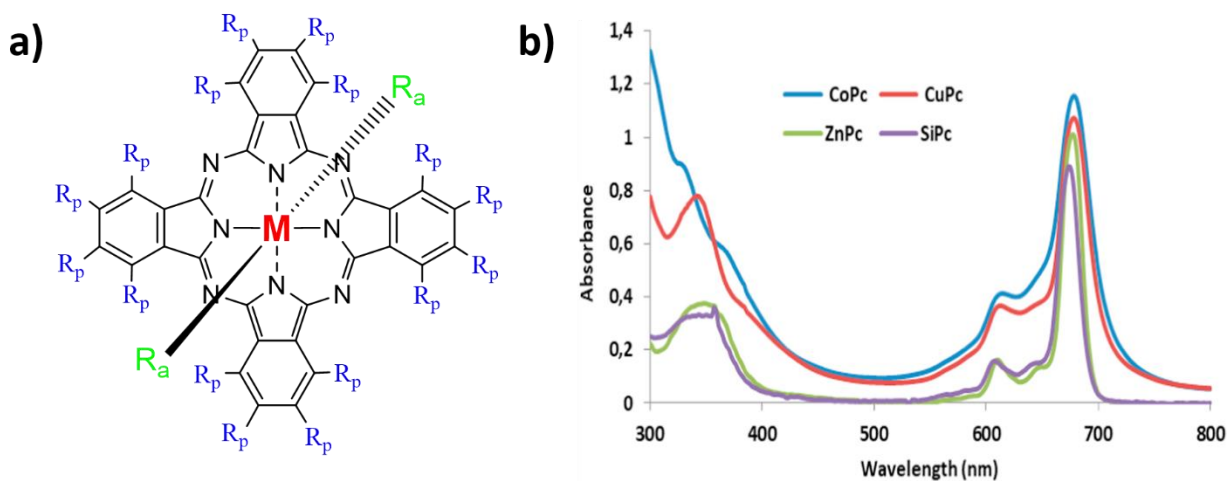


Figure 1.12. a) Structure of a tetravalent phthalocyanine with a metal center (M, in red), axial groups (Ra, in green) and peripheral groups (Rp, in blue); b) Absorption spectra of selected MPcs.

1.6 R₂-SiPcs as ternary additives

One of the main strategies to improve the performance of well-established donor-acceptor pairs is the introduction of a ternary additive. Such additives can have different functions, but typically they are introduced in the BHJ to improve morphology and spectral coverage. **Figure**

1.13 displays different morphologies that can be formed in a ternary BHJ. This is strategy is particularly interesting from an economical point of view as it can be easily implemented due to its simplicity.

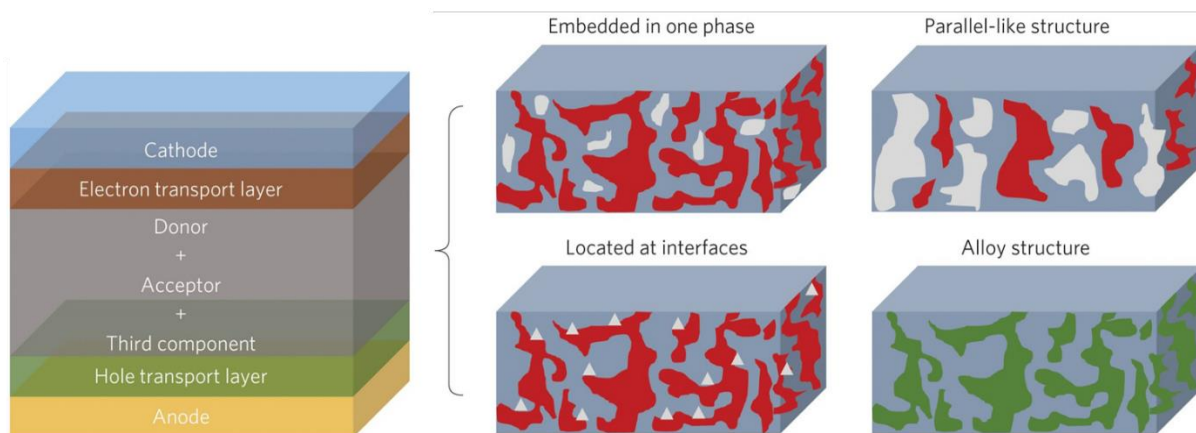


Figure 1.13. Possible morphologies of a ternary BHJ.

R_2 -SiPc have been effective additives due to their strong absorption in the near-infrared region, able to complement the coverage of P3HT/ $PC_{61}BM$ devices, as it can be seen by the external quantum efficiency (EQE) spectrum shown in **Figure 1.14**, leading to increases of up to 50% in the PCE and J_{SC} of the organic cell. This use of R_2 -SiPcs as ternary additives was first reported by Honda et al., who added the derivative bis(trihexyl)silyl oxide silicon phthalocyanine ($(3HS)_2$ -SiPc) to P3HT/ $PC_{61}BM$ BHJ.^{82,83} The same group also investigated the mechanism and morphology of this ternary blends and found that the $(3HS)_2$ -SiPc tends to migrate to the amorphous interface between P3HT and $PC_{61}BM$, as depicted in **Figure 1.13c**, where they boost charge collection and charge transfer, while contributing to spectral coverage.⁴⁶ These axially substituted derivatives also have been shown to compatibilize the surface energy of P3HT and $PC_{61}BM$, which further improves charge transfer at the domains' interface, underlining the effectiveness of R_2 -SiPcs as multi-function additives.⁴⁷

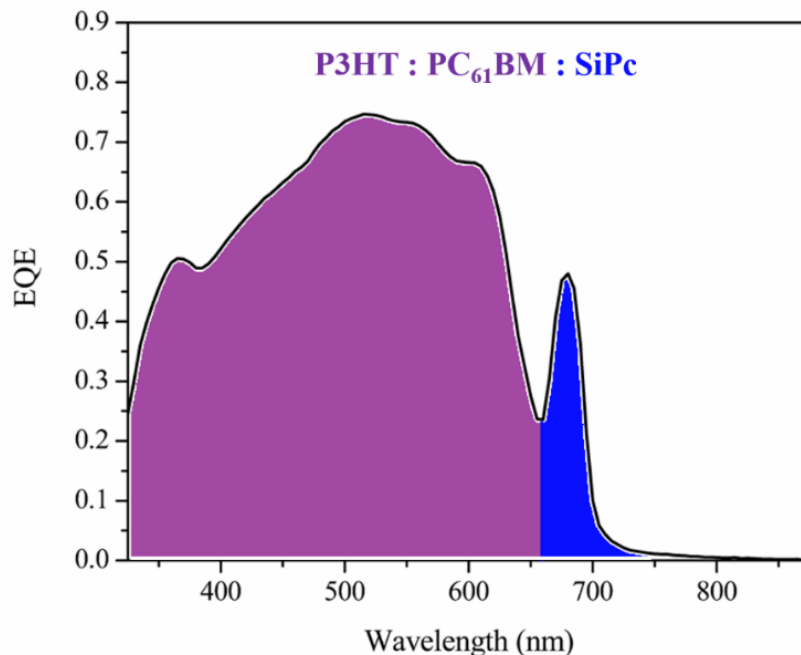


Figure 1.14. Extension of spectral coverage when adding 4 wt% of SiPc (blue) to a P3HT/PC61BM blend (purple).⁹³

1.7 R₂-SiPcs as non-fullerene acceptors (NFAs)

Another relevant issue with traditional OPVs is their reliance on fullerenes, such as PC₆₁BM. This class of compound have many desirable properties to be used as electron acceptors in organic electronics, namely delocalized LUMO in 3 dimensions, which form robust pathways for charge transfer, high electron mobilities, electron-affinity and the tendency to form extensive domains that improve charge collection. Nonetheless, fullerenes present weak absorption in the visible region, some degree of photo-instability and, above all, their synthesis has low efficiency, below 20% in most cases, and require time-consuming purification, leading to high costs and limitations to scale-up fabrication.^{94,95} These drawbacks prompted the research community to favour NFAs in the past decade.⁹⁶

Many organic NFAs have found application in high-performing OPVs, often specifically tailored to the donor polymer it is paired with, tuning their energy levels and absorption, in order to optimize charge transport while complementing the spectral coverage of the donor.⁹⁶ On the downside, NFAs are often 2D planar molecules, such as phthalocyanines, that typically present anisotropic electronic behavior, which may lead to unfavorable electron-transport, due to a limitation in the direction of transport. In principle, the crystalline domains can be oriented in the

preferred direction, however this is very hard to control in a bulk heterojunction and is very dependent on solid-state packing, film morphology and interactions with the polymer donor.^{51,96-98}

R₂-SiPcs present many of the characteristics that make a good acceptor, such as high electron mobility, high extinction coefficient, absorption in the red and near-infrared region, can be easily synthesized and purified. When paired with P3HT, R₂-SiPcs present a respectable V_{OC} , between 0.70-0.80 V, but very low J_{SC} , FF and PCE, often, below 1%.^{71,74,99} Dang *et al* demonstrated that the reason for the low PCEs of these system is due to bad BHJ morphology, indicating that tweaking molecular design, process conditions and solvent interactions may be the key for better performance.⁷¹ Nonetheless, studies that report the application of R₂-SiPcs as NFAs are scarce in the literature and lack optimization, constituting an open research topic that needs more investigation, especially considering that it has been estimated that the production of R₂-SiPc requires 70 to 150 times less energy than PC₆₁BM and PC₇₁BM, the fullerenes most often employed as acceptors in OPVs.^{100,101}

One of the limitations of R₂-SiPcs as electron acceptors is their relatively shallow HOMO and LUMO levels, which reduces their air-stability and narrows the range of possible donor pairs, as currently popular polymer donors often have HOMO levels deeper than -3.5 eV.¹⁰²⁻¹⁰⁴ The introduction of electron withdrawing groups to the R₂-SiPcs structure achieves those deeper energy levels. Fluorine is a popular choice of strong electron withdrawing group, that due to its small size does not disrupt molecular packing,¹⁰⁵ stabilize the electronic orbitals and enhance¹⁰⁶ the n-type conductivity of the semiconductor.¹⁰² Copper hexadecafluorophthalocyanines (CuF₁₆Pc) have been employed in OTFTs, with mobilities as high as 0.26 V⁻¹ s⁻¹,¹⁰⁷ and, to a lesser extent, as NFA in OPVs with improved performances when compared to their non-fluorinated counterpart.¹⁰⁸ Such devices are often fabricated by vapor deposition, as these unsubstituted F₁₆Pcs have very limited solubility. This problem can be circumvented by tetravalent, peripherally fluorinated phthalocyanines (F_xPcs, where x is between 1 and 16), such as fluorinated silicon phthalocyanines (R₂-F_xSiPc) whose solubility can be tuned with chemical modifications on the two axial bonds.¹⁰⁹ R₂-F_xSiPc have never been synthesized before and herein we proposed to attempt it and evaluated its properties and applications in OPVs.

1.8 Scope of the Thesis

In this chapter, I introduced some key concepts and contexts that are relevant in the study of OPVs. The OPV field has geared towards ever more complex structures to achieve high efficiencies, and it has become clear that without a compromise with cost and scalability, relevant applications will not be achieved in the near future. In that sense, SiPcs are promising candidates for n-type semiconductors that have not been widely explored for OPV applications. They have outstanding stability, intrinsic n-type conductivity and can be obtained through straightforward, low-cost synthetic pathways.

Herein we propose to explore R₂-SiPcs as acceptors in OPVs, and expand the knowledge on the donor/acceptor blends they form with select polymer donors, as we try to move away from trial-and-error approach to materials design, by establishing robust property-performance relationships.

- 1) *Can we correlate basic physical and thermodynamic properties of R₂-SiPcs to their performance in OPV devices?* (Chapter 2 and 3)
- 2) *Can the PCE of SiPc-containing OPVs be improved by pairing them with PTB7?* (Chapter 4)
- 3) *Can we combine R₂-SiPcs with a wider range of polymers while improving their n-type mobilities by peripheral fluorination of the phthalocyanine ring?* (Chapter 5)

1.9 References

- (1) A Fundamental Look At Supply Side Energy Reserves For The Planet. *SHC Sol. Updat.* **2015**. <https://doi.org/10.1016/j.eneco.2008.12.011>.
- (2) Fusella, M. A.; Lin, Y. L.; Rand, B. P. *20 - Organic Photovoltaics (OPVs): Device Physics*, 2nd ed.; Elsevier Ltd., 2019. <https://doi.org/10.1016/B978-0-08-102284-9.00020-6>.
- (3) Liu, J.; Yao, Y.; Xiao, S.; Gu, X. Review of Status Developments of High-Efficiency Crystalline Silicon Solar Cells. **2018**.
- (4) Zhang, Y.; Tao, J.; Chen, Y.; Xiong, Z.; Zhong, M.; Feng, Z.; Yang, P.; Chu, J. *RSC Advances*. **2016**, 58046–58054. <https://doi.org/10.1039/c6ra05765a>.
- (5) Mints, P. Global Photovoltaic Shipments Jump 15 % in 2014 Photovoltaic Technology Trends : A Supply Perspective. *IdTechEx* **2019**, 1–9.
- (6) Brabec, C. *Organic Photovoltaics : Materials, Device Physics, and Manufacturing Technologies*; Wiley: Hoboken, 2014.
- (7) Li, R.; Hu, W.; Liu, Y.; Zhu, D. Micro- and Nanocrystals of Organic Semiconductors. *Acc. Chem. Res.* **2010**, 43 (4), 529–540. <https://doi.org/10.1021/ar900228v>.

- (8) Liu, Q.; Jiang, Y.; Jin, K.; Qin, J.; Xu, J.; Li, W.; Xiong, J.; Liu, J.; Xiao, Z.; Sun, K.; et al. 18% Efficiency Organic Solar Cells. *Sci. Bull.* **2020**, *65* (4), 272–275. <https://doi.org/10.1016/j.scib.2020.01.001>.
- (9) Cui, Y.; Yao, H.; Zhang, J.; Xian, K.; Zhang, T.; Hong, L.; Wang, Y.; Xu, Y.; Ma, K.; An, C.; et al. Single-Junction Organic Photovoltaic Cells with Approaching 18% Efficiency. *Adv. Mater.* **2020**, *32* (19), 1–7. <https://doi.org/10.1002/adma.201908205>.
- (10) Cui, Y.; Xu, Y.; Yao, H.; Bi, P.; Hong, L.; Zhang, J.; Zu, Y.; Zhang, T.; Qin, J.; Ren, J.; et al. Single-Junction Organic Photovoltaic Cell with 19% Efficiency. *Adv. Mater.* **2021**, *33* (41), 1–8. <https://doi.org/10.1002/adma.202102420>.
- (11) Meyers, R. A. *Encyclopedia of Sustainability Science and Technology*; Springer Science, 2012. <https://doi.org/10.1007/978-1-4419-0851-3>.
- (12) Berny, S.; Blouin, N.; Distler, A.; Egelhaaf, H. J.; Krompiec, M.; Lohr, A.; Lozman, O. R.; Morse, G. E.; Nanson, L.; Pron, A.; et al. Solar Trees: First Large-Scale Demonstration of Fully Solution Coated, Semitransparent, Flexible Organic Photovoltaic Modules. *Adv. Sci.* **2015**, *3* (5), 1–7. <https://doi.org/10.1002/advs.201500342>.
- (13) Lee, S. Free of Carbon Emissions by Truly Green Energy. *Global Photovoltaic Business Magazine*. 2020, pp 2–3.
- (14) Hoppe, H.; Sariciftci, N. S. Organic Solar Cells: An Overview. *J. Mater. Res.* **2004**, *19* (7), 1924–1945. <https://doi.org/10.1557/JMR.2004.0252>.
- (15) Tang, C. W. Two-Layer Organic Photovoltaic Cell. *Appl. Phys. Lett.* **1986**, *48* (2), 183–185. <https://doi.org/10.1063/1.96937>.
- (16) Holliday, S.; Li, Y.; Luscombe, C. K. Recent Advances in High Performance Donor-Acceptor Polymers for Organic Photovoltaics. *Prog. Polym. Sci.* **2017**, *70*, 34–51. <https://doi.org/10.1016/j.progpolymsci.2017.03.003>.
- (17) Mazzi, K. A.; Luscombe, C. K. The Future of Organic Photovoltaics. *Chem. Soc. Rev.* **2015**, *44* (1), 78–90. <https://doi.org/10.1039/c4cs00227j>.
- (18) Kawashima, K.; Tamai, Y.; Ohkita, H.; Osaka, I.; Takimiya, K. High-Efficiency Polymer Solar Cells with Small Photon Energy Loss. *Nat. Commun.* **2015**, *6*. <https://doi.org/10.1038/ncomms10085>.
- (19) Brédas, J. L.; Beljonne, D.; Coropceanu, V.; Cornil, J. Charge-Transfer and Energy-Transfer Processes in π -Conjugated Oligomers and Polymers: A Molecular Picture. *Chem. Rev.* **2004**, *104* (11), 4971–5003. <https://doi.org/10.1021/cr040084k>.
- (20) Yu, Z. P.; Li, X.; He, C.; Wang, D.; Qin, R.; Zhou, G.; Liu, Z. X.; Andersen, T. R.; Zhu, H.; Chen, H.; et al. High-Efficiency Organic Solar Cells with Low Voltage-Loss of 0.46 V. *Chinese Chem. Lett.* **2020**, *31* (7), 1991–1996. <https://doi.org/10.1016/j.ccllet.2019.12.003>.
- (21) Pradhan, R.; Agrawal, A.; Bag, B. P.; Singhal, R.; Sharma, G. D.; Mishra, A. High-Efficiency Ternary Organic Solar Cells Enabled by Synergizing Dicyanomethylene-Functionalized Coumarin Donors and Fullerene-Free Acceptors. **2022**. <https://doi.org/10.1021/acsaem.2c01473>.
- (22) Liu, Y.; Zhang, J.; Zhou, G.; Liu, F.; Zhu, X.; Zhang, F. Electric Field Facilitating Hole Transfer in Non-Fullerene Organic Solar Cells with a Negative HOMO Offset. *J. Phys. Chem. C* **2020**, *124* (28), 15132–15139. <https://doi.org/10.1021/acs.jpcc.0c05654>.
- (23) Zhang, G.; Lin, F. R.; Qi, F.; Heumüller, T.; Distler, A.; Egelhaaf, H. J.; Li, N.; Chow, P. C. Y.; Brabec, C. J.; Jen, A. K. Y.; et al. Renewed Prospects for Organic Photovoltaics. *Chem. Rev.* **2021**. <https://doi.org/10.1021/acs.chemrev.1c00955>.

- (24) van der Staaij, F. M.; van Keulen, I. M.; von Hauff, E. Organic Photovoltaics: Where Are We Headed? *Sol. RRL* **2021**, *5* (8), 1–8. <https://doi.org/10.1002/solr.202100167>.
- (25) Shockley, W.; Queisser, H. J. Detailed Balance Limit of Efficiency of P-n Junction Solar Cells. *J. Appl. Phys.* **1961**, *32* (3), 510–519. <https://doi.org/10.1063/1.1736034>.
- (26) Rühle, S. Tabulated Values of the Shockley-Queisser Limit for Single Junction Solar Cells. *Sol. Energy* **2016**, *130*, 139–147. <https://doi.org/10.1016/j.solener.2016.02.015>.
- (27) Giebink, N. C.; Wiederrecht, G. P.; Wasielewski, M. R.; Forrest, S. R. Thermodynamic Efficiency Limit of Excitonic Solar Cells. *Phys. Rev. B - Condens. Matter Mater. Phys.* **2011**, *83* (19), 1–6. <https://doi.org/10.1103/PhysRevB.83.195326>.
- (28) Rand, B. P.; Burk, D. P.; Forrest, S. R. Offset Energies at Organic Semiconductor Heterojunctions and Their Influence on the Open-Circuit Voltage of Thin-Film Solar Cells. *Phys. Rev. B - Condens. Matter Mater. Phys.* **2007**, *75* (11), 1–11. <https://doi.org/10.1103/PhysRevB.75.115327>.
- (29) Riordan, C.; Hulstron, R. What Is an Air Mass 1.5 Spectrum. In *IEEE Photovoltaic Specialists Conference*; 1990; Vol. 2, pp 1085–1088.
- (30) Lee, C.; Lee, J. H.; Lee, H. H.; Nam, M.; Ko, D. H. Over 30% Efficient Indoor Organic Photovoltaics Enabled by Morphological Modification Using Two Compatible Non-Fullerene Acceptors. *Adv. Energy Mater.* **2022**, *12* (22), 1–10. <https://doi.org/10.1002/aenm.202200275>.
- (31) Gong, C.; Tong, S.; Huang, K.; Li, H.; Huang, H.; Zhang, J.; Yang, J. Flexible Planar Heterojunction Perovskite Solar Cells Fabricated via Sequential Roll-to-Roll Microgravure Printing and Slot-Die Coating Deposition. *Sol. RRL* **2020**, *4* (2), 1900204. <https://doi.org/10.1002/solr.201900204>.
- (32) Brabec, C. J.; Gowrisanker, S.; Halls, J. J. M.; Laird, D.; Jia, S.; Williams, S. P. Polymer-Fullerene Bulk-Heterojunction Solar Cells. *Adv. Mater.* **2010**, *22* (34), 3839–3856. <https://doi.org/10.1002/adma.200903697>.
- (33) Yu, G.; Gao, J.; Hummelen, J. C.; Wudi, F.; Heeger, A. J. Polymer Photovoltaic Cells: Enhanced Efficiencies via a Network of Internal Donor-Acceptor Heterojunctions. *Science (80-.)*. **1995**, *270*, 1–3.
- (34) Yilmaz, E. çetin; Yeşilyurt, M. K.; öner, I. V.; ömeroğlu, G.; özakin, A. N. Operational Stability and Degradation of Organic Solar Cells. *Period. Eng. Nat. Sci.* **2017**, *5* (2), 152–160. <https://doi.org/10.21533/pen.v5i2.105>.
- (35) Dang, M. T.; Hirsch, L.; Wantz, G. P3HT:PCBM, Best Seller in Polymer Photovoltaic Research. *Adv. Mater.* **2011**, *23* (31), 3597–3602. <https://doi.org/10.1002/adma.201100792>.
- (36) de Jong, M. P.; van Ijzendoorn, L. J.; de Voigt, M. J. A. Stability of the Interface between Indium-Tin-Oxide in Polymer Light-Emitting Diodes. *Appl. Phys. Lett.* **2000**, *77* (14), 2255–2257. <https://doi.org/10.1063/1.1315344>.
- (37) Wodo, O.; Tirthapura, S.; Chaudhary, S.; Ganapathysubramanian, B. A Graph-Based Formulation for Computational Characterization of Bulk Heterojunction Morphology. *Org. Electron.* **2012**, *13* (6), 1105–1113. <https://doi.org/10.1016/j.orgel.2012.03.007>.
- (38) Chen, L. M.; Hong, Z.; Li, G.; Yang, Y. Recent Progress in Polymer Solar Cells: Manipulation of Polymer: Fullerene Morphology and the Formation of Efficient Inverted Polymer Solar Cells. *Adv. Mater.* **2009**, *21* (14–15), 1434–1449. <https://doi.org/10.1002/adma.200802854>.
- (39) Vandewal, K.; Himmelberger, S.; Salleo, A. Structural Factors That Affect the Performance of Organic Bulk Heterojunction Solar Cells. *Macromolecules* **2013**, *46* (16), 6379–6387. <https://doi.org/10.1021/ma400924b>.

- (40) Liu, F.; Gu, Y.; Jung, J. W.; Jo, W. H.; Russell, T. P. On the Morphology of Polymer-Based Photovoltaics. *J. Polym. Sci. Part B Polym. Phys.* **2012**, *50* (15), 1018–1044. <https://doi.org/10.1002/polb.23063>.
- (41) Savikhin, V.; Babics, M.; Neophytou, M.; Liu, S.; Oosterhout, S. D.; Yan, H.; Gu, X.; Beaujuge, P. M.; Toney, M. F. Impact of Polymer Side Chain Modification on OPV Morphology and Performance. *Chem. Mater.* **2018**, *30* (21), 7872–7884. <https://doi.org/10.1021/acs.chemmater.8b03455>.
- (42) Chen, F. C.; Tseng, H. C.; Ko, C. J. Solvent Mixtures for Improving Device Efficiency of Polymer Photovoltaic Devices. *Appl. Phys. Lett.* **2008**, *92* (10), 2006–2009. <https://doi.org/10.1063/1.2898153>.
- (43) Hoppe, H.; Glatzel, T.; Niggemann, M.; Schwinger, W.; Schaeffler, F.; Hinsch, A.; Lux-Steiner, M. C.; Sariciftci, N. S. Efficiency Limiting Morphological Factors of MDMO-PPV:PCBM Plastic Solar Cells. *Thin Solid Films* **2006**, *511–512*, 587–592. <https://doi.org/10.1016/j.tsf.2005.12.071>.
- (44) Pavlopoulou, E.; Kim, C. S.; Lee, S. S.; Chen, Z.; Facchetti, A.; Toney, M. F.; Loo, Y. L. Tuning the Morphology of All-Polymer OPVS through Altering Polymer-Solvent Interactions. *Chem. Mater.* **2014**, *26* (17), 5020–5027. <https://doi.org/10.1021/cm502112z>.
- (45) Troshin, P. A.; Hoppe, H.; Renz, J.; Egginger, M.; Mayorova, J. Y.; Goryachev, A. E.; Peregudov, A. S.; Lyubovskaya, R. N.; Gobsch, G.; Sariciftci, N. S.; et al. Material Solubility-Photovoltaic Performance Relationship in the Design of Novel Fullerene Derivatives for Bulk Heterojunction Solar Cells. *Adv. Funct. Mater.* **2009**, *19* (5), 779–788. <https://doi.org/10.1002/adfm.200801189>.
- (46) Honda, S.; Ohkita, H.; Benten, H.; Ito, S. Selective Dye Loading at the Heterojunction in Polymer/Fullerene Solar Cells. *Adv. Energy Mater.* **2011**, *1* (4), 588–598. <https://doi.org/10.1002/aenm.201100094>.
- (47) Honda, S.; Yokoya, S.; Ohkita, H.; Benten, H.; Ito, S. Light-Harvesting Mechanism in Polymer/Fullerene/Dye Ternary Blends Studied by Transient Absorption Spectroscopy. *J. Phys. Chem. C* **2011**, *115* (22), 11306–11317. <https://doi.org/10.1021/jp201742v>.
- (48) Yang, X.; Loos, J.; Veenstra, S. C.; Verhees, W. J. H.; Wienk, M. M.; Kroon, J. M.; Michels, M. A. J.; Janssen, R. A. J. Nanoscale Morphology of High-Performance Polymer Solar Cells. *Nano Lett.* **2005**, *5* (4), 579–583. <https://doi.org/10.1021/nl048120i>.
- (49) Zommerman, D.; Kong, J.; McAfee, S. M.; Welch, G. C.; Kelly, T. L. Control and Characterization of Organic Solar Cell Morphology Through Variable-Pressure Solvent Vapor Annealing. *ACS Appl. Energy Mater.* **2018**, *1* (10), 5663–5674. <https://doi.org/10.1021/acsaem.8b01214>.
- (50) Ferreira, A. S.; Aguirre, J. C.; Subramanian, S.; Jenekhe, S. A.; Tolbert, S. H.; Schwartz, B. J. Understanding How Polymer Properties Control OPV Device Performance: Regioregularity, Swelling, and Morphology Optimization Using Random Poly(3-Butylthiophene-Co-3-Octylthiophene) Polymers. *J. Phys. Chem. C* **2016**, *120* (39), 22115–22125. <https://doi.org/10.1021/acs.jpcc.6b03300>.
- (51) Lyons, B. P.; Clarke, N.; Groves, C. The Relative Importance of Domain Size, Domain Purity and Domain Interfaces to the Performance of Bulk-Heterojunction Organic Photovoltaics. *Energy Environ. Sci.* **2012**, *5* (6), 7657–7663. <https://doi.org/10.1039/c2ee21327c>.
- (52) MacHui, F.; Langner, S.; Zhu, X.; Abbott, S.; Brabec, C. J. Determination of the P3HT:PCBM Solubility Parameters via a Binary Solvent Gradient Method: Impact of Solubility on the Photovoltaic Performance. *Sol. Energy Mater. Sol. Cells* **2012**, *100*, 138–146. <https://doi.org/10.1016/j.solmat.2012.01.005>.
- (53) MacHui, F.; Abbott, S.; Waller, D.; Koppe, M.; Brabec, C. J. Determination of Solubility Parameters for Organic Semiconductor Formulations. *Macromol. Chem. Phys.* **2011**, *212* (19), 2159–2165. <https://doi.org/10.1002/macp.201100284>.

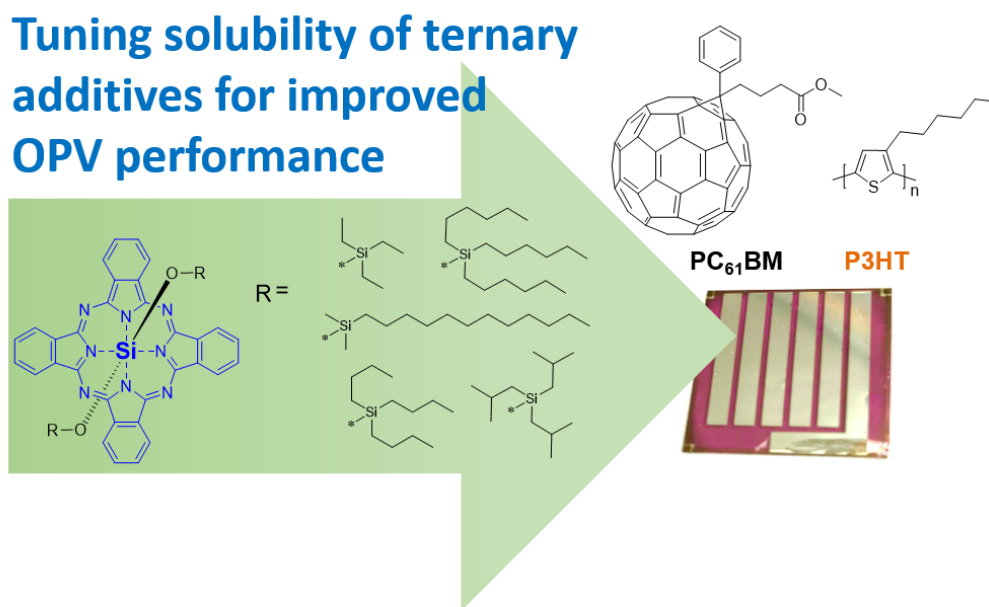
- (54) Reynolds, J. R.; Thompson, B. C.; Skotheim, T. A.; Langner, S.; Perea Ospina, J. D.; Zhang, C.; Li, N.; J. Brabec, C. The Relevance of Solubility and Miscibility for the Performance of Organic Solar Cells. *Conjug. Polym.* **2019**, 485–514. <https://doi.org/10.1201/9780429190520-15>.
- (55) Vezie, M. S.; Few, S.; Meager, I.; Pieridou, G.; Dörling, B.; Ashraf, R. S.; Goñi, A. R.; Bronstein, H.; McCulloch, I.; Hayes, S. C.; et al. Exploring the Origin of High Optical Absorption in Conjugated Polymers. *Nat. Mater.* **2016**, 15 (7), 746–753. <https://doi.org/10.1038/nmat4645>.
- (56) Ma, Y.; Zhang, M.; Wan, S.; Yin, P.; Wang, P.; Cai, D.; Liu, F.; Zheng, Q. Efficient Organic Solar Cells from Molecular Orientation Control of M-Series Acceptors. *Joule* **2021**, 5 (1), 197–209. <https://doi.org/10.1016/j.joule.2020.11.006>.
- (57) Doumon, N. Y.; Houard, F. V.; Dong, J.; Yao, H.; Portale, G.; Hou, J.; Koster, L. J. A. Energy Level Modulation of ITIC Derivatives: Effects on the Photodegradation of Conventional and Inverted Organic Solar Cells. *Org. Electron.* **2019**, 69 (February), 255–262. <https://doi.org/10.1016/j.orgel.2019.03.037>.
- (58) Firdaus, Y.; Le Corre, V. M.; Karuthedath, S.; Liu, W.; Markina, A.; Huang, W.; Chattopadhyay, S.; Nahid, M. M.; Nugraha, M. I.; Lin, Y.; et al. Long-Range Exciton Diffusion in Molecular Non-Fullerene Acceptors. *Nat. Commun.* **2020**, 11 (1). <https://doi.org/10.1038/s41467-020-19029-9>.
- (59) Li, N.; Brabec, C. J. Air-Processed Polymer Tandem Solar Cells with Power Conversion Efficiency Exceeding 10%. *Energy Environ. Sci.* **2015**, 8 (10), 2902–2909. <https://doi.org/10.1039/c5ee02145f>.
- (60) Zhao, J.; Li, Y.; Hunt, A.; Zhang, J.; Yao, H.; Li, Z.; Zhang, J.; Huang, F.; Ade, H.; Yan, H. A Difluorobenzoxadiazole Building Block for Efficient Polymer Solar Cells. *Adv. Mater.* **2016**, 28 (9), 1868–1873. <https://doi.org/10.1002/adma.201504611>.
- (61) Hwang, Y. J.; Li, H.; Courtright, B. A. E.; Subramaniyan, S.; Jenekhe, S. A. Nonfullerene Polymer Solar Cells with 8.5% Efficiency Enabled by a New Highly Twisted Electron Acceptor Dimer. *Adv. Mater.* **2016**, 28 (1), 124–131. <https://doi.org/10.1002/adma.201503801>.
- (62) Zhang, J.; Zhang, Y.; Fang, J.; Lu, K.; Wang, Z.; Ma, W.; Wei, Z. Conjugated Polymer-Small Molecule Alloy Leads to High Efficient Ternary Organic Solar Cells. *J. Am. Chem. Soc.* **2015**, 137 (25), 8176–8183. <https://doi.org/10.1021/jacs.5b03449>.
- (63) Yang Michael, Y.; Chen, W.; Dou, L.; Chang, W. H.; Duan, H. S.; Bob, B.; Li, G.; Yang, Y. High-Performance Multiple-Donor Bulk Heterojunction Solar Cells. *Nat. Photonics* **2015**, 9 (3), 190–198. <https://doi.org/10.1038/nphoton.2015.9>.
- (64) Po, R.; Bianchi, G.; Carbonera, C.; Pellegrino, A. “all That Glisters Is Not Gold”: An Analysis of the Synthetic Complexity of Efficient Polymer Donors for Polymer Solar Cells. *Macromolecules* **2015**, 48 (3), 453–461. <https://doi.org/10.1021/ma501894w>.
- (65) Cui, Y.; Yao, H.; Zhang, J.; Zhang, T.; Wang, Y.; Hong, L.; Xian, K.; Xu, B.; Zhang, S.; Peng, J.; et al. Over 16% Efficiency Organic Photovoltaic Cells Enabled by a Chlorinated Acceptor with Increased Open-Circuit Voltages. *Nat. Commun.* **2019**, 10 (1), 1–8. <https://doi.org/10.1038/s41467-019-10351-5>.
- (66) Yuan, J.; Zhang, Y.; Yuan, J.; Zhang, Y.; Zhou, L.; Zhang, G.; Yip, H.; Lau, T.; Lu, X. Single-Junction Organic Solar Cell with over 15 % Efficiency Using Fused-Ring Acceptor with Electron-Deficient Core Single-Junction Organic Solar Cell with over 15 % Efficiency Using Fused-Ring Acceptor with Electron-Deficient Core. *Joule* **2019**, 3, 1–12. <https://doi.org/10.1016/j.joule.2019.01.004>.
- (67) Grant, T. Molecular Engineering of Group 14 Phthalocyanines and Their Role in Organic Photovoltaic Devices, 2021.

- (68) Claessens, C. G.; Hahn, U.; Torres, T. Phthalocyanines: From Outstanding Electronic Properties to Emerging Applications. *Chem. Rec.* **2008**, *8* (2), 75–97. <https://doi.org/10.1002/tcr.20139>.
- (69) Lessard, B. H.; White, R. T.; Al-Amar, M.; Plint, T.; Castrucci, J. S.; Josey, D. S.; Lu, Z. H.; Bender, T. P. Assessing the Potential Roles of Silicon and Germanium Phthalocyanines in Planar Heterojunction Organic Photovoltaic Devices and How Pentafluoro Phenoxylation Can Enhance π - π Interactions and Device Performance. *ACS Appl. Mater. Interfaces* **2015**, *7* (9), 5076–5088. <https://doi.org/10.1021/am508491v>.
- (70) Yuen, A. P.; Jovanovic, S. M.; Hor, A. M.; Klenkler, R. A.; Devenyi, G. A.; Loutfy, R. O.; Preston, J. S. Photovoltaic Properties of M-Phthalocyanine/Fullerene Organic Solar Cells. *Sol. Energy* **2012**, *86* (6), 1683–1688. <https://doi.org/10.1016/j.solener.2012.03.019>.
- (71) Dang, M.-T.; Grant, T. M.; Yan, H.; Seferos, D. S.; Lessard, B. H.; Bender, T. P.; Miller, J. a.; Goethem, E. M. Van; Kenney, M. E.; Lu, Z.-H. Bis(Tri-n-Alkylsilyl Oxide) Silicon Phthalocyanines: A Start to Establishing a Structure Property Relationship as Both Ternary Additives and Non-Fullerene Electron Acceptors in Bulk Heterojunction Organic Photovoltaic Devices. *J. Mater. Chem. A* **2017**, *126*, 3378–3379. <https://doi.org/10.1039/C6TA10739G>.
- (72) Grant, T. M.; Gorisse, T.; Dautel, O.; Wantz, G.; Lessard, B. H. Multifunctional Ternary Additive in Bulk Heterojunction OPV: Increased Device Performance and Stability. *J. Mater. Chem. A* **2017**, *5* (4), 1581–1587. <https://doi.org/10.1039/C6TA08593H>.
- (73) Grant, T. M.; Rice, N. A.; Muccioli, L.; Castet, F.; Lessard, B. H. Solution-Processable n-Type Tin Phthalocyanines in Organic Thin Film Transistors and as Ternary Additives in Organic Photovoltaics. *ACS Appl. Electron. Mater.* **2019**, *1* (4), 494–504. <https://doi.org/10.1021/acsaelm.8b00113>.
- (74) Zysman-Colman, E.; Ghosh, S. S.; Xie, G.; Varghese, S.; Chowdhury, M.; Sharma, N.; Cordes, D. B.; Slawin, A. M. Z.; Samuel, I. D. W. Solution-Processable Silicon Phthalocyanines in Electroluminescent and Photovoltaic Devices. *ACS Appl. Mater. Interfaces* **2016**, *8* (14), 9247–9253. <https://doi.org/10.1021/acsami.5b12408>.
- (75) Pearson, A. J.; Plint, T.; Jones, S. T. E.; Lessard, B. H.; Credgington, D.; Bender, T. P.; Greenham, N. C. Silicon Phthalocyanines as Dopant Red Emitters for Efficient Solution Processed OLEDs. *J. Mater. Chem. C* **2017**, *5* (48), 12688–12698. <https://doi.org/10.1039/c7tc03946h>.
- (76) Plint, T.; Lessard, B. H.; Bender, T. P. Assessing the Potential of Group 13 and 14 Metal/Metalloid Phthalocyanines as Hole Transport Layers in Organic Light Emitting Diodes. *J. Appl. Phys.* **2016**, *119* (14), 1455021–1455029. <https://doi.org/10.1063/1.4945377>.
- (77) Melville, O. A.; Lessard, B. H.; Bender, T. P. Phthalocyanine-Based Organic Thin-Film Transistors: A Review of Recent Advances. *ACS Appl. Mater. Interfaces* **2015**, *7* (24), 13105–13118. <https://doi.org/10.1021/acsami.5b01718>.
- (78) Melville, O. A.; Grant, T. M.; Mirka, B.; Boileau, N. T.; Park, J.; Lessard, B. H. Ambipolarity and Air Stability of Silicon Phthalocyanine Organic Thin-Film Transistors. *Adv. Electron. Mater.* **2019**, *5* (1900087), 1–7. <https://doi.org/10.1002/aelm.201900087>.
- (79) Melville, O. A.; Grant, T. M.; Lessard, B. H. Silicon Phthalocyanines as N-Type Semiconductors in Organic Thin Film Transistors. *J. Mater. Chem. C* **2018**, *6* (20), 5482–5488. <https://doi.org/10.1039/c8tc01116h>.
- (80) Yutronkie, N. J.; Grant, T. M.; Melville, O. A.; Lessard, B. H.; Brusso, J. L. Old Molecule, New Chemistry: Exploring Silicon Phthalocyanines as Emerging N-Type Materials in Organic Electronics. *Materials (Basel)*. **2019**, *12* (8), 5–10. <https://doi.org/10.3390/ma12081334>.

- (81) Grant, T. M.; Rice, N. A.; Muccioli, L.; Castet, F.; Lessard, B. H. Solution-Processable n-Type Tin Phthalocyanines in Organic Thin Film Transistors and as Ternary Additives in Organic Photovoltaics. *ACS Appl. Electron. Mater.* **2019**, *1* (4), 494–504. <https://doi.org/10.1021/acsaelm.8b00113>.
- (82) Honda, S.; Ohkita, H.; Benten, H.; Ito, S. Multi-Colored Dye Sensitization of Polymer/Fullerene Bulk Heterojunction Solar Cells. *Chem. Commun.* **2010**, *46* (35), 6596–6598. <https://doi.org/10.1039/c0cc01787f>.
- (83) Honda, S.; Nogami, T.; Ohkita, H.; Benten, H.; Ito, S. Improvement of the Light-Harvesting Efficiency in Polymer/Fullerene Bulk Heterojunction Solar Cells by Interfacial Dye Modification. *ACS Appl. Mater. Interfaces* **2009**, *1* (4), 804–810. <https://doi.org/10.1021/am800229p>.
- (84) Lim, B.; Bloking, J. T.; Ponec, A.; McGehee, M. D.; Sellinger, A. Ternary Bulk Heterojunction Solar Cells: Addition of Soluble NIR Dyes for Photocurrent Generation beyond 800 Nm. *ACS Appl. Mater. Interfaces* **2014**, *6* (9), 6905–6913. <https://doi.org/10.1021/am5007172>.
- (85) Ke, L.; Min, J.; Adam, M.; Gasparini, N.; Hou, Y.; Perea, J. D.; Chen, W.; Zhang, H.; Fladischer, S.; Sale, A.-C.; et al. A Series of Pyrene-Substituted Silicon Phthalocyanines as Near-IR Sensitizers in Organic Ternary Solar Cells. *Adv. Energy Mater.* **2016**, *6* (7), 1502355. <https://doi.org/10.1002/aenm.201502355>.
- (86) Grant, T. M.; Dindault, C.; Rice, N. A.; Swaraj, S.; Lessard, B. H. Synthetically Facile Organic Solar Cells with >4% Efficiency Using P3HT and a Silicon Phthalocyanine Non-Fullerene Acceptor. *Mater. Adv.* **2021**. <https://doi.org/10.1039/d1ma00165e>.
- (87) Kim, D. Y.; Sarasqueta, G.; So, F. SnPc:C60 Bulk Heterojunction Organic Photovoltaic Cells with MoO₃ Interlayer. *Sol. Energy Mater. Sol. Cells* **2009**, *93* (8), 1452–1456. <https://doi.org/10.1016/j.solmat.2009.03.011>.
- (88) Lin, W. K.; Su, S. H.; Ma, C. K.; Yokoyama, M. Enhancing Conversion Efficiency of Inverted Organic Solar Cells Using Ag Nanoparticles and Long Wavelength Absorbing Tin (II) Phthalocyanine. *Org. Electron.* **2016**, *29*, 94–98. <https://doi.org/10.1016/j.orgel.2015.11.030>.
- (89) Rand, B. P.; Xue, J.; Yang, F.; Forrest, S. R. Organic Solar Cells with Sensitivity Extending into the near Infrared. *Appl. Phys. Lett.* **2005**, *87* (23), 1–3. <https://doi.org/10.1063/1.2140075>.
- (90) Yang, F.; Lunt, R. R.; Forrest, S. R. Simultaneous Heterojunction Organic Solar Cells with Broad Spectral Sensitivity. *Appl. Phys. Lett.* **2008**, *92* (5), 10–13. <https://doi.org/10.1063/1.2839408>.
- (91) Song, D.; Wang, H.; Zhu, F.; Yang, J.; Tian, H.; Geng, Y.; Yan, D. Phthalocyanato Tin(IV) Dichloride: An Air-Stable, High-Performance, n-Type Organic Semiconductor with a High Field-Effect Electron Mobility. *Adv. Mater.* **2008**, *20* (11), 2142–2144. <https://doi.org/10.1002/adma.200702439>.
- (92) Song, D.; Zhu, F.; Yu, B.; Huang, L.; Geng, Y.; Yan, D. Tin (IV) Phthalocyanine Oxide: An Air-Stable Semiconductor with High Electron Mobility. *Appl. Phys. Lett.* **2008**, *92* (14), 2–5. <https://doi.org/10.1063/1.2903486>.
- (93) Vebber, MC; Grant, TM; Brusso, JL; Lessard, BH. Bis(trialkylsilyl oxide) Silicon Phthalocyanines: Understanding the Role of Solubility in Device Performance as Ternary Additives in Organic Photovoltaics. *Langmuir* **2020**, *36*, 10, 2612–2621. <https://doi.org/10.1021/acs.langmuir.9b03772>.
- (94) Bloking, J. T.; Giovenzana, T.; Higgs, A. T.; Ponec, A. J.; Hoke, E. T.; Vandewal, K.; Ko, S.; Bao, Z.; Sellinger, A.; McGehee, M. D. Comparing the Device Physics and Morphology of Polymer Solar Cells Employing Fullerenes and Non-Fullerene Acceptors. *Adv. Energy Mater.* **2014**, *4* (12), 1–12. <https://doi.org/10.1002/aenm.201301426>.
- (95) Distler, A.; Sauermann, T.; Egelhaaf, H. J.; Rodman, S.; Waller, D.; Cheon, K. S.; Lee, M.; Guldi, D. M. The Effect of PCBM Dimerization on the Performance of Bulk Heterojunction Solar Cells. *Adv. Energy Mater.* **2014**, *4* (1), 1–6. <https://doi.org/10.1002/aenm.201300693>.

- (96) Yan, C.; Barlow, S.; Wang, Z.; Yan, H.; Jen, A. K.; Marder, S. R.; Zhan, X. Non-Fullerene Acceptors for Organic Solar Cells. *Nat. Publ. Gr.* **2018**, *3*, 1–19. <https://doi.org/10.1038/natrevmats.2018.3>.
- (97) Jinnai, S.; Ie, Y.; Karakawa, M.; Aernouts, T.; Nakajima, Y.; Mori, S.; Aso, Y. Electron-Accepting π -Conjugated Systems for Organic Photovoltaics: Influence of Structural Modification on Molecular Orientation at Donor-Acceptor Interfaces. *Chem. Mater.* **2016**, *28* (6), 1705–1713. <https://doi.org/10.1021/acs.chemmater.5b04551>.
- (98) Su, G. M.; Pho, T. V.; Eisenmenger, N. D.; Wang, C.; Wudl, F.; Kramer, E. J.; Chabynyc, M. L. Linking Morphology and Performance of Organic Solar Cells Based on Decacyclene Triimide Acceptors. *J. Mater. Chem. A* **2014**, *2* (6), 1781–1789. <https://doi.org/10.1039/c3ta14839d>.
- (99) Faure, M. D. M.; Grant, T. M.; Lessard, B. H. Silicon Phthalocyanines as Acceptor Candidates in Mixed Solution/Evaporation Processed Planar Heterojunction Organic Photovoltaic Devices. *Coatings* **2019**, *9* (3). <https://doi.org/10.3390/COATINGS9030203>.
- (100) Anctil, A.; Babbitt, C. W.; Raffaele, R. P.; Landi, B. J. Cumulative Energy Demand for Small Molecule and Polymer Photovoltaics. *Prog. Photovoltaics Res. Appl.* **2012**, *21*, 1541–1554. <https://doi.org/10.1002/pip>.
- (101) Anctil, A.; Babbitt, C. W.; Raffaele, R. P.; Landi, B. J. Material and Energy Intensity of Fullerene Production. *Environ. Sci. Technol.* **2011**, *45* (6), 2353–2359. <https://doi.org/10.1021/es103860a>.
- (102) Wannebroucq, A.; Meunier-Prest, R.; Chambron, J. C.; Brachais, C. H.; Suisse, J. M.; Bouvet, M. Synthesis and Characterization of Fluorophthalocyanines Bearing Four 2-(2-Thienyl)Ethoxy Moieties: From the Optimization of the Fluorine Substitution to Chemosensing. *RSC Adv.* **2017**, *7* (65), 41272–41281. <https://doi.org/10.1039/c7ra05325h>.
- (103) Chen, W.; Qi, D. C.; Huang, Y. L.; Huang, H.; Wang, Y. Z.; Chen, S.; Gao, X. Y.; Wee, A. T. S. Molecular Orientation Dependent Energy Level Alignment at Organic-Organic Heterojunction Interfaces. *J. Phys. Chem. C* **2009**, *113* (29), 12832–12839. <https://doi.org/10.1021/jp903139q>.
- (104) Marks, T. J. N-Channel Semiconductor Materials Design for Organic Complementary Circuits. **2011**, *44* (7), 501–510. <https://doi.org/10.1021/ar200006r>.
- (105) Grant, T. M.; McIntyre, V.; Vestfrid, J.; Raboui, H.; White, R. T.; Lu, Z. H.; Lessard, B. H.; Bender, T. P. Straightforward and Relatively Safe Process for the Fluoride Exchange of Trivalent and Tetravalent Group 13 and 14 Phthalocyanines. *ACS Omega* **2019**, *4* (3), 5317–5326. <https://doi.org/10.1021/acsomega.8b03202>.
- (106) Katz, H. E.; Johnson, J.; Lovinger, A. J.; Li, W. Naphthalenetetracarboxylic Diimide-Based n-Channel Transistor Semiconductors: Structural Variation and Thiol-Enhanced Gold Contacts. *J. Am. Chem. Soc.* **2000**, *122* (32), 7787–7792. <https://doi.org/10.1021/ja000870g>.
- (107) Shao, X.; Wang, S.; Li, X.; Su, Z.; Chen, Y.; Xiao, Y. Single Component P-, Ambipolar and n-Type OTFTs Based on Fluorinated Copper Phthalocyanines. *Dye. Pigment.* **2016**, *132*, 378–386. <https://doi.org/10.1016/j.dyepig.2016.05.020>.
- (108) Yang, J. L.; Schumann, S.; Hatton, R. A.; Jones, T. S. Copper Hexadecafluorophthalocyanine (F16CuPc) as an Electron Accepting Material in Bilayer Small Molecule Organic Photovoltaic Cells. *Org. Electron.* **2010**, *11* (8), 1399–1402. <https://doi.org/10.1016/j.orgel.2010.06.004>.
- (109) Sakamoto, K.; Ohno-Okumura, E. Syntheses and Functional Properties of Phthalocyanines. *Materials (Basel)*. **2009**, *2* (3), 1127–1179. <https://doi.org/10.3390/ma2031127>.

2. UNDERSTANDING THE ROLE OF SILICON PHTHALOCYANINE SOLUBILITY IN DEVICE PERFORMANCE AS TERNARY ADDITIVES IN ORGANIC PHOTOVOLTAICS



This chapter contains work published in *Langmuir*.

Mário C. Vebber, Trevor M. Grant, Jaclyn L. Brusso, and Benoît H. Lessard. *Langmuir* 2020, 36, 10, 2612–2621.

2.1 Context

The two available axial positions in SiPcs allow for easy functionalization of the silicon core, leading to molecules with tuned properties. While it is customary in literature to report fine-tuning of electrochemical properties, the control of solid-state structure and physical properties is relatively understudied. In the first part of my thesis, I synthesized and characterized eight different axially substituted silicon phthalocyanines and each compound differed from the other exclusively by the size of the alkyl chains connected to the axial silanes. This change should have a significant effect on physical properties in solid-state, while keeping the optical and electrochemical properties approximately constant, as they are mainly defined by the conjugated ring, which was unchanged in all compounds. If this hypothesis was correct, it should allow me to better isolate key properties, and their effect on how these compounds perform as ternary additives in organic photovoltaics (OPVs). I aimed to find correlations between the properties of the compounds and

the OPV metrics when employed as a ternary additive in P3HT/PC₆₀BM BHJs, because robust design rules for BHJ OPVs are still relatively scarce. Solubility specifically stood out in the survey, with a significant correlation that tied to known properties of the BHJ.

2.2 Contribution

I carried out the synthetic procedures and purification techniques required to obtain the final compounds, as well as the characterizations reported in this paper. I also produced all the OPV devices with the guidance of TG. Manuscript was also written by me with contributions from TG, BL and JB. BL and JB supervised the project.

2.3 Abstract

The use of ternary additives in organic photovoltaics (OPV) is a promising route to improve overall device performance. Silicon phthalocyanines (SiPcs) are ideal candidates due to their absorption profile, low cost and ease of synthesis and chemical tunability. However, to date only a few examples have been reported and specific strategies to help design improved ternary additives have not been established. In this study, we report a relationship between ternary additive solubility and device performance, demonstrating that device performance is maximized when the SiPc additive solubility is similar to that of the donor polymer (P3HT, in this case). This improved performance can be attributed to the favored interfacial precipitation of the SiPcs when its solubility matches that of the other components of the thin film. The power conversion efficiency (PCE) varied from 2.4% to 3.4% by using axially substituted SiPcs with different solubilities, where the best ternary additive led to a 25% increase in PCE compared to the baseline device.

2.4 Introduction

Organic photovoltaics (OPVs) are an emerging solar energy technology, presenting a number of advantages over their inorganic counterparts, such as low manufacturing cost, ease of integration onto flexible substrates, mechanical robustness and recyclability.¹⁻⁴ Recently, single-junction OPVs, on a laboratory scale, achieved record power conversion efficiency (PCE) between 15-17%.^{5,6} As OPV performance continues to rise and with the promise of high throughput manufacturing, it is predicted that their price will plunge below that of conventional inorganic cells.⁷

One of the main challenges with bulk heterojunction (BHJ) OPVs is to maximize light harvesting across the visible and near-infrared regions of the solar spectrum as most organic compounds tend to demonstrate a relatively narrow absorption band in the visible spectrum.^{8,9} The addition of a photosensitizing ternary additive to the donor/acceptor blend is a straightforward approach to increase the overall absorption of the active layer. Secondary functionality of these additives can also be achieved such as enhancement of the film microstructure,^{10,11} favoring phase separation in the nanoscale, and compatibilization of energy levels between donor and acceptor,¹² which can increase charge separation and even enhance device stability, through the use of crosslinking groups.^{13,14}

One class of materials that has been widely used for application in electronic devices are metal/metalloid containing phthalocyanines (MPcs). While divalent MPcs (Zn, Cu, etc) are widely reported in the literature as active materials, tetravalent MPcs are less studied. Tetravalent MPcs, such as silicon phthalocyanines (SiPcs), have two axial bonds available for chemical modification, imparting broader chemical versatility and facilitating the tuning of electronic and physical properties.^{15–18} MPcs have also demonstrated the ability to act as non-fullerene electron acceptors in bulk heterojunction (BHJ) OPVs.¹⁸ Furthermore, these dyes have found application as commercial photoreceptors for almost 50 years and, prior to that, as a commercial pigment.¹⁵ The chemistry and purification of MPcs is relatively simple and straightforward compared to conventional organic semiconductors, making them desirable candidates for commercially viable OPV devices.^{15–18} SiPcs have a high molar extinction coefficient and absorb light in the near infrared region, complimenting well-established donor/acceptor pairs, such as poly-3-hexylthiophene (P3HT) and phenyl-C₆₁-butyric-acid-methyl-ester (PCBM), that often show poor performance in that region of the solar spectrum.^{13,18,19}

Honda *et al.* first reported the use of bis(trihexyl)silyl oxide SiPc as an additive in a P3HT/PC₆₁BM BHJ OPV and obtained a 50% increase in current density (J_{sc}).^{20,21} The same group also found that the SiPc derivative had a high performance as an additive in OPVs due to their tendency to migrate to the donor-acceptor interface, where they improve charge collection and charge transfer between the donor and the acceptor.²² Silicon naphthalocyanines (SiNcs) have also been applied in OPVs, with similar increases in J_{sc} , by harvesting near infra-red light.²³ Alternatively, Ke *et al.* functionalized SiPcs with pyrenes in the axial position, resulting in effective ternary additives with increased absorption range, which were reported to increase J_{sc}

by 20% and PCE by 50%.²⁴ It has been demonstrated that the absorption coverage can be further improved by a combination of different SiPcs and SiNcs as ternary and quaternary additives.^{20,25} Moreover, SiPc derivatives have also been applied in light-emitting diodes (OLEDs)^{26–28} and in organic thin film transistors (OTFTs).^{29–33}

While most reports focus on energy level tuning of ternary additive materials, less attention is given to the role of other physical properties, such as solubility and crystal structure.^{6,34} In the case of SiPcs, it has been shown that axial functionalization has little to no effect on the frontier orbital energy levels or optical properties; however, it does lead to significant effects in molecular packing.^{16,35}

The solubility of active materials is often analyzed in the search for greener solvents, yet studies focused on the relationship between solubility and the performance of the resulting devices are surprisingly scarce, especially given the interest in solution processable OPVs.^{36,37} Troshin *et al.* have demonstrated that the solubility of fullerene acceptors significantly impacts the PCE of P3HT/fullerene devices, and that best performance is achieved when the solubility of the fullerene acceptor is close to that of P3HT, leading to favorable nanomorphology.³⁸ However, no similar studies have been performed on ternary additives. To that end, we present herein the synthesis and characterization of nine different SiPcs functionalized with a range of axial silanes, and their employment as additives in P3HT/PC₆₁BM BHJ OPVs. This study demonstrates that a small change in structure has a significant effect on the solubility and, ultimately, the performance of the resulting ternary BHJ/OPV devices. This investigation therefore represents the first report that facilitates the establishment of new design rules for ternary additives.

2.5 Experimental Section

2.5.1 Materials

N-butyldimethylchlorosilane (>95%), hexyldimethylchlorosilane (>95%), n-octyldimethylchlorosilane (>95%), n-dodecyldimethylchlorosilane (>95%), tri-n-ethylchlorosilane (>95%), tri-n-butylchlorosilane (>95%), tri-n-hexylchlorosilane (>95%) and n-octyldiisopropylchlorosilane (>95%) were purchased from Gelest and used as received. P3HT (MW = 75 kDa, 96% regioregular) was purchased from Rieke Metals and PC₆₁BM from Nano-C, respectively. All solvents were purchased from commercial suppliers and used without further

purification. Dichlorosilicon phthalocyanine ($\text{Cl}_2\text{-SiPc}$)³⁹ was synthesized according to reported procedures in the literature.

2.5.2 Synthesis of silicon phthalocyanine ternary additives

The general synthetic procedure for SiPc axial functionalization was performed as follows:⁴⁰ $\text{Cl}_2\text{-SiPc}$ (1.6 mmol), sodium hydroxide (8.6 mmol), trialkylchlorosilane (6 mmol), Aliquat HTA-1 (0.015 g) and chlorobenzene (10 ml) were added to a 100 ml flask and were stirred under reflux (132 °C). After 1 h, additional trialkylchlorosilane (1.9 mmol) was added to the reaction medium, which was left stirring at reflux for another hour. At this point, additional sodium hydroxide (3.4 mmol) and trialkylchlorosilane (1.9 mmol) were added to the mixture and refluxed for further 4 h before removing from heat. The dark-blue solution was then filtered to remove a purple residue, and the solvent was removed under reduced pressure. Methanol was added to the resulting residue affording the desired product, which was isolated upon filtration, washed with methanol and dried in a vacuum oven. Purification was carried out by train sublimation (180 °C to 250 °C, 130 mTorr) before their application in OPVs. Using this procedure, the soluble $(\text{R}_3\text{SiO})_2\text{-SiPc}$ derivatives shown in **Figure 2.1** were produced:

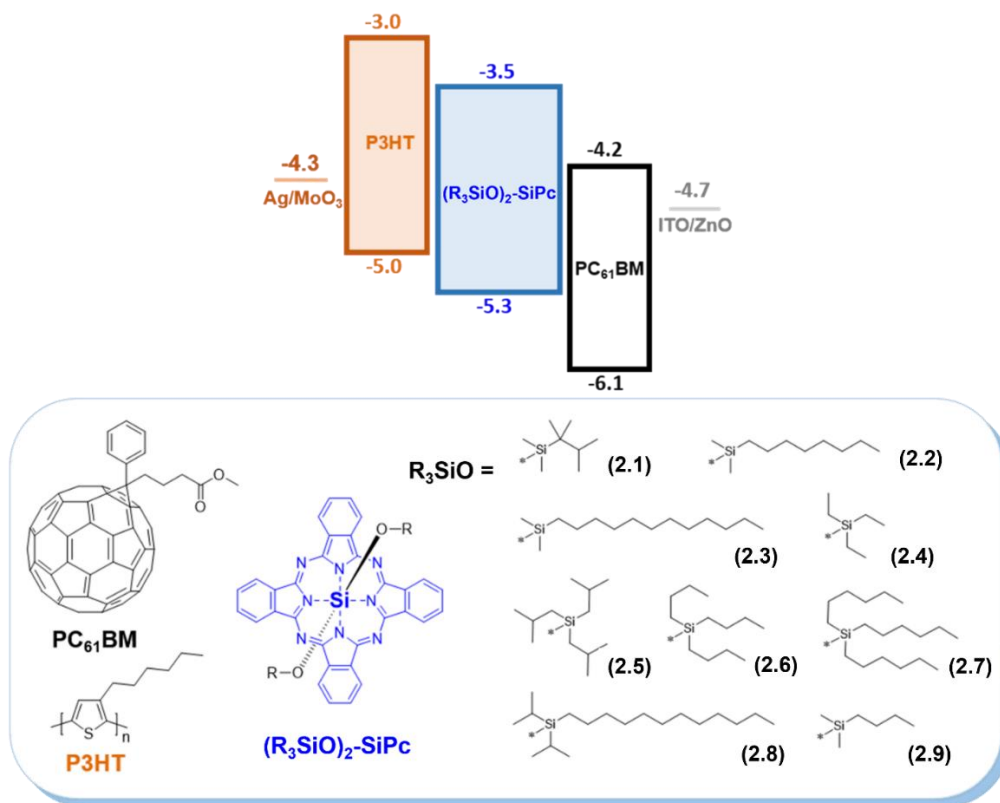


Figure 2.1. Axially substituted $(\text{R}_3\text{SiO})_2\text{-SiPc}$ synthesized and characterized in the present study.

(2.1) *Bis(thexyldimethylsilyl oxide) silicon phthalocyanine*: ^1H NMR 9.60 – 9.66 (m, 8 H), 8.28 – 8.34 (m, 8H), -0.95 – -1.0 (m, 2 H), -1.0 – -1.05 (d, 12 H) and -1.52 – -1.44 ppm (s, 12 H). ^{13}C NMR 148 , 136 , 130 , 123 (Aromatic); 32 , 22 , 17 , 16 and -5 ppm (Alkyl). MS (EI) expected mass: 858.37, obtained mass: 858.3. Yield: 0.45 g (30%).

(2.2) *Bis(n-octyldimethylsilyl oxide) silicon phthalocyanine*: ^1H NMR 9.60 – 9.66 (m, 8 H), 8.28 – 8.34 (m, 8H), 1.11 – 1.27 (m, 4 H), 0.92 – 1.04 (m, 4 H), 0.85 – 0.94 (t, 6H), 0.68 – 0.80 (m, 4H), 0.25 – 0.37 (m, 4H), -0.23 – -0.10 (m, 4H) and -1.17 – -1.04 ppm (m, 4H). ^{13}C NMR 148 , 136 , 130 , 123 (Aromatic); 32 (2), 29 , 23 , 21 , 15 , 14 n, -4 ppm (Alkyl). MS (EI) expected mass: 914.43, obtained mass: 914.4. Yield: 0.45 g (30%).

(2.3) *Bis(n-dodecyldimethylsilyl oxide) silicon phthalocyanine*: ^1H NMR 9.60 – 9.66 (m, 8 H), 8.28 – 8.34 (m, 8H), 1.20 – 1.39 (m, 20 H), 1.10 – 1.19 (m, 4 H), 0.95 – 1.02 (m, 4H), 0.88 – 0.95 (t, 6H), 0.64 – 0.73 (m, 4H), 0.19 – 0.31 (m, 4H), -0.29 – -0.18 (m, 4H) and -1.42 – -1.31 ppm (m, 4H). ^{13}C NMR 148 , 136 , 130 , 123 (Aromatic); 32 (2), 29 (5), 23 , 21 , 15 , 14 n, -4 ppm (Alkyl). MS (EI) expected mass: 1026.56, obtained mass: 1026.5. Yield: 0.50 g (28%).

(2.4) *Bis(tri-n-ethyl oxide) silicon phthalocyanine*: ^1H NMR 9.60 – 9.66 (m, 8 H), 8.28 – 8.34 (m, 8H) and -1.30 – -1.20 ppm (t, 12 H). ^{13}C NMR 148 , 136 , 130 , 123 (Aromatic); 5 and 3 ppm (Alkyl). MS (EI) expected mass: 802.31, obtained mass: 802.3. Yield: 0.28 g (20%).

(2.5) *Bis(triisobutylsilyl oxide) silicon phthalocyanine*: ^1H NMR 9.60 – 9.66 (m, 8 H), 8.28 – 8.34 (m, 8H), -0.58 – -0.50 (d, 12H) and -0.96 – -0.85 ppm (m, 2H). ^{13}C NMR 148 , 136 , 130 , 123 (Aromatic); 25 , 24 and 22 ppm (Alkyl). MS (EI) expected mass: 970.49, obtained mass: 970.5. Yield: 0.49 g (30%).

(2.6) *Bis(tri-n-butylsilyl oxide) silicon phthalocyanine*: ^1H NMR 9.60 – 9.66 (m, 8 H), 8.28 – 8.34 (m, 8H), -0.12 – 0.12 (m, 30H) and -1.36 – -1.22 ppm (m, 12H). Yield: 0.52g (30%). ^{13}C NMR and mass spec are published elsewhere. ¹⁸

(2.7) *Bis(tri-n-hexylsilyl oxide) silicon phthalocyanine*: ^1H NMR 9.60 – 9.66 (m, 8 H), 8.28 – 8.34 (m, 8H), 0.73 – 0.91 (m, 12H), 0.61 – 0.74 (t, 18H), 0.28 – 0.42 (m, 12H), -0.12 – 0.06 (m, 12H) and -1.38 – -1.22 ppm (m, 12H). Yield: 0.60g (31%). ^{13}C NMR and mass spec are published elsewhere. ⁴¹

(2.8) *Bis(diisopropyloctylsilyl oxide) silicon phthalocyanine*: ^1H NMR 9.60 – 9.66 (m, 8 H), 8.28 – 8.34 (m, 8H), 1.16 to 1.31 (m, 4H), 1.01 to 1.14 (m, 4 H), 0.77 to 0.95 (m, 8H), 0.33 to 0.45 (m, 4H), 0.05 to 0.22 (m, 4H), -1.05 to -0.90 (m, 4H) and -1.40 to -1.20 (m, 20H) and

-2.10 to -2.00 ppm (m, 2H). ^{13}C NMR 148, 136, 130, 123 (Aromatic); 33, 32, 29, 28, 22, 21, 15, 14, 11 and 10 ppm (Alkyl). MS (EI) expected mass: 1026.56, obtained mass: 1026.5. Yield: 0.28 g (17%).

(2.9) *Bis(n-butyl dimethyl oxide) silicon phthalocyanine*: No appreciable amount of this compound was obtained.

Mass obtained from MS was defined according to the fragment corresponding to the entire molecule.

2.5.3 Materials Characterizations

^1H NMR spectra were obtained on a Bruker Avance II spectrometer in CDCl_3 and operating frequency of 400 MHz. Molecular absorption spectra in the ultraviolet and visible regions (UV-Vis) were recorded on an Ocean Optics Flame spectrophotometer, using a DH-2000 light source and a quartz cuvette with a path length of 10 mm. Cyclic voltammograms were obtained using a VersaSTAT 3 potentiostat, a polished platinum disk as working electrode, a coiled platinum wire as counter electrode, and an Ag/AgCl electrode as reference. Three cycles from 0 V to 1.6 V were recorded at a scan rate of 0.1 V/s. Such experiments were carried out in dichloromethane (DCM) solutions with tetrabutylammonium perchlorate as the supporting electrolyte. Highest occupied molecular orbital (HOMO) energy levels were estimated according to the empirical correlation E_{HOMO} (eV) = $-(E_{\text{ox,onset}} - E_{\text{oxFc/Fc+,onset}}) - 4.80$ eV, where $E_{\text{ox,onset}}$ and $E_{\text{oxFc/Fc+,onset}}$ are the onset oxidation potentials of the sample and of the ferrocene standard, respectively. Solubility measurements were conducted by mixing 10, 20 or 40 mg of the axially substituted SiPcs in 0.15 ml of 1,2-dichlorobenzene and stirring the mixture for 1 h at 70°C, before allowing these mixtures to cool down to room temperature. The samples were then filtered through a 0.25 μm Teflon syringe filter and 100 μL samples of filtrate were collected, dried at 150°C under vacuum for 2 h and then weighted to calculate the solubility.

2.5.4 Device Preparation

The OPV devices were fabricated on indium tin oxide (ITO) coated glass slides (1 in x 1 in), which were cleaned in an ultrasonic bath with soapy water, deionized water, acetone then methanol, before being treated with air plasma for 15 min. 150 μL of a zinc solution constituted of zinc acetate (0.195 g), ethanolamine (0.055 ml) and ethanol (6 ml) was spincoated on the ITO

substrate at 2000 RPM for 1 min. These films were annealed at 180°C for 1 h, leading to the formation of the ZnO electron transport layer. The active layer solutions were prepared by dissolving P3HT and PC₆₁BM in DCB at a 1:0.8 ratio. Different amounts of (R₃SiO)₂-SiPc were added to the aforementioned mixture to form solutions with P3HT concentration of 20 mg ml⁻¹ and additive ratios of 2.7 wt %, 3.7 wt % and 4.8 wt %. These solutions were spincoated at 1000 RPM, for 35s inside a N₂ glovebox. The films were dried at room temperature, open to the glovebox atmosphere. Finally, the devices were moved into an evaporator chamber where MoO₃ (7 nm) and Ag (70 nm) films were evaporated at a pressure of 10⁻⁶ torr to make 5 devices per substrate, with areas of 0.32 cm², as defined by shadow masks. The device structure and its components' energy levels are depicted in **Figure 2.1**. Current density vs. voltage curves were obtained with a Keithley 2400 equipment, under 1000 W m⁻² illumination from an AM1.5 xenon lamp solar simulator, inside a glovebox. Devices were encapsulated using an optical adhesive (Norland NOA61), which was cured under an UV lamp (6 W), and a glass coverslip before EQE measurements in air, in a Newport Quantx-300 equipment.

2.6 Results and Discussion

2.6.1 Synthesis and Characterization of SiPcs

The (R₃SiO)₂-SiPc described here were all synthesized using the same experimental procedure, in which various trialkylchlorosilanes were used to afford the nine different derivatives outlined in **Figure 2.1**. The overall yields from diiminoisoindoline to axially substituted SiPcs varied from 20 to 40% by weight (see Experimental Section for details). The reactions affording the lowest yields were associated with low MW silanes, such as (2.4) and (2.9), which may be attributed to the preferential formation of siloxane (i.e., R–O–Si–O–R) byproducts. In fact, this reoccurring impurity may be present even after sublimation, which can be seen in the ¹H NMR spectrum as a strong singlet with a chemical shift of approximately 0.5 ppm (see Appendix A **Figure A1-A19** for NMR). Nonetheless, running the sublimation overnight or washing the solids with hexanes are both effective ways to remove this impurity. Unfortunately, no appreciable amounts of compound (2.9) were obtained due to the formation of this byproduct, which inhibited its incorporation into devices or further characterization. Nevertheless, this is a simple and

straightforward method to obtain various $(R_3SiO)_2$ -SiPc that does not require dry solvents or oxygen free environments.

2.6.2 UV-Vis Spectroscopy and Cyclic Voltammetry

The eight $(R_3SiO)_2$ -SiPc compounds were characterized optically and electrochemically to estimate their optical bandgap (E_g), highest occupied molecular orbital energy levels (E_{HOMO}) and lowest unoccupied molecular orbital energy levels, E_{LUMO} (**Table 2.1**). As expected, all SiPc derivatives have effectively the same energy levels and optical bandgap. The UV-Vis and CV spectra are presented in **Figure 2.2** except for compounds (2.6) and (2.7), which have been published elsewhere.¹⁸ These values are identical to our previously published bis(tri-n-hexylsilyl) SiPc and bis(tri-n-butylsilyl) SiPc derivatives (2.6 and 2.7, from **Figure 2.1**).¹⁸ For the current study these results indicate that the axial substituents have no effect on the absorption profiles, or frontier molecular orbitals, which is key when comparing their performance in OPVs with respect to their physical properties, such as solubility.

Table 2.1 Optical and electrochemical (CV) characterization of silicon phthalocyanine derivatives

Compound	λ_{max} ^a (nm)	E_{bg} ^a (nm)	E_{ox} ^b (V)	E_{HOMO} ^c (eV)	E_{LUMO} ^c (eV)
(2.1)	671	1.81	0.98	-5.31	-3.50
(2.2)	672	1.80	0.96	-5.29	-3.49
(2.3)	670	1.81	0.96	-5.29	-3.48
(2.4)	671	1.81	0.97	-5.30	-3.49
(2.5)	672	1.81	0.95	-5.28	-3.47
(2.6) ¹⁸	669	1.82	0.98	-5.31	-3.49
(2.7) ¹⁸	669	1.82	0.98	-5.31	-3.49
(2.8)	672	1.81	0.95	-5.28	-3.47

^a peak absorbance determined in DCM solution, E_{bg} = energy bandgap determined from the onset of UV-Vis absorption spectrum.

^b half wave potential of oxidation measured using an Ag/AgCl reference electrode and platinum rod working electrode in DCM solution. ^c E_{HOMO} = highest occupied molecular orbital energy level determined using the empirical correlation E_{HOMO} (eV) = $-(E_{ox,onset} - E_{ox}Fc/Fc+,onset) - 4.80$. Lowest unoccupied molecular orbital energy level calculated from $E_{LUMO} = E_{HOMO} + E_g$.

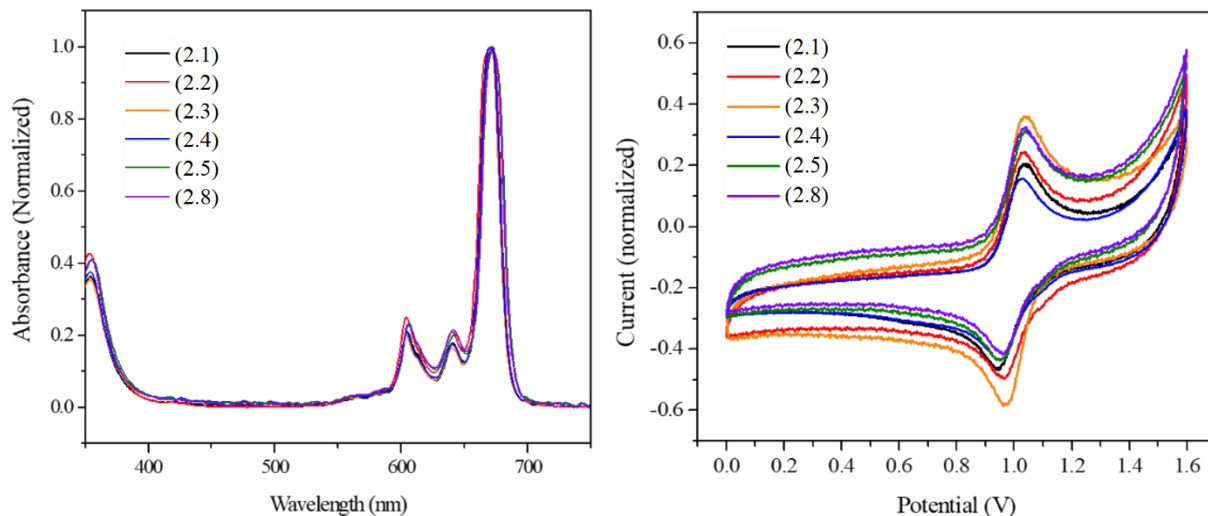


Figure 2.2. a) UV-Vis spectra of the $(R_3SiO)_2$ -SiPc and b) CV spectra and $(R_3SiO)_2$ -SiPc for HOMO level estimation.

2.6.3 Solubility

The solubility of P3HT, PC₆₁BM and all eight $(R_3SiO)_2$ -SiPc was determined in dichlorobenzene (see experimental section for details) and plotted in . It is clear that small changes in the alkylsilanes functional groups leads to a large difference in the solubility of the compounds, which varies from 8 to 190 mg mL⁻¹. It would appear that an increase in roughly one order of magnitude in solubility was observed for SiPc derivatives with alkyl chains going from 6 to 8 carbons (**Figure 2.3**). This type of significant increase in solubility has been observed in other small molecules such as fullerenes for example, where changing the alkyl solubilizing group from ethyl to butyl, increases the solubility from <1 mg mL⁻¹ to >70 mg mL⁻¹.³⁸ Unsubstituted SiPcs are very insoluble due to strong π - π intramolecular interactions. Since the SiPc radius (0.86 nm)¹⁵ is roughly equivalent to the length of a hexyl group (0.82 nm), one can hypothesize that alkyl groups longer than 6 carbons in the axial position will efficiently disrupt ring-ring interactions and cause the observed jump in solubility.

P3HT and PC₆₁BM were characterized to have a solubility of 100 and 140 mg mL⁻¹, respectively. It is important to note that the previously reported solubilities for PC₆₁BM and P3HT are within 50 to 80 mg mL⁻¹,³⁸ which are obtained by UV-Vis absorption spectroscopy. Nevertheless, all solubilities in this study were measured with the same procedure to ensure reliable comparisons can be made. These results further suggest that the changes in axial silane

groups on the SiPcs has little to no effect on optical, electrochemical or hydrophobicity properties but has a significant impact on the solubility.

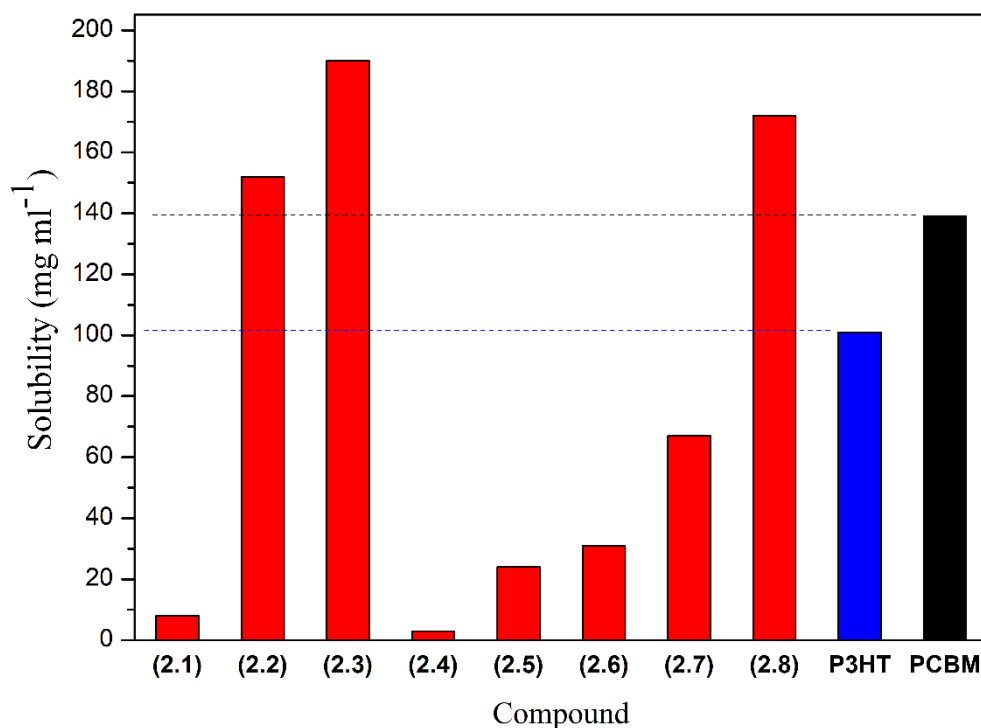


Figure 2.3. Solubility of different $(R_3SiO)_2$ -SiPcs, P3HT and PCBM in DCB.

2.6.4 Contact Angle

Contact angle measurements were carried out for $(R_3SiO)_2$ -SiPc, P3HT and PC₆₁BM films, spincoated on octyltrichlorosilane (OTS) treated glass slides and the surface energy was estimated using the iterative Neumann's method⁴². The results are shown in **Figure 2.4**. The $(R_3SiO)_2$ -SiPc films have intermediate surface energies to those of P3HT and PC₆₁BM. These results are in accordance with previous reports that found that $(R_3SiO)_2$ -SiPc compatibilize the surface energy of P3HT and PCBM and tend to migrate to the donor/acceptor interface¹². The measured surface energy was also very similar for all $(R_3SiO)_2$ -SiPc films (22.5 - 24.5 N mm⁻¹), which indicates that similar surface compatibilization effects can be expected when $(R_3SiO)_2$ -SiPc are added to P3HT/PC₆₁BM BHJ. Previously¹⁸ we have demonstrated via atomic force microscopy (AFM) that the addition of $(R_3SiO)_2$ -SiPc (at concentrations relevant to the current study), does not lead to significant changes in P3HT/PC₆₁BM BHJ morphology. The discrepancy observed for compound

(2.4) is attributed to bad film formation, resulting from its poor solubility (8 mg ml^{-1}) which led to nonhomogeneous films.

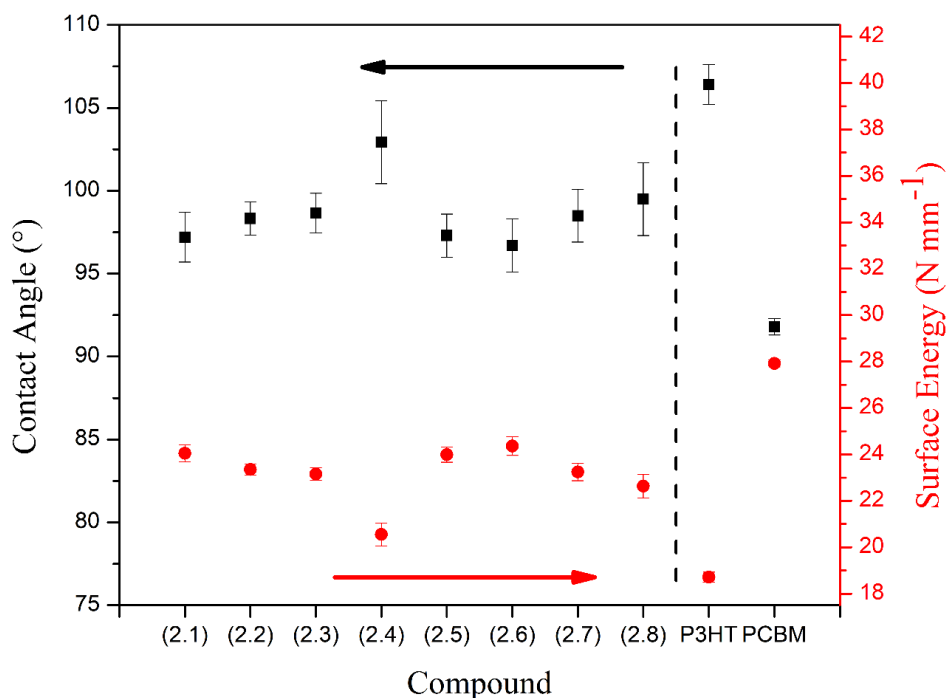


Figure 2.4. Contact angle and corresponding surface energy measurements of $(\text{R}_3\text{SiO})_2\text{-SiPc}$ films on OTS treated glass.

2.6.5 OPV performance

The eight $(\text{R}_3\text{SiO})_2\text{-SiPc}$ derivatives were employed as ternary additives in P3HT/ PC_{61}BM BHJ OPV devices in three different concentrations: 2.7 wt%, 3.7 wt% and 4.8 wt%. The results are presented on **Table 2.2**. The J_{sc} was measured by both current density vs. voltage (J - V) curves and EQE measurements. In general, J_{sc} values obtained with EQE are greater than those measured with the J - V curve. This is a common feature of thin-film devices due to photo current barrier effects.⁴³ Nevertheless, the difference is within 5-10%, which is consistent and acceptable for the purposes of this comparative work. With the exception of compound (2.1), the inclusion of all the $(\text{R}_3\text{SiO})_2\text{-SiPc}$ improve the overall device performance, through increased J_{sc} and FF . J_{sc} is increased due to extended light harvesting at long wavelengths ($>600 \text{ nm}$), which can be observed in the EQE spectra and overlaps with the absorption of SiPc chromophore (**Figure 2.2**). The additives also effectively collect and transport charges at the P3HT and PC_{61}BM interface, which causes the P3HT/ PC_{61}BM quantum efficiency contribution (300 nm to 600 nm) to increase as well.

Figure 2.5 displays the EQE spectra of every device listed on **Table 2.2**, where these features can be observed.

Table 2.2. Current density – voltage results for all the assembled OPVs and J_{sc} estimation from EQE measurements.

Compound	P3HT/PCBM: (R ₃ SiO) ₂ -SiPc ^a	V_{oc}^b	J_{sc}^b	J_{sc} (EQE) ^c	FF^b	PCE ^b
Baseline	1:0.8:0	0.53 ± 0.00	-9.44 ± 0.31	10.33	0.54 ± 0.00	2.70 ± 0.07
(2.1)	1:0.8:0.05	0.50 ± 0.01	-9.80 ± 0.75	9.84	0.48 ± 0.03	2.38 ± 0.37
	1:0.8:0.07	0.51 ± 0.01	-9.18 ± 0.19	8.80	0.50 ± 0.02	2.37 ± 0.14
	1:0.8:0.09	0.52 ± 0.01	-9.34 ± 0.48	9.51	0.51 ± 0.02	2.50 ± 0.26
(2.2)	1:0.8:0.05	0.53 ± 0.00	-10.35 ± 0.34	11.49	0.56 ± 0.01	3.07 ± 0.09
	1:0.8:0.07	0.54 ± 0.01	-10.62 ± 0.28	11.81	0.57 ± 0.01	3.27 ± 0.08
	1:0.8:0.09	0.54 ± 0.01	-10.98 ± 0.27	11.76	0.56 ± 0.02	3.32 ± 0.12
(2.3)	1:0.8:0.05	0.57 ± 0.01	-10.13 ± 0.30	12.07	0.59 ± 0.01	3.40 ± 0.12
	1:0.8:0.07	0.54 ± 0.01	-10.32 ± 0.22	11.73	0.57 ± 0.01	3.16 ± 0.05
	1:0.8:0.09	0.56 ± 0.01	-10.65 ± 0.41	11.69	0.57 ± 0.01	3.38 ± 0.09
(2.4)	1:0.8:0.05	0.52 ± 0.00	-10.64 ± 0.29	12.79	0.50 ± 0.01	2.74 ± 0.10
	1:0.8:0.07	0.53 ± 0.00	-11.00 ± 0.29	11.60	0.53 ± 0.01	3.08 ± 0.11
	1:0.8:0.09	0.52 ± 0.01	-10.81 ± 0.27	11.14	0.51 ± 0.00	2.87 ± 0.13
(2.5)	1:0.8:0.05	0.52 ± 0.00	-10.78 ± 0.33	12.16	0.53 ± 0.01	3.02 ± 0.11
	1:0.8:0.07	0.54 ± 0.01	-10.78 ± 0.10	12.56	0.56 ± 0.02	3.24 ± 0.07
	1:0.8:0.09	0.54 ± 0.01	-10.71 ± 0.28	12.00	0.56 ± 0.01	3.28 ± 0.08
(2.6)	1:0.8:0.05	0.52 ± 0.00	-10.97 ± 0.27	10.97	0.54 ± 0.00	3.11 ± 0.06
	1:0.8:0.07	0.54 ± 0.01	-10.51 ± 0.25	11.79	0.57 ± 0.01	3.27 ± 0.08
	1:0.8:0.09	0.56 ± 0.01	-10.65 ± 0.41	11.88	0.57 ± 0.01	3.38 ± 0.09
(2.7)	1:0.8:0.05	0.55 ± 0.00	-10.12 ± 0.23	11.10	0.57 ± 0.01	3.18 ± 0.08
	1:0.8:0.07	0.55 ± 0.00	-10.80 ± 0.16	11.78	0.58 ± 0.01	3.43 ± 0.05
	1:0.8:0.09	0.56 ± 0.00	-10.55 ± 0.27	11.14	0.58 ± 0.01	3.43 ± 0.11
(2.8)	1:0.8:0.05	0.55 ± 0.00	-9.75 ± 0.24	10.34	0.58 ± 0.01	3.13 ± 0.12
	1:0.8:0.07	0.55 ± 0.00	-10.05 ± 0.24	10.96	0.59 ± 0.01	3.25 ± 0.12
	1:0.8:0.09	0.56 ± 0.00	-9.54 ± 0.16	10.63	0.58 ± 0.00	3.08 ± 0.07

^a Made with 20 mg ml⁻¹ P3HT concentration, at 1000 RPM, dried in N₂ atmosphere, no annealing.

^b Measured from J - V curves, average of 5 devices, irradiation power of 1000 W m⁻².

^c Calculated by integrating the EQE spectra.

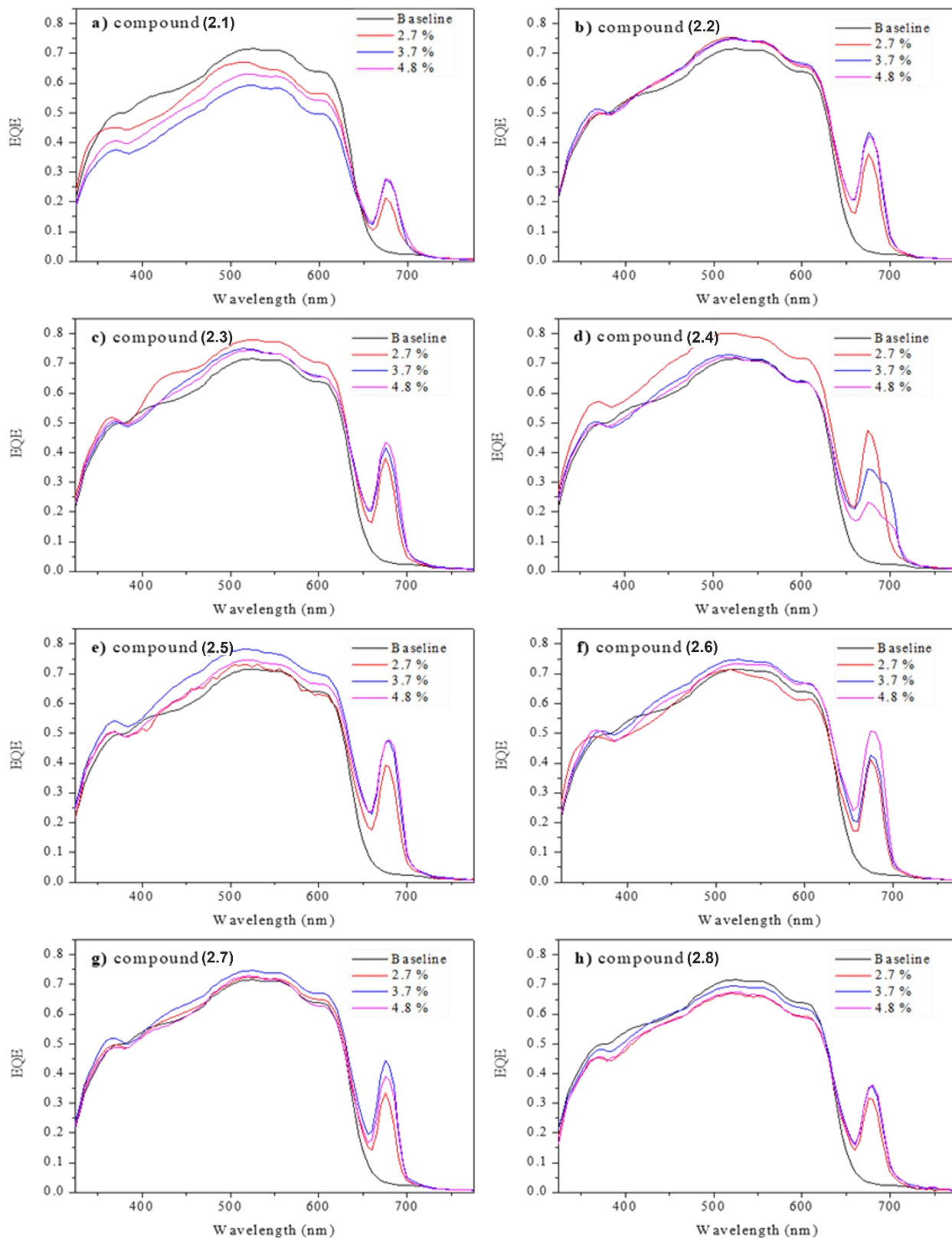


Figure 2.5. EQE spectra of all the devices produced in this work divided by $(R_3SiO)_2-SiPc$ compounds.

In most devices, the $(R_3SiO)_2$ -SiPc EQE contribution (≈ 675 nm) is almost a perfect match to the absorption profile of $(R_3SiO)_2$ -SiPc in solution, which indicates little to no solid-state aggregation of the $(R_3SiO)_2$ -SiPc,⁴⁴ further suggesting good dispersion of the SiPc derivative in the P3HT/PC₆₁BM blend. We observed this type of behavior for all SiPc derivatives except for (2.4; **Figure 2.5d**), the least soluble of the $(R_3SiO)_2$ -SiPc. At greater concentration of (2.4) we observe a red-shift and broadening of the EQE band, characteristic of solid-state interactions of SiPc aggregates. In fact, Honda *et al.*¹² demonstrated, through transient absorption spectroscopy, that bis(tri-n-hexylsilyl)-SiPc normally migrates to the amorphous P3HT/PC₆₁BM interface, where its efficiency is greatest. Taking into consideration the chemical similarities between all SiPc derivatives and the similar loading concentrations, we expect similar migration mechanism when blended in ternary films. We surmise the use of low solubility $(R_3SiO)_2$ -SiPc as a ternary additive lead to poor OPV performance due to the formation of tertiary semicrystalline domains. These aggregates form a third independent phase that is not found at the P3HT and PC₆₁BM interface and therefore disrupts efficient charge transfer, leading to no appreciable increase in EQE between 300 nm and 600 nm. While the devices containing compound (2.1) (second least soluble) do not show the same red-shift of the SiPc peak (**Figure 2.5a**), a decrease in the P3HT/PC₆₁BM EQE contribution (300 nm to 600 nm) is observed, which indicates that the preferred morphology is also not achieved.

In some instances, such as compounds (2.2) and (2.6), the greatest $(R_3SiO)_2$ -SiPc contribution to the photocurrent (e.g., EQE at 675 nm $\approx 42\%$) is achieved at the highest additive concentration (4.8%, pink line in **Figure 2.5b** and **Figure 2.5f**), but, overall, is approximately the same when compared to the medium concentration (3.7%, blue line **Figure 2.5**). However, the best P3HT/PC₆₁BM photocurrent generation is observed at the 3.7% concentration, as it is the case for compounds (2.2), (2.5), (2.6), (2.7) and (2.8) (**Figure 2.5b**, **Figure 2.5e**, **Figure 2.5f**, **Figure 2.5g** and **Figure 2.5h**) that display up to 10% EQE increase in the 300 – 600nm region. At lower additive loading concentrations, not enough SiPc is located at the interface; however, at greater concentrations, it is expected that SiPc is located not only at the interface leading to trapped charges. Therefore, the 3.7% concentration is often the one with the highest efficiency because it maximizes the amount of SiPc at the interface without diffusing into the bulk of the film.

Figure 2.6 shows the correlation between solubility *PCE*, *J_{sc}*, *V_{oc}* and fill factor, for the ternary BHJ OPV devices with the addition of 3.7 wt% $(R_3SiO)_2$ -SiPc.

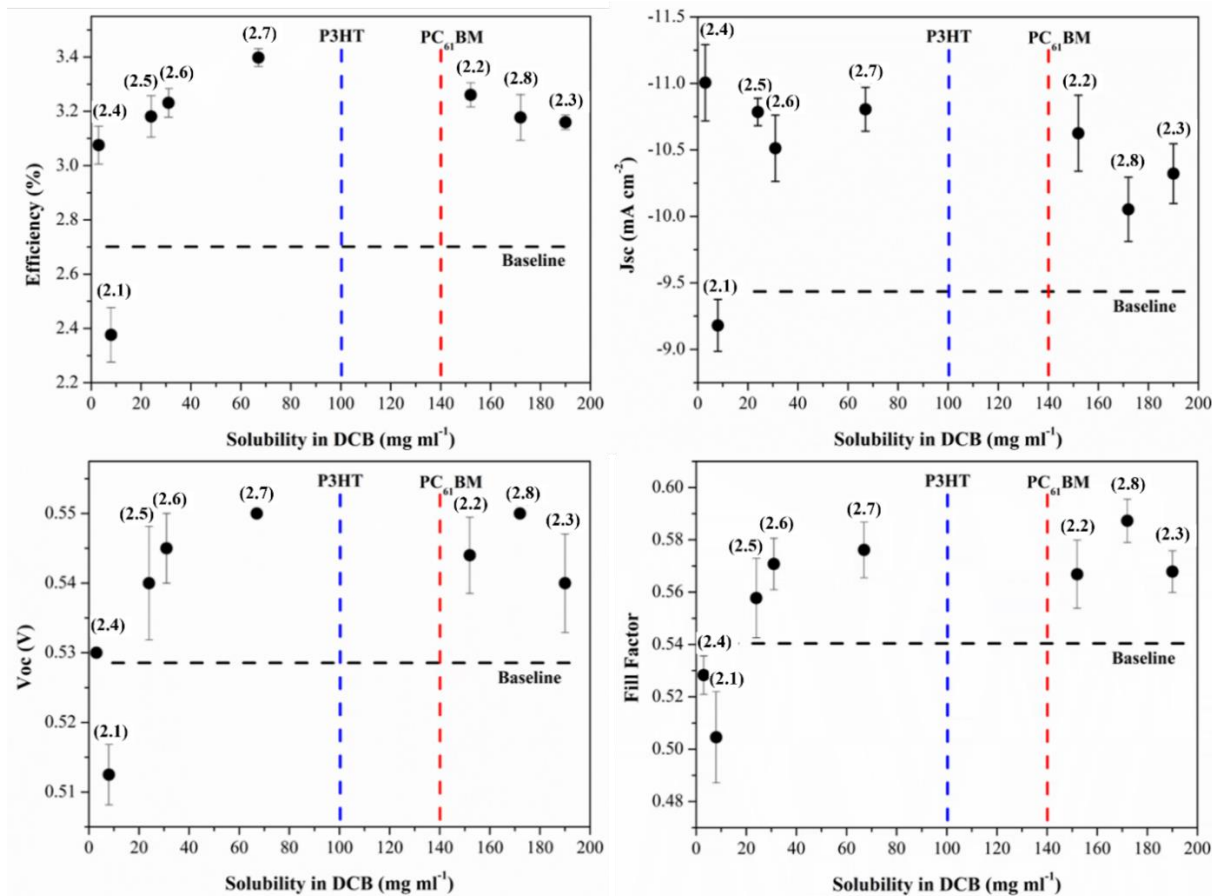


Figure 2.6. Solubility correlation with OPV performance parameters a) PCE, b) V_{oc} , c) J_{sc} and d) Fill Factor.

By simply changing the $(R_3SiO)_2-SiPc$, which only differ in solubility, the overall BHJ OPV PCE varies from 2.4% to 3.4%, compared to PCE = 2.7% for the P3HT/ $PC_{61}BM$ baseline. Therefore, even though all the $(R_3SiO)_2-SiPc$ solubilities are above processability range (minimum 8 mg ml⁻¹), the choice of additive can lead to improved or reduced OPV performance. The greatest PCE was obtained using compound (2.7), whose solubility is the closest to that of P3HT. We surmise this matching of solubility leads to more SiPc additive to be located at the donor/acceptor interface when the film dries. The same trend was found by Troshin *et al.*³⁸ where the authors reported that the best performance for P3HT/fullerene BHJ is achieved when the solubility of the donor/acceptor pair is similar, which leads to better nanomorphology. It would appear that in the case of the $(R_3SiO)_2-SiPc$, matching the solubility of P3HT has a stronger effect than matching $PC_{61}BM$'s solubility. We expect this to be a result of $(R_3SiO)_2-SiPc$'s stronger interaction with P3HT than with $PC_{61}BM$ ^{12,22}, i.e. they do not tend to solubilize in the $PC_{61}BM$ domains. Nonetheless, this is an area for further investigation.

The solubility of the $(R_3SiO)_2$ -SiPc ternary additive will determine the type of nanostructure formed during solvent evaporation, as a result of coprecipitation thermodynamics.^{22,38} More specifically, a low solubility additive, such as (2.4) and (2.1), will tend to precipitate before P3HT and PC61BM and may be forced beyond the P3HT and PC61BM interface, or even form its own crystalline domains. When the solubility of the additives is similar or higher than that of the other components of the BHJ, the precipitation kinetic will favor interfacial coverage. The proposed mechanism can be better visualized in **Figure 2.7**. Honda et al.¹² found that the P3HT/PC61BM nanostructure is composed of relatively pure crystalline phases and an amorphous interfacial phase (**Figure 2.7a**), and that the SiPcs performance is greatest when it is found at the amorphous interface where it can mediate the charge transfer between P3HT and PC61BM, thereby contributing to the photogeneration of charges at higher wavelengths. Obviously, the concentration of $(R_3SiO)_2$ -SiPc additive will also play a role in the drying mechanics, as previously stated. A low additive concentration can prevent the scenario illustrated in **Figure 2.7b** from happening; however, it will also limit the possible performance increase.

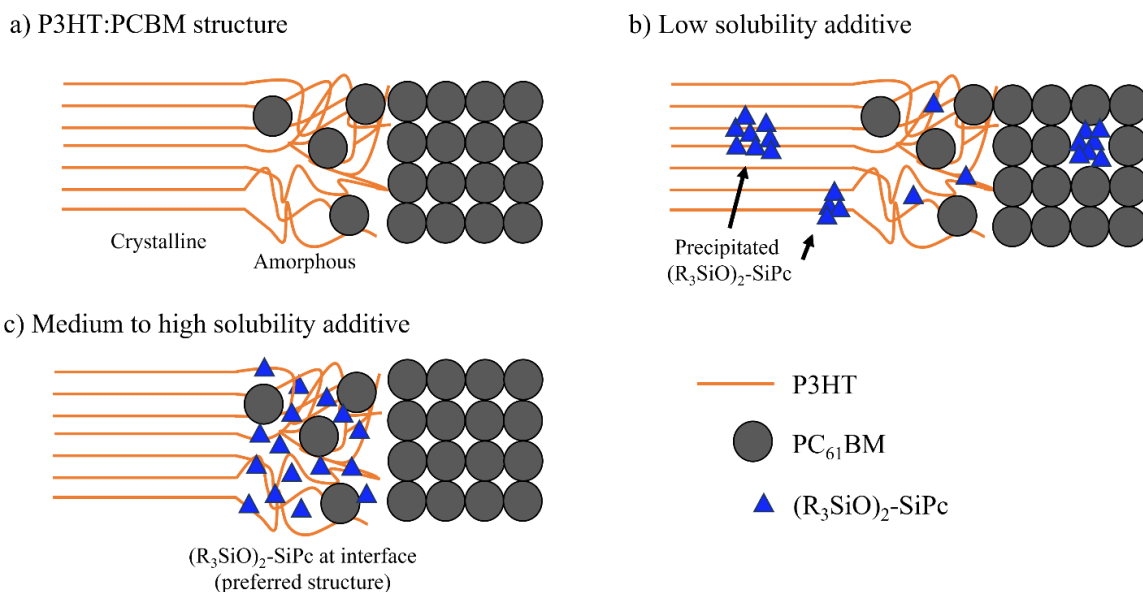


Figure 2.7. Proposed mechanism for the relationship found between additive and device performance: a) P3HT/PCBM structure when no additive is present; b) precipitation of low solubility $(R_3SiO)_2$ -SiPc, with low chance of interfacial coverage and possible formation of crystalline domains; and c) Preferred configuration, which happens when the additive solubility somewhat matches that of the polymer donor (P3HT).

Whereas we could not identify any signs of crystallization in the high solubility $(R_3SiO)_2$ -SiPc (2.2), (2.3) and (2.8), they demonstrate slightly lower performance than the additive (2.7), which indicates that an optimum window for additive solubility exists. This window is located near the solubility of the donor and acceptor materials. It is unclear why we observe a decrease in performance for the high solubility additives. It is possible that they tend to disperse in the P3HT phase, outside the interface. We have also observed that these compounds tend to dry slower and hold on to solvent molecules, which could happen during device fabrication, leading to some degree of charge trapping and slightly lower efficiency.

When we break down the PCE into its contributions, we can observe that both V_{oc} and J_{sc} increases with solubility up to a point and then slightly decreases with increased solubility. The $(R_3SiO)_2$ -SiPc located beyond the interface can act as charge traps, given that their LUMO is lower than that of P3HT, which could lead to photogenerated electrons in P3HT transferring to the $(R_3SiO)_2$ -SiPc that is physically separated from PCBM. This leads to charge recombination and, consequently, a reduction in V_{oc} and J_{sc} . The FF increases with solubility before reaching a plateau, which indicates a lower resistance across the film when the additive is more soluble. Overall, this study indicates that the solubility match between donor /acceptor phase and the ternary additive is critical for appropriate morphology and ultimately final device performance.

2.7 Conclusions

We successfully synthesized and characterized eight axially substituted SiPcs, which were then incorporated into P3HT/PCBM OPVs as ternary additives. The PCE of the devices varied from 2.4% to 3.4%, which represents up to 26% increase compared to the baseline (i.e., P3HT/PCBM OPVs with no ternary additives). Based on the results presented here, it is possible to conclude that changing the length of the axial alkylsilanes does not affect the energetics of the $(R_3SiO)_2$ -SiPc, yet drastically influences the solubility. Furthermore, the solubility of the additive has a significant effect on the performance of OPVs, with the best PCE achieved when the solubility of the $(R_3SiO)_2$ -SiPc is similar to that of P3HT, which favors the distribution of $(R_3SiO)_2$ -SiPc at the P3HT/PCBM interface, where its effectiveness is greatest. While the interaction of $(R_3SiO)_2$ -SiPc with the acceptor and donor pair also plays a role in the film nanomorphology and performance, we have shown that solubility is an important predictor of SiPcs performance as ternary additives. More research is needed to verify if this relationship is

true for other ternary additives and donor/acceptor pairs, though we expect similar trends. Nevertheless, the relationship between performance and solubility can be an important tool for device engineering containing SiPcs.

2.8 References

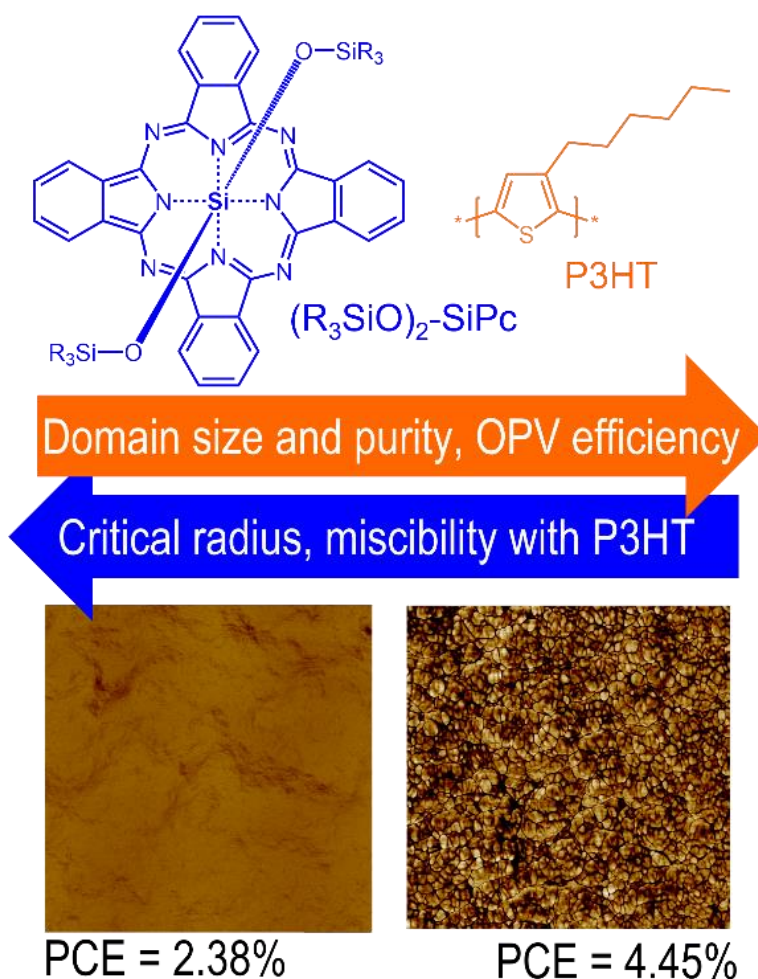
- (1) Cai, W.; Gong, X.; Cao, Y. Polymer Solar Cells: Recent Development and Possible Routes for Improvement in the Performance. *Sol. Energy Mater. Sol. Cells* 2010, 94 (2), 114–127. <https://doi.org/10.1016/j.solmat.2009.10.005>.
- (2) You, J.; Dou, L.; Yoshimura, K.; Kato, T.; Ohya, K.; Moriarty, T.; Emery, K.; Chen, C.; Gao, J.; Li, G.; et al. A Polymer Tandem Solar Cell with 10.6% Power Conversion Efficiency. *Nat. Commun.* 2013, 4, 1410–1446. <https://doi.org/10.1038/ncomms2411>.
- (3) Lipomi, D. J. Organic Photovoltaics: Focus on Its Strengths. *Joule* 2018, 2 (2), 195–198. <https://doi.org/10.1016/j.joule.2017.12.011>.
- (4) Fusella, M. A.; Lin, Y. L.; Rand, B. P. 20 - Organic Photovoltaics (OPVs): Device Physics. In *Handbook of Organic Materials for Electronic and Photonic Devices*; Elsevier Ltd., 2019; pp 665–693. <https://doi.org/10.1016/B978-0-08-102284-9.00020-6>.
- (5) Yuan, J.; Zhang, Y.; Yuan, J.; Zhang, Y.; Zhou, L.; Zhang, G.; Yip, H.; Lau, T.; Lu, X. Single-Junction Organic Solar Cell with over 15 % Efficiency Using Fused-Ring Acceptor with Electron-Deficient Core Single-Junction Organic Solar Cell with over 15 % Efficiency Using Fused-Ring Acceptor with Electron-Deficient Core. *Joule* 2019, 3, 1–12. <https://doi.org/10.1016/j.joule.2019.01.004>.
- (6) Cui, Y.; Yao, H.; Zhang, J.; Zhang, T.; Wang, Y.; Hong, L.; Xian, K.; Xu, B.; Zhang, S.; Peng, J.; et al. Over 16% Efficiency Organic Photovoltaic Cells Enabled by a Chlorinated Acceptor with Increased Open-Circuit Voltages. *Nat. Commun.* 2019, 10 (1), 1–8. <https://doi.org/10.1038/s41467-019-10351-5>.
- (7) Gambhir, A.; Sandwell, P.; Nelson, J. Solar Energy Materials & Solar Cells The Future Costs of OPV – A Bottom-up Model of Material and Manufacturing Costs with Uncertainty Analysis. *Sol. Energy Mater. Sol. Cells* 2016, 156, 49–58. <https://doi.org/10.1016/j.solmat.2016.05.056>.
- (8) Goubard, F.; Wantz, G. Ternary Blends for Polymer Bulk Heterojunction Solar Cells. *Polym. Int* 2013, 63 (July), 1362–1367. <https://doi.org/10.1002/pi.4636>.
- (9) Lu, L.; Kelly, M. A.; You, W.; Yu, L. Status and Prospects for Ternary Organic Photovoltaics. *Nat. Photonics* 2015, 9 (8), 491–500. <https://doi.org/10.1038/nphoton.2015.128>.
- (10) Kipp, D.; Verduzco, R.; Ganesan, V. Block Copolymer Compatibilizers for Ternary Blend Polymer Bulk Heterojunction Solar Cells-an Opportunity for Computation Aided Molecular Design. *Molecular Systems Design and Engineering*. Royal Society of Chemistry 2016, pp 353–369. <https://doi.org/10.1039/c6me00060f>.
- (11) Tsai, J. H.; Lai, Y. C.; Higashihara, T.; Lin, C. J.; Ueda, M.; Chen, W. C. Enhancement of P3HT/PCBM Photovoltaic Efficiency Using the Surfactant of Triblock Copolymer Containing Poly(3-Hexylthiophene) and Poly(4-Vinyltriphenylamine) Segments. *Macromolecules* 2010, 43 (14), 6085–6091. <https://doi.org/10.1021/ma1011182>.
- (12) Honda, S.; Yokoya, S.; Ohkita, H.; Benten, H.; Ito, S. Light-Harvesting Mechanism in Polymer/Fullerene/Dye Ternary Blends Studied by Transient Absorption Spectroscopy. *J. Phys. Chem. C* 2011, 115 (22), 11306–11317. <https://doi.org/10.1021/jp201742v>.

- (13) Grant, T. M.; Gorisse, T.; Dautel, O.; Wantz, G.; Lessard, B. H. Multifunctional Ternary Additive in Bulk Heterojunction OPV: Increased Device Performance and Stability. *J. Mater. Chem. A* 2017, 5 (4), 1581–1587. <https://doi.org/10.1039/C6TA08593H>.
- (14) Kim, H. J.; Han, A. R.; Cho, C. H.; Kang, H.; Cho, H. H.; Lee, M. Y.; Fréchet, J. M. J.; Oh, J. H.; Kim, B. J. Solvent-Resistant Organic Transistors and Thermally Stable Organic Photovoltaics Based on Cross-Linkable Conjugated Polymers. *Chem. Mater.* 2012, 24 (1), 215–221. <https://doi.org/10.1021/cm203058p>.
- (15) Claessens, C. G.; Hahn, U.; Torres, T. Phthalocyanines: From Outstanding Electronic Properties to Emerging Applications. *Chem. Rec.* 2008, 8 (2), 75–97. <https://doi.org/10.1002/tcr.20139>.
- (16) Lessard, B. H.; White, R. T.; Al-Amar, M.; Plint, T.; Castrucci, J. S.; Josey, D. S.; Lu, Z. H.; Bender, T. P. Assessing the Potential Roles of Silicon and Germanium Phthalocyanines in Planar Heterojunction Organic Photovoltaic Devices and How Pentafluoro Phenoxylation Can Enhance π - π Interactions and Device Performance. *ACS Appl. Mater. Interfaces* 2015, 7 (9), 5076–5088. <https://doi.org/10.1021/am508491v>.
- (17) Yuen, A. P.; Jovanovic, S. M.; Hor, A. M.; Klenkler, R. A.; Devenyi, G. A.; Loutfy, R. O.; Preston, J. S. Photovoltaic Properties of M-Phthalocyanine/Fullerene Organic Solar Cells. *Sol. Energy* 2012, 86 (6), 1683–1688. <https://doi.org/10.1016/j.solener.2012.03.019>.
- (18) Dang, M.-T.; Grant, T. M.; Yan, H.; Seferos, D. S.; Lessard, B. H.; Bender, T. P.; Miller, J. a.; Goethem, E. M. Van; Kenney, M. E.; Lu, Z.-H. Bis(Tri-n-Alkylsilyl Oxide) Silicon Phthalocyanines: A Start to Establishing a Structure Property Relationship as Both Ternary Additives and Non-Fullerene Electron Acceptors in Bulk Heterojunction Organic Photovoltaic Devices. *J. Mater. Chem. A* 2017, 126, 3378–3379. <https://doi.org/10.1039/C6TA10739G>.
- (19) Grant, T. M.; Rice, N. A.; Muccioli, L.; Castet, F.; Lessard, B. H. Solution-Processable n-Type Tin Phthalocyanines in Organic Thin Film Transistors and as Ternary Additives in Organic Photovoltaics. *ACS Appl. Electron. Mater.* 2019, 1 (4), 494–504. <https://doi.org/10.1021/acsaelm.8b00113>.
- (20) Honda, S.; Ohkita, H.; Benten, H.; Ito, S. Multi-Colored Dye Sensitization of Polymer/Fullerene Bulk Heterojunction Solar Cells. *Chem. Commun.* 2010, 46 (35), 6596–6598. <https://doi.org/10.1039/c0cc01787f>.
- (21) Honda, S.; Nogami, T.; Ohkita, H.; Benten, H.; Ito, S. Improvement of the Light-Harvesting Efficiency in Polymer/Fullerene Bulk Heterojunction Solar Cells by Interfacial Dye Modification. *ACS Appl. Mater. Interfaces* 2009, 1 (4), 804–810. <https://doi.org/10.1021/am800229p>.
- (22) Honda, S.; Ohkita, H.; Benten, H.; Ito, S. Selective Dye Loading at the Heterojunction in Polymer/Fullerene Solar Cells. *Adv. Energy Mater.* 2011, 1 (4), 588–598. <https://doi.org/10.1002/aenm.201100094>.
- (23) Lim, B.; Bloking, J. T.; Ponec, A.; McGehee, M. D.; Sellinger, A. Ternary Bulk Heterojunction Solar Cells: Addition of Soluble NIR Dyes for Photocurrent Generation beyond 800 Nm. *ACS Appl. Mater. Interfaces* 2014, 6 (9), 6905–6913. <https://doi.org/10.1021/am5007172>.
- (24) Ke, L.; Min, J.; Adam, M.; Gasparini, N.; Hou, Y.; Perea, J. D.; Chen, W.; Zhang, H.; Fladischer, S.; Sale, A.-C.; et al. A Series of Pyrene-Substituted Silicon Phthalocyanines as Near-IR Sensitizers in Organic Ternary Solar Cells. *Adv. Energy Mater.* 2016, 6 (7), 1502355. <https://doi.org/10.1002/aenm.201502355>.
- (25) Ke, L.; Gasparini, N.; Min, J.; Zhang, H.; Adam, M.; Rechberger, S.; Forberich, K.; Zhang, C.; Spiecker, E.; Tykwinski, R. R.; et al. Panchromatic Ternary/Quaternary Polymer/Fullerene BHJ Solar Cells Based on Novel Silicon Naphthalocyanine and Silicon Phthalocyanine Dye Sensitizers. *J. Mater. Chem. A* 2017, 5 (6), 2550–2562. <https://doi.org/10.1039/C6TA08729A>.

- (26) Zysman-Colman, E.; Ghosh, S. S.; Xie, G.; Varghese, S.; Chowdhury, M.; Sharma, N.; Cordes, D. B.; Slawin, A. M. Z.; Samuel, I. D. W. Solution-Processable Silicon Phthalocyanines in Electroluminescent and Photovoltaic Devices. *ACS Appl. Mater. Interfaces* 2016, 8 (14), 9247–9253. <https://doi.org/10.1021/acsami.5b12408>.
- (27) Pearson, A. J.; Plint, T.; Jones, S. T. E.; Lessard, B. H.; Credgington, D.; Bender, T. P.; Greenham, N. C. Silicon Phthalocyanines as Dopant Red Emitters for Efficient Solution Processed OLEDs. *J. Mater. Chem. C* 2017, 5 (48), 12688–12698. <https://doi.org/10.1039/c7tc03946h>.
- (28) Plint, T.; Lessard, B. H.; Bender, T. P. Assessing the Potential of Group 13 and 14 Metal/Metalloid Phthalocyanines as Hole Transport Layers in Organic Light Emitting Diodes. *J. Appl. Phys.* 2016, 119 (14), 1455021–1455029. <https://doi.org/10.1063/1.4945377>.
- (29) Melville, O. A.; Lessard, B. H.; Bender, T. P. Phthalocyanine-Based Organic Thin-Film Transistors: A Review of Recent Advances. *ACS Appl. Mater. Interfaces* 2015, 7 (24), 13105–13118. <https://doi.org/10.1021/acsami.5b01718>.
- (30) Melville, O. A.; Grant, T. M.; Mirka, B.; Boileau, N. T.; Park, J.; Lessard, B. H. Ambipolarity and Air Stability of Silicon Phthalocyanine Organic Thin-Film Transistors. *Adv. Electron. Mater.* 2019, 5 (1900087), 1–7. <https://doi.org/10.1002/aelm.201900087>.
- (31) Melville, O. A.; Grant, T. M.; Lessard, B. H. Silicon Phthalocyanines as N-Type Semiconductors in Organic Thin Film Transistors. *J. Mater. Chem. C* 2018, 6 (20), 5482–5488. <https://doi.org/10.1039/c8tc01116h>.
- (32) Yutronkie, N. J.; Grant, T. M.; Melville, O. A.; Lessard, B. H.; Brusso, J. L. Old Molecule, New Chemistry: Exploring Silicon Phthalocyanines as Emerging N-Type Materials in Organic Electronics. *Materials* (Basel). 2019, 12 (8), 5–10. <https://doi.org/10.3390/ma12081334>.
- (33) Grant, T. M.; Rice, N. A.; Muccioli, L.; Castet, F.; Lessard, B. H. Solution-Processable n-Type Tin Phthalocyanines in Organic Thin Film Transistors and as Ternary Additives in Organic Photovoltaics. *ACS Appl. Electron. Mater.* 2019, 1 (4), 494–504. <https://doi.org/10.1021/acsaelm.8b00113>.
- (34) Xue, Z.; Wang, S.; Yang, J.; Zhong, Y.; Qian, M.; Li, C.; Zhang, Z.; Xing, G.; Huettner, S.; Tao, Y.; et al. Enhanced Power Conversion Efficiency in Iridium Complex-Based Terpolymers for Polymer Solar Cells. *npj Flex. Electron.* 2018, 2 (1), 1–7. <https://doi.org/10.1038/s41528-017-0014-9>.
- (35) Lessard, B. H.; Grant, T. M.; White, R.; Thibau, E.; Lu, Z.-H.; Bender, T. P. The Position and Frequency of Fluorine Atoms Changes the Electron Donor/Acceptor Properties of Fluorophenoxy Silicon Phthalocyanines within Organic Photovoltaic Devices. *J. Mater. Chem. A* 2015, 3 (48), 24512–24524. <https://doi.org/10.1039/C5TA07173A>.
- (36) MacHui, F.; Langner, S.; Zhu, X.; Abbott, S.; Brabec, C. J. Determination of the P3HT:PCBM Solubility Parameters via a Binary Solvent Gradient Method: Impact of Solubility on the Photovoltaic Performance. *Sol. Energy Mater. Sol. Cells* 2012, 100, 138–146. <https://doi.org/10.1016/j.solmat.2012.01.005>.
- (37) Berriman, G. A.; Holmes, N. P.; Holdsworth, J. L.; Zhou, X.; Belcher, W. J.; Dastoor, P. C. A New Model for PCBM Phase Segregation in P3HT:PCBM Blends. *Org. Electron. physics, Mater. Appl.* 2016, 30, 12–17. <https://doi.org/10.1016/j.orgel.2015.12.014>.
- (38) Troshin, P. A.; Hoppe, H.; Renz, J.; Egginger, M.; Mayorova, J. Y.; Goryachev, A. E.; Peregudov, A. S.; Lyubovskaya, R. N.; Gobsch, G.; Sariciftci, N. S.; et al. Material Solubility-Photovoltaic Performance Relationship in the Design of Novel Fullerene Derivatives for Bulk Heterojunction Solar Cells. *Adv. Funct. Mater.* 2009, 19 (5), 779–788. <https://doi.org/10.1002/adfm.200801189>.
- (39) Lowbry, M. K.; Starshak, A. J.; John, S. J.; Esposito, N.; Krueger, P. C.; Kenney, M. E. DichloroCphthalocyaninoSilicon. *Inorg. Chem.* 1965, 4 (1), 128. <https://doi.org/10.1021/ic50023a036>.

- (40) Gessner, T.; Sens, R.; Ahlers, W.; Vamvakaris, C. Preparation of Silicon Phthalocyanines and Germanium Phthalocyanines and Related Substances. US 2010/0113767 2010.
- (41) Sauer, N. N. Green Chemistry: Frontiers in Benign Chemical Syntheses and Processes Edited by Paul T. Anastas and Tracy C. Williamson (U. S. Environmental Protection Agency). Oxford University Press: New York, NY. 1999. 360 Pp. \$115.00. ISBN 0-19-850170-6. J. Am. Chem. Soc. 2000, 122 (22), 5419–5420. <https://doi.org/10.1021/ja995756g>.
- (42) Li, D.; Neumann, A. W. A Reformulation of the Equation of State for Interfacial Tensions. J. Colloid Interface Sci. 1990, 137 (1), 1–4.
- (43) Scheer, R.; Schock, H. W. Chalcogenide Photovoltaics: Physics, Technologies, and Thin Film Devices; 2011. <https://doi.org/10.1002/9783527633708>.
- (44) Lessard, B. H.; Dang, J. D.; Grant, T. M.; Gao, D.; Seferos, D. S.; Bender, T. P. Bis(Tri- n -Hexylsilyl Oxide) Silicon Phthalocyanine: A Unique Additive in Ternary Bulk Heterojunction Organic Photovoltaic Devices. ACS Appl. Mater. Interfaces 2014, 6 (17), 15040–15051. <https://doi.org/10.1021/am503038t>.

3. THERMODYNAMIC PROPERTY-PERFORMANCE RELATIONSHIPS IN SILICON PHTHALOCYANINE-BASED ORGANIC PHOTOVOLTAICS.



This chapter contains work published in *ACS Appl. Energy Mater.*

Mario C. Vebber, Nicole A. Rice, Jaelyn L. Brusso, and Benoît H. Lessard. *ACS Appl. Energy Mater.* 2022, 5, 3, 3426–3435.

3.1 Context

While axially substituted $(R_3SiO)_2-SiPc$ have successfully found applications as ternary additives in BHJ, specifically in P3HT/PCBM blends, their performance has been historically below 1% as stand-alone acceptors, mainly due to the over-crystallization of the SiPc domains when casting BHJ films. Since the crystallization of $(R_3SiO)_2-SiPcs$ was an important factor to consider when casting these blends, in this work I aimed to assess how changing thermodynamic

properties associated with the crystallization of $(R_3SiO)_2-SiPc$ affect their overall efficiency as non-fullerene acceptors (NFAs) when paired with P3HT. While the results achieved are specific to SiPcs, this is potentially a step towards much needed robust design rules in OPVs. I measured properties such as $(R_3SiO)_2-SiPc$'s crystallization enthalpy, critical crystallization radius, and Flory-Huggings miscibility parameter for the BHJ components, and the $(R_3SiO)_2-SiPcs$ crystallization enthalpy and assessed their effects on the morphology of the films via AFM and, consequently, on the performance of devices.

3.2 Contribution

I carried out the synthetic procedures and purification techniques required to obtain the final compounds, as well as the characterization of each one of them. I also produced all the OPV devices and measured their performance metrics. NR obtained the AFM images of the BHJs. Manuscript was written by me with contributions from NR, BL and JB. BL and JB supervised the project.

3.3 Abstract

Axially substituted silicon phthalocyanines ($(R_3SiO)_2-SiPc$) have recently emerged as promising alternatives to fullerenes in organic photovoltaics (OPVs), with advances in both molecular design and device fabrication resulting in a 4-fold improvement in efficiency, bringing these materials closer to commercial viability. Further refinements in SiPc-based OPVs can only be achieved through exploration of their physical properties and correlation with performance metrics. In this work, we have synthesized seven $(R_3SiO)_2-SiPc$ derivatives and paired them with P3HT in OPV devices to explore how both the fundamental thermodynamic properties of the SiPcs and the blend morphology affect device performance. From these studies, $(R_3SiO)_2-SiPc$ derivatives with smaller critical radius (r_c) values correlated to higher power conversion efficiencies (PCEs) in devices, due to the tendency to form smaller domains in the active layer. Higher values for the Flory-Huggins miscibility parameter also correlated to higher PCEs, due to the formation of unadulterated, sharper domains. Both properties are dependent upon axial substituent size, with values minimized by smaller axial substituents, serving as a guideline for molecular design of SiPc-based non-fullerene acceptors (NFAs). Moreover, the majority of the

(R₃SiO)₂-SiPc materials reported herein outperformed the fullerene-based reference device, with one derivative resulting in a device with a PCE greater than 4%.

3.4 Introduction

In the coming decades, global energy security will depend heavily on our ability to find an inexpensive way to take advantage of the virtually endless energy the planet receives from the sun.^{1,2} Organic photovoltaics (OPVs) are a promising solar energy technology with the potential for low manufacturing cost and quick energy payback. OPVs can be fabricated through a variety of solution-based techniques, including smaller volume spin and blade-coating, as well as high throughput roll-to-roll printing techniques, facilitating their integration in continuous production lines, which is not feasible with traditional silicon technologies.²⁻⁵ Though the performance of OPVs has traditionally lagged in comparison to other emerging technologies, promising power conversion efficiencies (PCE) of 16 – 19% were recently reported by several research groups.⁶⁻⁸ Nonetheless, such high efficiency devices rely on small molecule acceptors and low-bandgap donor polymers, both of which are fabricated through low yielding, complex multi-step synthetic pathways and, therefore, are prohibitively expensive for large-scale production.⁹⁻¹³

Poly-3-hexylthiophene (P3HT) is a popular low-cost, synthetically scalable polymer donor,¹⁴ whose properties have been comprehensively studied over the past 30 years.¹⁵⁻¹⁷ As such, P3HT paired with phenyl-C₆₁-butyric acid methyl ester (PC₆₁BM) and other fullerenes is the benchmark OPV architecture that is often utilized as a reference device. However, P3HT/PC₆₁BM OPVs have limited efficiency, mainly due to low open-circuit voltage (*V_{oc}*).^{18,19} Recently, synthetically facile low-cost small molecules, such as O-IDFBR, DBFI-EDOT, and IDTBR, have been studied as non-fullerene acceptors (NFAs) to replace PC₆₁BM, resulting in *V_{oc}* values as high as 1.0 V.^{11,19-21} Enhancing efficiency in devices fabricated with simple small molecule NFAs may hold the key for commercial viability, as they simultaneously reduce overall materials costs while improving reproducibility, as they do not require the complex structure and chain length control of conjugated polymers.¹⁹

Metal phthalocyanines (MPcs) are commercial pigments, produced on the multi-ton scale annually, that have been explored in organic electronic applications for over 50 years. In fact, the first ever heterojunction OPV, developed by Tang in 1986, utilised copper phthalocyanine (CuPc) in combination with a perylene derivative as the donor and acceptor, respectively.^{22,23} Most widely

studied MPcs exhibit p-type characteristics, where they preferentially transport holes over electrons.^{24,25} Alternatively, silicon phthalocyanines (R₂-SiPcs) are tetravalent MPcs displaying impressive n-type characteristics,^{26,27} with demonstrated applications in light-emitting diodes (OLEDs),^{28–30} thin-film transistors (OTFTs)^{25,26,31–33} and OPVs.^{28,34–39} R₂-SiPcs have additional chemical versatility compared to most MPcs, with two axial sites available for chemical modification, facilitating tuning of electronic, chemical and physical properties, and ultimately improving the prospects for device optimization through fine-tuning such properties.^{23,40–42}

R₂-SiPc derivatives have historically been utilized as ternary additives in P3HT/PC₆₁BM OPVs, resulting in 25 – 50% increase in both short-circuit current (*J*_{sc}) and PCE when compared to the binary P3HT/PC₆₁BM blend, attributed to improved light absorption in the near-infrared region and to the mediation of the charge transfer between the donor and acceptor.^{34,42–44} Additionally, chemical modification of the R₂-SiPc axial groups can provide further functionality to the additive, such as crosslinking R₂-SiPcs reported by Grant et al,³⁹ which in addition to improved performance also resulted in enhanced device stability and longevity. Until recently, application of R₂-SiPcs as NFAs has been limited to a few reports, with the majority of devices possessing efficiencies below 1%.^{28,42,45} Such suboptimal performance can be attributed to poor bulk heterojunction (BHJ) nanomorphology, namely over crystallization of the R₂-SiPc phase.⁴² Recently, our group reported R₂-SiPc-based OPVs using P3HT⁴⁶ and PBDB-T⁴⁷ as donor polymers, achieving respectable efficiencies between 3.5 and 4.5% and *V*_{oc} values between 0.7 and 1.1 V, respectively, renewing interest in this class of materials.^{46,47} Considering that R₂-SiPc production and purification requires 70 – 150 times less energy than fullerenes,^{48,49} and that R₂-SiPcs have a synthetic complexity index (SC) 3 to 5 times smaller than prominent NFAs, including ITIC, Y6 and A1,^{46,50} further refinement of R₂-SiPc-based OPVs could be key to realizing economically viable OPVs. Despite this enormous potential, R₂-SiPc-based devices are understudied and lack clear design rules to guide materials scientists and engineers in optimization of these OPVs.

The present work utilized seven different axially substituted R₂-SiPcs ((R₃SiO)₂-SiPc) as NFAs paired with P3HT in OPVs, with property-performance relationships established to elucidate how the thermodynamic and physical properties of NFAs can impact OPV device performance. The active layer components of the BHJ devices were thoroughly characterized, with crystallization enthalpy, critical crystallization radius, and Flory-Huggings miscibility parameters

calculated and correlated with device efficiency, enabling us to propose design rules based on molecular characteristics that optimized such parameters.

3.5 Experimental

3.5.1 Materials

P3HT ($M_w = 35$ kDa, 96% regioregular) was purchased from Rieke Metals, and all solvents were purchased from commercial suppliers and used as received unless otherwise specified. Dichlorosilicon phthalocyanine ($\text{Cl}_2\text{-SiPc}$)⁵¹ and its axially substituted derivatives ($(\text{R}_3\text{SiO})_2\text{-SiPc}$)^{52,53} were synthesized according to reported procedures in the literature.

3.5.2 Materials Characterization

Differential scanning calorimetry (DSC) spectra for the binary mixtures and a P3HT reference were obtained with a TA Instruments Discovery 2500, where each sample was cycled from 0 °C to 250 °C three times with a heating/cooling rate of 5 °C min⁻¹. Binary mixtures of P3HT and $(\text{R}_3\text{SiO})_2\text{-SiPc}$ at 1:1 weight ratio were prepared by thoroughly dissolving both compounds in chloroform, with the aid of an ultrasonic bath, and then drying the samples under reduced pressure. Nuclear magnetic resonance (¹H NMR and ¹³C NMR), cyclic voltammetry (CV), mass spectroscopy (MS), UV-Vis spectroscopy,⁵³ thermogravimetric analysis (TGA) and DSC of the pure $(\text{R}_3\text{SiO})_2\text{-SiPcs}$ have already been published elsewhere.⁵⁴

3.5.3 Device Preparation and Characterization

Indium tin oxide (ITO) coated glass substrates (1" x 1", 20 Ω/sq) were cleaned in an ultrasonic bath sequentially with soapy water, distilled water, acetone, and methanol, and then treated with oxygen plasma prior to film deposition. A zinc oxide (ZnO) electron transport layer was deposited on top of the ITO slides by spin coating 200 μL of a zinc acetate solution (0.195g of $\text{Zn}(\text{AcO})_2 \cdot 2\text{H}_2\text{O}$; 0.054 ml of ethanolamine; and 6 ml of ethanol) followed by thermal annealing in air for 1 h at 180 °C. The substrates were transferred into a N₂ glovebox where the remainder of the fabrication process was carried out. Active layer solutions comprised of a 1:1 ratio of P3HT and a $(\text{R}_3\text{SiO})_2\text{-SiPc}$ at a concentration of 15 mg ml⁻¹ were prepared in dichlorobenzene (DCB). The active layers were spin coated (static) from these solutions at 2000 RPM, for 90 s, with a 10 s acceleration ramp to avoid film defects. The chips were then transferred

into an evaporator chamber, where the back electrodes of MoO₃ (7 nm) and Ag (70 nm) were deposited to yield 5 devices per chip, each with an area of 0.32 cm². Current density vs. voltage curves (*J-V* curves) were obtained with a Keithley 2400 under 1000 W m⁻² illumination from an AM1.5 xenon lamp solar simulator, in a N₂ atmosphere. Short-circuit current (*J_{sc}*) was also calculated from External Quantum Efficiency (EQE) curves, obtained using a Newport Quantx-300; for this characterization, the chips were encapsulated using an optical adhesive (Norland NOA61) and cured under an UV lamp (6 W). Active layer thickness was measured by scratching the film and measuring the height difference with Bruker Dektak XTL stylus profilometer. Atomic force microscopy (AFM) height and phase images of the OPVs were recorded with a Bruker Dimension Icon using FESPA-V2 probes in soft tapping mode, at a frequency of 0.8 Hz. The films were also characterized by UV-Vis spectroscopy using an Ocean Optics Flame spectrophotometer, and low angle X-ray diffraction (XRD) from 5° to 20°, with a 0.02° step size and 0.5° min⁻¹ scanning speed, in a Rigaku Ultima IV Diffractometer.

3.6 Results and Discussion

3.6.1 OPV performance

The various device components' energy levels, as well as the structures of the seven axially substituted ((R₃SiO)₂-SiPc) derivatives investigated, are depicted in **Figure 3.1**. We have previously established that functionalizing SiPcs with different axial silane groups has little to no significant impact on the optical and electrochemical properties of the resulting (R₃SiO)₂-SiPc, as the length of the axial alkylsilanes does not significantly impact the energetics of the phthalocyanine ring, where the HOMO and LUMO orbitals are located.⁵³ This property arises due to the fact that the different alkyl groups are not directly bonded to, nor increase the size of the SiPc ring resonance system, having minimal impact on the relevant energy transitions.^{27,53,55,56} As such, all the (R₃SiO)₂-SiPc derivatives in **Figure 3.1** were characterized with nearly identical HOMO and LUMO levels. Therefore, herein we attempted to correlate the (R₃SiO)₂-SiPc solid-state properties, such as crystallization enthalpy, miscibility with the donor polymer, and molecular radius, with their performance as NFAs when paired with P3HT in OPVs. Seven different P3HT/(R₃SiO)₂-SiPc devices were fabricated, along with a P3HT/PC₆₁BM baseline (BL) for reference, with the corresponding *J-V* characteristics summarized in **Table 3.1**. EQE curves for

the same devices are presented in **Figure B1** (Appendix B), from which J_{sc} was also independently estimated. Previous work by our group⁴⁶ found that optimized OPV performance in $(R_3SiO)_2$ -SiPc devices was achieved with a 1:1 ratio of donor polymer to NFA at a concentration of 15 mg mL⁻¹, which differs slightly from the optimized procedure for P3HT/PCBM devices. Using this fabrication recipe, the majority of our NFA compounds yielded OPVs with superior performance compared to our PC₆₁BM baseline. While the $(R_3SiO)_2$ -SiPc-based OPVs display J_{sc} values similar (or slightly lower) to those with PC₆₁BM as the acceptor, their V_{oc} values were on average 50% greater. Devices **3** and **4** had the premier performance, reaching PCEs of nearly 4.5 and 4.0%, respectively, which are among the best reported PCEs for SiPc-based OPVs.⁴⁶ For the class of $(R_3SiO)_2$ -SiPcs reported here, with no peripheral substitution, we have found that axial tripropylsilane groups are the smallest possible alkyl length that provides enough solubility for use as NFA, given that compound (3.7), which contains triethyl groups, was not soluble enough to produce working devices.

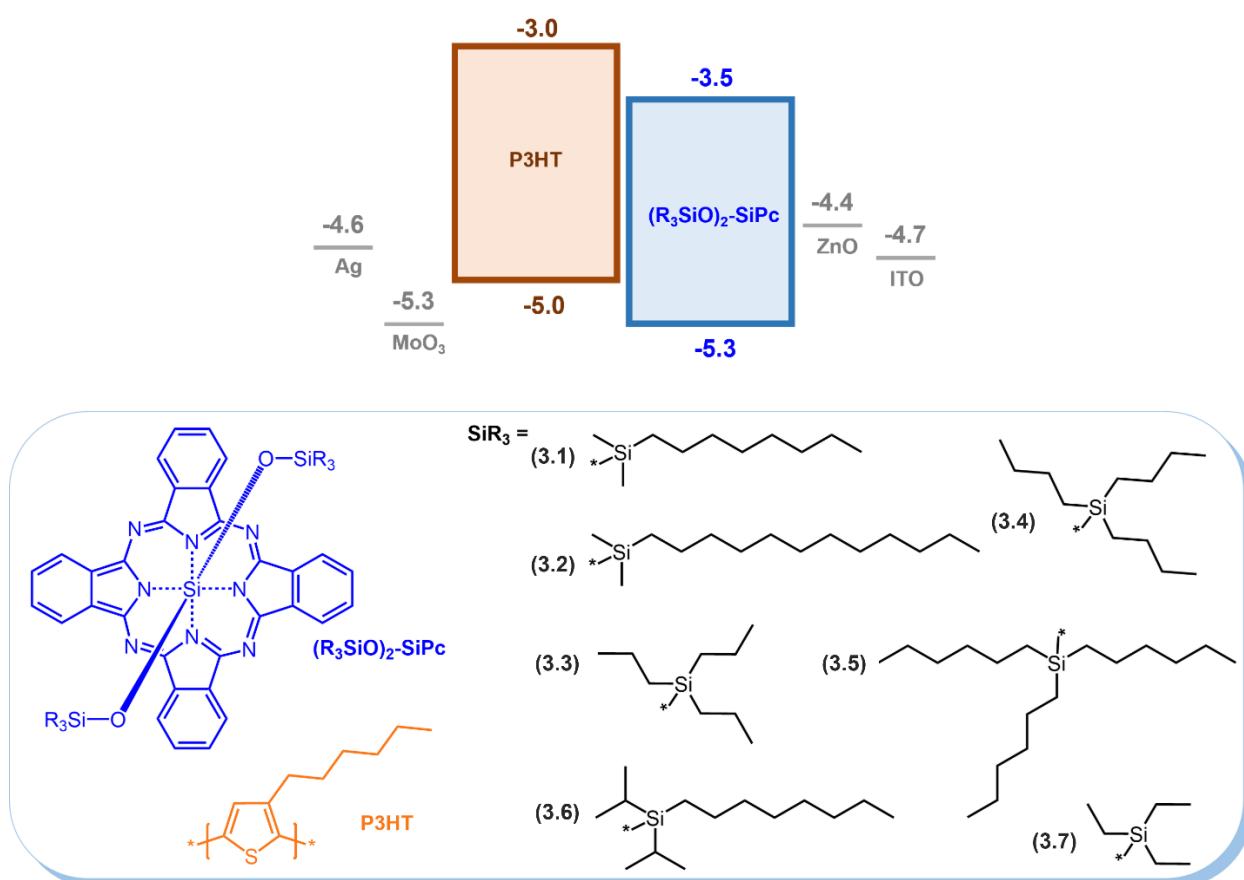


Figure 3.1. Axially substituted R_3SiO -SiPcs applied as NFAs in the present study.

Table 3.1. Current density – voltage results for all the assembled OPVs and J_{sc} estimation from EQE measurements.

Device	NFA ^a	Thickness (nm) ^c	V_{oc} (V) ^d	J_{sc} (mA cm ⁻²) ^d	J_{sc} (EQE) (mA cm ⁻²) ^e	FF ^d	PCE (%) ^{c, d}
BL	PC ₆₁ BM ^b	200 ± 5	0.52 ± 0.01	9.51 ± 0.06	9.82 ± 0.11	0.58 ± 0.00	2.88 ± 0.05
1	(3.1)	93 ± 1	0.76 ± 0.01	7.27 ± 0.28	8.60 ± 0.05	0.54 ± 0.01	2.98 ± 0.10
2	(3.2)	93 ± 1	0.77 ± 0.01	5.56 ± 0.37	5.47 ± 0.16	0.51 ± 0.02	2.25 ± 0.14
3	(3.3)	95 ± 7	0.79 ± 0.01	9.25 ± 0.39	9.24 ± 0.12	0.60 ± 0.01	4.33 ± 0.11
4	(3.4)	90 ± 4	0.77 ± 0.01	8.93 ± 0.17	9.90 ± 0.21	0.57 ± 0.01	3.92 ± 0.13
5	(3.5)	87 ± 3	0.77 ± 0.01	5.33 ± 0.14	5.66 ± 0.02	0.48 ± 0.01	2.02 ± 0.07
6	(3.6)	102 ± 4	0.74 ± 0.01	8.41 ± 0.14	8.43 ± 0.04	0.52 ± 0.01	3.27 ± 0.10
7	(3.7)	No working devices					

^{a)} Made with 15 mg ml⁻¹ P3HT/(R₃SiO)₂-SiPc concentration, at 2000 RPM, dried in N₂ atmosphere, no annealing.

^{b)} Made with 20 mg ml⁻¹ P3HT/ PC₆₁BM concentration, at 1000 RPM, dried in N₂ atmosphere, no annealing.

^{c)} From contact profilometry measurements.

^{d)} Measured from J-V curves, average of 8 devices, in two fabrication blocks, irradiation power of 1000 W m⁻².

^{e)} Calculated by integrating the EQE spectra.

The average thickness of all the P3HT/(R₃SiO)₂-SiPc active layers was approximately 93 ± 5 nm (**Table 3.1**). Only device **6** had a thickness outside this range (102 nm), which is likely attributed to its increased viscosity. The thickness of the optimized P3HT/(R₃SiO)₂-SiPc active layer is significantly smaller than that of both P3HT/PC₆₁BM (200 nm), as well as previously reported P3HT/(R₃SiO)₂-SiPc BHJs (150 – 200 nm).^{42,47} For example, Dang *et al*⁴² fabricated similar devices with compounds (3.4) and (3.5) and achieved PCEs between 0.25 of 1.07%, while Zysman-Colman and coworkers⁵⁷ employed a different (RO)₂-SiPc and achieved a PCE of 0.4% when paired with P3HT. The reduction in active layer film thickness seems to be related to the increase in performance in our (R₃SiO)₂-SiPc-based devices. PC₆₁BM charge transport can occur in 3D networks throughout the active layer. In contrast, current studies have demonstrated that (R₃SiO)₂-SiPcs tend to exhibit only 1D and 2D charge transfer processes,^{54,58,59} which can greatly hinder the ability of these NFAs to conduct charges from the interface to the electrodes in thick BHJ OPVs. Therefore, a thinner film is beneficial to overall performance by facilitating efficient charge transport and collection. This fact is supported by the FF of 0.59 measured for thin devices (~90 nm, **Table 3.1**), while a lower FF of 0.4 was obtained for thicker P3HT/(R₃SiO)₂-SiPc BHJ devices (~180 nm, **Table 3**),⁴² indicating the presence of charge traps and high rates of recombination in the latter. Additionally, UV-Vis analysis (**Figure B2**) of the devices listed in

Table 3.1 shows that these BHJs were less opaque, with 63% of the visible light transmitted through, enabling applications in translucent OPVs, such as smart windows, where some a certain degree of light transmission is necessary.

AFM analysis enables assessment of BHJ film nanostructure and phase separation, both of which play a major role in device performance. Representative AFM height and phase images from each of the devices produced are displayed in **Figure 3.2**. The size and shape of the domains varies considerably with incorporation of different $(R_3SiO)_2$ -SiPc derivatives. Devices **2** and **5** have the largest domains on average (**Figure 3.2b** and **Figure 3.2e**), with a lack of fine features between the blended P3HT/ $(R_3SiO)_2$ -SiPc phases; conversely, these two devices resulted in the lowest PCE values. Alternatively, AFM images from the top performing device **3** show small domain sizes and defined nanometer-sized features in the phase image (**Figure 3.2c**), which are characteristics correlated with superior performance in BHJ OPVs, due to improved charge separation at the donor/acceptor interface and reduced charge trapping, respectively.⁶⁰ The phase images in **Figure 3.2** also inform about the solid-state interactions between P3HT and $(R_3SiO)_2$ -SiPc, with device **3** showing clear phase separation (**Figure 3.2i**), whereas compound (3.2) presents nearly as a single phase (**Figure 3.2h**). These observed differences are connected to how the $(R_3SiO)_2$ -SiPc solubility in P3HT changes with increasing alkyl length, which will be discussed further in the next session.

3.6.2 Relationship Between Thermodynamic Properties and Photovoltaic Efficiency

To further understand the role of the $(R_3SiO)_2$ -SiPc axial group on device morphology and resulting device performance we explored the effect of key physical properties, which are compiled in **Table 3.2**. Crystallization enthalpies (ΔH_c), along with melting temperatures of the individual $(R_3SiO)_2$ -SiPc components (T_m) and their mixtures with P3HT (T_{P3HT}^{mix}), were obtained from DSC measurements. The molar volume (V_m) and molecular radius (r_m) were calculated from the results of single-crystal X-ray analysis (SC-XRD).⁵⁴ Solubility and surface energy (γ_s) characteristics have been previously reported.⁵³

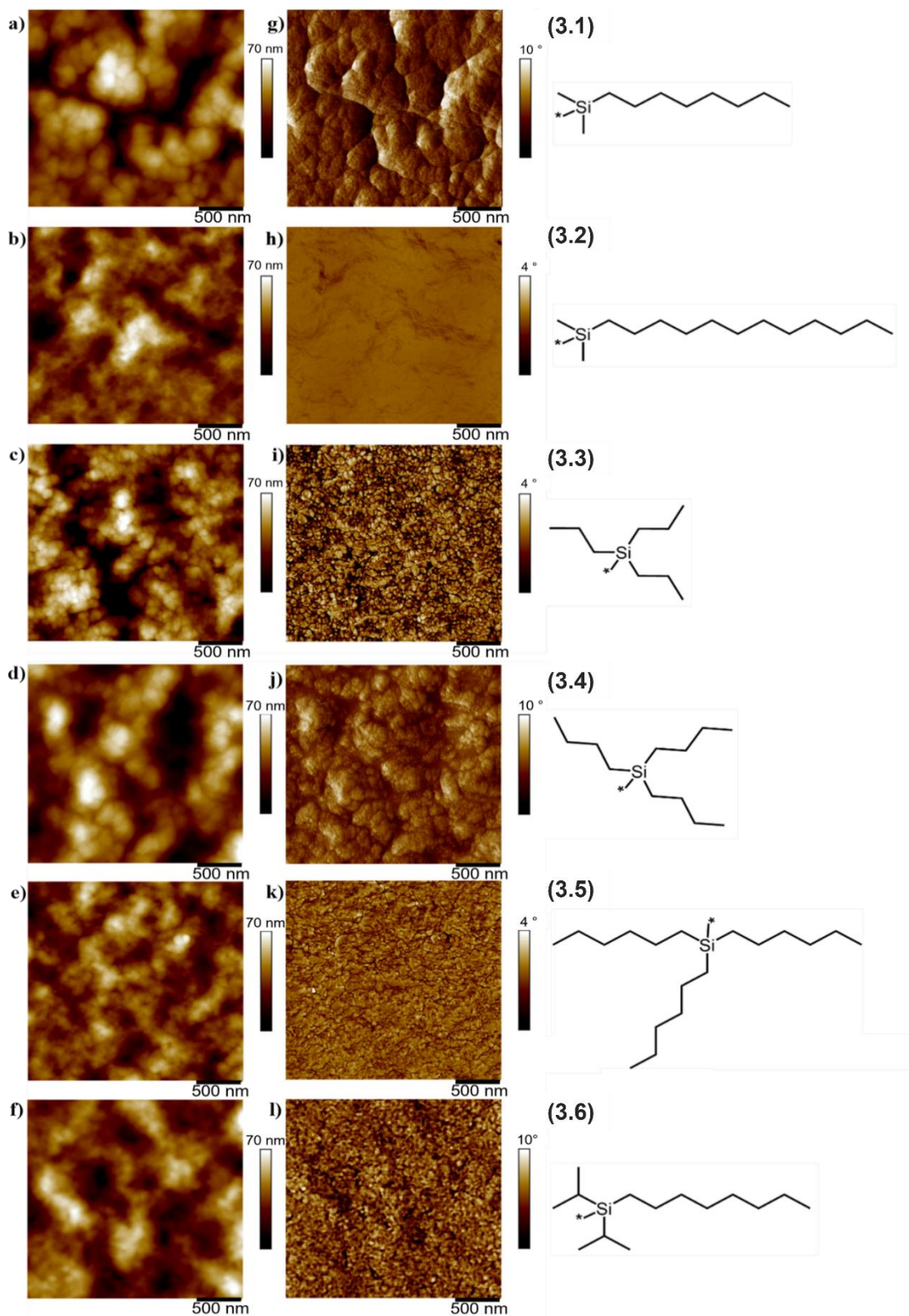


Figure 3.2. Representative atomic force microscopy (AFM) height (**a-f**) and phase (**g-l**) images of the P3HT/(R₃SiO)₂-SiPc active layers fabricated with compounds (3.1) – (3.6).

Table 3.2. Selected physical properties of (R₃SiO)₂-SiPcs, P3HT, and their blends.

	T_m (°C) ^{a)}	T_{P3HT}^{mix} (°C) ^{b)}	ΔH_c (J g ⁻¹) ^{a)}	Solubility (g L ⁻¹) ^{c)}	γ_s (mJ m ⁻²) ^{d)}	r_m (nm) ^{e)}	V_m (L mol ⁻¹) ^{e)}
(3.1)	178	209	46.7	150	23.8	0.662	0.732
(3.2)	127	209	48.7	190	24.1	0.697	0.857
(3.3)	-	228	-	25	22.5	0.652	0.698
(3.4)	231	223	30.7	31	22.7	0.675	0.776
(3.5)	173	216	23.5	67	24.0	0.721	0.944
(3.6)	148	212	30.0	170	24.7	0.743	0.822
(3.7)	-	-	-	8	-	-	-
P3HT	233	-	24.3	100	19.0		0.153

^{a)} From DSC curves of pure compounds.⁵⁴ Compound (3.3) did not show any thermal event up to 250°C. Enthalpies at 25°C were calculated using thermodynamic transformations.⁶¹

^{b)} From DSC curves of binary (R₃SiO)₂-SiPc:P3HT mixtures.

^{c)} Measured with filtration method, as previously reported.⁵³

^{d)} Estimated by the Neumann method, from Tessile drop contact angle measurements.⁵³

^{e)} Obtained from SC-XRD.⁵⁴

In solution-processed BHJs, the nanomorphology is largely determined by the processes involved in the solidification of the dissolved components into a condensed film. Solidification usually takes place through two different processes: nucleation and crystal growth, both of which are correlated to the fundamental thermodynamic properties of the components and the mixture. Nucleation is the first step of a phase change, where the initial onset of the new domains are formed, and is a result of statistical mechanical fluctuations once the Gibbs free energy (ΔG) of the system is favorable to the process.^{62,63} **Equation (3.1)** defines the critical radius (r_c) of a pure substance solidification nuclei as a function the V_m , γ_s , boltzman constant (k_B) and supersaturation of the medium (S), which is the driving force for solidification from melts and solutions.⁶²⁻⁶⁴

$$r_s = r_c \ln S = \frac{2\gamma_s V_m}{k_B T} \quad (1.1)$$

By using **Equation (3.1)**, it is possible to estimate the supersaturation-independent critical radius r_s of a solidifying solute. The supersaturation (S) is a complex, hard to quantify function precipitation variables, mainly evaporation rate and physicochemical properties of the blend. For

that reason, it is not being individually evaluated here.^{64–66} In **Figure 3.3**, the r_s of each $(R_3SiO)_2$ -SiPc is plotted against the PCE of their respective devices. The PCE versus r_s plot shows that $(R_3SiO)_2$ -SiPc derivatives with smaller r_s values tend to perform better in OPVs, even when excluding interactions with the polymer. Smaller r_s values are associated with faster rates of nucleation and smaller domains,⁶² which typically results in improved BHJ OPV performance due to more efficient charge separation.⁶⁰ The smallest r_s values were calculated for devices **3** and **4**, which were also the devices with the highest recorded efficiencies. This is corroborated by the AFM images depicted in **Figure 3.2a-f**, where films from devices **3** and **4** had domains smaller than devices 2 and 5, which contained $(R_3SiO)_2$ -SiPcs with higher r_s values, larger domains, and inferior performance. Additionally, the molecular radius r_m (**Figure B3**) show similar trends along the series when plotted with PCE. The r_m here is analogous to the molecular excluded volume and reducing the excluded volume in a given NFA motif has been correlated with a smaller degree of phase separation and improved OPV performance.⁶⁷

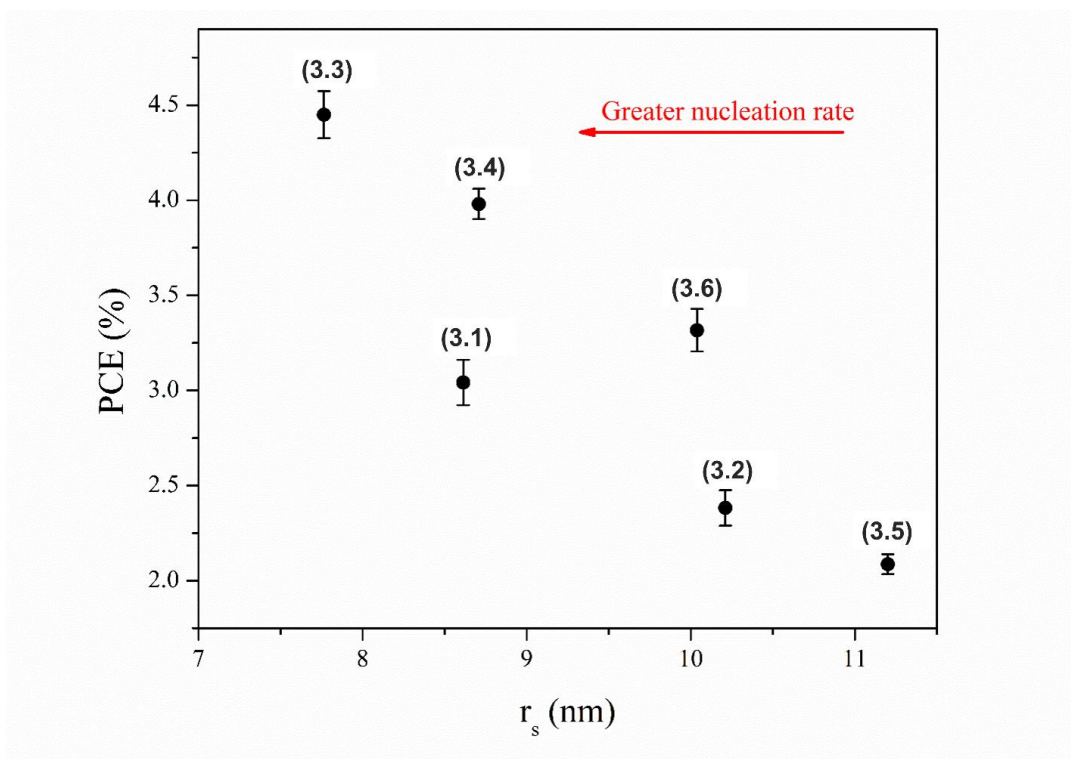


Figure 3.3. Power conversion efficiency (PCE) of P3HT/ $(R_3SiO)_2$ -SiPc OPV devices as a function of the critical radius (r_s) of $(R_3SiO)_2$ -SiPcs.

An important implication from **Equation (3.1)** is that r_s is a function of only V_m and γ_s . This implies that, if supersaturation is similar, smaller domains will be formed by $(R_3SiO)_2$ -SiPc

derivatives with smaller axial substituents, which tend to have smaller V_m and lower γ_s . While we see that the smallest derivative, compound (3.3), had the smallest domains and best performance, additional studies with in-situ crystallization analysis needs to be carried out to confirm the trend is really followed when controlling for supersaturation. Variations in the supersaturation degrees achieved by each of the compounds studied here can also be the reason why the morphology of device **1** is not as refined as its r_s value would suggest, falling outside of the overall trend. Additionally, the concrete relationship between nucleation parameters, morphology and device efficiency suggests that in P3HT/(R₃SiO)₂-SiPc BHJs, the nucleation step of film formation plays an important role in the final morphology.

The previous section discussed the BHJ morphology as function of pure (R₃SiO)₂-SiPc characteristics, and while the correlations are informative it is important to also consider the thermodynamic contribution of P3HT during film formation. Lyons *et al.* have demonstrated that domain purity plays a key role in OPV performance, often a more pronounced effect than domain size.⁶⁰ The miscibility of a polymer and a small molecule can be estimated from thermal properties and melting temperature suppression through **Equation (3.2)**, where the melting temperature depression of a polymer $\left(\frac{1}{T_{P3HT}} - \frac{1}{T_{P3HT}^{mix}}\right)$ is a function of the ideal gas constant (R), the polymer melting enthalpy (Hm_{P3HT} , equivalent to $-Hc_{P3HT}$), the molar volume of each component (V_{P3HT} , V_{SiPc}), the molar fraction of polymer in the mixture (Φ_{P3HT}), and the Flory–Huggins' miscibility parameter (χ_{12}), which is a measure of the miscibility of a small molecule in the polymeric network.⁶⁸ A large χ_{12} indicates that the polymer and small molecule phases will have a tendency to separate rather than be miscible.^{60,68}

$$\frac{1}{T_{P3HT}} - \frac{1}{T_{P3HT}^{mix}} = \frac{RV_{P3HT}}{\Delta Hm_{P3HT}V_{SiPc}}(\Phi_{P3HT} - \chi_{12} \Phi_{P3HT}^2) \quad (3.2)$$

The χ_{12} was calculated for each (R₃SiO)₂-SiPc P3HT blend using T_{P3HT} and T_{P3HT}^{mix} , which were obtained experimentally by DSC (**Table 3.2**). **Figure 3.4** demonstrates the relationship between OPV PCE and the resulting χ_{12} . Larger χ_{12} values suggest increased domain purity, through a reduction in miscibility, and sharper interfaces, both of which correlate to improved OPV performance through the reduction in trap states and charge recombination.⁶⁰ The model is corroborated by the phase images in **Figure 3.2g-1**, as device **3** was calculated to have the largest χ_{12} and subsequently has the sharpest edges between domains in AFM images. In contrast, the phase image for device **2** shows indistinguishable features, and this device was characterized by

the lowest χ_{12} values, indicating that this $(R_3SiO)_2$ -SiPc derivative has high miscibility in the P3HT phase. Increased domain purity also resulted in increased crystallinity of the $(R_3SiO)_2$ -SiPc NFAs, which was observed in PXRD diffractograms (**Figure B4**). Comparing films of similar thicknesses prepared under identical processing conditions, we observed that only the film containing compound (3.4), second lowest miscibility, displayed semicrystalline peaks at 8.2° diffraction angle (**Figure B4**). We believe that compound (3.3) did not present a clear peak in PXRD due to the small domain size, which leads to broadening of the diffraction peaks and lower intensity.

The $(R_3SiO)_2$ -SiPcs with smaller alkyl chains possessed the largest χ_{12} , likely due to reduced interactions between $(R_3SiO)_2$ -SiPc functional groups and the hexyl substituents in P3HT. It is also important to note that the length of the alkyl chains on the $(R_3SiO)_2$ -SiPcs influences miscibility in P3HT, rather than the total number of carbon atoms. For example, compounds (3.2) and (3.6) have the same number of carbon atoms, but (3.2) is significantly more miscible in P3HT than (3.6). While (3.1) and (3.6) have dissimilar number of carbon atoms, they possess a chain with the same maximum length (octyl) and exhibit very similar miscibility. This suggests that $(R_3SiO)_2$ -SiPcs with branched solubilizing groups should have similar miscibility in P3HT than their non-branched analogues and could be a potential way to optimize other properties such as crystallization enthalpy and molecular radius, with limited effect on miscibility.

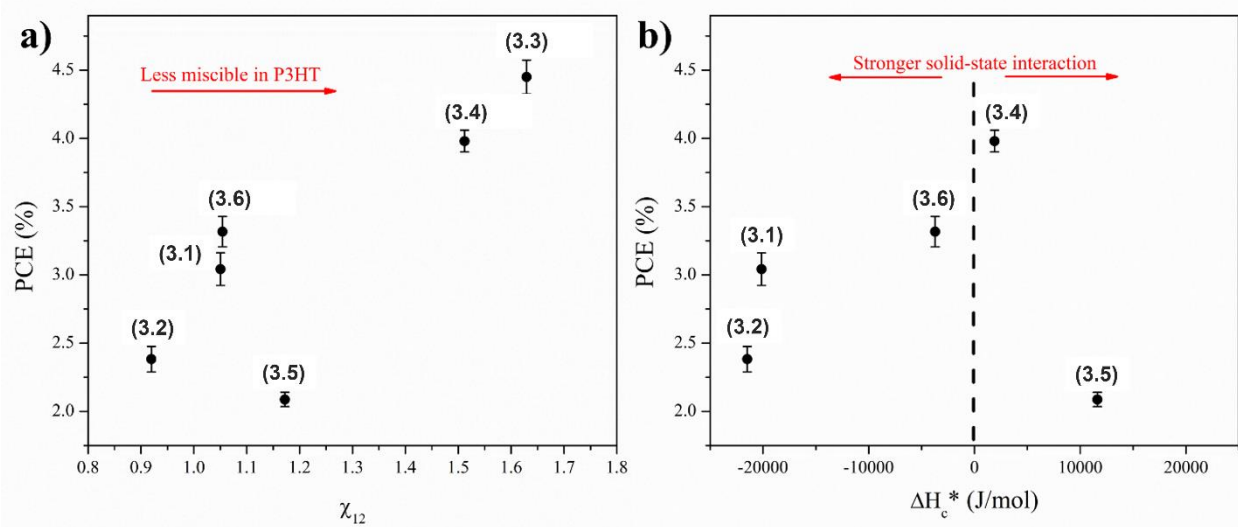


Figure 3.4. Device PCE as a function of (a) the Flory–Huggins’ miscibility parameter (χ_{12}) and (b) of excess crystallization enthalpy (ΔH_c^*) for blends of $(R_3SiO)_2$ -SiPc in P3HT.

Miscibility can also be indirectly evaluated by the excess crystallization enthalpy (ΔH_c^*), which is the difference between the ΔH_c of pure $(R_3SiO)_2$ -SiPcs and the ΔH_c of the corresponding $(R_3SiO)_2$ -SiPc and P3HT blend.⁶¹ For each P3HT/ $(R_3SiO)_2$ -SiPc blend, ΔH_c^* is plotted against PCE in **Figure 3.4b**. Larger excess crystallization enthalpy indicates the two components have more interactions and greater miscibility. Compound (3.4) resulted the smallest ΔH_c^* , while compound (3.2) exhibited the highest, both of which are in agreement with the χ_{12} values calculated above. Compound 3 is not included in **Figure 3.4b** because it does not have a melting point before its degradation temperature, therefore ΔH_c could not be evaluated.

Crystal growth is a function of crystallization equilibrium constant, surface energy, and diffusivity of species. If the growth is not limited by diffusion, the crystallization rate constant of a $(R_3SiO)_2$ -SiPc is related to their crystallization enthalpy (ΔH_c), which consequently affects the size of the $(R_3SiO)_2$ -SiPc domains in the final thin film.^{62,63} However, as shown in **Figure 3.5a**, no clear trend was observed by comparing ΔH_c of our isolated pure $(R_3SiO)_2$ -SiPc compounds to the PCE of the optimized devices (**Table 3.3**). The relationship between the crystallization rate constant and ΔH_c is complex and subject to many important considerations.^{61–63} Moreover, while there are no reports on the crystallization kinetics or diffusion parameters of $(R_3SiO)_2$ -SiPcs, the crystallization of P3HT has been reported to not be limited by diffusion,⁶⁹ Thus, we hypothesized that the lack of a trend could be attributed to the fast evaporation rates observed for these thinner films (less than 100 nm), further suggesting that nucleation plays a greater role than growth in the crystallization kinetics of $(R_3SiO)_2$ -SiPc for this set of devices.^{62,63}

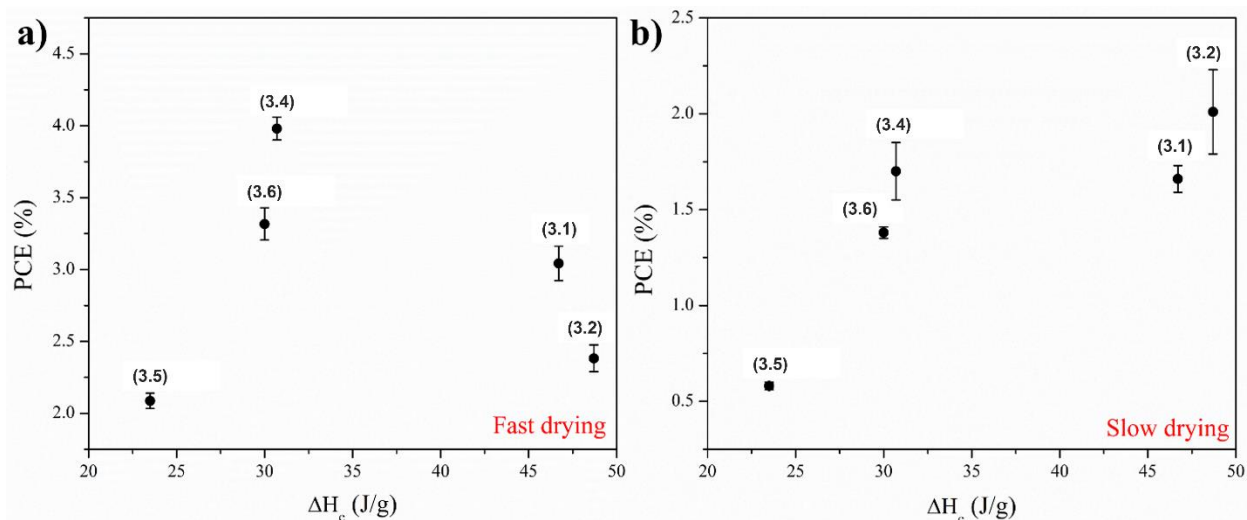


Figure 3.5. Relationship between $(R_3SiO)_2$ -SiPc crystallization enthalpy and device performance for (a) fast drying and (b) slow drying conditions.

To further probe this hypothesis, we fabricated a second series of BHJ OPV devices (**Table 3.3**) using conditions that should favour crystallization. A higher molecular weight P3HT (80 kDa) was used, combined with a reduced spin-coating rotation speed of 1000 RPM, resulting in thicker films (180 nm on average, as measured by profilometry) and ultimately slower evaporation rates. As previously reported, similar fabrication conditions encouraged over-crystallization of the $(R_3SiO)_2$ -SiPcs, which had domains larger than 1 μm and poor device performance.⁴² Plotting the PCE values for this second set of OPV devices against ΔH_c indicated a dramatically different trend (**Figure 3.5b**). A nearly linear relationship with ΔH_c was observed, where greater ΔH_c values correlated with improved device performance. Given that r_c , r_m , and χ_{12} or each $(R_3SiO)_2$ -SiPc/P3HT blend will remain comparable between the two sets of OPV devices, the shift to a crystallization enthalpy-specific trend, coupled with the over-crystallization previously observed in such devices,⁴² suggests that crystal growth was the dominant process in the film formation for the slow drying devices. As such, it is important to distinguish between nucleation and growth-dominated film formation when optimizing OPVs, as our results show that the dominating properties in each case are very different.

Table 3.3. Current density – voltage results for the OPVs containing thicker active layers.

NFA ^{a)}	V_{oc} (V) ^{b)}	J_{sc} (mA cm ⁻²) ^{b)}	FF ^{b)}	PCE (%) ^{b)}
(3.1)	0.77 ± 0.01	4.72 ± 0.20	0.45 ± 0.01	1.66 ± 0.07
(3.2)	0.75 ± 0.05	6.42 ± 0.25	0.42 ± 0.03	2.01 ± 0.22
(3.3)	No working devices			
(3.4)	0.74 ± 0.01	5.04 ± 0.22	0.45 ± 0.02	1.70 ± 0.15
3.5	0.54 ± 0.02	2.68 ± 0.15	0.40 ± 0.00	0.58 ± 0.02
3.6	0.67 ± 0.01	3.55 ± 0.03	0.39 ± 0.01	1.38 ± 0.03

^{a)} Made with 20 mg ml⁻¹ $(R_3SiO)_2$ -SiPc/ PC₆₁BM concentration, at 1000 RPM, dried in N₂ atmosphere, no annealing.

^{b)} Measured from J-V curves, average of 5 devices, irradiation power of 1000 W m⁻².

3.7 Conclusions

$(R_3SiO)_2$ -SiPcs are exciting candidates for cost-effective NFAs in OPVs, however, further refinement of both molecular structures and OPV architecture are required before their true potential can be realized. In this study seven $(R_3SiO)_2$ -SiPc derivatives were incorporated into OPVs as NFAs to assess structure-performance relationships. The optimized device fabrication process promoted rapid drying of the active layer, resulting in the SiPc NFA devices outperforming

the PCBM:P3HT baseline devices, with a maximum PCE of 4.4% achieved (*cf.* 2.9% for PCBM:P3HT). Our results show that P3HT/(R₃SiO)₂-SiPc OPVs benefit from relatively thin (100 nm) active layers and smaller domain sizes, both of which promote improved charge separation. Correlating PCE results to calculated critical radius (r_s) values for all (R₃SiO)₂-SiPc NFAs reveal that smaller r_s values promote enhanced OPV performance. Note that lower r_s values also correlate with higher nucleation rates and enhanced performance. As r_s is a function of the molar volume (V_m), we also demonstrated that (R₃SiO)₂-SiPcs with shorter axial alkyl chains, such as the tri-propyl and tri-butyl (R₃SiO)₂-SiPc derivatives (3.3 and 3.4, respectively), produce OPVs with superior performance, which is an important guideline for future molecular designs. Shorter alkyl chains also resulted in (R₃SiO)₂-SiPcs that are less miscible in P3HT, creating more unadulterated NFA domains when blended with this polymer. This was observed in AFM images of the blended films and confirmed through calculation of the Flory-Huggings miscibility parameter, where higher values effectuated devices with improved PCEs. Moreover, these results suggest that formation of P3HT/(R₃SiO)₂-SiPc active layers with less than 100 nm thickness are dominated by nucleation, rather than crystal growth. When OPV fabrication conditions were adjusted to produce active layers with almost a two-fold increase in thickness, the resulting PCE values correlated almost linearly with crystallization enthalpy. These results suggest that at these slow drying-rates nucleation slows down, and crystal growth plays a larger role in the final morphology, leading to different correlations with the thermodynamic properties of the P3HT/(R₃SiO)₂-SiPc blends. The trends outlined in this report, combined with the chemical versatility of SiPc molecules, will help to facilitate fine tuning OPV active layers with these exciting NFAs, advancing device performance while maintaining low-cost production.

3.8 Acknowledgements

The Natural Sciences and Engineering Research Council of Canada (NSERC) (2015-509 03987 and STPGP 506661-17 to B.H.L), the Canada Research Chairs Program 950-230724 (B.H.L.). We also thank the Centre for Research in Photonics at the University of Ottawa (CRPuO) for access to the AFM.

3.9 References

- (1) A Fundamental Look At Supply Side Energy Reserves For The Planet. *SHC Sol. Updat.* 2015. <https://doi.org/10.1016/j.eneco.2008.12.011>.
- (2) Fusella, M. A.; Lin, Y. L.; Rand, B. P. 20 - Organic Photovoltaics (OPVs): Device Physics, 2nd ed.; Elsevier Ltd., 2019. <https://doi.org/10.1016/B978-0-08-102284-9.00020-6>.
- (3) Cai, W.; Gong, X.; Cao, Y. Polymer Solar Cells: Recent Development and Possible Routes for Improvement in the Performance. *Sol. Energy Mater. Sol. Cells* 2010, 94 (2), 114–127. <https://doi.org/10.1016/j.solmat.2009.10.005>.
- (4) You, J.; Dou, L.; Yoshimura, K.; Kato, T.; Ohya, K.; Moriarty, T.; Emery, K.; Chen, C.; Gao, J.; Li, G.; et al. A Polymer Tandem Solar Cell with 10.6% Power Conversion Efficiency. *Nat. Commun.* 2013, 4, 1410–1446. <https://doi.org/10.1038/ncomms2411>.
- (5) Lipomi, D. J. Organic Photovoltaics: Focus on Its Strengths. *Joule* 2018, 2 (2), 195–198. <https://doi.org/10.1016/j.joule.2017.12.011>.
- (6) Yuan, J.; Zhang, Y.; Yuan, J.; Zhang, Y.; Zhou, L.; Zhang, G.; Yip, H.; Lau, T.; Lu, X. Single-Junction Organic Solar Cell with over 15 % Efficiency Using Fused-Ring Acceptor with Electron-Deficient Core Single-Junction Organic Solar Cell with over 15 % Efficiency Using Fused-Ring Acceptor with Electron-Deficient Core. *Joule* 2019, 3, 1–12. <https://doi.org/10.1016/j.joule.2019.01.004>.
- (7) Cui, Y.; Yao, H.; Zhang, J.; Zhang, T.; Wang, Y.; Hong, L.; Xian, K.; Xu, B.; Zhang, S.; Peng, J.; et al. Over 16% Efficiency Organic Photovoltaic Cells Enabled by a Chlorinated Acceptor with Increased Open-Circuit Voltages. *Nat. Commun.* 2019, 10 (1), 1–8. <https://doi.org/10.1038/s41467-019-10351-5>.
- (8) Liu, Q.; Jiang, Y.; Jin, K.; Qin, J.; Xu, J.; Li, W.; Xiong, J.; Liu, J.; Xiao, Z.; Sun, K.; et al. 18% Efficiency Organic Solar Cells. *Sci. Bull.* 2020, 65 (4), 272–275. <https://doi.org/10.1016/j.scib.2020.01.001>.
- (9) Li, N.; Brabec, C. J. Air-Processed Polymer Tandem Solar Cells with Power Conversion Efficiency Exceeding 10%. *Energy Environ. Sci.* 2015, 8 (10), 2902–2909. <https://doi.org/10.1039/c5ee02145f>.
- (10) Zhao, J.; Li, Y.; Hunt, A.; Zhang, J.; Yao, H.; Li, Z.; Zhang, J.; Huang, F.; Ade, H.; Yan, H. A Difluorobenzoxadiazole Building Block for Efficient Polymer Solar Cells. *Adv. Mater.* 2016, 28 (9), 1868–1873. <https://doi.org/10.1002/adma.201504611>.
- (11) Hwang, Y. J.; Li, H.; Courtright, B. A. E.; Subramaniyan, S.; Jenekhe, S. A. Nonfullerene Polymer Solar Cells with 8.5% Efficiency Enabled by a New Highly Twisted Electron Acceptor Dimer. *Adv. Mater.* 2016, 28 (1), 124–131. <https://doi.org/10.1002/adma.201503801>.
- (12) Zhang, J.; Zhang, Y.; Fang, J.; Lu, K.; Wang, Z.; Ma, W.; Wei, Z. Conjugated Polymer-Small Molecule Alloy Leads to High Efficient Ternary Organic Solar Cells. *J. Am. Chem. Soc.* 2015, 137 (25), 8176–8183. <https://doi.org/10.1021/jacs.5b03449>.
- (13) Yang Michael, Y.; Chen, W.; Dou, L.; Chang, W. H.; Duan, H. S.; Bob, B.; Li, G.; Yang, Y. High-Performance Multiple-Donor Bulk Heterojunction Solar Cells. *Nat. Photonics* 2015, 9 (3), 190–198. <https://doi.org/10.1038/nphoton.2015.9>.
- (14) Bannock, J. H.; Krishnadasan, S. H.; Nightingale, A. M.; Yau, C. P.; Khaw, K.; Burkitt, D.; Halls, J. J. M.; Heeney, M.; De Mello, J. C. Continuous Synthesis of Device-Grade Semiconducting Polymers in Droplet-Based Microreactors. *Adv. Funct. Mater.* 2013, 23 (17), 2123–2129. <https://doi.org/10.1002/adfm.201203014>.

- (15) Yang, C.; Lee, K.; Heeger, J.; Wudl, F. Well-Defined Donor – Acceptor Rod – Coil Diblock Copolymers Based on P3HT Containing C 60 : The Morphology and Role as a Surfactant in Bulk-Heterojunction Solar Cells †‡. 2009, 5416–5423. <https://doi.org/10.1039/b901732a>.
- (16) Tsai, J. H.; Lai, Y. C.; Higashihara, T.; Lin, C. J.; Ueda, M.; Chen, W. C. Enhancement of P3HT/PCBM Photovoltaic Efficiency Using the Surfactant of Triblock Copolymer Containing Poly(3-Hexylthiophene) and Poly(4-Vinyltriphenylamine) Segments. *Macromolecules* 2010, 43 (14), 6085–6091. <https://doi.org/10.1021/ma1011182>.
- (17) MacHui, F.; Langner, S.; Zhu, X.; Abbott, S.; Brabec, C. J. Determination of the P3HT:PCBM Solubility Parameters via a Binary Solvent Gradient Method: Impact of Solubility on the Photovoltaic Performance. *Sol. Energy Mater. Sol. Cells* 2012, 100, 138–146. <https://doi.org/10.1016/j.solmat.2012.01.005>.
- (18) Dang, M. T.; Hirsch, L.; Wantz, G. P3HT:PCBM, Best Seller in Polymer Photovoltaic Research. *Adv. Mater.* 2011, 23 (31), 3597–3602. <https://doi.org/10.1002/adma.201100792>.
- (19) Baran, D.; Ashraf, R. S.; Hanifi, D. A.; Abdelsamie, M.; Gasparini, N.; Röhr, J. A.; Holliday, S.; Wadsworth, A.; Lockett, S.; Neophytou, M.; et al. Reducing the Efficiency-Stability-Cost Gap of Organic Photovoltaics with Highly Efficient and Stable Small Molecule Acceptor Ternary Solar Cells. *Nat. Mater.* 2017, 16 (3), 363–369. <https://doi.org/10.1038/nmat4797>.
- (20) Pascual-San-José, E.; Rodríguez-Martínez, X.; Adel-Abdelaleim, R.; Stella, M.; Martínez-Ferrero, E.; Campoy-Quiles, M. Blade Coated P3HT:Non-Fullerene Acceptor Solar Cells: A High-Throughput Parameter Study with a Focus on up-Scalability. *J. Mater. Chem. A* 2019, 7 (35), 20369–20382. <https://doi.org/10.1039/c9ta07361b>.
- (21) Wadsworth, A.; Moser, M.; Marks, A.; Little, M. S.; Gasparini, N.; Brabec, C. J.; Baran, D.; McCulloch, I. Critical Review of the Molecular Design Progress in Non-Fullerene Electron Acceptors towards Commercially Viable Organic Solar Cells. *Chem. Soc. Rev.* 2019, 48 (6), 1596–1625. <https://doi.org/10.1039/c7cs00892a>.
- (22) Tang, C. W. Two-Layer Organic Photovoltaic Cell. *Appl. Phys. Lett.* 1986, 48 (2), 183–185. <https://doi.org/10.1063/1.96937>.
- (23) Claessens, C. G.; Hahn, U.; Torres, T. Phthalocyanines: From Outstanding Electronic Properties to Emerging Applications. *Chem. Rec.* 2008, 8 (2), 75–97. <https://doi.org/10.1002/tcr.20139>.
- (24) Boileau, N. T.; Cranston, R.; Mirka, B.; Melville, O. A.; Lessard, B. H. Metal Phthalocyanine Organic Thin-Film Transistors: Changes in Electrical Performance and Stability in Response to Temperature and Environment. *RSC Adv.* 2019, 9 (37), 21478–21485. <https://doi.org/10.1039/c9ra03648b>.
- (25) Melville, O. A.; Lessard, B. H.; Bender, T. P. Phthalocyanine-Based Organic Thin-Film Transistors: A Review of Recent Advances. *ACS Appl. Mater. Interfaces* 2015, 7 (24), 13105–13118. <https://doi.org/10.1021/acsami.5b01718>.
- (26) Melville, O. A.; Grant, T. M.; Mirka, B.; Boileau, N. T.; Park, J.; Lessard, B. H. Ambipolarity and Air Stability of Silicon Phthalocyanine Organic Thin-Film Transistors. *Adv. Electron. Mater.* 2019, 5 (8), 1–7. <https://doi.org/10.1002/aelm.201900087>.
- (27) Lessard, B. H. The Rise of Silicon Phthalocyanine: From Organic Photovoltaics to Organic Thin Film Transistors. *ACS Appl. Mater. Interfaces* 2021, 13 (27), 31321–31330. <https://doi.org/10.1021/acsami.1c06060>.
- (28) Zysman-Colman, E.; Ghosh, S. S.; Xie, G.; Varghese, S.; Chowdhury, M.; Sharma, N.; Cordes, D. B.; Slawin, A. M. Z.; Samuel, I. D. W. Solution-Processable Silicon Phthalocyanines in Electroluminescent and Photovoltaic Devices. *ACS Appl. Mater. Interfaces* 2016, 8 (14), 9247–9253. <https://doi.org/10.1021/acsami.5b12408>.

- (29) Pearson, A. J.; Plint, T.; Jones, S. T. E.; Lessard, B. H.; Credgington, D.; Bender, T. P.; Greenham, N. C. Silicon Phthalocyanines as Dopant Red Emitters for Efficient Solution Processed OLEDs. *J. Mater. Chem. C* 2017, 5 (48), 12688–12698. <https://doi.org/10.1039/c7tc03946h>.
- (30) Plint, T.; Lessard, B. H.; Bender, T. P. Assessing the Potential of Group 13 and 14 Metal/Metalloid Phthalocyanines as Hole Transport Layers in Organic Light Emitting Diodes. *J. Appl. Phys.* 2016, 119 (14), 1455021–1455029. <https://doi.org/10.1063/1.4945377>.
- (31) Melville, O. A.; Grant, T. M.; Lessard, B. H. Silicon Phthalocyanines as N-Type Semiconductors in Organic Thin Film Transistors. *J. Mater. Chem. C* 2018, 6 (20), 5482–5488. <https://doi.org/10.1039/c8tc01116h>.
- (32) Yutronkie, N. J.; Grant, T. M.; Melville, O. A.; Lessard, B. H.; Brusso, J. L. Old Molecule, New Chemistry: Exploring Silicon Phthalocyanines as Emerging N-Type Materials in Organic Electronics. *Materials (Basel)*. 2019, 12 (8), 5–10. <https://doi.org/10.3390/ma12081334>.
- (33) Grant, T. M.; Rice, N. A.; Muccioli, L.; Castet, F.; Lessard, B. H. Solution-Processable n-Type Tin Phthalocyanines in Organic Thin Film Transistors and as Ternary Additives in Organic Photovoltaics. *ACS Appl. Electron. Mater.* 2019, 1 (4), 494–504. <https://doi.org/10.1021/acsaelm.8b00113>.
- (34) Honda, S.; Ohkita, H.; Benten, H.; Ito, S. Multi-Colored Dye Sensitization of Polymer/Fullerene Bulk Heterojunction Solar Cells. *Chem. Commun.* 2010, 46 (35), 6596–6598. <https://doi.org/10.1039/c0cc01787f>.
- (35) Ke, L.; Gasparini, N.; Min, J.; Zhang, H.; Adam, M.; Rechberger, S.; Forberich, K.; Zhang, C.; Spiecker, E.; Tykwinski, R. R.; et al. Panchromatic Ternary/Quaternary Polymer/Fullerene BHJ Solar Cells Based on Novel Silicon Naphthalocyanine and Silicon Phthalocyanine Dye Sensitizers. *J. Mater. Chem. A* 2017, 5 (6), 2550–2562. <https://doi.org/10.1039/C6TA08729A>.
- (36) Honda, S.; Yokoya, S.; Ohkita, H.; Benten, H.; Ito, S. Light-Harvesting Mechanism in Polymer/Fullerene/Dye Ternary Blends Studied by Transient Absorption Spectroscopy. *J. Phys. Chem. C* 2011, 115 (22), 11306–11317. <https://doi.org/10.1021/jp201742v>.
- (37) Ke, L.; Min, J.; Adam, M.; Gasparini, N.; Hou, Y.; Perea, J. D.; Chen, W.; Zhang, H.; Fladischer, S.; Sale, A.-C.; et al. A Series of Pyrene-Substituted Silicon Phthalocyanines as Near-IR Sensitizers in Organic Ternary Solar Cells. *Adv. Energy Mater.* 2016, 6 (7), 1502355. <https://doi.org/10.1002/aenm.201502355>.
- (38) Grant, T. M.; Josey, D. S.; Sampson, K. L.; Mudigonda, T.; Bender, T. P.; Lessard, B. H. Boron Subphthalocyanines and Silicon Phthalocyanines for Use as Active Materials in Organic Photovoltaics. *Chem. Rec.* 2019, 19 (6), 1093–1112. <https://doi.org/10.1002/tcr.201800178>.
- (39) Grant, T. M.; Gorisse, T.; Dautel, O.; Wantz, G.; Lessard, B. H. Multifunctional Ternary Additive in Bulk Heterojunction OPV: Increased Device Performance and Stability. *J. Mater. Chem. A* 2017, 5 (4), 1581–1587. <https://doi.org/10.1039/C6TA08593H>.
- (40) Lessard, B. H.; White, R. T.; Al-Amar, M.; Plint, T.; Castrucci, J. S.; Josey, D. S.; Lu, Z. H.; Bender, T. P. Assessing the Potential Roles of Silicon and Germanium Phthalocyanines in Planar Heterojunction Organic Photovoltaic Devices and How Pentafluoro Phenoxylation Can Enhance π - π Interactions and Device Performance. *ACS Appl. Mater. Interfaces* 2015, 7 (9), 5076–5088. <https://doi.org/10.1021/am508491v>.
- (41) Yuen, A. P.; Jovanovic, S. M.; Hor, A. M.; Klenkler, R. A.; Devenyi, G. A.; Loutfy, R. O.; Preston, J. S. Photovoltaic Properties of M-Phthalocyanine/Fullerene Organic Solar Cells. *Sol. Energy* 2012, 86 (6), 1683–1688. <https://doi.org/10.1016/j.solener.2012.03.019>.
- (42) Dang, M.-T.; Grant, T. M.; Yan, H.; Seferos, D. S.; Lessard, B. H.; Bender, T. P.; Miller, J. a.; Goethem, E. M. Van; Kenney, M. E.; Lu, Z.-H. Bis(Tri-n-Alkylsilyl Oxide) Silicon Phthalocyanines: A Start to Establishing a Structure Property Relationship as Both Ternary Additives and Non-Fullerene Electron Acceptors in Bulk

Heterojunction Organic Photovoltaic Devices. *J. Mater. Chem. A* 2017, 126, 3378–3379. <https://doi.org/10.1039/C6TA10739G>.

(43) Honda, S.; Ohkita, H.; Benten, H.; Ito, S. Selective Dye Loading at the Heterojunction in Polymer/Fullerene Solar Cells. *Adv. Energy Mater.* 2011, 1 (4), 588–598. <https://doi.org/10.1002/aenm.201100094>.

(44) Lessard, B. H.; Dang, J. D.; Grant, T. M.; Gao, D.; Seferos, D. S.; Bender, T. P. Bis(Tri-*n*-Hexylsilyl Oxide) Silicon Phthalocyanine: A Unique Additive in Ternary Bulk Heterojunction Organic Photovoltaic Devices. *ACS Appl. Mater. Interfaces* 2014, 6 (17), 15040–15051. <https://doi.org/10.1021/am503038t>.

(45) Faure, M. D. M.; Grant, T. M.; Lessard, B. H. Silicon Phthalocyanines as Acceptor Candidates in Mixed Solution/Evaporation Processed Planar Heterojunction Organic Photovoltaic Devices. *Coatings* 2019, 9 (3). <https://doi.org/10.3390/COATINGS9030203>.

(46) Grant, T. M.; Dindault, C.; Rice, N. A.; Swaraj, S.; Lessard, B. H. Synthetically Facile Organic Solar Cells with > 4% Efficiency Using P3HT and a Silicon Phthalocyanine Non-Fullerene Acceptor. *Mater. Adv.* 2021. <https://doi.org/10.1039/D1MA00165E>.

(47) Grant, T. M.; Kaller, K. L. C.; Coathup, T. J.; Rice, N. A.; Hinzer, K.; Lessard, B. H. High Voc Solution-Processed Organic Solar Cells Containing Silicon Phthalocyanine as a Non-Fullerene Electron Acceptor. *Org. Electron.* 2020, 87 (June), 105976. <https://doi.org/10.1016/j.orgel.2020.105976>.

(48) Anctil, A.; Babbitt, C. W.; Raffaele, R. P.; Landi, B. J. Cumulative Energy Demand for Small Molecule and Polymer Photovoltaics. *Prog. Photovoltaics Res. Appl.* 2012, 21, 1541–1554. <https://doi.org/10.1002/pip>.

(49) Anctil, A.; Babbitt, C. W.; Raffaele, R. P.; Landi, B. J. Material and Energy Intensity of Fullerene Production. *Environ. Sci. Technol.* 2011, 45 (6), 2353–2359. <https://doi.org/10.1021/es103860a>.

(50) Po, R.; Bianchi, G.; Carbonera, C.; Pellegrino, A. “all That Glisters Is Not Gold”: An Analysis of the Synthetic Complexity of Efficient Polymer Donors for Polymer Solar Cells. *Macromolecules* 2015, 48 (3), 453–461. <https://doi.org/10.1021/ma501894w>.

(51) Lowbry, M. K.; Starshak, A. J.; John, S. J.; Esposito, N.; Krueger, P. C.; Kenney, M. E. DichloroCphthalocyaninoSilicon. *Inorg. Chem.* 1965, 4 (1), 128. <https://doi.org/10.1021/ic50023a036>.

(52) Gessner, T.; Sens, R.; Ahlers, W.; Vamvakaris, C. Preparation of Silicon Phthalocyanines and Germanium Phthalocyanines and Related Substances. *US 2010/0113767* 2010.

(53) Vebber, M. C.; Grant, T. M.; Brusso, J. L.; Lessard, B. H. Bis (Tri-Alkylsilyl Oxide) Silicon Phthalocyanines: Understanding the Role of Solubility on Device Performance as Ternary Additives in Organic Photovoltaics. *Langmuir* 2020, 36, 2612–2621. <https://doi.org/10.1021/acs.langmuir.9b03772>.

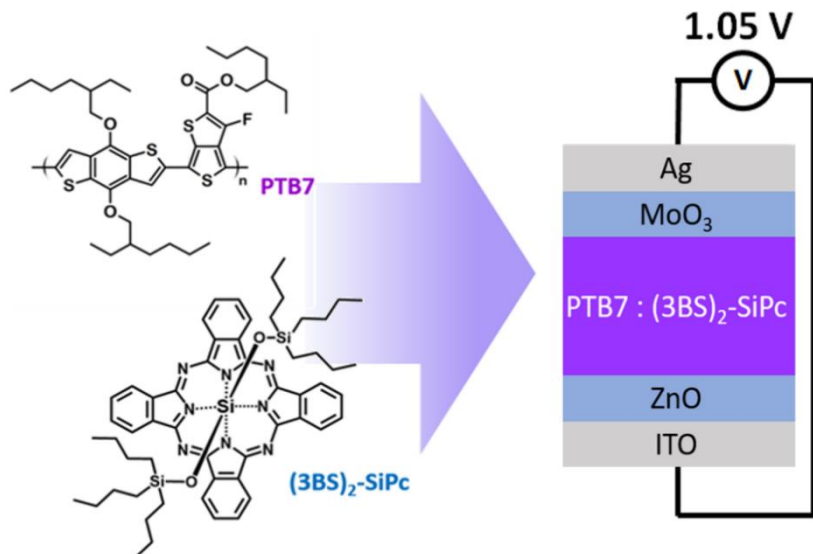
(54) Cranston, R.; Vebber, M. C.; Berbigier, J.; Rice, N. A.; Tonnelé, C.; Comeau, Z.; Boileau, N. T.; Brusso, J.; Shuhendler, A. J.; Castet, F.; et al. Thin-Film Engineering of Solution-Processable *n*-Type Silicon Phthalocyanines for Organic Thin-Film Transistors. *ACS Appl. Mater. Interfaces* 2020.

(55) Pal, A. K.; Varghese, S.; Cordes, D. B.; Slawin, A. M. Z.; Samuel, I. D. W.; Zysman-Colman, E. Near-Infrared Fluorescence of Silicon Phthalocyanine Carboxylate Esters. *Sci. Rep.* 2017, 7 (1), 1–14. <https://doi.org/10.1038/s41598-017-12374-8>.

(56) De Simone, B. C.; Alberto, M. E.; Russo, N.; Toscano, M. Photophysical Properties of Heavy Atom Containing Tetrasulfonyl Phthalocyanines as Possible Photosensitizers in Photodynamic Therapy. *J. Comput. Chem.* 2021, 42 (25), 1803–1808. <https://doi.org/10.1002/jcc.26714>.

- (57) Zysman-Colman, E.; Ghosh, S. S.; Xie, G.; Varghese, S.; Chowdhury, M.; Sharma, N.; Cordes, D. B.; Slawin, A. M. Z.; Samuel, I. D. W. Solution-Processable Silicon Phthalocyanines in Electroluminescent and Photovoltaic Devices. *ACS Appl. Mater. Interfaces* 2016, 8 (14), 9247–9253. <https://doi.org/10.1021/acsami.5b12408>.
- (58) Manoj Gali, S.; Matta, M.; H. Lessard, B.; Castet, F.; Muccioli, L. Ambipolarity and Dimensionality of Charge Transport in Crystalline Group 14 Phthalocyanines: A Computational Study. *J. Phys. Chem. C* 2018, 122 (5), 2554–2563. <https://doi.org/10.1021/acs.jpcc.7b11588>.
- (59) King, B.; Melville, O. A.; Rice, N. A.; Kashani, S.; Tonnelé, C.; Raboui, H.; Swaraj, S.; Grant, T. M.; McAfee, T.; Bender, T. P.; et al. Silicon Phthalocyanines for N-Type Organic Thin-Film Transistors: Development of Structure–property Relationships. *ACS Appl. Electron. Mater.* 2021. <https://doi.org/10.1021/acsaelm.0c00871>.
- (60) Lyons, B. P.; Clarke, N.; Groves, C. The Relative Importance of Domain Size, Domain Purity and Domain Interfaces to the Performance of Bulk-Heterojunction Organic Photovoltaics. *Energy Environ. Sci.* 2012, 5 (6), 7657–7663. <https://doi.org/10.1039/c2ee21327c>.
- (61) Ragone, D. V. *Thermodynamics of Materials, Volume 1. Thermodyn. Mater. Vol. 1*, by David V. Ragone, pp. 336. ISBN 0-471-30885-4. Wiley-VCH, Oct. 1994. 1994, 227 (2), 336.
- (62) Thanh, N. T. K.; Maclean, N.; Mahiddine, S. Mechanisms of Nucleation and Growth of Nanoparticles in Solution. *Chem. Rev.* 2014, 114 (15), 7610–7630. <https://doi.org/10.1021/cr400544s>.
- (63) Lakatos, B. G.; Szilágyi, B. Modeling Crystallization from Solution with Heat Effects. *Cryst. Growth Des.* 2015, 15 (12), 5726–5737. <https://doi.org/10.1021/acs.cgd.5b00863>.
- (64) Abbas, M.; Zeng, L.; Guo, F.; Rauf, M.; Cai, B. A Critical Review on Crystal Growth Techniques for Scalable Deposition of Photovoltaic Perovskite Thin Films. *Materials (Basel)*. 2020, 13, 4851–4892.
- (65) He, G.; Bhamid, V.; Tan, R. B. H.; Kenis, P. J. A.; Zukoski, C. F. Determination of Critical Supersaturation from Microdroplet Evaporation Experiments. *Cryst. Growth Des.* 2006, 6 (5), 1175–1180.
- (66) Liu, C.; Cheng, Y. B.; Ge, Z. Understanding of Perovskite Crystal Growth and Film Formation in Scalable Deposition Processes. *Chem. Soc. Rev.* 2020, 49 (6), 1653–1687. <https://doi.org/10.1039/c9cs00711c>.
- (67) Roders, M.; Pitch, G. M.; Garcia-Vidales, D.; Ayzner, A. L. Influence of Molecular Excluded Volume and Connectivity on the Nanoscale Morphology of Conjugated Polymer/Small Molecule Blends. *J. Phys. Chem. C* 2018, 122 (7), 3700–3708. <https://doi.org/10.1021/acs.jpcc.7b11065>.
- (68) Reynolds, J. R.; Thompson, B. C.; Skotheim, T. A.; Langner, S.; Perea Ospina, J. D.; Zhang, C.; Li, N.; J. Brabec, C. The Relevance of Solubility and Miscibility for the Performance of Organic Solar Cells. *Conjug. Polym.* 2019, 485–514. <https://doi.org/10.1201/9780429190520-15>.
- (69) Nguyen, N. A.; Shen, H.; Liu, Y.; Mackay, M. E. Kinetics and Mechanism of Poly(3-Hexylthiophene) Crystallization in Solution under Shear Flow. *Macromolecules* 2020. <https://doi.org/10.1021/acs.macromol.0c00717>.

4. VARIANCE-RESISTANT PTB7 AND AXIALLY-SUBSTITUTED SILICON PHTHALOCYANINES AS ACTIVE MATERIALS FOR HIGH-VOC ORGANIC PHOTOVOLTAICS



This chapter contains work published in *Scientific Reports*.

Mario C. Vebber, Nicole Rice, Jaclyn Brusso and Benoît H. Lessard. *Sci Rep* **11**, 15347 (2021).

4.1 Context

After exploring a wide-range of axially substituted $(R_3SiO)_2$ -SiPcs (Chapters 2 and 3), along with parallel work carried out by other members of our research group, we started to approach a limit to how high we could make the PCE of $(R_3SiO)_2$ -SiPcs:P3HT blends. While P3HT is a benchmark OPV material and arguably the best studied polymeric donor, its photovoltaic performance has long been surpassed by other conjugated polymers, such as PBDB-T and PM6. However, pairing $(R_3SiO)_2$ -SiPcs with modern-generation blends is a challenging endeavor, primarily due to the relatively shallow energy levels associated with $(R_3SiO)_2$ -SiPcs, which limits the number of donors they can be paired with. One exception is the donor PTB7 whose frontier molecular orbitals match those of $(R_3SiO)_2$ -SiPcs, with a small energy offset between them, which maximizes the voltage developed by devices. This pairing serves to evaluate whether $(R_3SiO)_2$ -SiPcs-based devices can function with a small driving force, as is the case with state-of-the-art acceptors, namely Y6 and ITIC. In this work, I aimed to begin exploring properties of the $(R_3SiO)_2$ -

SiPcs:PTB7 blend, as well as optimizing its performance and assess if it was possible to push the efficiency beyond that achieved with P3HT.

4.2 Contribution

I produced all the OPV devices and assessed all the performance metrics. NR obtained AFM images of the BHJ. Manuscript was also written by me with contributions from NR, BL and JB. BL and JB supervised the project.

4.3 Abstract

While the efficiency of organic photovoltaics (OPV) has improved drastically in the past decade, such devices rely on exorbitantly expensive materials that are unfeasible for commercial applications. Moreover, examples of high voltage single-junction devices, which are necessary for several applications, particularly low-power electronics and rechargeable batteries, are lacking in literature. Alternatively, silicon phthalocyanines (R_2 -SiPc) are inexpensive, industrially scalable organic semiconductors, having a minimal synthetic complexity (SC) index, and are capable of producing high voltages when used as acceptors in OPVs. In the present work, we have developed high voltage OPVs composed of Poly({4,8-bis[(2-ethylhexyl)oxy]benzo[1,2-b:4,5-b']dithiophene-2,6-diyl}{3-fluoro-2-[(2-ethylhexyl)carbonyl]thieno [3,4 b]thiophenediyl}) (PTB7) and an SiPc derivative ((3BS)₂-SiPc). While changes to the solvent system had a strong effect on performance, interestingly, the PTB7/(3BS)₂-SiPc active layer were robust to spin speed, annealing and components ratio. This invariance is a desirable characteristic for industrial production. All PTB7/(3BS)₂-SiPc devices produced high open circuit voltages between 1.0 and 1.07 V, while maintaining 80% of the overall efficiency, when compared to their fullerene-based counterpart.

4.4 Introduction

Organic photovoltaics (OPVs) are a promising solar energy technology with the potential for low manufacturing cost and quick energy payback.^{1,2} OPVs can be fabricated by solution-based techniques, such as spin-coating, blade-coating and a variety of printing techniques, facilitating their integration into continuous, high throughput processing, which is unachievable with traditional silicon technology.^{1,3-5} In the past 5 years, single-junction OPVs with record power conversion efficiencies (PCE) of 15 - 19% have been reported,⁶⁻⁹ approaching commercial solar

cell performances. However, these high efficiencies are achieved using expensive small molecules and polymers, the production of which is not scalable as they require complex multi-step synthesis and purification methods.^{10–14} Most of these state-of-the-art OPVs often excel in high current densities (J_{sc}) and fill factor (FF), while providing middling open-circuit voltage (V_{oc}), between 0.7 and 0.8 V.^{6–9,15}

High-voltage OPVs are of great interest for certain applications, particularly in rechargeable batteries and low-power electronics, which always require a minimum voltage to operate.^{16–18} While high V_{ocs} can be obtained by tandem cells or cells in series, this requires all cells to produce similar currents, which is virtually impossible to achieve in applications where lighting is inhomogeneous.¹⁶ Some ternary BHJs with V_{ocs} above 0.9 V have been reported,^{19,20} albeit relying on high-cost, non-scalable materials. It remains that the V_{oc} of the majority of single-junction photovoltaics rarely surpasses 0.8 V, including silicon-based devices. Recently, a few research groups have used simple and low-cost small molecules as non-fullerene acceptors (NFAs) in OPVs, and achieved $V_{oc} \geq 1.0$ V.^{12,21–24} Such architectures may hold the key for commercial viability as they can be manufactured on an industrial scale, provided that the efficiency and stability of the devices is sufficiently high.^{21,25}

Axially substituted silicon phthalocyanines (R_2 -SiPc) are ideal candidates for low-cost, high- V_{oc} acceptor materials.^{24,26,27} While metal phthalocyanine (MPc) have been investigated in organic electronic applications for more than 50 year, R_2 -SiPcs are relatively understudied, having emerged in recent years²⁸ and successfully incorporated in multiple new application, including organic thin-film transistors (OTFTs),^{29–34} organic light-emitting diodes (OLEDs)^{35–37} and in OPVs^{24,35,38–41}. The synthetic complexity (SC) index⁴² of R_2 -SiPcs have been calculated to be at least three times lower ($SC = 12$)²⁷ than that of several prominent OPV acceptors materials, such as PC₆₁BM ($SC = 36$)⁴³, Y6 ($SC = 59$)⁴⁴ and ITIC ($SC = 67$)⁴⁵. The exceptionally low SC index of R_2 -SiPcs makes them exceedingly promising organic semiconductors for OPVs. Historically, R_2 -SiPcs have mainly been employed as ternary additives in OPVs.^{38–41,46} However, in a recent study by Grant *et. al.*, an OPV composed of a blend of R_2 -SiPc and poly-3-hexylthiophene (P3HT) achieved higher V_{oc} and PCE than the fullerene-based analogue. Remarkably, when paired with poly[[4,8-bis[5-(2-ethylhexyl)-2-thienyl]benzo[1,2-b:4,5-b']dithiophene-2,6-diyl]-2,5-thiophenediyl [5,7-bis(2-ethylhexyl)-4,8-dioxo-4H,8H-benzo[1,2-c:4,5-c']dithiophene-1,3-diyl]] (PBDB-T), yielded a device with an exceptionally high V_{oc} of nearly 1.1 V.²⁴ Additionally,

relatively simple chemical modification of R_2 -SiPcs can address other common issues in OPVs, such as stability, by including cross-linking groups in the SiPc structure to improve the stability of the active layer's nanostructure.⁴⁷ Nonetheless, there are relatively few reports investigating the use of R_2 -SiPc as stand-alone acceptors in OPVs.^{24,26,27} therefore it is vital to investigate pairing these cost-effective molecules with different donor polymers and optimizing these devices to exploit their full potential in OPVs.

In the present work we have fabricated OPVs using poly[[4,8-bis[(2-ethylhexyl)oxy]benzo[1,2-b:4,5-b']dithiophene-2,6-diyl][3-fluoro-2-[(2-ethylhexyl) carbonyl]thieno[3,4-b]thiophenediyl]] (PTB7, **Figure 4.1**) and bis(tri-n-butylsilyl oxide) silicon phthalocyanine ((3BS)₂-SiPc; **Figure 4.1**). Our group has recently reported similar devices, by pairing ((3BS)₂-SiPc with PBDB-T, and here we continue to explore this NFA with PTB7, another high performing polymer, that possesses more adequate energy level alignment with respect to (3BS)₂-SiPc (**Figure 4.1**). These devices were characterized by atomic force microscopy (AFM) and external quantum efficiency (EQE). The OPVs were optimized and yielded devices with a high *V_{oc}* of 1.05 V, while maintaining 80% of the overall PCE, when compared to a fullerene-based analogue.

4.5 Experimental section

4.5.1 Materials

Two different molecular weights of PTB7 (93 kDa, PDI 2.6 and 16 kDa, PDI 2.4) was purchased from 1-Material and used as received. Bis(tri-n-butyl siloxy) silicon phthalocyanine ((3BS)₂-SiPc) was synthesized and purified according to the literature.⁴⁶ Dichlorobenzene (DCB, 99%), chlorobenzene (CB, 99%), chloroform (CF, 99%), dichloromethane (DCM, 99%), diiodooctane (DIO, 98%) and diphenylether (DPE, 99%), zinc acetate dehydrate (Zn(Ac)₂ · 2 H₂O, 99%), ethylamine (97%) were all purchased from Sigma-Aldrich and used without further purification. Ag (99.99 %) was purchased from Angstrom Engineering Inc. and MoO₃ (99.99%) was purchased from Strem.

4.5.2 Devices

Indium-tin-oxide (ITO) coated glass substrates (100 nm, 20 Ω/sq, 1 in by 1 in), purchased from Thin Film Devices Inc., were cleaned in an ultrasound bath sequentially with soapy water,

DI water, acetone (99 %) and methanol (95 %) to remove any debris. The ITO slides were then dried with a N₂ jet and placed in an air plasma cleaner for 15 min to remove any residual organics. The zinc oxide (ZnO) electron-transport layer was deposited by spin coating 150 µl of an ethanolic solution of Zn(Ac)₂ · 2 H₂O (3.3 %) and ethanolamine (0.9 %) at 2000 RPM, followed by annealing for 1 h in air at 180 °C. The substrates were then move into a N₂ glovebox where the remainder of the procedure was carried out. Preparation of the active layer was achieved using a variety of conditions, details of which are provided in **Table 4.1**. The active layer components are illustrated in **Figure 4.1a**. After deposition, the films were dried in the glovebox, at room temperature, for 1h before being transferred to an evaporation chamber (Angstrom EvoVac), where MoO₃ (7 nm) and silver electrodes (70 nm) were deposited by physical vapor deposition at a pressure below 10⁻⁶ torr, to yield 5 individual 0.32 cm² devices per substrate, as defined by shadow masks. Energy level diagram and device architecture are shown in **Figure 4.1b** and **Figure 4.1c**, respectively. Device performance was characterized using a custom push pin probe station connected to multiplexer and Keithley 2400 source meter. All OPVs were assessed under 1000 W m⁻² light intensity, provided by a solar simulator (Xenon lamp, AM1.5) and scanned between -2.0 and 2.0 V. Light intensity was verified using an NREL certified silicon standard cell prior to every run. Series and shunt resistances have been calculated from the slope of the *J-V* curves, at the *J_{sc}* and *V_{oc}*, respectively. External quantum efficiency (EQE) plots were recorded using a Newport Quantx-300 instrument outside of the glovebox. Prior to EQE measurements, the devices were encapsulated in an epoxy resin (Norland NOA61) cured under UV-light. Atomic force microscopy (AFM) topography images of the active layer films were obtained using a Bruker Dimension Icon instrument, with ScanAsyst-Air probes in tapping mode, at a frequency of 0.8 Hz; image processing was performed with NanoScope Analysis v1.8.

4.6 Results and Discussion

Bulk heterojunction (BHJ) OPV devices (**Figure 4.1c**) were fabricated by combining PTB7 (donor) with (3BS)₂-SiPc (acceptor, **Figure 4.1a**). The energy levels of PTB7, (3BS)₂-SiPc and the other materials in the BHJ OPV devices are shown in **Figure 4.1b**. Extensive optimization of the active layer was performed, as shown in **Table 4.1**. The optimized parameters were spin-rate, annealing, donor:acceptor ratio and choice of solvent. Parameters including spin-rate, annealing time and temperature, donor:acceptor ratio, and choice of solvent were all investigated.

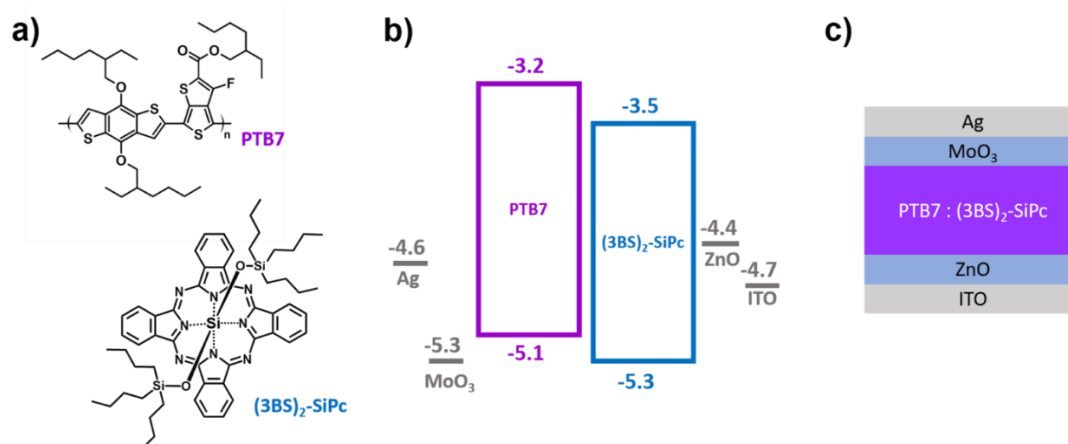


Figure 4.1. a) Chemical structure of donor and acceptor materials; b) energy level diagram of the device components; and c) schematic representation of device architecture.

Table 4.1. Experimental conditions and resulting performance of PTB7/((3BS)₂-SiPc BHJ OPV devices.

#	D:A Ratio	Solvent	Spin speed: Annealing (RPM : °C /min)	$V_{oc}^{a)}$ (V)	$J_{sc}^{a)}$ (mA·cm ⁻²)	FF ^{a)}	PCE ^{a)} (%)
1	1:1.5 ^{b)}	CB	1500 : N/A	0.76 ± 0.01	12.57 ± 0.3	0.49 ± 0.02	4.73 ± 0.03
2	1:1.5 ^{b)}	CB +DIO (3%) +DPE (2%)	1500 : N/A	0.70 ± 0.01	14.66 ± 0.09	0.65 ± 0.01	6.67 ± 0.09
3	1:1.5 ^{c)}	CB	2000 : N/A	1.05 ± 0.01	7.66 ± 0.08	0.45 ± 0.01	3.64 ± 0.05
4	1:1.5 ^{c)}	CB	1500 : N/A	1.06 ± 0.004	7.61 ± 0.04	0.45 ± 0.01	3.59 ± 0.01
5	1:1.5 ^{c)}	CB	1000 : N/A	1.06 ± 0.004	7.51 ± 0.05	0.43 ± 0.01	3.49 ± 0.01
6	1:1.5	CB	1500 : 100/15	1.07 ± 0.01	7.58 ± 0.04	0.46 ± 0.01	3.55 ± 0.03
7	1:1.5	CB	1500: 100/30	1.00 ± 0.1	7.31 ± 0.05	0.47 ± 0.02	3.41 ± 0.2
8	1:1.5	CB	1500: 150/15	1.06 ± 0.01	7.11 ± 0.05	0.46 ± 0.02	3.48 ± 0.2
9	1:1.5	CB	1500: 150/30	1.03 ± 0.01	6.88 ± 0.09	0.44 ± 0.01	3.11 ± 0.08
10	1:1	CB	1500 : N/A	1.06 ± 0.01	7.24 ± 0.04	0.44 ± 0.01	3.38 ± 0.02
11	1:1.5	CB	1500 : N/A	1.05 ± 0.01	7.68 ± 0.2	0.46 ± 0.01	3.76 ± 0.1
12	1:1.8	CB	1500 : N/A	1.05 ± 0.01	7.68 ± 0.07	0.48 ± 0.01	3.82 ± 0.04
13	1:2	CB	1500 : N/A	1.04 ± 0.01	7.59 ± 0.03	0.48 ± 0.01	3.79 ± 0.03
14	1:1	DCB	1500 : N/A	1.02 ± 0.004	7.48 ± 0.09	0.40 ± 0.01	3.06 ± 0.01
15	1:1.8	CB:CF 3:1	1500 : N/A	1.04 ± 0.01	7.84 ± 0.09	0.45 ± 0.01	3.68 ± 0.04
16	1:1.8	CB:DCM 3:1	1500 : N/A	1.06 ± 0.01	7.81 ± 0.05	0.45 ± 0.01	3.73 ± 0.01
17	1:1.8	CF	3000 : N/A	1.02 ± 0.01	4.67 ± 0.1	0.38 ± 0.01	1.79 ± 0.08
18	1:1.5	CB +DIO (3%) +DPE (2%)	1500 : N/A	No functioning device			
19	1:1.8 ^{d)}	CB	1000 : N/A	1.04 ± 0.004	5.84 ± 0.05	0.41 ± 0.01	2.47 ± 0.02
20	1:1.8 ^{d)}	CB	1500 : N/A	1.04 ± 0.004	6.19 ± 0.07	0.43 ± 0.01	2.74 ± 0.05

^{a)}All BHJ OPVs were assessed under 1000 W m⁻² light intensity, and scanned between -2.0 and 2.0 V. The open circuit voltage (V_{oc}), short circuit current (J_{sc}), fill factor (FF) and the power conversion efficiency (PCE) were obtained

from an average of 4-8 devices with an individual area 0.32 cm^2 per device. Devices that have not been annealed are marked as “N/A”.

^{b)} Baseline device composed of PTB7/PC₆₁BM at a 1:1.5 ratio.

^{c)} Solution was not filtered before deposition.

^{d)} PTB7 with M_w of 96 kDa was used for all devices except device 19 and 20 where a M_w of 16 kDa was used.

The best PTB7/(3BS)₂-SiPc BHJ OPV device (**12**) was obtained with an excess of (3BS)₂-SiPc (1:1.8 ratio) in CB, at a spin rate of 1500 RPM, resulting in a high V_{oc} of $1.05 \pm 0.01 \text{ V}$, a modest J_{sc} of $7.68 \pm 0.07 \text{ mA}\cdot\text{cm}^{-2}$, fill factor (FF) of 0.48 ± 0.01 and an overall PCE of 3.82 ± 0.04 (**Table 4.1**). While benchmark OPVs often have FF between 0.6 and 0.7,⁴⁸ these values are comparable to those of the PTB7/PC₆₁BM baseline device prepared (**1**). The average performance of device **12** is comparable to the champion device in the series, which achieved a PCE of 3.85% ($V_{oc} = 1.06 \text{ V}$, $J_{sc} = 7.71 \text{ mA}\cdot\text{cm}^{-2}$, $FF = 0.47$), within one standard deviation. These results are also slightly superior to the high- V_{oc} devices previously reported by our group, based on PBDB-T:(3BS)₂-SiPc devices (PCE = 3.4 %).²⁴ This improvement comes from a 10% improvement in current density, which can be attributed to the favourable energy level alignment between PTB7 and (3BS)₂-SiPc, with a 0.2-0.3 eV separation between HOMO and LUMO levels (**Figure 4.1**). This energy gap facilitates charge separation and can lead to greater currents.

When optimizing the PTB7/(3BS)₂-SiPc BHJ OPV devices we found that PCE improves only slightly when deposition spin rate is increased from 1000 to 2000 RPM (devices **3** to **5**), demonstrating that the PTB7/(3BS)₂-SiPc active layer can be successfully deposited at different spin-rates. Interestingly, film thickness remains relatively constant, decreasing slightly from 129 nm to 115 nm, when varying spin rate from 1000 to 2000 RPM, which does not follow the typical spin-coating equation, that predicts a thickness variation of nearly 50% between the two films.⁴⁹ This behaviour suggests a strong dilatant characteristic of the PTB7/(3BS)₂-SiPc solution, resisting the centrifugal force. In general, annealing also showed a weak effect on device PCE (devices **6** to **9**), slightly increasing FF while decreasing J_{sc} . **Figure 4.2** shows AFM images before (**Figure 4.2a**) and after annealing for 15 min at 100 °C (**Figure 4.2b**). Comparison of the films at various length scales shows that some larger amorphous features are formed during the annealing step, which is reflected in the increased roughness of the films: $r_q = 1.31 \text{ nm}$ before annealing and $r_q = 2.0 \text{ nm}$ after. Nonetheless, in general overall surface morphology and height features are mostly retained. Longer annealing times were slightly detrimental to device performance, most likely due to disruption of the active layer through formation of large agglomerates, as suggested in **Figure**

4.2b. The (3BS)₂-SiPc to PTB7 ratio (devices **10** to **13**) only had a noticeable effect on the PCE when the ratio was reduced below 1.5, which is observed when comparing devices **10** and **11**, with ratios of 1.0 and 1.5, respectively. Alternatively, devices **11**, **12** and **13**, with ratios of 1.5, 1.8 and 2.0, respectively, have remarkably similar performances. While PTB7/PC₆₁BM devices have been optimized at a 1:1.5 ratio,⁵⁰ the PTB7/(3BS)₂-SiPc BHJ OPV devices had the best performance when using a 1:1.8 ratio (**Table 4.1**). In summary, we found that the (3BS)₂-SiPc:PTB7 blend is fairly invariant to spin rate, acceptor:donor ratio and annealing conditions. This low variability is a desirable property for high throughput manufacture, where minor variations are inevitable.

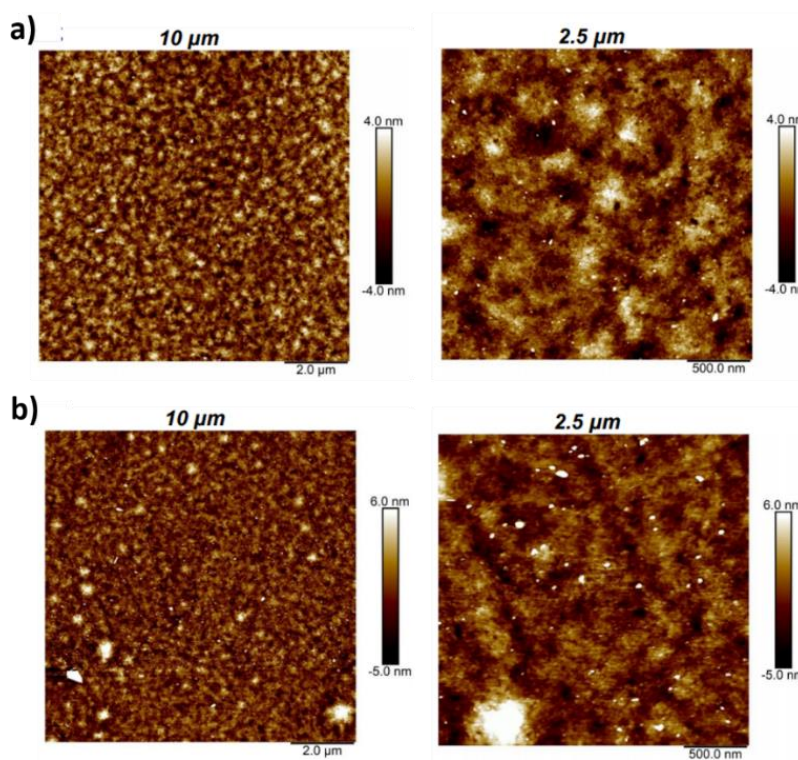


Figure 4.2. AFM height images of the PTB7/(3BS)₂-SiPc films on two different scales (10 and 2.5 μm **a**) before annealing and **b**) after annealing (15 min at 100 °C).

Alternatively, modification of the active layer solvent system had a significant impact on device performance. Solvent additives, namely DIO and DPE, have been previously reported to play a critical role in the film morphology of the active layer in PTB7/PC₆₁BM devices, resulting in significant improvements in current density and PCE.⁵¹ Such high boiling point additives promote higher crystallinity and improved nanomorphology in PTB7/fullerene blends,⁵¹ typically resulting in increases of more than 40% in PCE. We have observed these improvements as well in

our baseline PTB7/PC₆₁BM baselines (**1** and **2**, **Table 4.1**). However, when incorporating these additives in the fabrication of PTB7/(3BS)₂-SiPc BHJ OPV devices (device **18**), we were unable to obtain functioning devices. This may be attributed to (3BS)₂-SiPc, which has been reported to crystallize rapidly,^{47,52,53} and the use of high boiling point additives thereby exacerbating this behaviour, creating micrometric or even submillimetric domains (patterns are visible to the naked eye) as opposed to the nanometric phase separation required for functioning OPVs.^{54,55} In attempt to counter this crystallization we explored the use of low-boiling point solvent additives, such as DCM and CF (devices **15** and **16**) but these solvent changes led to negligible improvements in performance. Using CF as a single low-boiling point solvent (device **17**) resulted in thicker films due to rapid evaporation, which approximately halved the PCE when compared to the best devices deposited with solutions in CB. We have also investigated if incorporating a low a low-M_w PTB7 (16 kDa) instead of the conventional PTB7 (M_w = 96 Kda) could improve the crystallinity of the P7B7 phase without additives. Functioning devices were obtained (**19** and **20**), but with lower efficiency compared to the optimized device achieved from low-M_w PTB7 (**12**).

While the *J*_{sc} and FF of the PTB7/(3BS)₂-SiPc BHJ OPV devices were modest, it is important to note the consistently high *V*_{oc} between 1.00 – 1.07 V, which is a very desirable and often rare characteristic in OPVs. Note that current state-of-the-art OPVs typically display *V*_{oc} values around 0.8V.⁷⁻⁹ The high voltages can be attributed to the large difference between the energy levels of the donor's highest occupied molecular orbital (HOMO) and the acceptor's lowest unoccupied molecular orbital (LUMO), as illustrated in **Figure 4.1b**.

Table 4.2 compares the series and shunt resistances of our optimized device **12** with literature-based devices containing either PTB7 or P3HT as the donor and PC₆₁BM or (3BS)₂-SiPc as the acceptor. Strikingly, the shunt resistance of the PTB7/(3BS)₂-SiPc BHJ OPV device is significantly lower than the others, which indicates a high rate of charge recombination in the active layer film and may offer a potential explanation for the relatively low *J*_{sc} compared to PTB7/PC₆₁BM devices (**Table 4.1** and **Table 4.2**). This may be ascribed to the small energy level offset only 0.2 eV between the donor and acceptor, which could be impairing the dissociation of excitons at the PTB7/(3BS)₂-SiPc interface.¹ Moreover, AFM images (**Figure 4.2**) show that domain sizes are in the hundreds of nm range, which is often too large for optimal BHJ OPV operation, given the average distance travelled by excitons before recombination is around 5 - 15 nm.^{1,55,56}

Table 4.2. Thickness, series and shunt resistances of the optimized devices and relevant comparative devices.

Device	Series (Ω)	Shunt (Ω)	Thickness (nm)
P3HT/PC ₆₁ BM ^{46 a)}	11	1676	200
P3HT/(3BS) ₂ -SiPc ^{24 a)}	15	816	100
PTB7/PC ₆₁ BM (1)	9	1352	90
PTB7/(3BS) ₂ -SiPc (12)	22	463	115

^{a)} Devices have been previously reported and further characterized here.

Figure 4.3a shows the J - V curves for the optimized PTB7/(3BS)₂-SiPc device (**12**) compared to the PTB7/PC₆₁BM baseline (**1**) and **Figure 4.3b** displays the EQE curves for the same devices. While (3BS)₂-SiPc provides some extra light absorption around 700 nm, the overall quantum efficiency is lower than that of the fullerene-based device. This trade off is often seen in SiPc-based devices.²⁴ Moreover, the EQE spectrum of device **12** is slightly blue-shifted and sharper in comparison to the baseline (**1**), which is associated with smaller crystallinity of the polymeric phase.^{51,57} This suggests that (3BS)₂-SiPc inhibits the crystallization of PTB7, and it is one of the causes for the lower current observed when compared to the fullerene baseline. The lower crystallinity of the polymeric network can also impair charge conduction and contribute to the low shunt resistance measured for such devices. We surmise that a new type of additive, that simultaneously promotes the crystallization of PTB7 while keeping the SiPc domain size small, could push the efficiency of this class of devices beyond that of the PTB7/PC₆₁BM baseline, but the authors are not familiar with any additive that fits these requirements.

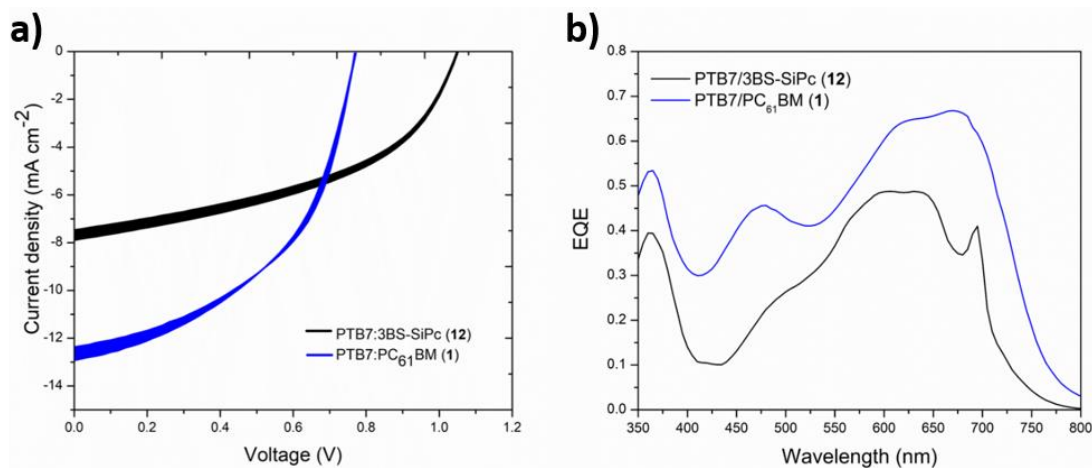


Figure 4.3. OPV characteristics **a)** J - V curves, where line thickness corresponds to the standard deviation of 4 devices, and **b)** EQE spectra of the optimized device (**12**) and the fullerene-containing baseline (**1**).

R₂-SiPcs continue to show promise as NFAs in BHJ OPVs. However, their tendency to quickly crystallize and their shallow LUMO level have been detrimental to achieving high performance. Moving forward, the chemical versatility of R₂-SiPc molecules, would facilitate fine tuning of the material properties such as their frontier orbital energy levels and the solid-state packing properties, providing the potential for improving device performance while still remaining a synthetically simple molecule to produce.

4.7 Conclusion

We paired PTB7, a high performing donor polymer, with a low cost and easy to synthesize acceptor (3BS)₂-SiPc in OPVs and observed a significant improvement in *V_{oc}* values. Device performance was robust to changes in the spin speed, acceptor:donor ratio and annealing; although this hinders a route towards device optimization, it is ultimately a desirable property for high throughput fabrication of OPVs. When replacing the fullerene acceptor with (3BS)₂-SiPc, 80% of the overall device efficiency was retained, while a high average *V_{oc}* of 1.05 V was obtained. These findings further establish SiPc-based acceptors as promising NFA candidates for high voltage OPV devices. Control of the crystallization of the SiPc will be key to yield the desired nanomorphology in the active layer will be key in the development of high performing device.

4.8 Acknowledgements

The Natural Sciences and Engineering Research Council of Canada (NSERC) (2015-509 03987 and STPGP 506661-17 to B.H.L), the Canada Research Chairs Program 950-230724 (B.H.L.). We also thank the Centre for Research in Photonics at the University of Ottawa (CRPuO) for access to the AFM.

4.9 References

- (1) Fusella, M. A.; Lin, Y. L.; Rand, B. P. 20 - Organic Photovoltaics (OPVs): Device Physics, 2nd ed.; Elsevier Ltd., 2019. <https://doi.org/10.1016/B978-0-08-102284-9.00020-6>.
- (2) Parida, B.; Iniyar, S.; Goic, R. A Review of Solar Photovoltaic Technologies. *Renew. Sustain. Energy Rev.* 2011, 15 (3), 1625–1636. <https://doi.org/10.1016/j.rser.2010.11.032>.
- (3) Cai, W.; Gong, X.; Cao, Y. Polymer Solar Cells: Recent Development and Possible Routes for Improvement in the Performance. *Sol. Energy Mater. Sol. Cells* 2010, 94 (2), 114–127. <https://doi.org/10.1016/j.solmat.2009.10.005>.

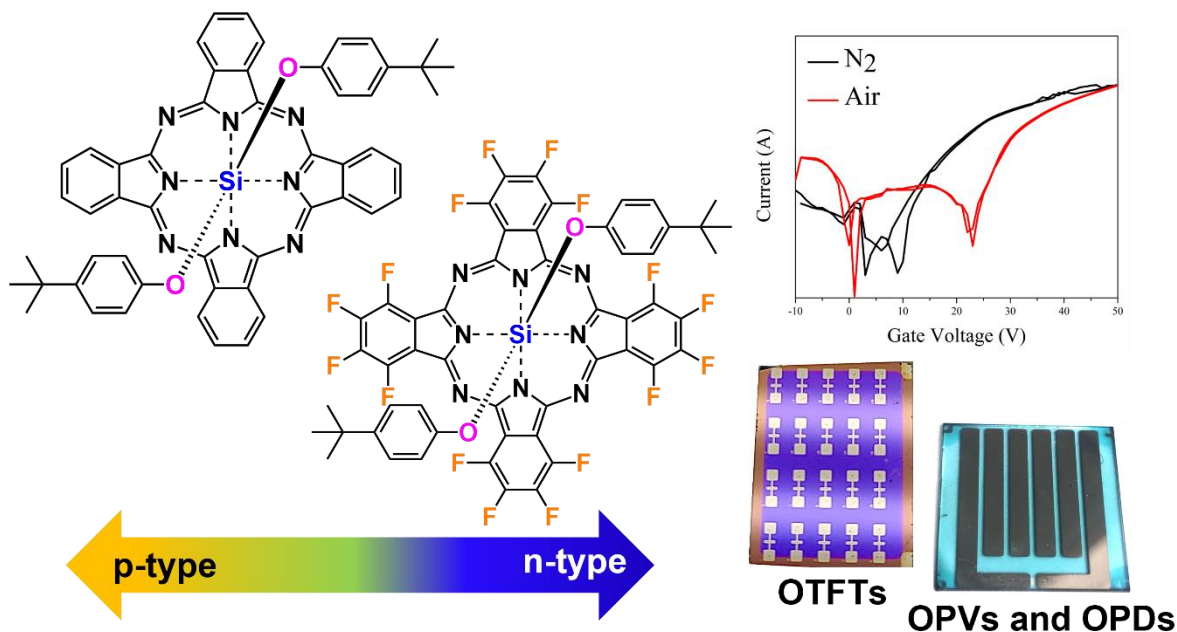
- (4) You, J.; Dou, L.; Yoshimura, K.; Kato, T.; Ohya, K.; Moriarty, T.; Emery, K.; Chen, C.; Gao, J.; Li, G.; et al. A Polymer Tandem Solar Cell with 10.6% Power Conversion Efficiency. *Nat. Commun.* 2013, 4, 1410–1446. <https://doi.org/10.1038/ncomms2411>.
- (5) Lipomi, D. J. Organic Photovoltaics: Focus on Its Strengths. *Joule* 2018, 2 (2), 195–198. <https://doi.org/10.1016/j.joule.2017.12.011>.
- (6) Yuan, J.; Zhang, Y.; Yuan, J.; Zhang, Y.; Zhou, L.; Zhang, G.; Yip, H.; Lau, T.; Lu, X. Single-Junction Organic Solar Cell with over 15 % Efficiency Using Fused-Ring Acceptor with Electron-Deficient Core Single-Junction Organic Solar Cell with over 15 % Efficiency Using Fused-Ring Acceptor with Electron-Deficient Core. *Joule* 2019, 3, 1–12. <https://doi.org/10.1016/j.joule.2019.01.004>.
- (7) Cui, Y.; Yao, H.; Zhang, J.; Zhang, T.; Wang, Y.; Hong, L.; Xian, K.; Xu, B.; Zhang, S.; Peng, J.; et al. Over 16% Efficiency Organic Photovoltaic Cells Enabled by a Chlorinated Acceptor with Increased Open-Circuit Voltages. *Nat. Commun.* 2019, 10 (1), 1–8. <https://doi.org/10.1038/s41467-019-10351-5>.
- (8) Liu, Q.; Jiang, Y.; Jin, K.; Qin, J.; Xu, J.; Li, W.; Xiong, J.; Liu, J.; Xiao, Z.; Sun, K.; et al. 18% Efficiency Organic Solar Cells. *Sci. Bull.* 2020, 65 (4), 272–275. <https://doi.org/10.1016/j.scib.2020.01.001>.
- (9) Cui, Y.; Yao, H.; Zhang, J.; Xian, K.; Zhang, T.; Hong, L.; Wang, Y.; Xu, Y.; Ma, K.; An, C.; et al. Single-Junction Organic Photovoltaic Cells with Approaching 18% Efficiency. *Adv. Mater.* 2020, 32 (19), 1–7. <https://doi.org/10.1002/adma.201908205>.
- (10) Li, N.; Brabec, C. J. Air-Processed Polymer Tandem Solar Cells with Power Conversion Efficiency Exceeding 10%. *Energy Environ. Sci.* 2015, 8 (10), 2902–2909. <https://doi.org/10.1039/c5ee02145f>.
- (11) Zhao, J.; Li, Y.; Hunt, A.; Zhang, J.; Yao, H.; Li, Z.; Zhang, J.; Huang, F.; Ade, H.; Yan, H. A Difluorobenzoxadiazole Building Block for Efficient Polymer Solar Cells. *Adv. Mater.* 2016, 28 (9), 1868–1873. <https://doi.org/10.1002/adma.201504611>.
- (12) Hwang, Y. J.; Li, H.; Courtright, B. A. E.; Subramaniyan, S.; Jenekhe, S. A. Nonfullerene Polymer Solar Cells with 8.5% Efficiency Enabled by a New Highly Twisted Electron Acceptor Dimer. *Adv. Mater.* 2016, 28 (1), 124–131. <https://doi.org/10.1002/adma.201503801>.
- (13) Zhang, J.; Zhang, Y.; Fang, J.; Lu, K.; Wang, Z.; Ma, W.; Wei, Z. Conjugated Polymer-Small Molecule Alloy Leads to High Efficient Ternary Organic Solar Cells. *J. Am. Chem. Soc.* 2015, 137 (25), 8176–8183. <https://doi.org/10.1021/jacs.5b03449>.
- (14) Yang Michael, Y.; Chen, W.; Dou, L.; Chang, W. H.; Duan, H. S.; Bob, B.; Li, G.; Yang, Y. High-Performance Multiple-Donor Bulk Heterojunction Solar Cells. *Nat. Photonics* 2015, 9 (3), 190–198. <https://doi.org/10.1038/nphoton.2015.9>.
- (15) Doumon, N. Y.; Houard, F. V.; Dong, J.; Yao, H.; Portale, G.; Hou, J.; Koster, L. J. A. Energy Level Modulation of ITIC Derivatives: Effects on the Photodegradation of Conventional and Inverted Organic Solar Cells. *Org. Electron.* 2019, 69 (February), 255–262. <https://doi.org/10.1016/j.orgel.2019.03.037>.
- (16) Sullivan, P.; Schumann, S.; Da Campo, R.; Howells, T.; Duraud, A.; Shipman, M.; Hatton, R. A.; Jones, T. S. Ultra-High Voltage Multijunction Organic Solar Cells for Low-Power Electronic Applications. *Adv. Energy Mater.* 2013, 3 (2), 239–244. <https://doi.org/10.1002/aenm.201200560>.
- (17) Sullivan, P.; Duraud, A.; Hancox, L.; Beaumont, N.; Mirri, G.; Tucker, J. H. R.; Hatton, R. A.; Shipman, M.; Jones, T. S. Halogenated Boron Subphthalocyanines as Light Harvesting Electron Acceptors in Organic Photovoltaics. *Adv. Energy Mater.* 2011, 1 (3), 352–355. <https://doi.org/10.1002/aenm.201100036>.

- (18) Tipnis, R.; Bernkopf, J.; Jia, S.; Krieg, J.; Li, S.; Storch, M.; Laird, D. Large-Area Organic Photovoltaic Module-Fabrication and Performance. *Sol. Energy Mater. Sol. Cells* 2009, 93 (4), 442–446. <https://doi.org/10.1016/j.solmat.2008.11.018>.
- (19) Cheng, H. W.; Zhang, H.; Lin, Y. C.; She, N. Z.; Wang, R.; Chen, C. H.; Yuan, J.; Tsao, C. S.; Yabushita, A.; Zou, Y.; et al. Realizing Efficient Charge/Energy Transfer and Charge Extraction in Fullerene-Free Organic Photovoltaics via a Versatile Third Component. *Nano Lett.* 2019, 19 (8), 5053–5061. <https://doi.org/10.1021/acs.nanolett.9b01344>.
- (20) Zhao, W.; Li, S.; Zhang, S.; Liu, X.; Hou, J. Ternary Polymer Solar Cells Based on Two Acceptors and One Donor for Achieving 12.2% Efficiency. *Adv. Mater.* 2017, 29 (2). <https://doi.org/10.1002/adma.201604059>.
- (21) Baran, D.; Ashraf, R. S.; Hanifi, D. A.; Abdelsamie, M.; Gasparini, N.; Röhr, J. A.; Holliday, S.; Wadsworth, A.; Lockett, S.; Neophytou, M.; et al. Reducing the Efficiency-Stability-Cost Gap of Organic Photovoltaics with Highly Efficient and Stable Small Molecule Acceptor Ternary Solar Cells. *Nat. Mater.* 2017, 16 (3), 363–369. <https://doi.org/10.1038/nmat4797>.
- (22) Pascual-San-José, E.; Rodríguez-Martínez, X.; Adel-Abdelaleim, R.; Stella, M.; Martínez-Ferrero, E.; Campoy-Quiles, M. Blade Coated P3HT:Non-Fullerene Acceptor Solar Cells: A High-Throughput Parameter Study with a Focus on up-Scalability. *J. Mater. Chem. A* 2019, 7 (35), 20369–20382. <https://doi.org/10.1039/c9ta07361b>.
- (23) Wadsworth, A.; Moser, M.; Marks, A.; Little, M. S.; Gasparini, N.; Brabec, C. J.; Baran, D.; McCulloch, I. Critical Review of the Molecular Design Progress in Non-Fullerene Electron Acceptors towards Commercially Viable Organic Solar Cells. *Chem. Soc. Rev.* 2019, 48 (6), 1596–1625. <https://doi.org/10.1039/c7cs00892a>.
- (24) Grant, T. M.; Kaller, K. L. C.; Coathup, T. J.; Rice, N. A.; Hinzer, K.; Lessard, B. H. High Voc Solution-Processed Organic Solar Cells Containing Silicon Phthalocyanine as a Non-Fullerene Electron Acceptor. *Org. Electron.* 2020, 87 (June), 105976. <https://doi.org/10.1016/j.orgel.2020.105976>.
- (25) Doumon, N. Y.; Wang, G.; Qiu, X.; Minnaard, A. J.; Chiechi, R. C.; Koster, L. J. A. 1,8-Diiodooctane Acts As a Photo-Acid in Organic Solar Cells. *Sci. Rep.* 2019, 9 (1), 1–14. <https://doi.org/10.1038/s41598-019-40948-1>.
- (26) Zysman-Colman, E.; Ghosh, S. S.; Xie, G.; Varghese, S.; Chowdhury, M.; Sharma, N.; Cordes, D. B.; Slawin, A. M. Z.; Samuel, I. D. W. Solution-Processable Silicon Phthalocyanines in Electroluminescent and Photovoltaic Devices. *ACS Appl. Mater. Interfaces* 2016, 8 (14), 9247–9253. <https://doi.org/10.1021/acsami.5b12408>.
- (27) Grant, T. M.; Dindault, C.; Rice, N. A.; Swaraj, S.; Lessard, B. H. Synthetically Facile Organic Solar Cells with > 4% Efficiency Using P3HT and a Silicon Phthalocyanine Non-Fullerene Acceptor. *Mater. Adv.* 2021. <https://doi.org/10.1039/D1MA00165E>.
- (28) Mitra, K.; Hartman, M. C. T. Silicon Phthalocyanines: Synthesis and Resurgent Applications. *Org. Biomol. Chem.* 2021. <https://doi.org/10.1039/d0ob02299c>.
- (29) Melville, O. A.; Lessard, B. H.; Bender, T. P. Phthalocyanine-Based Organic Thin-Film Transistors: A Review of Recent Advances. *ACS Appl. Mater. Interfaces* 2015, 7 (24), 13105–13118. <https://doi.org/10.1021/acsami.5b01718>.
- (30) Melville, O. A.; Grant, T. M.; Mirka, B.; Boileau, N. T.; Park, J.; Lessard, B. H. Ambipolarity and Air Stability of Silicon Phthalocyanine Organic Thin-Film Transistors. *Adv. Electron. Mater.* 2019, 5 (1900087), 1–7. <https://doi.org/10.1002/aelm.201900087>.
- (31) Melville, O. A.; Grant, T. M.; Lessard, B. H. Silicon Phthalocyanines as N-Type Semiconductors in Organic Thin Film Transistors. *J. Mater. Chem. C* 2018, 6 (20), 5482–5488. <https://doi.org/10.1039/c8tc01116h>.

- (32) Yutronkie, N. J.; Grant, T. M.; Melville, O. A.; Lessard, B. H.; Brusso, J. L. Old Molecule, New Chemistry: Exploring Silicon Phthalocyanines as Emerging N-Type Materials in Organic Electronics. *Materials* (Basel). 2019, 12 (8), 5–10. <https://doi.org/10.3390/ma12081334>.
- (33) Grant, T. M.; Rice, N. A.; Muccioli, L.; Castet, F.; Lessard, B. H. Solution-Processable n-Type Tin Phthalocyanines in Organic Thin Film Transistors and as Ternary Additives in Organic Photovoltaics. *ACS Appl. Electron. Mater.* 2019, 1 (4), 494–504. <https://doi.org/10.1021/acsaelm.8b00113>.
- (34) King, B.; Melville, O. A.; Rice, N. A.; Kashani, S.; Tonnelé, C.; Raboui, H.; Swaraj, S.; Grant, T. M.; McAfee, T.; Bender, T. P.; et al. Silicon Phthalocyanines for N-Type Organic Thin-Film Transistors: Development of Structure–property Relationships. *ACS Appl. Electron. Mater.* 2021. <https://doi.org/10.1021/acsaelm.0c00871>.
- (35) Zysman-Colman, E.; Ghosh, S. S.; Xie, G.; Varghese, S.; Chowdhury, M.; Sharma, N.; Cordes, D. B.; Slawin, A. M. Z.; Samuel, I. D. W. Solution-Processable Silicon Phthalocyanines in Electroluminescent and Photovoltaic Devices. *ACS Appl. Mater. Interfaces* 2016, 8 (14), 9247–9253. <https://doi.org/10.1021/acsaami.5b12408>.
- (36) Pearson, A. J.; Plint, T.; Jones, S. T. E.; Lessard, B. H.; Credgington, D.; Bender, T. P.; Greenham, N. C. Silicon Phthalocyanines as Dopant Red Emitters for Efficient Solution Processed OLEDs. *J. Mater. Chem. C* 2017, 5 (48), 12688–12698. <https://doi.org/10.1039/c7tc03946h>.
- (37) Plint, T.; Lessard, B. H.; Bender, T. P. Assessing the Potential of Group 13 and 14 Metal/Metalloid Phthalocyanines as Hole Transport Layers in Organic Light Emitting Diodes. *J. Appl. Phys.* 2016, 119 (14), 1455021–1455029. <https://doi.org/10.1063/1.4945377>.
- (38) Honda, S.; Ohkita, H.; Benten, H.; Ito, S. Multi-Colored Dye Sensitization of Polymer/Fullerene Bulk Heterojunction Solar Cells. *Chem. Commun.* 2010, 46 (35), 6596–6598. <https://doi.org/10.1039/c0cc01787f>.
- (39) Ke, L.; Gasparini, N.; Min, J.; Zhang, H.; Adam, M.; Rechberger, S.; Forberich, K.; Zhang, C.; Spiecker, E.; Tykwinski, R. R.; et al. Panchromatic Ternary/Quaternary Polymer/Fullerene BHJ Solar Cells Based on Novel Silicon Naphthalocyanine and Silicon Phthalocyanine Dye Sensitizers. *J. Mater. Chem. A* 2017, 5 (6), 2550–2562. <https://doi.org/10.1039/C6TA08729A>.
- (40) Honda, S.; Yokoya, S.; Ohkita, H.; Benten, H.; Ito, S. Light-Harvesting Mechanism in Polymer/Fullerene/Dye Ternary Blends Studied by Transient Absorption Spectroscopy. *J. Phys. Chem. C* 2011, 115 (22), 11306–11317. <https://doi.org/10.1021/jp201742v>.
- (41) Ke, L.; Min, J.; Adam, M.; Gasparini, N.; Hou, Y.; Perea, J. D.; Chen, W.; Zhang, H.; Fladischer, S.; Sale, A.-C.; et al. A Series of Pyrene-Substituted Silicon Phthalocyanines as Near-IR Sensitizers in Organic Ternary Solar Cells. *Adv. Energy Mater.* 2016, 6 (7), 1502355. <https://doi.org/10.1002/aenm.201502355>.
- (42) Po, R.; Bianchi, G.; Carbonera, C.; Pellegrino, A. “all That Glisters Is Not Gold”: An Analysis of the Synthetic Complexity of Efficient Polymer Donors for Polymer Solar Cells. *Macromolecules* 2015, 48 (3), 453–461. <https://doi.org/10.1021/ma501894w>.
- (43) Andersen, T. R.; Weyhe, A. T.; Tao, Q.; Zhao, F.; Qin, R.; Zhang, S.; Chen, H.; Yu, D. Novel Cost-Effective Acceptor:P3HT Based Organic Solar Cells Exhibiting the Highest Ever Reported Industrial Readiness Factor. *Mater. Adv.* 2020, 1 (4), 658–665. <https://doi.org/10.1039/d0ma00133c>.
- (44) Brabec, C. J.; Distler, A.; Du, X.; Egelhaaf, H. J.; Hauch, J.; Heumueller, T.; Li, N. Material Strategies to Accelerate OPV Technology Toward a GW Technology. *Adv. Energy Mater.* 2020, 10 (43), 1–10. <https://doi.org/10.1002/aenm.202001864>.
- (45) Du, X.; Heumueller, T.; Gruber, W.; Classen, A.; Unruh, T.; Li, N.; Brabec, C. J. Efficient Polymer Solar Cells Based on Non-Fullerene Acceptors with Potential Device Lifetime Approaching 10 Years. *Joule* 2019, 3 (1), 215–226. <https://doi.org/10.1016/j.joule.2018.09.001>.

- (46) Vebber, M. C.; Grant, T. M.; Brusso, J. L.; Lessard, B. H. Bis (Tri-Alkylsilyl Oxide) Silicon Phthalocyanines: Understanding the Role of Solubility on Device Performance as Ternary Additives in Organic Photovoltaics. *Langmuir* 2020, 36, 2612–2621. <https://doi.org/10.1021/acs.langmuir.9b03772>.
- (47) Grant, T. M.; Gorisse, T.; Dautel, O.; Wantz, G.; Lessard, B. H. Multifunctional Ternary Additive in Bulk Heterojunction OPV: Increased Device Performance and Stability. *J. Mater. Chem. A* 2017, 5 (4), 1581–1587. <https://doi.org/10.1039/c6ta08593h>.
- (48) Mazziio, K. A.; Luscombe, C. K. The Future of Organic Photovoltaics. *Chem. Soc. Rev.* 2015, 44 (1), 78–90. <https://doi.org/10.1039/c4cs00227j>.
- (49) Mouhamad, Y.; Mokarian-Tabari, P.; Clarke, N.; Jones, R. A. L.; Geoghegan, M. Dynamics of Polymer Film Formation during Spin Coating. *J. Appl. Phys.* 2014, 116 (12). <https://doi.org/10.1063/1.4896674>.
- (50) Ebenhoch, B.; Thomson, S. A. J.; Genevičius, K.; Juška, G.; Samuel, I. D. W. Charge Carrier Mobility of the Organic Photovoltaic Materials PTB7 and PC71BM and Its Influence on Device Performance. *Org. Electron.* 2015, 22, 62–68. <https://doi.org/10.1016/j.orgel.2015.03.013>.
- (51) Zheng, Y.; Wang, G.; Huang, D.; Kong, J.; Goh, T. H.; Huang, W.; Yu, J.; Taylor, A. D. Binary Solvent Additives Treatment Boosts the Efficiency of PTB7:PCBM Polymer Solar Cells to Over 9.5%. *Sol. RRL* 2018, 2 (4), 1–8. <https://doi.org/10.1002/solr.201700144>.
- (52) Lessard, B. H.; Dang, J. D.; Grant, T. M.; Gao, D.; Seferos, D. S.; Bender, T. P. Bis(Tri- n -Hexylsilyl Oxide) Silicon Phthalocyanine: A Unique Additive in Ternary Bulk Heterojunction Organic Photovoltaic Devices. *ACS Appl. Mater. Interfaces* 2014, 6 (17), 15040–15051. <https://doi.org/10.1021/am503038t>.
- (53) Dang, M.-T.; Grant, T. M.; Yan, H.; Seferos, D. S.; Lessard, B. H.; Bender, T. P.; Miller, J. a.; Goethem, E. M. Van; Kenney, M. E.; Lu, Z.-H. Bis(Tri-n-Alkylsilyl Oxide) Silicon Phthalocyanines: A Start to Establishing a Structure Property Relationship as Both Ternary Additives and Non-Fullerene Electron Acceptors in Bulk Heterojunction Organic Photovoltaic Devices. *J. Mater. Chem. A* 2017, 126, 3378–3379. <https://doi.org/10.1039/C6TA10739G>.
- (54) Wodo, O.; Tirthapura, S.; Chaudhary, S.; Ganapathysubramanian, B. A Graph-Based Formulation for Computational Characterization of Bulk Heterojunction Morphology. *Org. Electron.* 2012, 13 (6), 1105–1113. <https://doi.org/10.1016/j.orgel.2012.03.007>.
- (55) Lyons, B. P.; Clarke, N.; Groves, C. The Relative Importance of Domain Size, Domain Purity and Domain Interfaces to the Performance of Bulk-Heterojunction Organic Photovoltaics. *Energy Environ. Sci.* 2012, 5 (6), 7657–7663. <https://doi.org/10.1039/c2ee21327c>.
- (56) Martín-Gomis, L.; Seetharaman, S.; Herrero, D.; Karr, P. A.; Fernández-Lázaro, F.; D'Souza, F.; Sastre-Santos, Á. Distance-Dependent Electron Transfer Kinetics in Axially Connected Silicon Phthalocyanine-Fullerene Conjugates. *ChemPhysChem* 2020, 21 (20), 2254–2262. <https://doi.org/10.1002/cphc.202000578>.
- (57) Grell, M.; Bradley, D. D. C.; Long, X.; Chamberlain, T.; Inbasekaran, M.; Woo, E. P.; Soliman, M. Chain Geometry, Solution Aggregation and Enhanced Dichroism in the Liquid-Crystalline Conjugated Polymer Poly(9,9-Dioctylfluorene). *Acta Polym.* 1998, 49 (8), 439–444. [https://doi.org/10.1002/\(SICI\)1521-4044\(199808\)49:8<439::AID-APOL439>3.0.CO;2-A](https://doi.org/10.1002/(SICI)1521-4044(199808)49:8<439::AID-APOL439>3.0.CO;2-A).

5. FROM P-TYPE TO N-TYPE: PERIPHERAL FLUORINATION OF AXIALLY SUBSTITUTED SILICON PHTHALOCYANINES ENABLES FINE TUNING OF CHARGE TRANSPORT.



This chapter contains work published in *The Canadian Journal of Chemical Engineering*.

Mário C. Veber, Benjamin King, Callum French, Mathieu Tousignant, Bahar Ronnasi, Chloé Dindault, Guillaume Wantz, Lionel Hirsch, Jaclyn Brusso, and Benoît H. Lessard. *Can J Chem Eng.* **2023**; 1–13.

5.1 Context

After exploring the properties of $(R_3SiO)_2$ -SiPc:P3HT blends followed by attempts to pair these acceptors with different conjugated polymers, it became clear that tailoring the electrochemical properties of SiPcs was required in order to facilitate their application with modern conjugated polymers. Presently, it appears that $(R_3SiO)_2$ -SiPc derivatives require a large driving force for effective charge transfer to occur, similarly to fullerene acceptors, which therefore necessitates lowering the energy level of the frontier molecular orbitals. Deepening of these energy levels has also been associated with improved n-type behaviour, electron affinity and air-stability. Fluorination is known to achieve that goal in organic semiconductors, while the relatively small size of fluorine atoms tends not to disrupt the solid-state intermolecular interactions (i.e., π - π interactions). Due to the relative difficulty in obtaining these compounds, fluorinated SiPcs have

only recently (2021) been reported for the first time and are widely understudied when compared to other metal phthalocyanine analogues. Here, I attempted to improve the existing chemistry (as reported in the literature) and synthesize for the first time fluorinated SiPcs ($(\text{tb-Ph})_2\text{-F}_X\text{SiPc}$) axially substituted with phenoxy groups. Assessment of how the degree of fluorination affects their electrochemical and physical properties was also carried out. The materials produced here were incorporated in OPVs, OTFTs and OPDs (organic photodetectors), to better evaluate their potential and the changes that occur in their semiconducting behaviour. We will also assess if improved n-type mobility and air-stability can be achieved. 0

5.2 Contributions

I synthesized and characterized all the $(\text{tb-Ph})_2\text{-F}_X\text{SiPc}$ derivatives, produced all the OPV devices and assessed all the performance metrics. BK and CF produced all OTFT devices and assessed performance metrics. CD, GW, LH produced all OPD devices and assessed performance metrics. BK and MT obtained thin film AFM images. BR carried out DSC analysis. Manuscript was also written by me with contributions from all authors. BL and JB supervised the project.

5.3 Abstract

Silicon phthalocyanines ($\text{R}_2\text{-SiPcs}$) are a family of promising tunable materials for organic electronic applications. We report the chemistry for the synthesis of axially substituted fluorinated SiPcs $(\text{tb-Ph})_2\text{-F}_X\text{SiPc}$ (where $X=0, 4, 8$ or 16) and explored how the degree of fluorination effects optical and electronic properties. A new treatment with boron trichloride was included to obtain $\text{Cl}_2\text{-F}_X\text{SiPcs}$ from $\text{F}_2\text{-F}_X\text{SiPcs}$, activating the axial position for further functionalization. We observed that, as the degree of fluorination increased, so did the electron affinity of the compounds, leading to a drop in the frontier orbital energy levels, as measured by electrochemistry and ultraviolet photoelectron spectroscopy (UPS). The deeper energy levels enabled successful $(\text{tb-Ph})_2\text{-F}_4\text{SiPc}$ and PTQ10 blends for organic photovoltaics and photodetectors. All four compounds were incorporated in organic thin-film transistors (OTFTs) where the degree of fluorination influenced device operation, changing it from p-type conduction for $(\text{tb-Ph})_2\text{-F}_0\text{SiPc}$, to ambipolar for $(\text{tb-Ph})_2\text{-F}_4\text{SiPc}$, and n-type for $(\text{tb-Ph})_2\text{-F}_8\text{SiPc}$ and $(\text{tb-Ph})_2\text{-F}_{16}\text{SiPc}$. The OTFT devices made with $(\text{tb-Ph})_2\text{-F}_{16}\text{SiPc}$ achieved a low average threshold voltage of 7.0 V in N_2 and retained its n-type mobility when exposed to air.

5.4 Introduction

The range of available synthetic techniques and functional groups in organic chemistry brings unique opportunities in fine-tuning physical and electrochemical properties of active materials for applications in electronic devices.^{1,2} As such, metal and metalloid-containing phthalocyanines (MPcs) have had an important role in the history of semiconductors, due to their chemical versatility, highly delocalized electron density, good thermal stability, and facile, low-cost synthesis.^{3–5} The majority of reported MPcs are divalent such as zinc or copper containing MPcs, however, trivalent and tetravalent MPcs have also experienced increased interest in recent years.

Silicon phthalocyanines (R_2 -SiPcs) are an exciting class of MPcs, exhibiting enhanced electron-transporting behavior in thin-film electronics,^{6,7} and possessing two axial handles for functionalization and property fine-tuning.^{8–11} R_2 -SiPcs also have a synthetic complexity index (SC) which is many times lower than most high performing electron transport materials, making them favourable candidates for commercial printed electronics.^{12,13} R_2 -SiPcs have been incorporated into a wide range of organic electronic devices, namely organic thin-film transistors (OTFTs) and organic photovoltaics (OPVs).^{6,14,23–26,15–22} While classically paired with P3HT, the highest occupied molecular orbital (HOMO) and lowest unoccupied molecular orbital (LUMO) energy levels of R_2 -SiPcs are not typically compatible with state-of-the-art polymer donors, such as poly[N-9'-heptadecanyl-2,7-carbazole-alt-5,5-(4',7'-di-2-thienyl-2',1',3'-benzothiadiazole)] (PCDTBT) and poly[[6,7-difluoro[(2-hexyldecyl)oxy]-5,8-quinoxalinediyl]-2,5-thiophenediyl] (PTQ10).^{25,27–34} In OTFTs, the electron-rich nature of the R_2 -SiPc ring may limit its electron affinity and hence lead to high threshold voltages (V_T), limited charge carrier mobilities (μ) and poor air-stability.^{6,7,26,35} Air-stability in n-type or electron-transporting organic semiconductors incorporated into OTFTs is an ongoing challenge.^{36–39} The electron transfer from organic semiconductors with shallow LUMO levels onto oxygen present in air is generally favored, leading oxygen to act as a charge trap in such devices.³⁷

The introduction of electron-withdrawing groups to the periphery of the MPc ring may be key to address n-type air stability, by removing electron density from the MPc ring and deepening the HOMO and LUMO levels. Fluorine is a promising choice for a peripheral electron-withdrawing group, since its small atomic radius does not disrupt molecular packing,⁴⁰ and in fact may improve intermolecular interactions,^{2,41,42} favoring face-to-face and face-on packing of

conjugated molecules,^{41,43} stabilize the electronic orbitals,⁴⁴ and enhance the n-type conductivity of the semiconductor.³² A few examples of fluorinated phthalocyanines (F_XMPc) have been reported in literature, such as F_XCoPc ,^{42,45} F_XFePc ,⁴⁶ and F_XZnPc .^{42,47,48} Copper hexadecafluorophthalocyanines ($F_{16}CuPc$) is arguably the most extensively studied F_XMPc ,^{42,43,49,50} and has been employed in evaporated OTFTs with mobilities as high as $0.26 \text{ cm}^2 \text{ V}^{-1} \text{ s}^{-1}$, owing to improved electron conductivity and solid-state packing.^{51,52}

While these F_XMPc s have been studied for over two decades, the synthesis of a peripherally-fluorinated silicon phthalocyanine (R_2-F_XSiPc) was first reported by our group in 2021.²⁶ $F_{16}SiPc$ s are relatively complex to synthesize because, unlike most MPc s, they are not obtainable in appreciable yields when directly reacting a silicon source to phthalonitriles,¹⁶ requiring coupling of isoindoline groups.⁵ This increases the probability of side-reactions and degradation, which become more prominent when using partially fluorinated starting materials that tend to be more reactive than their nonfluorinated counterparts, due to uneven electron cloud distribution.⁵³ In addition, the currently reported procedure produces axially fluorinated $F_2-F_{16}SiPc$, as opposed to $Cl_2-F_{16}SiPc$, which is the preferred starting material for further axial functionalization of $SiPc$ s.⁵ Therefore, in the present work we develop the chemistry and report the characterization of novel R_2-F_XSiPc derivatives and assess how the degree of fluorination affects thermal, electrochemical and physical properties. We also integrated the R_2-F_XSiPc into preliminary OPVs, OPDs and OTFTs and found that as the number of peripheral fluorine atoms on the R_2-SiPc ring increases, the n-type characteristics of the films incorporated into devices become more prominent. Furthermore, air-stable electron transport was observed in perfluorinated $F_{16}SiPc$ devices.

5.5 Experimental

5.5.1 Materials

Tetrafluorophthalonitrile (98%), 4,5-Difluorophthalonitrile(95%) and 4-Fluorophthalonitrile (98%) were purchased from TCI America. Lithium bis(trimethylsilyl)amide (LiHMDS, 97%), silicon tetrachloride (99%), tetraline (anhydrous, 99%), chlorobenzene (anhydrous,99%) and 4-tertbutylphenol (99%) were purchased from Sigma-Aldrich. PTQ10 (60 kDa, PDI 2.3) was purchased from Brilliant Matters.

5.5.2 Synthesis

Synthesis of hexadecafluoro silicon phthalocyanine difluoride ($F_2-F_{16}SiPc$): in a typical procedure,²⁶ tetrafluorophthalonitrile (5 g, 0.025 mol) was charged into a pre-dried 500 ml 3-neck round bottom flask, which was connected to a condenser and a bubbler. The flask was then sealed with rubber septa and purged for 45 min with N_2 . Anhydrous tetraline (250 mL) was introduced to the flask via cannula, with gentle stirring. Most of the tetrafluorophthalonitrile dissolved, but larger chunks remained. After that, LiHMDS·Et₂O (3.5 g, 0.015 mol) was added while keeping a strong N_2 flow, to avoid moisture and air from entering the reaction medium. Upon addition, the solution quickly turned orange, brown and then practically black. The flask was sealed again, and the reaction was left to stir (600 RPM) at room temperature. After 2 hours, silicon tetrachloride (4 ml, 0.035 mol) was added to the solution via syringe through a septum, and the temperature was set to 200°C. After 16 h of vigorous stirring (1000 RPM) under N_2 the reaction mixture was cooled to room temperature, admixed with hexanes (200 ml), and filtered through a medium porosity fritted glass filter, with the aid of a vacuum pump. The collected precipitate was subsequently washed with methanol (300-500 ml), acetone (200 ml), toluene (100 ml) and hexanes (100 ml), affording a blueish green powder in the filter. Crude yield: 1.2 g (22%).

Synthesis of octafluoro silicon phthalocyanine difluoride (F_2-F_8SiPc): same procedure as $F_2-F_{16}SiPc$ was followed, replacing tetrafluorophthalonitrile by 4,5-difluorophthalonitrile, and keeping the same molar ratios. Crude yield: 1.6 g (21%).

Synthesis of tetrafluoro silicon phthalocyanine difluoride (F_2-F_4SiPc): same procedure as $F_2-F_{16}SiPc$ was followed, replacing tetrafluorophthalonitrile by 4-fluorophthalonitrile, and keeping the same molar ratios. Crude yield: 2.4 g (43%).

Chlorination of the axial position (Cl_2-F_xSiPc): in a typical procedure, F_2-F_xSiPc (1g) was charged into a 250 ml round bottom flask and after purging with N_2 for 30 min anhydrous chlorobenzene (100 ml) was added to the flask via cannula. Upon ceasing N_2 flow, boron trichloride (4 ml, 1M solution in heptanes) was added to the reaction mixture through a septum. Moderate stirring (500 RPM) was kept while the reaction mixture was heated to 100°C. While heating the reaction mixture, a needle was kept on the septum, to prevent pressure from building up, and was removed when the target temperature was achieved. The reaction was carried out in the sealed container for 72-96h. The mixture was subsequently cooled to room temperature and

filtered by gravity. The product was washed with methanol (100 ml) and hexanes (100ml). Crude product used as is in the next steps. Crude yield: 0.95- 1.0g.

Synthesis of Bis(Tertbutylphenoxy) silicon hexadecafluorophthalocyanine ((tb-Ph)₂-F₁₆SiPc): procedure was adapted from Melville *et al.*⁵⁴ Cl₂-F₁₆SiPc (500 mg, 0.57 mmol) was charged in a 100 ml 3-neck round bottom flask with 4-tertbutylphenol (866 mg, 5.7 mmol). The flask was purged with N₂ for 30 minutes, before adding anhydrous chlorobenzene (10 ml) via cannula. The reaction was carried out at reflux (132°C) for 16h. The reaction mixture was filtered and washed with warm chloroform (50-60°C, 100-300 ml) until the filtrate ran clear. Solvents in the filtrate were removed under reduced pressure in a rotary evaporator. Affording a waxy, teal residue, at which point MeOH was added in 50 ml portions and filtered, to remove unreacted phenols. After 3-5 washes, only powdery dark blue solids remained. Purification was carried out by train sublimation at 130 mtorr and 280°C. Purified yield: 148 mg (23%). ¹HNMR: 5.72 ppm (m, 4H); 2.40 ppm (m, 4H); 0.67 ppm (s, 18H). ¹⁹FNMR: -137.2 ppm; -146.0 ppm. HR-MS: expected mass 1126.2, obtained mass 1127.2. Connectivity confirmed by SC-XRD.

Synthesis of Bis(Tertbutylphenoxy) silicon octafluorophthalocyanine ((tb-Ph)₂-F₈SiPc): same procedure as (tb-Ph)₂-F₁₆SiPc, respecting molar ratios. Cl₂-F₈SiPc (300 mg, 0.42 mmol) was used as starting material. Purified yield: 94 mg (19%). ¹HNMR: 9.31 ppm (m, 8H); 5.56 ppm (m, 4H); 2.19 ppm (m, 4H); 0.58 ppm (s, 18H). ¹⁹FNMR: -128.5 ppm (s). HR-MS: expected mass 982.2, obtained mass 983.3. Connectivity confirmed by SC-XRD.

Synthesis of Bis(Tertbutylphenoxy) silicon tetrafluorophthalocyanine ((tb-Ph)₂-F₄SiPc): same procedure as (tb-Ph)₂-F₁₆SiPc, respecting molar quantities. Cl₂-F₄SiPc (300 mg, 0.48 mmol) was used as starting material. Purified yield: 182 mg (40%). ¹HNMR: 9.53 ppm (m, 4H); 9.16 ppm (m, 4H); 8.02 ppm (m, 4H); 5.56 ppm (m, 4H); 2.26 ppm (m, 4H); 0.58 ppm (s, 18H). ¹⁹FNMR: -106.5 ppm (s). HR-MS: expected mass 910.3, obtained mass 911.3. Connectivity confirmed by SC-XRD.

Bis(Tertbutylphenoxy) silicon phthalocyanine ((tb-Ph)₂-F₀SiPc): the synthesis of (tb-Ph)₂-F₀SiPc was conducted according to previously reported procedures.⁵⁵ Purified yield: 205 mg (32%). ¹HNMR: 9.58 ppm (m, 8H); 8.31 ppm (m, 8H); 5.30 ppm (m, 4H); 2.33 ppm (m, 4H); 0.54 ppm (s, 18H). HR-MS: expected mass 838.3, obtained mass 839.3.

5.5.3 Materials Characterizations

The optical properties of (tb-Ph)₂-F_xSiPc in DCM solution were evaluated by UV-Vis spectroscopy in a Cary 5000 spectrometer, dual-beam mode, from 350 to 800 nm. Electrochemical properties were obtained from both cyclic voltammetry (CV) and ultraviolet photoelectric spectroscopy (UPS). CV voltammograms were obtained from solutions in THF, using three platinum wires as the working, reference and counter electrodes, under N₂, from -1.5 to 1.0 V. Tetrabutylammonium (0.1 M) was used as the electrolyte and ferrocene oxidation as reference potential, allowing LUMO level estimation from the equation $E_{\text{LUMO}} (\text{eV}) = -E_{\text{red,onset}} + E_{\text{oxFc}} - 4.80$. Energy levels were also independently calculated from UPS spectra, using gold as reference and radiation source of 21.2 eV. Thermogravimetric analysis (TGA) was carried out from 25°C to 600°C in a TA instruments Q5000 instrument and decomposition temperatures were calculated at 5% mass drop. Single crystals for X-ray diffraction (SC-XRD) were grown by slow evaporation of chloroform or THF solutions. Powder X-ray diffraction (PXRD) measurements on 50 nm evaporated ((tb-Ph)₂-F_xSiPc films deposited on OTS-functionalized substrates (no electrodes) were performed using a Rigaku Ultima IV powder diffractometer with an X-ray source of Cu K α ($\lambda = 1.5418 \text{ \AA}$) at a scan range of $5^\circ < 2\theta < 20^\circ$ and a scan rate of 0.5°/min. Atomic force microscopy (AFM) images were obtained with a Bruker Dimension Icon using ScanAsyst-Air probes, in the ScanAsyst mode with a scan rate of 0.85 Hz.

5.5.4 Device Preparation

The OPV preparation procedure has been adapted from Vebber *et al.*²⁵ Substrate, transport layers and electrode deposition have not been altered, with overall device structure ITO/ZnO/PTQ10/(tb-Ph)₂-F_xSiPc/MoO_x/Ag. Active layers were spincoated at 1250 RPM, for 60 s, from PTQ10/(tb-Ph)₂-F_xSiPc solutions at 8 mg mL⁻¹ and 1:1 ratio. For OPDs, a (tb-Ph)₂-F₄SiPc acceptor was blended with PTQ10 donor in a 1:1 donor/acceptor weight ratio in chlorobenzene. Polyethylenimine ethoxylated (PEIE) in deionized water solution was spin coated on ITO in order to reduce its work-function. OPDs had an ITO/ZnO/PEIE/bulk active layer/MoO_x/Ag stack structure. Active layer was spincoated from 40 mg mL⁻¹ solutions, first at 400 RPM for 30 s and then at 2000 RPM for 60 s.^{56,57} For OTFT devices, N-doped silicon substrates with a 230 nm thermally grown SiO₂ dielectric layer purchased from WaferPro were washed sequentially with acetone and isopropanol to remove the protective photoresist and dried with nitrogen. Substrates

were then sonicated for 5 min in an acetone bath and then were transferred to a methanol bath and sonicated for an additional five minutes. Sonicated substrates were dried under a nitrogen stream and treated with oxygen plasma under vacuum for 15 min in a Harrick Plasma Cleaner (model no. PDC-32G). The cleaned substrates were rinsed with water followed by isopropanol, dried under nitrogen, and then reacted for 1 h in 20 mL scintillation vials (VWR) containing 3 mL of a 1% v/v solution of n-octyltrichlorosilane (OTS) in toluene. OTS-treated substrates were removed from their vials and washed with toluene before being dried under a nitrogen stream and subsequently dried under vacuum at 70 °C for 1 h to remove residual toluene. Bottom-gate top-contact OTFTs were fabricated from each of the four R₂-SiPc derivatives. First, a 500 Å-thick film was thermally deposited onto OTS-treated substrates held at room temperature in an Angstrom EvoVac evaporator by physical vapor deposition (PVD) through a square shadow mask at a rate of 0.2 Å/s ($P < 2 \times 10^{-6}$ Torr). Substrates were then removed from the evaporator and two corners were scratched with a diamond-tipped pen to expose bare silicon for deposition of the gate electrode. Source and drain electrodes (channel length $L = 30 \mu\text{m}$, width $W = 1000 \mu\text{m}$) as well as gate electrodes in the corners of each substrate were obtained by depositing 100 Å of Mn at a rate of 0.5 Å/s, followed by 500 Å of Ag at a rate of 1 Å/s through shadow masks (Ossila) to yield 20 individual transistors per substrate. Additional devices fabricated with Ag-only electrodes (500 Å) were also prepared using the same deposition rate and shadow masks.

5.5.5 Device Characterization

OPV testing has been carried out following literature procedures,⁵⁸ from -2.0 V to 2.0 V, and device areas of 0.32 cm². OPD testing was carried out according to literature,⁵⁶ from literature,⁵⁹ from 0 V to -2.0 V bias, under dark and 528 nm visible green illumination, All OTFTs were measured at room temperature in a nitrogen glovebox and in air with electrical characterization performed using a custom-built autotester with brass alloy contact tips plated with 20 μm of gold on 100 μm of nickel. The tester was connected to a Keithley 2614B source meter to set the gate-source voltage (V_G) and source-drain voltage (V_{SD}) and measure the source-drain current (I_{DS}). Output curves were obtained by fixing five evenly distributed and discrete V_G values from -10 and +50 V for n-type measurements and +10 to -50V or -70 V for p-type measurements, and sweeping V_{SD} from 0 to +50V for n-type measurements or 0 to -50V for p-type measurements. Transfer curves were obtained by fixing V_{SD} in the saturation region at +50 V for n-type

measurements and -50V for p-type measurements, while sweeping V_G values from -10 and +50 V for n-type measurements and +10 to -50V or -70 V for p-type measurements.

The electron and hole field-effect mobilities (μ) was calculated using equation (1):

$$I_{DS} = \frac{\mu C_i W}{2L} (V_{GS} - V_T)^2 \quad (1)$$

where L and W represent the channel length and width, respectively. The capacitance of the gate dielectric (C_i) is calculated using $C_i = \frac{\epsilon_0 \epsilon_r}{d}$, where d is the thickness of the SiO₂ dielectric (230 nm), ϵ_r is the relative dielectric constant of SiO₂ and ϵ_0 is the permittivity of free space. μ_e was determined by calculating the slope of best fit of a 10V region of $\sqrt{I_{DS}}$ as a function of V_G when the curve became linear. The threshold voltage (V_T) was calculated from the x -intercept of linearized data for $\sqrt{I_{DS}}$ vs V_G in the same measurement range.

5.6 Results and Discussion

5.6.1 Synthesis

We synthesized four novel R₂-F_xSiPc derivatives with varying degrees of peripheral fluorination and axially functionalized with tertbutylphenol (tb-Ph) groups: (tb-Ph)₂-F₀SiPc, (tb-Ph)₂-F₄SiPc, (tb-Ph)₂-F₈SiPc, (tb-Ph)₂-F₁₆SiPc. **Figure 5.1** illustrates the synthetic pathway used where reactions i and ii, have been adapted from Yutronkie *et al.*²⁶ It is not possible to obtain R₂-F_xSiPcs directly from phthalonitriles (**Figure 5.1**), requiring first the formation of the isoindoline group (step i).^{8,16,60} In step ii, which is carried out in the same reaction flask, the cyclization of these groups takes place at high temperatures to form the phthalocyanine ring. High-resolution mass spectroscopy results show the predominance of difluoride species in the crude products, instead of the expected dichloride derivative (**Table 5.1**), which signals that partial degradation of the phthalonitrile core must be taking place, since that is the only source of fluorine in the reaction medium. This seems to also affect the crude yield of the overall reaction, which is \approx 40% for F₂-F₄SiPc and 20-25% for F₂-F₈SiPc and F₂-F₁₆SiPc, compared to typical 80% obtained for non-fluorinated R₂-SiPcs.^{7,27,61}

We attempted different synthetic approaches to increase the yield and favor the production of Cl₂-F₁₆SiPc (**Table C1**, see Appendix C), but the formation of F₂-F₁₆SiPc persisted. Nonetheless, we did improve the F₂-F₁₆SiPc crude yield from our initial report²⁶ going from 9%

to 23%, by reducing the amount of LiHDMS employed, rendering the F_X -phthalonitriles as the excess reagents in the reaction. We surmise R_2-F_XSiPcs , and more specifically $R_2-F_{16}SiPcs$, are very sensitive to attack by bases. This attack has been observed with NaOH, amines, pyridine and bicarbonate solutions, where $R_2-F_{16}SiPcs$ mixtures get discolored (going from teal to dark brown) after a few minutes of mild heating (50-100°C) in the presence of these bases. R_2-F_4SiPc appears to be more resistant, suggesting that the increase in degree of fluorination makes the phthalocyanine ring more susceptible to this type of attack. Regardless of the approach taken we have not been able to favor the formation of Cl_2-F_XSiPcs over F_2-F_XSiPcs .

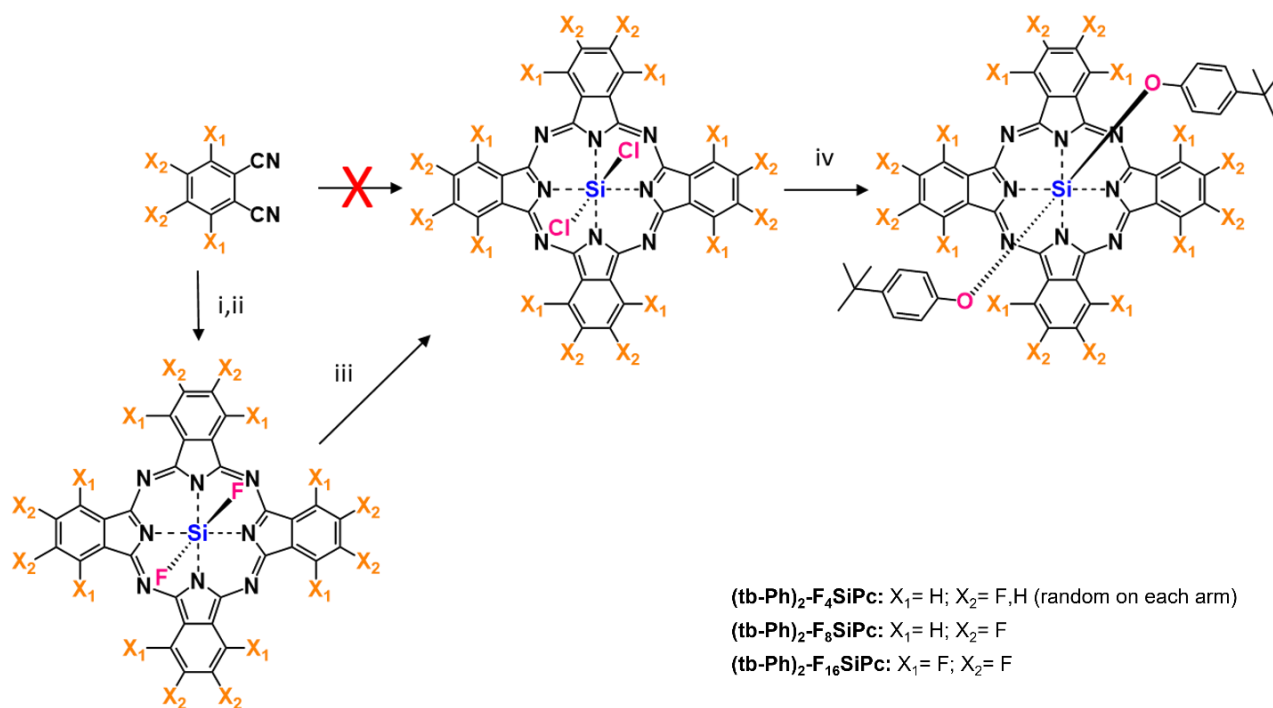


Figure 5.1. Synthetic pathway used in the production of functionalized F_XSiPcs i) Tetraline, LiHDMS, 2 h; ii) $SiCl_4$, 200°C, 16 h; iii) Cl-Benzene, BCl_3 , 100°C, 72h; iv) Cl-Benzene, 4-Tertbutylphenol, 130°C, 16 h.

While axially fluorinated phthalocyanines have their applications and advantages,^{9,26,40,62} they pose a problem when further functionalization is desired. The silicon-fluorine bond is very strong, ~580 kJ/mol, when compared to ~450 kJ/mol bond energy of silicon-oxygen bonds, making it difficult to displace the fluoride ion when reacting with oxygen-containing groups such as phenols, carboxylic acids or even hydroxyls, all of which readily react with $Cl_2-SiPcs$ at high temperatures (>100°C).^{7,60} Therefore, obtaining the Cl_2-F_XSiPcs was imperative to enable

functionalization of this class of $(\text{tb-Ph})_2\text{-F}_x\text{SiPc}$. Step iii then was required to convert the $\text{F}_2\text{-F}_x\text{SiPcs}$ to $\text{Cl}_2\text{-F}_x\text{SiPcs}$. The reaction is slow and requires multiple days, but BCl_3 was able to exchange halogens with the $\text{R}_2\text{-F}_x\text{SiPcs}$,⁶³ leading to the formation of the desired product, as indicated by the increase in the $\text{Cl}_2\text{-F}_x\text{SiPc}$ signal in MS (**Table 5.1**). The percentages of $\text{R}_2\text{-F}_x\text{SiPcs}$ that could be converted to $\text{Cl}_2\text{-F}_x\text{SiPcs}$ is presented in **Table 5.1**, based on the yield of the subsequent reactions with tertbutylphenol (step iv in **Figure 5.1**). Just like the yield, the percentages of $\text{R}_2\text{-F}_x\text{SiPcs}$ that could be converted to $\text{Cl}_2\text{-F}_x\text{SiPcs}$ decreased with increasing peripheral fluorination, likely because there are larger fractions of the product present as $\text{F}_2\text{-F}_x\text{SiPc}$ and not as $\text{Cl}_2\text{-F}_x\text{SiPc}$. For example, $\text{F}_2\text{-F}_{16}\text{SiPcs}$ samples are completely unreactive with phenols and carboxylic acids before the treatment with BCl_3 . All yields increased after treatment with BCl_3 . Therefore, the new step iii implemented here was a crucial point that enabled the exploration of functionalized $\text{R}_2\text{-F}_x\text{SiPc}$ such as adding solubilizing axial groups which enables purification and solution processing.

Table 5.1. Ratio between the $\text{Cl}_2\text{-F}_x\text{SiPc}$ and $\text{F}_2\text{-F}_x\text{SiPc}$ signals in mass spectroscopy analysis and fraction of the $\text{X}_2\text{-F}_x\text{SiPc}$ samples that can be axially functionalized by phenols (Cl-benzene, reflux, 16h).

	Crude		After BCl_3 treatment	
	Chloride/fluoride MS signal ratio	Reaction yield	Chloride/fluoride MS signal ratio	Reaction yield
$\text{X}_2\text{-F}_4\text{SiPc}$	1/100	24%	1/100	40%
$\text{X}_2\text{-F}_8\text{SiPc}$	0	4%	1/100	19%
$\text{X}_2\text{-F}_{16}\text{SiPc}$	0	0%	1/10	23%

5.6.2 Material characterization

The optical and electrochemical properties of the $(\text{tb-Ph})_2\text{-F}_x\text{SiPcs}$ have been evaluated by UV-Vis spectroscopy (**Figure 5.2a**), cyclic voltammetry (CV, **Figure 5.2b**) and ultraviolet photoelectron spectroscopy (UPS, **Figure C1**, see Appendix C). The compounds characteristics, derived from abovementioned techniques, are summarized in **Table 5.2**. The absorption maximum and optical band gap (E_{bg}) measured from both solution and thin films have only small variations across the $(\text{tb-Ph})_2\text{-F}_x\text{SiPcs}$ compounds. This result is consistent with the effect of fluorination of organic semiconductors, which leads to energy drops in both frontier orbitals energy levels, while keeping the E_{bg} relatively constant.⁵¹ HOMO and LUMO levels were estimated from solution

(CV) and thin films (UPS, **Figure 5.3**), yielding mostly consistent results. The potential required to reduce the $(\text{tb-Ph})_2\text{-F}_X\text{SiPc}$ ($E_{\text{Red},1/2}$) gets closer to zero as fluorine content increases, indicating higher electron-affinity. The exception was $(\text{tb-Ph})_2\text{-F}_8\text{SiPc}$, whose solution HOMO level was considerably shallower than the one measured by UPS on thin films. The root cause of this observed difference is not yet clear, but we hypothesize that the $(\text{tb-Ph})_2\text{-F}_8\text{SiPc}$ reduction peak in **Figure 5.2** is the result of a two-electron process, causing the discrepancy observed. Further experimentation should be performed to confirm the hypothesis, however, for the purposes of this work we decided to use the UPS results as primary method to estimate HOMO and LUMO levels. UPS results, demonstrate that as more fluorine atoms are located on the periphery of the $(\text{tb-Ph})_2\text{-F}_X\text{SiPc}$ ring, both HOMO and LUMO levels become deeper, up to 0.8 eV drop when comparing $(\text{tb-Ph})_2\text{-F}_0\text{SiPc}$ to both $(\text{tb-Ph})_2\text{-F}_8\text{SiPc}$ and $(\text{tb-Ph})_2\text{-F}_{16}\text{SiPc}$, which is consistent with reported values for F_{16}CuPc ⁵¹ and fluoro aluminum phthalocyanine (F-AlPc).⁶²

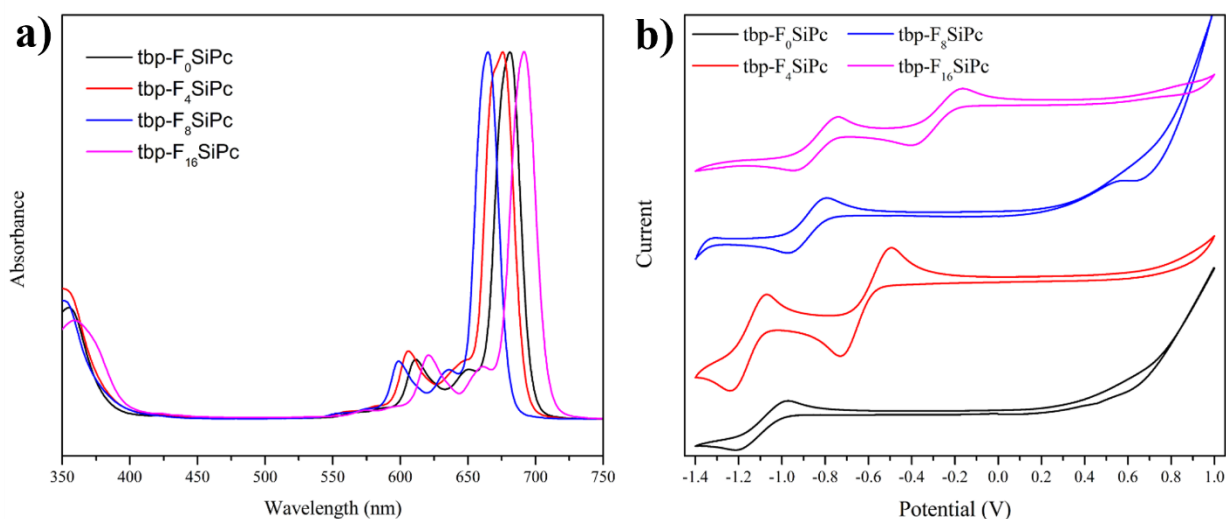


Figure 5.2. a) Solution UV-Vis spectra (in DCM) and b) voltammograms of $(\text{tb-Ph})_2\text{-F}_{16}\text{SiPc}$.

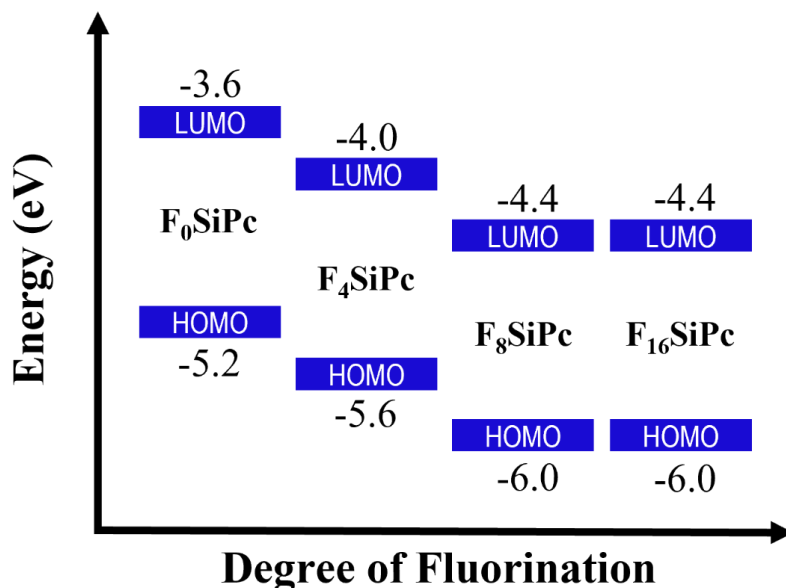


Figure 5.3. HOMO and LUMO energy levels of $(\text{tb-Ph})_2\text{-F}_{16}\text{SiPc}$ estimated from UPS data.

The thermal properties of the $(\text{tb-Ph})_2\text{-F}_x\text{SiPcs}$ have been evaluated by thermal gravimetric analysis (TGA) and differential scanning calorimetry (DSC) (**Figure C2**). While we observed lower chemical stability for $\text{R}_2\text{-F}_x\text{SiPcs}$, compared to the non-fluorinated counterparts, specifically towards bases, the thermal stability is less significantly altered. Only $(\text{tb-Ph})_2\text{-F}_{16}\text{SiPc}$ has a modest decrease in thermal stability, calculated from 5% mass loss cutoff. Regardless, all $(\text{tb-Ph})_2\text{-F}_x\text{SiPcs}$ have degradation temperatures (T_d) above 350 °C, which is typical for phenol-substituted $\text{R}_2\text{-SiPcs}$.^{64,65} No DSC transitions were observed up to 250 °C, demonstrating that $(\text{tb-Ph})_2\text{-F}_x\text{SiPcs}$ remain solid over a wide range of temperatures. The thermal stability coupled with the solubility imparted by the tert-butylphenol groups means such compounds can be processed by both solution and evaporation.

Table 5.2. Optical, electrochemical and UPS characteristics of functionalized F_xSiPcs .

Compound	λ_{max}^a (nm)	E_{bg}^a THF / Film (eV)	$E_{Red,1/2}^b$ (mV)	$LUMO / HOMO_{CV}^b$ (eV)	Φ^c (eV)	Δe^c (eV)	$LUMO / HOMO_{UPS}^c$ (eV)
$(\text{tb-Ph})_2\text{-F}_0\text{SiPc}$	681	1.8 / 1.6	-1090	-3.5 / -5.3	3.4	1.8	-3.6 / -5.2
$(\text{tb-Ph})_2\text{-F}_4\text{SiPc}$	676	1.8 / 1.6	-610, -1160	-3.9 / -5.7	3.5	2.0	-4.0 / -5.6
$(\text{tb-Ph})_2\text{-F}_8\text{SiPc}$	665	1.8 / 1.6	-880	-3.7 / -5.5	4.3	1.7	-4.4 / -6.0
$(\text{tb-Ph})_2\text{-F}_{16}\text{SiPc}$	691	1.8 / 1.6	-300, -860	-4.3 / -6.0	3.7	2.3	-4.4 / -6.0

^a Peak absorbance from a THF solution and Optical band gap characterized using the onset of the absorption in both solution and thin film.

^b Half-wave reduction potential from solution CV, carried out in dry, O₂-free THF, using platinum wires as electrodes and LUMO/HOMO calculated according to $LUMO = -E_{Red,1/2} + E_{Ox,ferrocene} - 4.8$, $HOMO = LUMO - E_{G,THF}$.

^c Energy levels and work function estimated from UPS spectra, with a + 9 V bias, 21.22 eV emission source and calibrated using an Au reference. We estimated the ionization energy (IE) to be equal to the HOMO energy level and $LUMO = HOMO + E_{G,Film}$.

5.6.3 Light-absorbing devices

The (tb-Ph)₂-F_xSiPcs have been incorporated as non-fullerene acceptors in OPVs, paired with poly [(thiophene)-alt-(6,7-difluoro-2-(2-hexyldecyloxy)quinoxaline)] (PTQ10) a scalable, low-cost polymer. The device metrics are summarized in (**Table 5.3**). Films spincoated from (tb-Ph)₂-F₈SiPc and (tb-Ph)₂-F₁₆SiPc did not display favorable morphology, with visible phase separation, and led to devices with very poor J-V characteristics and over 50% of shorted devices. This was likely due to their low solubility (**Table 5.3**). The films cast from (tb-Ph)₂-F₀SiPc and (tb-Ph)₂-F₄SiPc solutions, alternatively, were smooth and clear. AFM images showed they possess comparable morphologies (**Figure C4**) and allow for a more straightforward comparison of the effect of fluorination. The device based on (tb-Ph)₂-F₀SiPc displayed high open circuit voltage (V_{oc}) and very low short circuit current (J_{sc}), likely due to improper energy level alignment between its HOMO and that of the PQT10 donor (**Figure 5.4a**). However, the device containing (tb-Ph)₂-F₄SiPc had much better J-V characteristics, leading to modest currents (**Table 5.3, Figure 5.4c**). The 0.4 eV drop in HOMO helps align the frontier orbital levels of the PTQ10, making (tb-Ph)₂-F₄SiPc a suitable acceptor. The champion devices achieved a power conversion efficiency (PCE) of 3.3%, which is comparable to other R₂-SiPc-based devices.²⁵ These results demonstrate that peripheral fluorination of R₂-F_xSiPc enables the pairing with PTQ10, by deepening their HOMO/LUMO levels. That is further evidenced by the results obtained from the incorporation of (tb-Ph)₂-F₄SiPc in OPDs, also paired with PTQ10 (**Figure 5.4d, Table 5.3**). With an average dark current J_d at -2 V of 5.06 nA cm⁻², the PTQ10/(tb-Ph)₂-F₄SiPc devices perform very similarly to previously reported PTQ10-integrating OPDs with $J_d = 1.1$ nA cm⁻² for the system PTQ10/FBR,⁶⁶ and $J_d = 0.13$ nA cm⁻² for the system PTQ10/EH-TCNBT.⁶⁷ At an average of $4.45 \cdot 10^{12}$ Jones, PTQ10/(tb-Ph)₂-F₄SiPc devices also displayed detectivity D* at higher or the same order of magnitude as the comparable devices,^{59,66,67} all of which were composed of high SC acceptors.¹³ **Figure C6** shows that PTQ10/(tb-Ph)₂-F₄SiPc devices responds linearly with varying irradiance

over 5 orders of magnitude. These results demonstrate the potential of R₂-F_xSiPc as low-cost acceptors in light-absorbing devices, such as detectors and solar cells.

Table 5.3. Current density-voltage results for all assembled OPVs, including photoconversion efficiency (*PCE*), open circuit voltage (*V_{OC}*), short circuit current (*J_{SC}*), fill factor (*FF*) and number of devices (*n*); and OPDs, including dark current (*J_{dark}*), responsivity (*R*) and detectivity (*D**).

OPV Characteristics						
Device ^a	Solub. (mg mL ⁻¹)	PCE ^b (%)	Voc ^b (V)	Jsc ^b (mA cm ⁻²)	FF ^b	n ^b
(tb-Ph) ₂ -F ₀ SiPc	13	0.12 ± 0.01	1.05 ± 0.03	0.42 ± 0.01	0.27 ± 0.01	9
(tb-Ph) ₂ -F ₄ SiPc	17	3.16 ± 0.06	1.03 ± 0.01	6.63 ± 0.19	0.46 ± 0.01	10
(tb-Ph) ₂ -F ₈ SiPc	5	0.13 ± 0.03	0.64 ± 0.14	0.72 ± 0.02	0.35 ± 0.02	3
(tb-Ph) ₂ -F ₁₆ SiPc	8	0.13 ± 0.01	0.42 ± 0.00	1.00 ± 0.01	0.31 ± 0.01	4

OPD Characteristics					
Device ^c	Bias (V)	Irra. at 528 nm (W m ⁻²)	J _{dark} (nA m ⁻²) ^d	R (A W ⁻¹) ^d	D (Jones) ^d n ^d
(tb-Ph) ₂ -F ₄ SiPc	-2.0	37.7	5.06 ± 3.1	0.16	4.45·10 ¹² 11

^a active layer spincoated from PTQ10/(tb-Ph)₂-F_xSiPc, 8 mg ml⁻¹, 50°C, spin-coated at 1500 RPM, dried in nitrogen, no annealing.

^b values calculated from *J-V* curves, average of *n* devices, 1000 W m⁻² irradiation power calibrated with silicon reference cell.

^c active layer spincoated from PTQ10/(tb-Ph)₂-F_xSiPc, 40 mg ml⁻¹, spin-coated in two steps, 1) 400 RPM and 2) 2000 RPM, dried in nitrogen, no annealing.

^d responsivity R=Jph / Irradiance calculated and detectivity D*=R/√2qJd are reported at -2.0 V bias, and 37.7 W m⁻² irradiation power at 528nm, averaged over *n* devices.

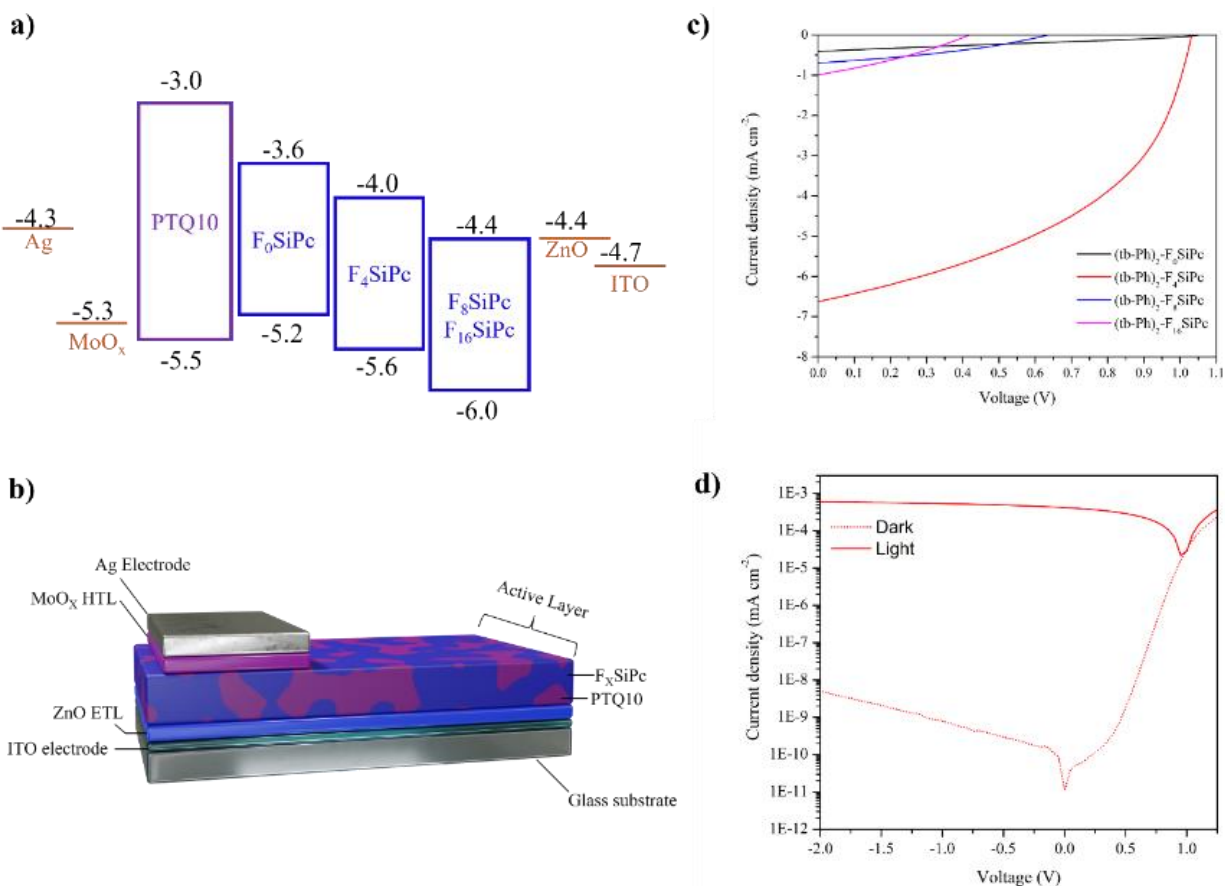


Figure 5.4. **a)** Energy levels of the semiconductors and electrodes; **b)** OPV device structure; **c)** J-V curves for OPVs prepared from PTQ10 and (tb-Ph)₂-F_xSiPcs; and **d)** J-V curves for OPD devices prepared from PTQ10 and (tb-Ph)₂-F₄SiPcs.

5.6.4 OTFT devices

(tb-Ph)₂-F_xSiPcs were incorporated as the active layers in bottom-gate top-contact OTFTs by thermal evaporation on a silane-functionalized Si/SiO₂ substrate using Ag or Ag/Mn as source and drain electrodes. Both n-type and p-type behaviors were characterized for all devices. **Figure 5.5** displays the transfer curves for devices fabricated with (tb-Ph)₂-F₁₆SiPc characterized in N₂, and OTFT characteristics are summarized in **Table 5.4** and **Table 5.5**. The V_T and electron mobility (μ_e) of (tb-Ph)₂-F_xSiPc materials in OTFTs are comparable to previously reported R₂-SiPcs.^{35,68} This modest μ_e can also be a result of the relatively large distance between phthalocyanine rings in most directions in the crystal packing structure. As observed in SC-XRD images (**Figure C3**), close-packing of the phthalocyanine rings happens only in one dimension. (tb-Ph)₂-F_xSiPcs exhibited negligible diffraction in the XRD diffractograms (**Figure C7**) suggesting all derivatives form amorphous films which is not ideal for OTFT performance. This

lack of crystallinity is thought to be caused by the bulky tert-butyl groups, which do not favour close-packing of adjacent molecules. AFM images show mainly featureless, amorphous domains for (tb-Ph)₂-F₀SiPc, (tb-Ph)₂-F₄SiPc and (tb-Ph)₂-F₈SiPc (**Figure C8**). AFM images of thin films of (tb-Ph)₂-F₁₆SiPc, while not highly crystalline, displayed some ordered feather-like domains. Fluorine-fluorine interactions are known to increase intermolecular interactions in organic materials,^{2,41,42,69} and can lead to close-packing in solid state, as observed with F₂F₁₆SiPc.²⁶

When analyzing the data in **Table 5.4** and **Table 5.5** it is notable that the n-type behavior is enhanced as peripheral fluorination of the (tb-Ph)₂-F_xSiPc macrocycle increases. (tb-Ph)₂-F₀SiPc displays only p-type behavior, whereas (tb-Ph)₂-F₄SiPc is ambipolar in N₂. Alternatively, (tb-Ph)₂-F₈SiPc and (tb-Ph)₂-F₁₆SiPc exhibit n-type behavior in N₂, with the latter able to transport electrons in air. This is illustrated in **Figure 5.6**. The fluorination of phthalocyanine brings significantly increases electron affinity (**Figure 5.2**) and reduces the energy level of the frontier orbitals (Error! Reference source not found.), facilitating charge injection. *V_t* for devices fabricated with (tb-Ph)₂-F₁₆SiPc is lower compared to other derivatives suggesting the ease of electron injection due to peripheral fluorination. When using a Mn interlayer the *V_t* drops below 10 V, which is relatively low for typical R₂-SiPcs in similar device structures.¹⁸

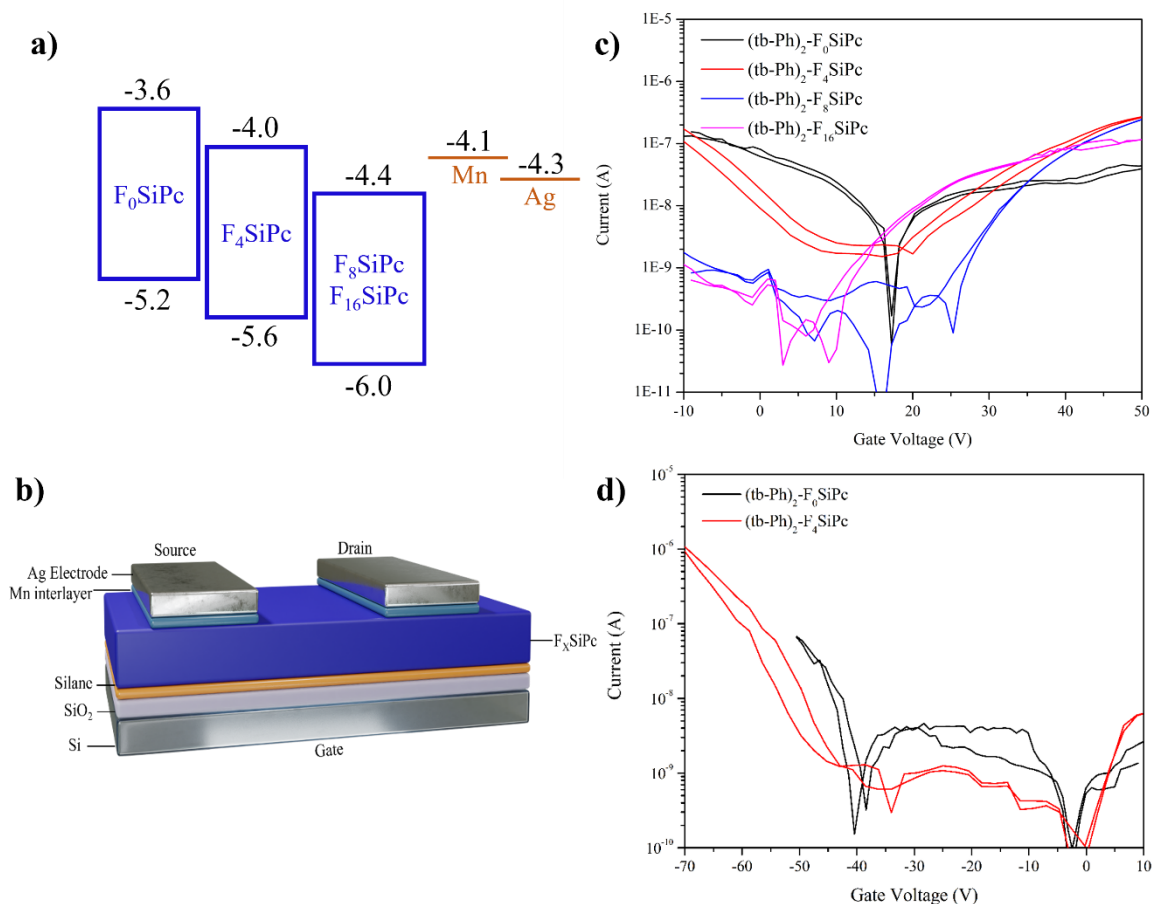


Figure 5.5. a) Energy levels of the semiconductors and electrodes; b) OTFT device configurations; and curves of evaporated (tb-Ph)₂-F_xSiPcs transistors characterized at room temperature in N₂, with Ag electrodes, operating as c) n-type ($V_{DS} = + 50V$) and d) p-type ($V_{DS} = - 50V$) semiconductors.

Table 5.4. Summary of OTFT n-type characteristics, measured at room temperature in a nitrogen atmosphere.

Material	Electrode	μ_e [cm ² ·V ⁻¹ ·s ⁻¹] ^a	V_T [V] ^a	I_{on} [A] ^b	I_{on}/I_{off}	n^a
(tb-Ph) ₂ -F ₀ SiPc	Ag	--	--	--	--	--
	Ag/Mn	--	--	--	--	--
(tb-Ph) ₂ -F ₄ SiPc	Ag	$(4.45 \pm 2.16) \cdot 10^{-4}$	23.08 ± 2.46	$2.20 \cdot 10^{-6}$	10^3 - 10^4	29
	Ag/Mn	$(2.13 \pm 0.80) \cdot 10^{-3}$	19.53 ± 3.87	$7.19 \cdot 10^{-7}$	10^4 - 10^5	27
(tb-Ph) ₂ -F ₈ SiPc	Ag	$(5.03 \pm 1.87) \cdot 10^{-4}$	23.54 ± 2.28	$2.43 \cdot 10^{-7}$	10^4 - 10^5	36

(tb-Ph) ₂ -F ₁₆ SiPc	Ag/Mn	(2.06 ± 0.42)·10 ⁻³	34.72 ± 0.07	2.50·10 ⁻⁸	10 ⁴ -10 ⁵	38
	Ag	(2.15 ± 0.90)·10 ⁻⁴	11.27 ± 2.73	1.77·10 ⁻⁷	10 ³ -10 ⁴	38
	Ag/Mn	(1.58 ± 0.59)·10 ⁻³	7.06 ± 4.20	2.66·10 ⁻⁷	10 ² -10 ³	40

^a μ_e and V_T were calculated based on mean values of n transistors.

^b I_{on} calculated based on median values

Table 5.5. Summary of OTFT p-type characteristics, measured at room temperature in a nitrogen atmosphere.

Material	Electrode	μ_h [cm ² ·V ⁻¹ ·s ⁻¹] ^a	V_T [V] ^a	I_{on} [A] ^b	I_{on}/I_{off}	n
(tb-Ph) ₂ -F ₀ SiPc	Ag	(4.15 ± 7.26)·10 ⁻⁵	2.83 ± 4.60	3.37·10 ⁻⁸	10 ² -10 ³	17
	Ag/Mn	(4.36 ± 2.92)·10 ⁻⁴	-40.67 ± 5.28	3.21·10 ⁻⁸	10 ³ -10 ⁴	18
(tb-Ph) ₂ -F ₄ SiPc	Ag	(3.68 ± 5.48)·10 ⁻³	-51.03 ± 2.58	7.19·10 ⁻⁷	10 ³ -10 ⁵	14
	Ag/Mn	--	--	--	--	--
(tb-Ph) ₂ -F ₈ SiPc	Ag	--	--	--	--	--
	Ag/Mn	--	--	--	--	--
(tb-Ph) ₂ -F ₁₆ SiPc	Ag	--	--	--	--	--
	Ag/Mn	--	--	--	--	--

^a μ_e and V_T were calculated based on mean values of n transistors.

^b I_{on} calculated based on median values

(tb-Ph)₂-F₁₆SiPc, is also the only (tb-Ph)₂-F_XSiPc in the series that maintained n-type μ_e in air. OTFT metrics of (tb-Ph)₂-F₁₆SiPc devices characterized in air are shown in **Table 5.6** and **Figure C9**. Devices fabricated with (tb-Ph)₂-F₁₆SiPc as the semiconductor showed higher V_t in air than in N₂, but maintained a comparable μ_e . The improved air stability is likely due to the drop in the LUMO level with increased peripheral fluorination, as observed by UPS. Air-stability is expected to increase significantly when the semiconductor's LUMO drops below -4.0 eV,^{70,71} by making the transfer of electrons from semiconductor to O₂ in air less favorable. However, it is unclear why (tb-Ph)₂-F₈SiPc, having similar HOMO and LUMO levels to (tb-Ph)₂-F₁₆SiPc, has not retained μ_e after devices were exposed to air. Additional research needs to be conducted to understand the fundamental mechanisms that lead (tb-Ph)₂-F₈SiPc to be an outlier in many of the trends observed. Overall, we demonstrate the synthesis and characterization of novel peripherally

fluorinated silicon phthalocyanines leading to an effective route towards tuning the energy levels and enabling air stable operation of SiPc-based n-type thin-film transistors.

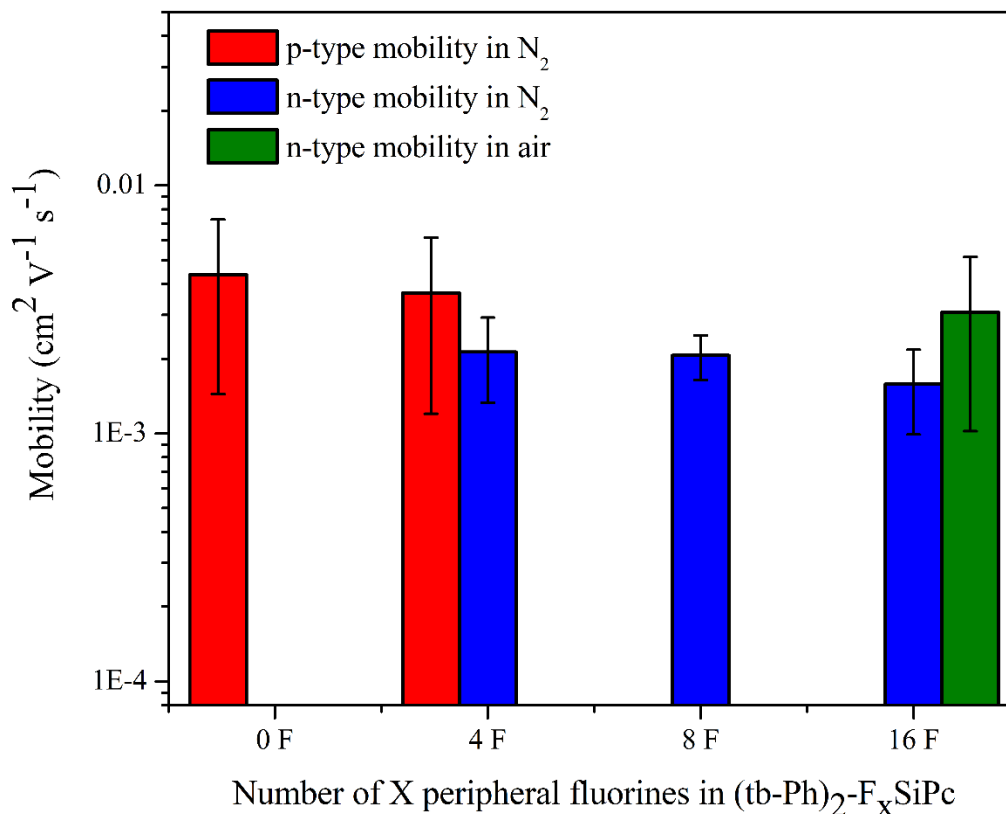


Figure 5.6. N-type and p-type mobilities of (tb-Ph)₂-F_xSiPc as function of peripheral fluorination.

Table 5.6. OTFT n-type characteristics of (tb-Ph)₂-F₁₆SiPc devices tested in air.

Condition	Electrode	μ_e [cm ² ·V ⁻¹ ·s ⁻¹] ^a	V_T [V] ^a	I_{on} [A] ^b	I_{on}/I_{off}	n
Air	Ag	$(2.44 \pm 1.57) \cdot 10^{-4}$	25.75 ± 4.51	$4.92 \cdot 10^{-8}$	10^2 - 10^3	33
	Ag/Mn	$(3.08 \pm 2.06) \cdot 10^{-4}$	24.32 ± 4.49	$4.87 \cdot 10^{-8}$	10^3 - 10^4	38

^a μ_e and V_T were calculated based on mean values of n transistors.

^b I_{on} calculated based on median values

5.7 Conclusions

We reported the synthesis and characterization of functionalized R₂-F_xSiPcs with different degrees of peripheral fluorination. Four novel (tb-Ph)₂-F_xSiPcs were synthesized by relatively simple synthetic methods, which have been optimized. A novel pathway for the substitution of R₂-

F_x SiPc was also reported. As the degree of fluorination increased, the electron affinity increased and HOMO and LUMO levels were lowered, which highlights the effect of the addition of electron withdrawing groups to the periphery of the R_2-F_x SiPc macrocycle, as measured by CV and UPS. The change in energy levels between $(tb-Ph)_2-F_0$ SiPc and $(tb-Ph)_2-F_{16}$ SiPc was 0.8 eV. The deeper energy levels enabled $(tb-Ph)_2-F_4$ SiPc to be paired with PTQ10 in OPV and OPD devices, with respectable metrics. When incorporated in OTFTs, devices based on $(tb-Ph)_2-F_{16}$ SiPc as the semiconductor yielded similar mobilities to unfluorinated R_2 -SiPcs but at a lower operating voltage, owing to its higher electron affinity. The type of charge carrier mobility displayed was also a function of the degree of fluorination of the R_2-F_x SiPc core. $(tb-Ph)_2-F_0$ SiPc displayed only p-type conductivity in OTFTs, whereas $(tb-Ph)_2-F_4$ SiPc was ambipolar, and $(tb-Ph)_2-F_8$ SiPc and $(tb-Ph)_2-F_{16}$ SiPc only conducted electrons. $(tb-Ph)_2-F_{16}$ SiPc retained its electron mobility after exposure to air which is an important characteristic for the development of next-generation n-type semiconductors and enables a wider range of applications. The results presented here demonstrate the potential for further development of R_2-F_x SiPc derivatives as effective low-cost, air-stable organic semiconductors.

5.8 Acknowledgements

We thank Natural Sciences and Engineering Research Council of Canada (NSERC) for RGPIN-2015-509 03987 and STPGP 506661-17 to B.H.L) and CGS-D (B.K). The research was undertaken, in part, thanks to funding from the Canada Research Chair program (B.H.L). Authors are thankful for the funding France Relance AD 21-498 and the national research agency ANR Labcom project « SPRINT » ANR 19-LCV1-0006-01 (C.D, G.W and L.H). The authors would also like to acknowledge the Surface Science Western (SSW) at Western University for performing UPS, the Centre for Research in Photonics at the University of Ottawa for access to the AFM and Dr. Jeffery Ovens for performing single crystal XRD.

5.9 References

- (1) Bronstein, H.; Nielsen, C. B.; Schroeder, B. C.; McCulloch, I. The Role of Chemical Design in the Performance of Organic Semiconductors. *Nat. Rev. Chem.* **2020**, *4* (2), 66–77. <https://doi.org/10.1038/s41570-019-0152-9>.
- (2) Mei, J.; Diao, Y.; Appleton, A. L.; Fang, L.; Bao, Z. Integrated Materials Design of Organic Semiconductors for Field-Effect Transistors. *J. Am. Chem. Soc.* **2013**, *135* (18), 6724–6746. <https://doi.org/10.1021/ja400881n>.

- (3) Bottomley, L. A.; Gorce, J. N.; Goedken, V. L.; Ercolani, C. Spectroelectrochemistry of a μ -Nitrido-Bridged Iron Phthalocyanine Dimer. *Inorg. Chem.* **1985**, *24* (23), 3733–3737. <https://doi.org/10.1021/ic00217a008>.
- (4) Leznoff, C. C.; Lever, A. B. P. *Phthalocyanines, Properties and Applications*; Wiley, 1996; Vol. 1.
- (5) Smith, K. M.; Guillard, R.; History, M. *The Porphyrin Handbook*; Academic Press, 2000.
- (6) Melville, O. A.; Grant, T. M.; Mirka, B.; Boileau, N. T.; Park, J.; Lessard, B. H. Ambipolarity and Air Stability of Silicon Phthalocyanine Organic Thin-Film Transistors. *Adv. Electron. Mater.* **2019**, *5* (8), 1–7. <https://doi.org/10.1002/aelm.201900087>.
- (7) Lessard, B. H. The Rise of Silicon Phthalocyanine: From Organic Photovoltaics to Organic Thin Film Transistors. *ACS Appl. Mater. Interfaces* **2021**, *13* (27), 31321–31330. <https://doi.org/10.1021/acsmi.1c06060>.
- (8) Claessens, C. G.; Hahn, U.; Torres, T. Phthalocyanines: From Outstanding Electronic Properties to Emerging Applications. *Chem. Rec.* **2008**, *8* (2), 75–97. <https://doi.org/10.1002/tcr.20139>.
- (9) Lessard, B. H.; White, R. T.; Al-Amar, M.; Plint, T.; Castrucci, J. S.; Josey, D. S.; Lu, Z. H.; Bender, T. P. Assessing the Potential Roles of Silicon and Germanium Phthalocyanines in Planar Heterojunction Organic Photovoltaic Devices and How Pentafluoro Phenoxylation Can Enhance π - π Interactions and Device Performance. *ACS Appl. Mater. Interfaces* **2015**, *7* (9), 5076–5088. <https://doi.org/10.1021/am508491v>.
- (10) Yuen, A. P.; Jovanovic, S. M.; Hor, A. M.; Klenkler, R. A.; Devenyi, G. A.; Loutfy, R. O.; Preston, J. S. Photovoltaic Properties of M-Phthalocyanine/Fullerene Organic Solar Cells. *Sol. Energy* **2012**, *86* (6), 1683–1688. <https://doi.org/10.1016/j.solener.2012.03.019>.
- (11) Dang, M.-T.; Grant, T. M.; Yan, H.; Seferos, D. S.; Lessard, B. H.; Bender, T. P.; Miller, J. a.; Goethem, E. M. Van; Kenney, M. E.; Lu, Z.-H. Bis(Tri-n-Alkylsilyl Oxide) Silicon Phthalocyanines: A Start to Establishing a Structure Property Relationship as Both Ternary Additives and Non-Fullerene Electron Acceptors in Bulk Heterojunction Organic Photovoltaic Devices. *J. Mater. Chem. A* **2017**, *126*, 3378–3379. <https://doi.org/10.1039/C6TA10739G>.
- (12) Po, R.; Bianchi, G.; Carbonera, C.; Pellegrino, A. “all That Glisters Is Not Gold”: An Analysis of the Synthetic Complexity of Efficient Polymer Donors for Polymer Solar Cells. *Macromolecules* **2015**, *48* (3), 453–461. <https://doi.org/10.1021/ma501894w>.
- (13) Grant, T. M.; Dindault, C.; Rice, N. A.; Swaraj, S.; Lessard, B. H. Synthetically Facile Organic Solar Cells with >4% Efficiency Using P3HT and a Silicon Phthalocyanine Non-Fullerene Acceptor. *Mater. Adv.* **2021**, *2* (8), 2594–2599. <https://doi.org/10.1039/d1ma00165e>.
- (14) Melville, O. A.; Lessard, B. H.; Bender, T. P. Phthalocyanine-Based Organic Thin-Film Transistors: A Review of Recent Advances. *ACS Appl. Mater. Interfaces* **2015**, *7* (24), 13105–13118. <https://doi.org/10.1021/acsmi.5b01718>.
- (15) Melville, O. A.; Grant, T. M.; Lessard, B. H. Silicon Phthalocyanines as N-Type Semiconductors in Organic Thin Film Transistors. *J. Mater. Chem. C* **2018**, *6* (20), 5482–5488. <https://doi.org/10.1039/c8tc01116h>.
- (16) Yutronkie, N. J.; Grant, T. M.; Melville, O. A.; Lessard, B. H.; Brusso, J. L. Old Molecule, New Chemistry: Exploring Silicon Phthalocyanines as Emerging N-Type Materials in Organic Electronics. *Materials (Basel)*. **2019**, *12* (8), 5–10. <https://doi.org/10.3390/ma12081334>.
- (17) Grant, T. M.; Rice, N. A.; Muccioli, L.; Castet, F.; Lessard, B. H. Solution-Processable n-Type Tin Phthalocyanines in Organic Thin Film Transistors and as Ternary Additives in Organic Photovoltaics. *ACS Appl. Electron. Mater.* **2019**, *1* (4), 494–504. <https://doi.org/10.1021/acsaelm.8b00113>.

- (18) King, B.; Melville, O. A.; Rice, N. A.; Kashani, S.; Tonnelé, C.; Raboui, H.; Swaraj, S.; Grant, T. M.; McAfee, T.; Bender, T. P.; et al. Silicon Phthalocyanines for N-Type Organic Thin-Film Transistors: Development of Structure–property Relationships. *ACS Appl. Electron. Mater.* **2021**. <https://doi.org/10.1021/acsaelm.0c00871>.
- (19) Cranston, R.; King, B.; Dindault, C.; Grant, T. M.; Rice, N.; Tonnelé, C.; Muccioli, L.; Castet, F.; Swaraj, S.; Lessard, B. H. Highlighting the Processing Versatility of a Silicon Phthalocyanine Derivative for Organic Thin-Film Transistors. *J. Mater. Chem. C* **2022**. <https://doi.org/10.1039/d1tc05238a>.
- (20) Honda, S.; Ohkita, H.; Benten, H.; Ito, S. Multi-Colored Dye Sensitization of Polymer/Fullerene Bulk Heterojunction Solar Cells. *Chem. Commun.* **2010**, 46 (35), 6596–6598. <https://doi.org/10.1039/c0cc01787f>.
- (21) Honda, S.; Ohkita, H.; Benten, H.; Ito, S. Selective Dye Loading at the Heterojunction in Polymer/Fullerene Solar Cells. *Adv. Energy Mater.* **2011**, 1 (4), 588–598. <https://doi.org/10.1002/aenm.201100094>.
- (22) Pal, A. K.; Varghese, S.; Cordes, D. B.; Slawin, A. M. Z.; Samuel, I. D. W.; Zysman-Colman, E. Near-Infrared Fluorescence of Silicon Phthalocyanine Carboxylate Esters. *Sci. Rep.* **2017**, 7 (1). <https://doi.org/10.1038/s41598-017-12374-8>.
- (23) Zysman-Colman, E.; Ghosh, S. S.; Xie, G.; Varghese, S.; Chowdhury, M.; Sharma, N.; Cordes, D. B.; Slawin, A. M. Z.; Samuel, I. D. W. Solution-Processable Silicon Phthalocyanines in Electroluminescent and Photovoltaic Devices. *ACS Appl. Mater. Interfaces* **2016**, 8 (14), 9247–9253. <https://doi.org/10.1021/acsami.5b12408>.
- (24) Grant, T. M.; Kaller, K. L. C.; Coathup, T. J.; Rice, N. A.; Hinzer, K.; Lessard, B. H. High V Oc Solution-Processed Organic Solar Cells Containing Silicon Phthalocyanine as a Non-Fullerene Electron Acceptor. *Org. Electron.* **2020**, 87 (October), 105976. <https://doi.org/10.1016/j.orgel.2020.105976>.
- (25) Vebber, M. C.; Rice, N. A.; Brusso, J. L.; Lessard, B. H. Thermodynamic Property–Performance Relationships in Silicon Phthalocyanine-Based Organic Photovoltaics. *ACS Appl. Energy Mater.* **2022**, 5 (3), 3426–3435. <https://doi.org/10.1021/acsaem.1c04013>.
- (26) Yutronkie, N. J.; King, B.; Melville, O. A.; Lessard, B. H.; Brusso, J. L. Attaining Air Stability in High Performing N-Type Phthalocyanine Based Organic Semiconductors. *J. Mater. Chem. C* **2021**, 9 (31), 10119–10126. <https://doi.org/10.1039/d1tc02275j>.
- (27) Vebber, M. C.; Grant, T. M.; Brusso, J. L.; Lessard, B. H. Bis(Trialkylsilyl Oxide) Silicon Phthalocyanines: Understanding the Role of Solubility in Device Performance as Ternary Additives in Organic Photovoltaics. *Langmuir* **2020**, 36 (10), 2612–2621. <https://doi.org/10.1021/acs.langmuir.9b03772>.
- (28) Grant, T. M.; Dindault, C.; Rice, N. A.; Swaraj, S.; Lessard, B. H. Synthetically Facile Organic Solar Cells with > 4% Efficiency Using P3HT and a Silicon Phthalocyanine Non-Fullerene Acceptor. *Mater. Adv.* **2021**, 2 (8), 2594–2599. <https://doi.org/10.1039/D1MA00165E>.
- (29) Yan, J.; Saunders, B. R. Third-Generation Solar Cells: A Review and Comparison of Polymer:Fullerene, Hybrid Polymer and Perovskite Solar Cells. *RSC Adv.* **2014**, 4 (82), 43286–43314. <https://doi.org/10.1039/c4ra07064j>.
- (30) Liu, Y.; Zhang, J.; Zhou, G.; Liu, F.; Zhu, X.; Zhang, F. Electric Field Facilitating Hole Transfer in Non-Fullerene Organic Solar Cells with a Negative HOMO Offset. *J. Phys. Chem. C* **2020**, 124 (28), 15132–15139. <https://doi.org/10.1021/acs.jpcc.0c05654>.
- (31) Faure, M. D. M.; Grant, T. M.; Lessard, B. H. Silicon Phthalocyanines as Acceptor Candidates in Mixed Solution/Evaporation Processed Planar Heterojunction Organic Photovoltaic Devices. *Coatings* **2019**, 9 (3). <https://doi.org/10.3390/COATINGS9030203>.
- (32) Wannebroucq, A.; Meunier-Prest, R.; Chambron, J. C.; Brachais, C. H.; Suisse, J. M.; Bouvet, M. Synthesis and Characterization of Fluorophthalocyanines Bearing Four 2-(2-Thienyl)ethoxy Moieties: From the Optimization

of the Fluorine Substitution to Chemosensing. *RSC Adv.* **2017**, *7* (65), 41272–41281. <https://doi.org/10.1039/c7ra05325h>.

(33) Chen, W.; Qi, D. C.; Huang, Y. L.; Huang, H.; Wang, Y. Z.; Chen, S.; Gao, X. Y.; Wee, A. T. S. Molecular Orientation Dependent Energy Level Alignment at Organic-Organic Heterojunction Interfaces. *J. Phys. Chem. C* **2009**, *113* (29), 12832–12839. <https://doi.org/10.1021/jp903139q>.

(34) Usta, H.; Facchetti, A.; Marks, T. J. N -Channel Semiconductor Materials Design for Organic Complementary Circuits. *Acc. Chem. Res.* **2011**, *44* (7), 501–510. <https://doi.org/10.1021/ar200006r>.

(35) King, B.; Melville, O. A.; Rice, N. A.; Kashani, S.; Tonnelé, C.; Raboui, H.; Swaraj, S.; Grant, T. M.; McAfee, T.; Bender, T. P.; et al. Silicon Phthalocyanines for N-Type Organic Thin-Film Transistors: Development of Structure-Property Relationships. *ACS Appl. Electron. Mater.* **2021**, *3* (1), 325–336. <https://doi.org/10.1021/acsaelm.0c00871>.

(36) Zschieschang, U.; Amsharov, K.; Jansen, M.; Kern, K.; Klauk, H.; Weitz, R. T. Separating the Impact of Oxygen and Water on the Long-Term Stability of n-Channel Perylene Diimide Thin-Film Transistors. *Org. Electron.* **2015**, *26*, 340–344. <https://doi.org/10.1016/j.orgel.2015.07.060>.

(37) Aguirre, C. M.; Levesque, P. L.; Paillet, M.; Lapointe, F.; St-Antoine, B. C.; Desjardins, P.; Martel, R. The Role of the Oxygen/Water Redox Couple in Suppressing Electron Conduction in Field-Effect Transistors. *Adv. Mater.* **2009**, *21* (30), 3087–3091. <https://doi.org/10.1002/adma.200900550>.

(38) Chen, H. Z.; Ling, M. M.; Mo, X.; Shi, M. M.; Wang, M.; Bao, Z. Air Stable n -Channel Organic Semiconductors for Thin Film Transistors Based on Fluorinated Derivatives of Perylene Diimides. *Chem. Mater.* **2007**, *19* (4), 816–824. <https://doi.org/10.1021/cm062352w>.

(39) Gaál, G.; Mawin, M. J.; Alvarez, F.; Rodrigues, V.; Riul, A. Influence of Water on Electrical and Mechanical Properties of Self-Assembled and Self-Healing PEM Films. *Prog. Org. Coatings* **2021**, *150* (October 2020). <https://doi.org/10.1016/j.porgcoat.2020.105980>.

(40) Grant, T. M.; McIntyre, V.; Vestfrid, J.; Raboui, H.; White, R. T.; Lu, Z. H.; Lessard, B. H.; Bender, T. P. Straightforward and Relatively Safe Process for the Fluoride Exchange of Trivalent and Tetravalent Group 13 and 14 Phthalocyanines. *ACS Omega* **2019**, *4* (3), 5317–5326. <https://doi.org/10.1021/acsomega.8b03202>.

(41) Jung, B. J.; Tremblay, N. J.; Yeh, M. L.; Katz, H. E. Molecular Design and Synthetic Approaches to Electron-Transporting Organic Transistor Semiconductors. *Chem. Mater.* **2011**, *23* (3), 568–582. <https://doi.org/10.1021/cm102296d>.

(42) Jiang, H.; Ye, J.; Hu, P.; Wei, F.; Du, K.; Wang, N.; Ba, T.; Feng, S.; Kloc, C. Fluorination of Metal Phthalocyanines: Single-Crystal Growth, Efficient N-Channel Organic Field-Effect Transistors, and Structure-Property Relationships. *Sci. Rep.* **2014**, *4*, 1–6. <https://doi.org/10.1038/srep07573>.

(43) Zhang, A.; Xiao, C.; Wu, Y.; Li, C.; Ji, Y.; Li, L.; Hu, W.; Wang, Z.; Ma, W.; Li, W. Effect of Fluorination on Molecular Orientation of Conjugated Polymers in High Performance Field-Effect Transistors. *Macromolecules* **2016**, *49* (17), 6431–6438. <https://doi.org/10.1021/acs.macromol.6b01446>.

(44) Katz, H. E.; Johnson, J.; Lovinger, A. J.; Li, W. Naphthalenetetracarboxylic Diimide-Based n-Channel Transistor Semiconductors: Structural Variation and Thiol-Enhanced Gold Contacts. *J. Am. Chem. Soc.* **2000**, *122* (32), 7787–7792. <https://doi.org/10.1021/ja000870g>.

(45) Ngassam, F.; Urbain, E.; Joly, L.; Boukari, S.; Arabski, J.; Bertran, F.; Le Fèvre, P.; Garreau, G.; Wetzel, P.; Alouani, M.; et al. Fluorinated Phthalocyanine Molecules on Ferromagnetic Cobalt: A Highly Polarized Spininterface. *J. Phys. Chem. C* **2019**, *123* (43), 26475–26480. <https://doi.org/10.1021/acs.jpcc.9b09150>.

- (46) Greulich, K.; Belser, A.; Bölke, S.; Grüninger, P.; Karstens, R.; Sättele, M. S.; Ovsyannikov, R.; Giangrisostomi, E.; Basova, T. V.; Klyamer, D.; et al. Charge Transfer from Organic Molecules to Molybdenum Disulfide: Influence of the Fluorination of Iron Phthalocyanine. *J. Phys. Chem. C* **2020**, *124* (31), 16990–16999. <https://doi.org/10.1021/acs.jpcc.0c03862>.
- (47) Klyamer, D.; Bonegardt, D.; Basova, T. Fluoro-Substituted Metal Phthalocyanines for Active Layers of Chemical Sensors. *Chemosensors* **2021**, *9* (6). <https://doi.org/10.3390/chemosensors9060133>.
- (48) Pucelik, B.; Gürol, I.; Ahsen, V.; Dumoulin, F.; Dąbrowski, J. M. Fluorination of Phthalocyanine Substituents: Improved Photoproperties and Enhanced Photodynamic Efficacy after Optimal Micellar Formulations. *Eur. J. Med. Chem.* **2016**, *124*, 284–298. <https://doi.org/10.1016/j.ejmech.2016.08.035>.
- (49) Peisert, H.; Knupfer, M.; Schwieger, T.; Fuentes, G. G.; Olligs, D.; Fink, J.; Schmidt, T. Fluorination of Copper Phthalocyanines: Electronic Structure and Interface Properties. *J. Appl. Phys.* **2003**, *93* (12), 9683–9692. <https://doi.org/10.1063/1.1577223>.
- (50) De Oteyza, D. G.; El-Sayed, A.; Garcia-Lastra, J. M.; Goiri, E.; Krauss, T. N.; Turak, A.; Barrena, E.; Dosch, H.; Zegenhagen, J.; Rubio, A.; et al. Copper-Phthalocyanine Based Metal-Organic Interfaces: The Effect of Fluorination, the Substrate, and Its Symmetry. *J. Chem. Phys.* **2010**, *133* (21), 214703. <https://doi.org/10.1063/1.3509394>.
- (51) Shao, X.; Wang, S.; Li, X.; Su, Z.; Chen, Y.; Xiao, Y. Single Component P-, Ambipolar and n-Type OTFTs Based on Fluorinated Copper Phthalocyanines. *Dye. Pigment.* **2016**, *132*, 378–386. <https://doi.org/10.1016/j.dyepig.2016.05.020>.
- (52) Jiang, H.; Hu, P.; Ye, J.; Li, Y.; Li, H.; Zhang, X.; Li, R.; Dong, H.; Hu, W.; Kloc, C. Molecular Crystal Engineering: Tuning Organic Semiconductor from p-Type to n-Type by Adjusting Their Substitutional Symmetry. *Adv. Mater.* **2017**, *29* (10), 1605053. <https://doi.org/10.1002/adma.201605053>.
- (53) Busch, M. A. Halogen Chemistry. *Encycl. Phys. Sci. Technol.* **2003**, 197–222. <https://doi.org/10.1016/b0-12-227410-5/00307-0>.
- (54) Melville, O. A.; Grant, T. M.; Mirka, B.; Boileau, N. T.; Park, J.; Lessard, B. H. Ambipolarity and Air Stability of Silicon Phthalocyanine Organic Thin-Film Transistors. *Adv. Electron. Mater.* **2019**, *5* (1900087), 1–7. <https://doi.org/10.1002/aelm.201900087>.
- (55) Raboui, H.; Lough, A. J.; Plint, T.; Bender, T. P. Position of Methyl and Nitrogen on Axial Aryloxy Substituents Determines the Crystal Structure of Silicon Phthalocyanines. *Cryst. Growth Des.* **2018**, *18* (5), 3193–3201. <https://doi.org/10.1021/acs.cgd.8b00298>.
- (56) Kielar, M.; Dhez, O.; Pecastaings, G.; Curutchet, A.; Hirsch, L. Long-Term Stable Organic Photodetectors with Ultra Low Dark Currents for High Detectivity Applications. *Sci. Rep.* **2016**, *6* (November), 1–11. <https://doi.org/10.1038/srep39201>.
- (57) Xu, H.; Ohkita, J.; Tamai, Y.; Bente, H.; Ito, S. A Universal Method to Produce Low-Work Function Electrodes for Organic Electronics. *Science (80-.)*. **2012**, *336*, 327–332.
- (58) Vebber, M. C.; Rice, N. A.; Brusso, J. L.; Lessard, B. H. Variance-Resistant PTB7 and Axially-Substituted Silicon Phthalocyanines as Active Materials for High-Voc Organic Photovoltaics. *Sci. Rep.* **2021**, *11* (1), 1–8. <https://doi.org/10.1038/s41598-021-94704-5>.
- (59) Gasparini, N.; Bristow, H.; Jacoutot, P.; Scaccabarozzi, A. D.; Babics, M.; Moser, M.; Wadsworth, A.; Anthopoulos, T. D.; Bakulin, A.; McCulloch, I. Nonfullerene-Based Organic Photodetectors for Ultrahigh Sensitivity Visible Light Detection. *ACS Appl. Mater. Interfaces* **2020**, *12* (43), 48836–48844. <https://doi.org/10.1021/acsami.0c14016>.

- (60) Mitra, K.; Hartman, M. C. T. Silicon Phthalocyanines: Synthesis and Resurgent Applications. *Org. Biomol. Chem.* **2021**, No. 19, 1168–1190. <https://doi.org/10.1039/d0ob02299c>.
- (61) Grant, T. M.; Josey, D. S.; Sampson, K. L.; Mudigonda, T.; Bender, T. P.; Lessard, B. H. Boron Subphthalocyanines and Silicon Phthalocyanines for Use as Active Materials in Organic Photovoltaics. *Chem. Rec.* **2019**, *19* (6), 1093–1112. <https://doi.org/10.1002/tcr.201800178>.
- (62) Lessard, B. H.; Al-Amar, M.; Grant, T. M.; White, R.; Lu, Z. H.; Bender, T. P. From Chloro to Fluoro, Expanding the Role of Aluminum Phthalocyanine in Organic Photovoltaic Devices. *J. Mater. Chem. A* **2015**, *3* (9), 5047–5053. <https://doi.org/10.1039/c4ta06759b>.
- (63) Deck, P. A.; Fisher, T. S.; Downey, J. S. Boron-Silicon Exchange Reactions of Boron Trihalides with Trimethylsilyl-Substituted Metallocenes. *Organometallics* **1997**, *16* (6), 1193–1196. <https://doi.org/10.1021/om961026v>.
- (64) Lessard, B. H.; Grant, T. M.; White, R.; Thibau, E.; Lu, Z.-H.; Bender, T. P. The Position and Frequency of Fluorine Atoms Changes the Electron Donor/Acceptor Properties of Fluorophenoxy Silicon Phthalocyanines within Organic Photovoltaic Devices. *J. Mater. Chem. A* **2015**, *3* (48), 24512–24524. <https://doi.org/10.1039/C5TA07173A>.
- (65) Lessard, B. H.; White, R. T.; Al-Amar, M.; Plint, T.; Castrucci, J. S.; Josey, D. S.; Lu, Z. H.; Bender, T. P. Assessing the Potential Roles of Silicon and Germanium Phthalocyanines in Planar Heterojunction Organic Photovoltaic Devices and How Pentafluoro Phenoxylation Can Enhance π - π Interactions and Device Performance. *ACS Appl. Mater. Interfaces* **2015**, *7* (9), 5076–5088. <https://doi.org/10.1021/am508491v>.
- (66) Zhang, T.; Moser, M.; Scaccabarozzi, A. D.; Bristow, H.; Jacoutot, P. Ternary Organic Photodetectors Based on Pseudo- Binaries Nonfullerene-Based Acceptors. *J. Phys. Mater.* **2021**, *4*, 045001.
- (67) Kafourou, P.; Qiao, Z.; Ani, F.; Eisner, F.; Gasparini, N.; Heeney, M. Low Dark Current Organic Photodetectors Utilizing Highly Cyanated Non-Fullerene Acceptors. *Appl. Mater. Interfaces* **2022**, *14* (34), 39141–39148. <https://doi.org/10.1021/acsami.2c10197>.
- (68) Cranston, R. R.; Vebber, M. C.; Berbigier, J. F.; Rice, N. A.; Tonnelé, C.; Comeau, Z. J.; Boileau, N. T.; Brusso, J. L.; Shuhendler, A. J.; Castet, F.; et al. Thin-Film Engineering of Solution-Processable n-Type Silicon Phthalocyanines for Organic Thin-Film Transistors. *ACS Appl. Mater. Interfaces* **2021**, *13* (1), 1008–1020. <https://doi.org/10.1021/acsami.0c17657>.
- (69) Cranston, R. R.; Vebber, M. C.; Faleiro Berbigier, J.; Brusso, J.; Kelly, T. L.; Lessard, B. H. High Performance Solution Processed N-Type OTFTs through Surface Engineered F-F Interactions Using Asymmetric Silicon Phthalocyanines. *Adv. Electron. Mater.* **2022**, *8* (12), 2200696. <https://doi.org/10.1002/aelm.202200696>.
- (70) Ferreira, A. S.; Aguirre, J. C.; Subramaniyan, S.; Jenekhe, S. A.; Tolbert, S. H.; Schwartz, B. J. Understanding How Polymer Properties Control OPV Device Performance: Regioregularity, Swelling, and Morphology Optimization Using Random Poly(3-Butylthiophene-Co-3-Octylthiophene) Polymers. *J. Phys. Chem. C* **2016**, *120* (39), 22115–22125. <https://doi.org/10.1021/acs.jpcc.6b03300>.
- (71) Anthony, J. E.; Facchetti, A.; Heeney, M.; Marder, S. R.; Zhan, X. N-Type Organic Semiconductors in Organic Electronics. *Adv. Mater.* **2010**, *22* (34), 3876–3892. <https://doi.org/10.1002/adma.200903628>.

6. CONCLUSIONS AND FUTURE WORK

6.1 Summary and Main Findings

The development of scalable, low-cost organic semiconductors is paramount to enable relevant commercial applications of organic photovoltaics (OPVs). Silicon phthalocyanines (SiPcs) compose a versatile group of compounds that can be produced and purified using methods already employed for large-scale manufacture in chemical plants. It remains, however, that their performance has been limited by the poor understanding of the physical properties and microstructure of SiPc-containing bulk heterojunctions (BHJ) films. In fact, this is a general issue within the field of OPVs, which has relied on a trial-and-error approach to advance the field. Therefore, during my PhD I aimed to better understand how the physical and electrochemical properties of individual SiPc compounds interplay with their performance in OPVs.

In chapter 2, a roster of novel axially substituted $(R_3SiO)_2$ -SiPcs was synthesized and characterized. These $(R_3SiO)_2$ -SiPcs were then incorporated as ternary additives in P3HT/PC₆₁BM OPVs, to assess how different axial groups effect the performance. By changing only the length of the axial silane groups, it was possible to maintain similar electrochemical properties for all compounds and isolate the effect of solubility on the overall efficiency of the devices. We found that matching the solubility of the ternary additive with that of the P3HT polymer optimizes the PCE of resulting devices. Since $(R_3SiO)_2$ -SiPcs ternary additives need to populate the interface between P3HT/PC₆₁BM for effective charge transfer to occur, in addition to compatible surface energies, matching the solubility is also important to ensure none of the components precipitate too soon and migrate to the interface. We observed that additives with lower solubilities will form semicrystalline domains of their own, instead of migrating to the amorphous interface. This rule can be used by materials engineers to guide their choice or even design of ternary additives, when deciding how long solubilizing groups should be.

In chapter 3, we chose to assess a few of the $(R_3SiO)_2$ -SiPcs as stand-alone acceptors paired with P3HT in OPVs. The performance of P3HT/ $(R_3SiO)_2$ -SiPcs has historically been limited to below 1% due to the over crystallization of SiPc domains. Therefore, I aimed to find out relationships between their thermodynamic properties and performance in OPVs. We observed that the drying rate is linked to SiPc precipitation behavior, being growth-dominated for slow-drying films (lower spin speed), and nucleation-dominated for fast-drying films (higher spin

speed). The latter showed better results across the compounds tested, in virtue of leading to smaller domains. Additionally, we established that $(R_3SiO)_2$ -SiPcs with smaller critical radii, tended to form smaller domains in the blended films, consequently leading to better performance. The miscibility of $(R_3SiO)_2$ -SiPcs in the polymer phase was another important parameter, where lower miscibility led to purer and sharper domains. This is due to a reduction in trap states and improves overall performance. Lower miscibility correlated with shorter alkyl chains rather than total number of carbons, whereas critical radii correlated with total molecular volume, which increases with total number of carbons. The groundwork laid out here is an important tool for semiconductor design and engineering, increasing the property-performance relationships available in the field so we are able to rely on trial-and-error approach less.

With the studies and improvements listed above, we were able to reach PCEs of 4.3% in P3HT/ $(R_3SiO)_2$ -SiPcs, which is significantly higher than the fullerene-based blend that averages at around 3% in AM 1.5 G illumination. Therefore, in chapter 4, we aimed at exploring a new blend employing a better-performing polymer donor, thereby focusing on PTB7/ $(Bu_3SiO)_2$ -SiPcs blends. A high voltage of 1.05V was obtained from such devices, with a maximum PCE of 3.8% after the processing parameters had been optimized, or around 80% of the baseline containing PC₆₁BM. The efficiency of the devices obtained from this blend did not vary significantly with changes to spin speed, acceptor:donor ratio and annealing. This is possibly due to the non-Newtonian behavior of the solutions employed in spin-coating. Robustness is a desired property that can greatly facilitate manufacturing devices and goes towards the goal of economically viable OPVs.

In the search for other polymers we could pair $(R_3SiO)_2$ -SiPcs with, and assess the property-performance relationships, it was clear that the shallow HOMO (-5.3 eV) and LUMO (-3.5 eV) levels of $(R_3SiO)_2$ -SiPcs was a great limiting factor. It limits the number of polymer donors $(R_3SiO)_2$ -SiPc derivatives are compatible with, and can also be correlated to lower electron affinities and mobilities. Therefore, in chapter 5 we attempted to deepen those energy levels and explore how that affects the SiPc properties. We synthesized four silicon phthalocyanines axially substitute with tertbutylphenol groups ($(tb-Ph)_2$ -F_XSiPcs) and containing varying number of fluorine atoms (X = 0, 4, 8 or 16). The HOMO and LUMO levels, as estimated from UPS analysis, deepen as the degree of fluorination increases. This allowed $(tb-Ph)_2$ -F₄SiPcs to be successfully employed in OPVs, paired with PTQ10, a scalable, high performing polymer donor, which the

unfluorinated SiPcs are not compatible with due to their shallow energy levels. By incorporating the (tb-Ph)₂-F_xSiPcs in OTFTs we observed that we were able to control the type of mobility in the (tb-Ph)₂-F_xSiPcs semiconductor by changing the degree of fluorination. Only p-type behaviour was observed for (tb-Ph)₂-F₀SiPc, whereas (tb-Ph)₂-F₄SiPcs was ambipolar, (tb-Ph)₂-F₈SiPcs was only n-type but not stable in air, and (tb-Ph)₂-F₁₆SiPcs was n-type and air-stable. Air-stable electron conduction in organic semiconductors is an elusive property and the results achieved here can open a wide range of applications for such devices.

In the final analysis, this thesis has advanced the understanding of SiPc-containing organic electronics, with a focus on OPVs. Several basic properties of SiPcs have been correlated to their performance in OPVs, which may serve as a guide for molecular engineering and material selection when designing organic electronic devices. New optimization pathways have been open in the field. Several new SiPc derivatives have been synthesized for the first time and thoroughly characterized. The functionalization of F_xSiPcs required the development of new chemistry routes that are now available to chemists. We compromised on overall PCE, in order to advance a group of readily scalable and low-cost semiconductors, which now have new possibilities for efficiency and stability improvements, and may lead to commercially relevant devices in the future.

6.2 Recommendations for Future Work

6.2.1 Evaluate different donor/acceptor systems

The property-performance relationships explored in this thesis have been limited to SiPc derivatives. The way acceptors interact in a BHJ depend on multiple factors, including their shape, symmetry and which heteroatoms are present in the conjugated core.¹ Therefore a wider range of donor/acceptor systems needs to be evaluated to assess the if the trends observed here remain true. Recently, Li *et al*² explored four different high-performing A-D-A type acceptors (Y6 derivatives) and found that shorter solubilizing groups led to better performance as acceptors, when paired with PM6, which is congruent with the results found in Chapter 4. Additional thermodynamic studies can be performed in this system to verify if the underlying reasons for the trend are the same as in SiPcs. Symmetry of small-molecule donor also plays an important role and is often correlated to

better morphological outcomes in OPV films, while asymmetry can improve intermolecular charge transfer.^{2,3} Phthalocyanine cores are highly symmetric, therefore evaluating how asymmetry correlated with side chain length/branching is an immediate area to be studied. Similar studies have assessed the effect of side chain on polymer donors, mainly focused on engineering a face-on self-assembly.^{4,5} It remains however, that most studies are performed from a trial-and-error approach and customarily do not include discuss how intrinsic, measurable physical properties of these materials lead to the trends observed. If a more robust groundwork can be drawn for other systems, it will be a great tool for device engineering and promote faster advancement of the field.

Robust assessment of multiple donor/acceptor systems is necessary to develop artificial intelligence (AI) tools for OPVs. Machine learning has been increasingly targeted in recent years to accelerate the development of the OPVs.^{6,7} The number of publications on the topic has increased from one article every few years, to dozens a year since 2019.^{7,8} Since different acceptor cores tend to have different behaviors from one another, specific property-performance relationships, much like the ones developed in this thesis, are often incorporated in the algorithms.^{7,8} More importantly, due to the wide array of properties and interactions at play in organic photovoltaics, broad studies, with many derivatives, are necessary to feed the AIs enough data points and improve their accuracy and overall applicability. It is widely believed that AI-assisted material design and selection is the future of organic electronics.⁷

6.2.2 *Stability studies*

In addition to high efficiency and low-cost, the issue that has limited the application of organic photovoltaics has been their stability. While the efficiency of OPVs has been improved by a factor of 10 in the past 2 decades, stability studies are relatively scarce and organic photovoltaics lifetime is still long ways from approaching that of inorganic materials. Most viability studies have established that a 5-year stability threshold needs to be achieved in OPVs before commercialization is possible.⁹⁻¹¹ The mains pathways for efficiency degradation in OPVs are related to the degradation of the materials under long light exposure and alterations in the nanomorphology.^{1,12} SiPcs are promising candidates in both those aspects. They possess overall high stability and we have demonstrated that fluorination allows operation in air. The axial handles are convenient to engineer solid-state interactions with other polymer donors and for crosslinking. OPVs crosslinked with SiPc additives have been demonstrated in the past,¹² and lead to morphologies more resistant

to change, and can be explored further. New scalable and relatively low-cost blends based on PTQ10 polymer have been employed in recent years,¹ and crosslinkable SiPc-based ternary additives are good candidates to improve both charge generation and long-term stability in these systems. SiPcs applications in OPVs have been mostly confined to P3HT-based active layers, but the energetic compatibilization of SiPcs with PTQ10 has been made possible by the synthesis of fluorinated derivatives (See Section 7.2.3).

It has become clear in recent years that a compromise between efficiency and long-term stability is hard to avoid.¹³ For instance, it has been demonstrated while planar molecules with strong backbones will tend to have better immediate performance, they tend to aggregate over long operational times, leading to a drop in overall current. Alternatively, when structural hinderance is introduced via bulky side-chains, the demixing effect is weakened, leading to more stable performance over longer periods of time.¹⁴ Based on that, similar relationships as the ones that were presented in Chapters 2, 3 and 5 should be assessed with respect to stability, as opposed to efficiency, towards a better understanding and quantification of the properties that lead to high stability in OPVs.

Most studies on the stability of OPVs employ accelerated aging comparisons that, while useful, may not reflect the real aging of organic modules.^{9,13} Thus, it should also be mentioned that to fully assess OPV lifetimes, long-term studies need to be carried out.

6.2.3 *Explore other F_x SiPc derivatives*

While only a few devices have been produced in this thesis, the fluorination of SiPcs makes a wide range of donor: F_x SiPcs systems energetically compatible. **Figure 7.1** compares the HOMO and LUMO levels of SiPcs at different degrees of fluorination with relevant, commercial polymer donors. On paper, F_4 SiPc becomes compatible with all the displayed polymer donors, by having lower lying HOMO and LUMO energies. F_{16} SiPc, which is also compatible, can be explored if the energy level offsets are found to be too small. Nonetheless, as discussed previously, morphological considerations.

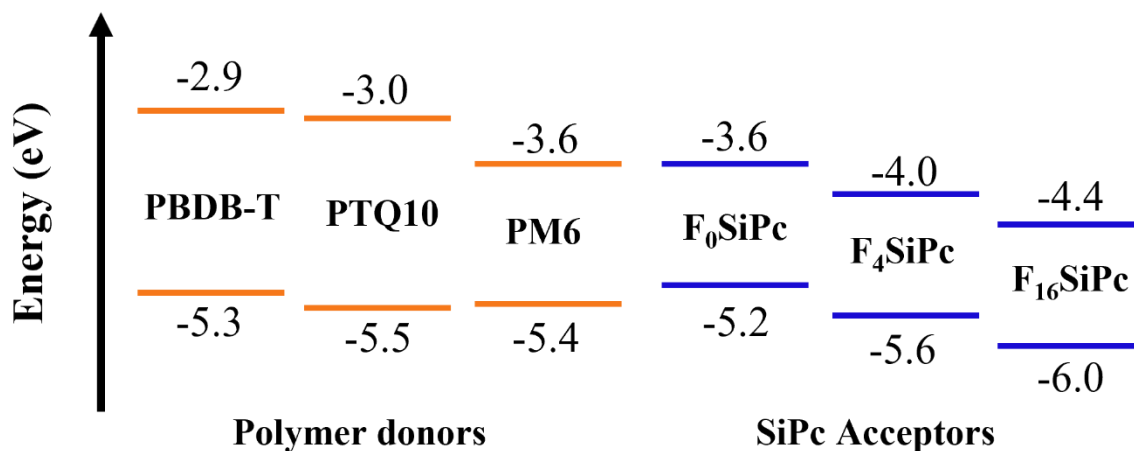


Figure 6.1. Frontier orbital energy levels of commercial polymer donors and SiPcs with different degrees of fluorination

Only a few derivatives of the fluorinated F_xSiPcs have been developed in this thesis which pales in comparison to the number of unfluorinated SiPcs derivatives. What's more, (tb-Ph)₂-F_xSiPcs had processability issues in solution that impeded the evaluation of the full potential of such materials in OPVs. Therefore, obtaining derivatives that may lead to better morphologies is required to grasp the full potential of such acceptors in terms of efficiency, when paired with new polymer donors. These derivatives can be assessed as both stand-alone acceptors as well as ternary additives. **Figure 7.2a** illustrates a derivative of F₄SiPc with tripropylsilane groups in the axial positions, which is a great candidate given that the unfluorinated counterpart showed the best performance when paired with P3HT. The solubility imparted by the axial silanes also greatly improve processability. **Figure 7.2b**, illustrates an asymmetric F₁₆SiPc derivative, with a solubilizing silane group on one axial position and a thiophene on the other. Heavily fluorinated molecules tend to separate due to their unpaired surface energies, therefore, including a thiophene molecule to interact with the polymer phases can improve mixing and nanomorphology. This derivative is a good candidate for air-stable application because we have demonstrated F₁₆SiPc's ability to conduct electrons in air. This characteristic can alleviate the requirements for device encapsulation and, consequently, improving processability in large scale. **Figure 7.2c** shows the structure of a presumably soluble F₄SiPc that is capable of crosslink, owing to the terminal azide groups.¹² This derivative would be a good candidate for ternary additive in high-performing donor/acceptor pairs, such as PTQ10/ITIC-F, with the role of improving light absorption and stability.

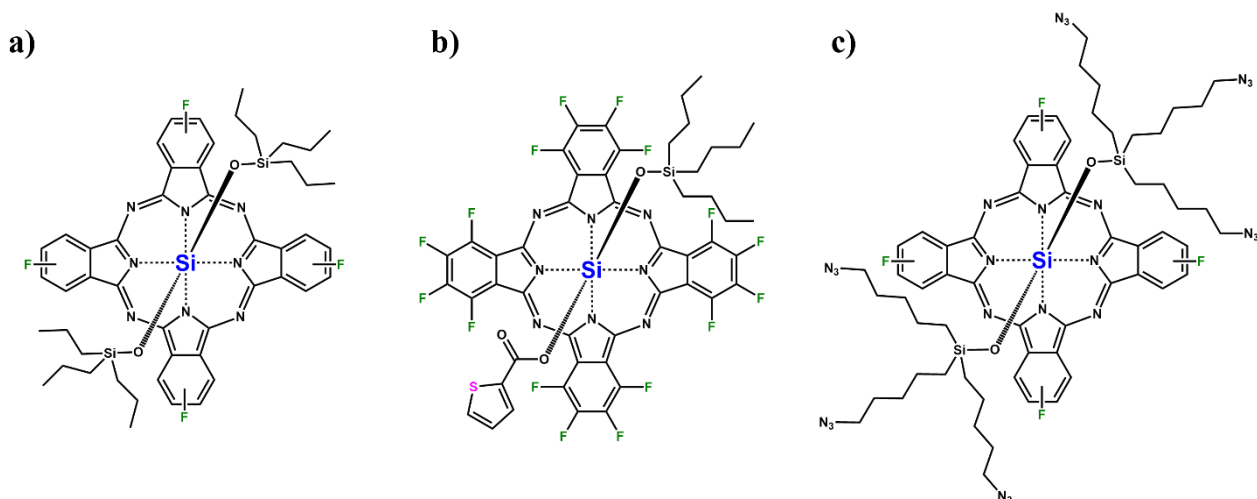


Figure 6.2. Structure of F_xSiPcs derivatives proposed for future studies.

While time limitation of the PhD thesis prevented us from exploring such possibilities, the new chemical routes developed here along with the thorough characterization of F_xSiPcs prepared the foundations necessary for such studied to be carried out.

6.3 References

- (1) Zhang, G.; Lin, F. R.; Qi, F.; Heumüller, T.; Distler, A.; Egelhaaf, H. J.; Li, N.; Chow, P. C. Y.; Brabec, C. J.; Jen, A. K. Y.; et al. Renewed Prospects for Organic Photovoltaics. *Chem. Rev.* **2021**. <https://doi.org/10.1021/acs.chemrev.1c00955>.
- (2) Li, S.; Zhan, L.; Yao, N.; Xia, X.; Chen, Z.; Yang, W.; He, C.; Zuo, L.; Shi, M.; Zhu, H.; et al. Unveiling Structure-Performance Relationships from Multi-Scales in Non-Fullerene Organic Photovoltaics. *Nat. Commun.* **2021**, *12* (1), 1–11. <https://doi.org/10.1038/s41467-021-24937-5>.
- (3) He, C.; Bi, Z.; Chen, Z.; Guo, J.; Xia, X.; Lu, X.; Min, J.; Zhu, H.; Ma, W.; Zuo, L.; et al. Compromising Charge Generation and Recombination with Asymmetric Molecule for High-Performance Binary Organic Photovoltaics with Over 18% Certified Efficiency. *Adv. Funct. Mater.* **2022**, *32* (18), 1–8. <https://doi.org/10.1002/adfm.202112511>.
- (4) Lo, C. K.; Reynolds, J. R. Structural and Morphological Effects of Alkyl Side Chains on Flanking Thiophenes of Diketopyrrolopyrrole Polymers for Organic Photovoltaic Devices. *Polymer (Guildf)*. **2016**, *99*, 741–747. <https://doi.org/10.1016/j.polymer.2016.07.066>.
- (5) Yamanaka, K.; Saito, M.; Mikie, T.; Osaka, I. Effect of Ester Side Chains on Photovoltaic Performance in Thiophene-Thiazolothiazole Copolymers. *Bull. Chem. Soc. Jpn.* **2021**, *94* (8), 2019–2027. <https://doi.org/10.1246/bcsj.20210172>.
- (6) Sun, W.; Zheng, Y.; Zhang, Q.; Yang, K.; Chen, H.; Cho, Y.; Fu, J.; Odunmbaku, O.; Shah, A. A.; Xiao, Z.; et al. Artificial Intelligence Designer for Highly-Efficient Organic Photovoltaic Materials. *J. Phys. Chem. Lett.* **2021**, *12* (36), 8847–8854. <https://doi.org/10.1021/acs.jpcllett.1c02554>.
- (7) Miyake, Y.; Saeki, A. Machine Learning-Assisted Development of Organic Solar Cell Materials: Issues, Analyses, and Outlooks. *J. Phys. Chem. Lett.* **2021**, *12* (51), 12391–12401.

<https://doi.org/10.1021/acs.jpcelett.1c03526>.

- (8) Saeki, A.; Kranthiraja, K. A High Throughput Molecular Screening for Organic Electronics via Machine Learning: Present Status and Perspective. *Jpn. J. Appl. Phys.* **2020**, *59* (SD). <https://doi.org/10.7567/1347-4065/ab4f39>.
- (9) Moser, M.; Wadsworth, A.; Gasparini, N.; McCulloch, I. Challenges to the Success of Commercial Organic Photovoltaic Products. *Adv. Energy Mater.* **2021**, *11* (18). <https://doi.org/10.1002/aenm.202100056>.
- (10) Osedach, T. P.; Andrew, T. L.; Bulović, V. Effect of Synthetic Accessibility on the Commercial Viability of Organic Photovoltaics. *Energy Environ. Sci.* **2013**, *6* (3), 711–718. <https://doi.org/10.1039/c3ee24138f>.
- (11) Mulligan, C. J.; Wilson, M.; Bryant, G.; Vaughan, B.; Zhou, X.; Belcher, W. J.; Dastoor, P. C. A Projection of Commercial-Scale Organic Photovoltaic Module Costs. *Sol. Energy Mater. Sol. Cells* **2014**, *120* (PART A), 9–17. <https://doi.org/10.1016/j.solmat.2013.07.041>.
- (12) Grant, T. M.; Gorisse, T.; Dautel, O.; Wantz, G.; Lessard, B. H. Multifunctional Ternary Additive in Bulk Heterojunction OPV: Increased Device Performance and Stability. *J. Mater. Chem. A* **2017**, *5* (4), 1581–1587. <https://doi.org/10.1039/c6ta08593h>.
- (13) Yang, W.; Wang, W.; Wang, Y.; Sun, R.; Guo, J.; Li, H.; Shi, M.; Guo, J.; Wu, Y.; Wang, T.; et al. Balancing the Efficiency, Stability, and Cost Potential for Organic Solar Cells via a New Figure of Merit. *Joule* **2021**, *5* (5), 1209–1230. <https://doi.org/10.1016/j.joule.2021.03.014>.
- (14) Fan, B.; Gao, W.; Wu, X.; Xia, X.; Wu, Y.; Lin, F. R.; Fan, Q.; Lu, X.; Li, W. J.; Ma, W.; et al. Importance of Structural Hinderance in Performance–Stability Equilibrium of Organic Photovoltaics. *Nat. Commun.* **2022**, *13* (1), 1–11. <https://doi.org/10.1038/s41467-022-33754-3>.

7. ADDITIONAL CONTRIBUTIONS

Throughout my PhD, I was part of a few projects with other member of our research group and other groups. My contributions were mainly related to the synthesis and characterization of phthalocyanines for varied organic electronic devices.

7.1 Low-Cost Silicon Phthalocyanine as a Non-Fullerene Acceptor for Flexible Large Area Organic Photovoltaics.

ACS Omega 2023, 8, 1, 1588–1596.

Chithiravel Sundaresan, Mário C. Vebber, Jaclyn L. Brusso, Ye Tao, Salima Alem, and Benoît H. Lessard.

7.1.1 Abstract

We demonstrate large-area (1 cm^2) organic photovoltaic (OPVs) devices based on bis(tri-n-butylsilyl oxide) silicon phthalocyanine $(3\text{BS})_2\text{-SiPc}$ as a non-fullerene acceptor (NFA) with low synthetic complexity paired with poly(3-hexylthiophene) (P3HT) as a donor polymer. Environment-friendly nonhalogenated solvents were used to process large area OPVs on flexible indium tin oxide (ITO)-coated polyethylene terephthalate (PET) substrates. An alternate sequentially (Alt-Sq) blade-coated active layer with bulk heterojunction-like morphology is obtained when using $(3\text{BS})_2\text{-SiPc}$ processing with o-xylene/1,3,5-trimethylbenzene solvents. The sequential (Sq) active layer is prepared by first blade-coating $(3\text{BS})_2\text{-SiPc}$ solution followed by P3HT coated on the top without any post-treatment. The conventional sequentially (Sq) blade-coated active layer presents very low performance due to the $(3\text{BS})_2\text{-SiPc}$ bottom layer being partially washed off by processing the top layer of P3HT. In contrast, alternate sequentially (Alt-Sq) blade-coated layer-by-layer film shows even better device performance compared to the bulk heterojunction (BHJ) active layer. Time-of-flight secondary ion mass spectroscopy (TOF-SIMS) and atomic force microscopy (AFM) reveal that the Alt-Sq processing of the active layer leads to a BHJ-like morphology with a well-intermixed donor–acceptor component in the active layer while providing a simpler processing approach to low-cost and large-scale OPV production.

7.1.2 Contributions

I synthesized and purified the silicon phthalocyanine used in this work and contributed to the discussion section in the manuscript.

7.2 High Performance Solution Processed n-Type OTFTs through Surface Engineered F–F Interactions Using Asymmetric Silicon Phthalocyanines

Adv. Electron. Mater. 2022, 2200696.

Rosemary R. Cranston, Mário C. Vebber, Jônatas Faleiro Berbigier, Jaclyn Brusso, Timothy L. Kelly, and Benoît H. Lessard.

7.2.1 Abstract

Two novel asymmetric silicon phthalocyanine (SiPc) derivatives consisting of one axially substituted fluorine and one tri-alkyl silane group are synthesized and characterized in n-type solution processed bottom-gate top-contact organic thin-film transistors (OTFTs). The effect of surface energy and fluorination are investigated at the dielectric/semiconductor interface by thin-film X-ray diffraction, atomic force microscopy, bright field real-color microscopy, and grazing-incidence wide-angle X-ray scattering to assess alterations in film conformation, microstructure, and morphology. Low surface energy dielectric modification and the presence of fluorine interactions produce films with large area crystalline domains that promote charge carrier transport resulting in high performing OTFTs, with a clear relationship determined between surface energy, fluorination, and OTFT operation. Through modifying deposition solvent and the exploitation of fluorine–fluorine interactions, the asymmetric SiPc derivative, (tri-*n*-hexylsilyl oxide) fluorosilicon phthalocyanine (F-3HS-SiPc), leads to high performing n-type OTFTs with an average field-effect mobility of $0.13 \text{ cm}^2 \text{ V}^{-1} \text{ s}^{-1}$ and a threshold voltage of 26.3 V. These results successfully demonstrate the use of asymmetric axial fluorination as a route to high performance n-type OTFT devices through controlled self-assembly by fluorine–fluorine interactions.

7.2.2 Contributions

I synthesized and purified the novel asymmetric SiPcs used in this work. I characterized their thermal (DSC and TGA), electrochemical (CV), optical (UV-Vis) properties and grew single-crystals for SC-XRD analysis.

7.3 Polymeric Composites for Industrial Water Treatment: An Overview

Book chapter in Industrial Wastewater Treatment: Emerging Technologies for Sustainability Springer International Publishing: Cham, 2022; pp 257–283.

Jordana Bortoluz, Mário C. Vebber, Nayrim B. Guerra, Janaina da Silva Crespo, and Marcelo Giovanela.

7.3.1 Abstract

Several advanced techniques for water treatment depend on materials and chemicals that can pose a secondary pollution risk if not removed, such as nanoparticles, catalysts, and disinfectants. The removal of these compounds requires the use of additional unit operations, making the water treatment process more expensive or even non-scalable. Immobilizing active materials in polymeric composites is an effective way to address these concerns. Such hybrid materials possess a combination of properties that are not normally found in a single constituent, combining the thermal and chemical stabilities of inorganic materials with the processability and flexibility of organic compounds while avoiding dangerous chemicals leech into the treated water. Given that water producers are required to provide high-quality drinking water, polymeric composites have been broadly employed to abate several pollutants. In this context, several nanometric materials have been integrated into polymeric matrices to form state-of-the-art water treatment composites, finding application in microbiological treatment, adsorption and photocatalysis. Due to their chemical flexibility, high surface area, optimal mechanical properties, and cost-effectiveness, such composites have great potential in water purification. The possibilities for tuning polymeric networks are virtually endless, which allows for relatively simple control of functionality (chemical modification, surface modification) and nanomorphology (porosity, structure) of the composites, and fine-tuning of these materials for specific applications and contaminants. In this chapter, we provide an up-to-date review of the importance of polymeric composites in removing several pollutants from water. The main techniques and materials employed in preparing nanocomposites for water treatment, along with their target contaminants, will be addressed, as well as a discussion on their economic feasibility and comparison with well-established techniques.

7.3.2 Contributions

I co-wrote this review chapter with JB and NBG, under supervision of JSC and MG.

7.4 Design of ternary additive for organic photovoltaics: a cautionary tale

RSC Adv., 2022, 12, 10029.

Chithiravel Sundaresan, Pierre Josse, Mario C. Vebber, Jaclyn Brusso, Jianping Lu, Ye Tao, Salima Alem, and Benoit H. Lessard.

7.4.1 Abstract

Silicon phthalocyanines as ternary additives are a promising way to increase the performance of organic photovoltaics. The miscibility of the additive and the donor polymer plays a significant role in the enhancement of the device performance, therefore, ternary additives can be designed to better interact with the conjugated polymer. We synthesized N-90-heptadecanyl-2,7-carbazole functionalized SiPc ((CBzPho)₂-SiPc), a ternary additive with increased miscibility in poly[N-90-heptadecanyl-2,7-carbazolealt-5,5-(40,70-di-2-thienyl-20,10,30-benzothiadiazole)] (PCDTBT). The resulting additive was included into PCDTBT and [6,6]-phenyl C71 butyric acid methyl ester as bulk (PC71BM) heterojunction OPV devices as a ternary additive. While the (CBzPho)₂-SiPc demonstrated strong EQE >30% contribution in the range of 650–730 nm, the overall performance was reduced because (CBzPho)₂-SiPc acted as a hole trap due to its high-lying HOMO energy level. This study demonstrates the importance of the solubility, miscibility, and energy level engineering of the ternary additive when designing organic photovoltaic devices.

7.4.2 Contributions

I carried out the electrochemical characterization of (CBzPho)₂-SiPc by cyclic voltammetry (CV) and helped with the thermal characterization.

7.5 N-Type Solution-Processed Tin versus Silicon Phthalocyanines: A Comparison of Performance in Organic Thin-Film Transistors and in Organic Photovoltaic

ACS Appl. Electron. Mater. 2021, 3, 1873–1885

Rosemary R. Cranston, Mário C. Vebber, Nicole A. Rice, Claire Tonnelé, Frédéric Castet, Luca Muccioli, Jaclyn L. Brusso, and Benoît H. Lessard.

7.5.1 Abstract

Tin(IV) phthalocyanines (SnPcs) are promising candidates for low-cost organic electronic devices, and have been employed in organic photovoltaics (OPVs) and organic thin-film transistors (OTFTs). However, they remain relatively understudied compared to their silicon phthalocyanine (SiPc) analogues. Previously, we reported the first solution-processed SnPc semiconductors for OTFTs and OPVs; however, the performances of these derivatives were unexpected. Herein to further study the behavior of these derivatives in OPVs and OTFTs, we report the synthesis along with optical and thermal characterization of seven axially substituted (OR)₂-SnPcs, five of which were synthesized for the first time. Density functional theory (DFT) was used to predict charge-carrier mobilities for our materials in their crystal state. The application of these SnPcs as ternary additives in poly(3-hexylthiophene) (P3HT)/phenyl-C₆₁-butyric acid methyl ester (PC61BM) OPVs and as semiconductors in solution-processed n-type OTFTs was also investigated. When employed as ternary additives in OPVs, all (OR)₂-SnPcs decreased the power conversion efficiency, open-circuit voltage, short-circuit current, and fill factor. However, in OTFTs, four of the seven materials exhibited greater electron field-effect mobility with similar threshold voltages compared to their previously studied SiPc analogues. Among these SnPcs, bis(triisobutylsilyl oxide) SnPc displayed the greatest electron field-effect mobility of 0.014 cm² V⁻¹ s⁻¹, with a threshold voltage of 31.4 V when incorporated into OTFTs. This difference in electrical performance between OTFT and OPV devices was attributed to the low photostability of SnPcs.

7.5.2 Contributions

I synthesized and purified all the silicon and tin phthalocyanines used in this work. I also characterized their thermal properties (TGA, DSC), opto-electronical properties (UV-Vis, CV), grew single-crystals for SC-XRD analysis, produced and characterized all the OPV devices. I co-wrote the manuscript with RRC.

7.6 Thin-Film Engineering of Solution-Processable n-Type Silicon Phthalocyanines for Organic Thin-Film Transistors

***ACS Appl. Mater. Interfaces* 2021, 13, 1008–1020.**

Rosemary R. Cranston, Mário C. Vebber, Jônatas Faleiro Berbigier, Nicole A. Rice, Claire Tonnelé, Zachary J. Comeau, Nicholas T. Boileau, Jaclyn L. Brusso, Adam J. Shuhendler, Frédéric Castet, Luca Muccioli, Timothy L. Kelly, and Benoît H. Lessard.

7.6.1 Abstract

Metal and metalloid phthalocyanines are an abundant and established class of materials widely used in the dye and pigment industry as well as in commercial photoreceptors. Silicon phthalocyanines (SiPcs) are among the highest-performing n-type semiconductor materials in this family when used in organic thin-film transistors (OTFTs) as their performance and solid-state arrangement are often increased through axial substitution. Herein, we study eight axially substituted SiPcs and their integration into solution-processed n-type OTFTs. Electrical characterization of the OTFTs, combined with atomic force microscopy (AFM), determined that the length of the alkyl chain affects device performance and thin-film morphology. The effects of high-temperature annealing and spin coating time on film formation, two key processing steps for fabrication of OTFTs, were investigated by grazing-incidence wide-angle X-ray scattering (GIWAXS) and X-ray diffraction (XRD) to elucidate the relationship between thin-film microstructure and device performance. Thermal annealing was shown to change both film crystallinity and SiPc molecular orientation relative to the substrate surface. Spin time affected film crystallinity, morphology, and interplanar d-spacing, thus ultimately modifying device performance. Of the eight materials studied, bis(tri-n-butylsilyl oxide) SiPc exhibited the greatest electron field-effect mobility ($0.028 \text{ cm}^2 \text{ V}^{-1} \text{ s}^{-1}$, a threshold voltage of 17.6 V) of all reported solution-processed SiPc derivatives.

7.6.2 Contributions

I synthesized and purified all the silicon phthalocyanines used in this work. I also characterized their thermal properties (TGA, DSC), measured their solubility in various solvents and grew single-crystals for SC-XRD analysis.

7.7 Mechanism of formation, characterization and cytotoxicity of green synthesized zinc oxide nanoparticles obtained from *Ilex paraguariensis* leaves extract

Nano-Structures & Nano-Objects 24 (2020) 100532.

Marina Bandeira, André L. Possan, Sandra S. Pavin, Camila S. Raota, Mario C. Vebber, Marcelo Giovanela, Mariana Roesch-Ely, Declan M. Devine, Janaina S. Crespo.

7.7.1 Abstract

Zinc oxide nanoparticles (ZnONPs) was produced using *Ilex paraguariensis* (mate) leaves extract using a green synthesis process. The influence of ethanolic and aqueous plant extract and zinc source on the green synthesis of ZnONPs was studied. Cyclic voltammetry and Fourier transform infrared spectroscopy (FTIR) were used for the assessment of the mechanism route of ZnONPs while the formation of this nanomaterial was confirmed by X-ray diffraction (XRD) analysis. The morphology and size of the ZnONPs synthesized were evaluated using field emission scanning microscopy (FESEM) and transmission electron microscopy (TEM) analysis. In general, all different synthesized ZnONPs exhibited a hexagonal crystalline structure whereas the size and shape varied depending on the extract and zinc salt used. Nonetheless, the most uniform and smallest ZnONPs were obtained using ethanolic extract and zinc nitrate, showing spherical morphology and a diameter of about 18 nm. With the use of cyclic voltammetry and FTIR analysis, it was concluded that the formation of ZnONPs through green synthesis occurred due to complexation of Zn(II) ions by antioxidants compounds present in the *Ilex paraguariensis* extract and further thermal degradation of the complexes. Concerning the cytotoxicity assays, the L929 cell viability decreases in a dose-dependent manner for all samples tested. In general, nanoparticles with reduced size and uniform shape exhibited no cytotoxic effects up to a concentration of 10 g mL⁻¹. However, higher ZnONPs concentrations caused a decrease in cell viability. This was possibly due an autophagic induction process triggered by the internalization of the nanomaterial. Finally, this work provides a better understanding of the mechanism route to obtain ZnONPs via green method and their potential to be used as a biomedical material.

7.7.2 Contribution

I have contributed to the characterization of the ZnO nanoparticles, namely UV-Vis spectroscopy, cyclic voltammetry and X-ray diffraction.

7.8 Preparation, characterization and application of polymeric thin films containing silver and copper nanoparticles with bactericidal activity

Journal of Environmental Chemical Engineering 8 (2020) 103745.

Fabiana Z. Eltz, Mario C. Vebber, Cesar Aguzzoli, Giovanna Machado, Janaina S. Crespo, Marcelo Giovanela.

7.8.1 Abstract

The aim of this work was to prepare and characterize self-assembled thin films (SATFs) of poly(allylamine hydrochloride) and poly(acrylic acid) containing silver (AgNPs) and copper nanoparticles (CuNPs) for their subsequent application in the disinfection of an industrial wastewater. The AgNPs and CuNPs were synthesized by direct irradiation of SATFs with ultraviolet light after immersion in silver and copper (II) salt solutions. At the end of the self-assembly procedure, the SATFs were thoroughly characterized by different instrumental techniques, including glow discharge optical emission spectroscopy (GD-OES), atomic force microscopy (AFM), field emission scanning electron microscopy (FESEM), X-ray photoelectron spectroscopy (XPS), inductively coupled plasma optical emission spectrometry (ICP-OES), and transmission electron microscopy (TEM). In general, the GD-OES spectra confirmed the incorporation/formation of AgNPs and CuNPs/copper (II) oxide in the SATFs. Moreover, it was observed through the FESEM and TEM analyses that a change in the salt concentration promoted a variation in the nanoparticle size incorporated into the SATFs (10–250 nm for AgNPs, and 10–170 nm for CuNPs). The disinfection process of the industrial wastewater with the SATFs reduced the total count of coliforms by 91 and 100 % compared to the raw industrial wastewater (untreated), being the SATF prepared with a concentration of $0.1098 \text{ mmol Ag}^+ \text{ L}^{-1}$ the most efficient material. Finally, the SATFs developed in this work present great potential for a possible application in the tertiary treatment of industrial wastewater due to ease of application, reduced environmental impact, and satisfactory inhibitory action.

7.8.2 Contribution

I contributed with the production and testing of self-assembled thin films and contributed to the final manuscript.

7.9 Influence of silver nanoparticle deposition on self-assembled thin films of weak polyelectrolytes/TiO₂ for bezafibrate photodegradation through central composite experimental design.

Journal of Environmental Chemical Engineering 8 (2020) 103619.

Jonas Kerwald, Mario Cesar Vebber, Cesar Aguzzoli, Janaina da Silva Crespo, Marcelo Giovanela.

7.9.1 *Abstract*

This study evaluated, through a central composite experimental design, the influence of silver nanoparticles (AgNPs) deposition, synthesized at different pH and silver concentration $[Ag^+]$, on the photocatalytic efficiency of self-assembled thin films (SATFs) of poly(allylamine hydrochloride) (PAH)/poly(acrylic acid) (PAA) and TiO_2 over bezafibrate (BZF) drug. The SATFs were produced by dip coating on glass substrates using the layer-by-layer technique and were characterized by ultraviolet and visible absorption spectroscopy, scanning electron microscopy with a field emission gun and energy dispersive spectroscopy. The results revealed that the SATF that represents the optimum point of the central composite design (pH = 7.0 and $[Ag^+] = 0.46 \text{ mmol L}^{-1}$) reduced the initial concentration of BZF by 81.4 %. The presence of AgNPs on the polyelectrolytes/ TiO_2 thin film was responsible for an increase of 64 % in its photocatalytic efficiency when compared to the film containing only polyelectrolytes and TiO_2 . Silver is present mostly in the form of nanoparticle agglomerates with sizes under 90 nm. Moreover, the optimized SATF showed no reduction in its photocatalytic efficiency after four reuse cycles. Finally, the data set showed that the SATFs of this work possess a high potential for photo-oxidation, which makes them attractive for domestic and industrial wastewater treatment.

7.9.2 *Contribution*

I helped produce and test the self-assembled thin films, as well as characterize their physico-chemical properties and contributed to the final manuscript

APPENDIX A - Supporting information for Chapter 2.

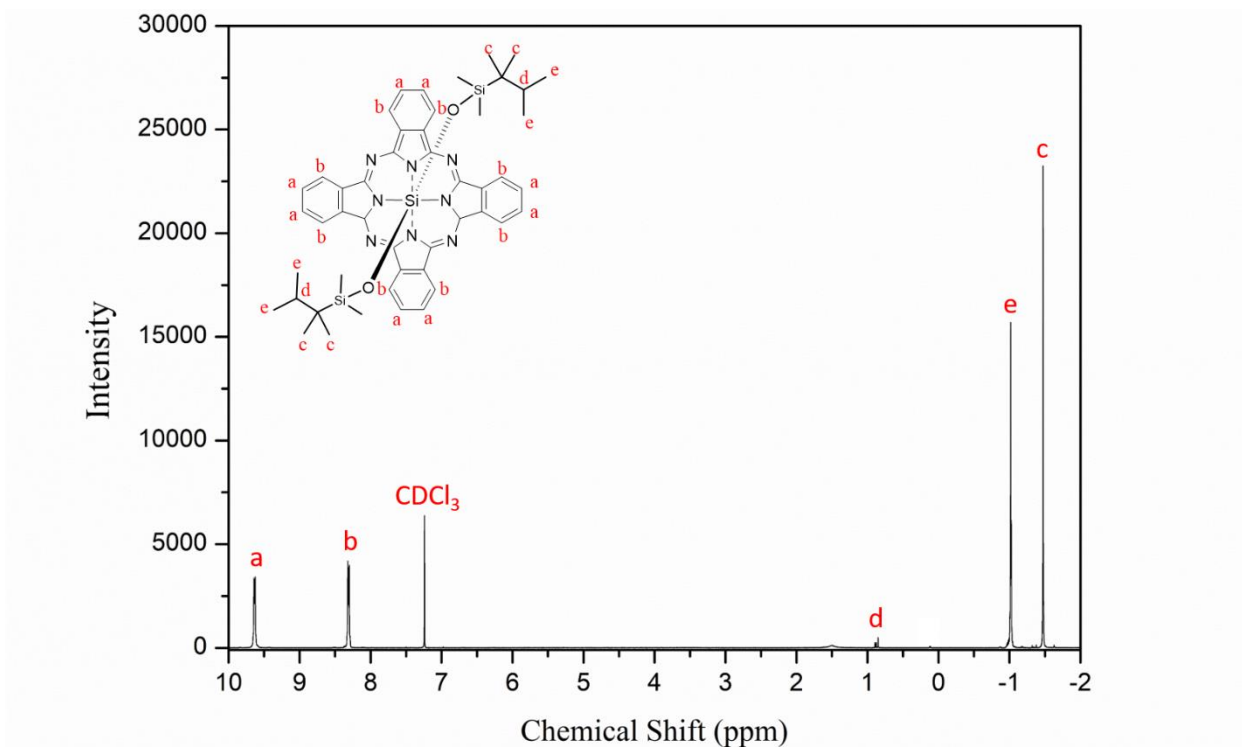
Bis (tri-alkylsilyl oxide) silicon phthalocyanines: understanding the role of solubility on device performance as ternary additives in organic photovoltaics.

Figure A1. ¹H NMR spectrum of compound (2.1) Bis(thexyldimethylsilyl oxide) silicon phthalocyanine in CDCl₃.

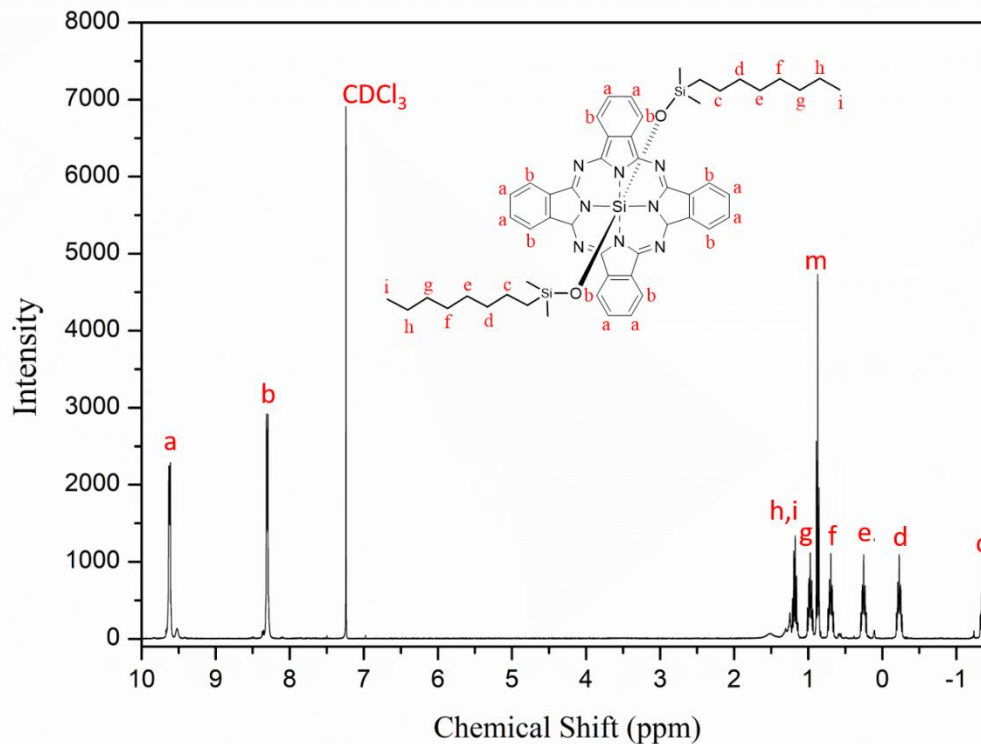


Figure A2. ¹H NMR spectrum of compound (2.2) Bis(n-octyldimethylsilyl oxide) silicon phthalocyanine in CDCl₃.

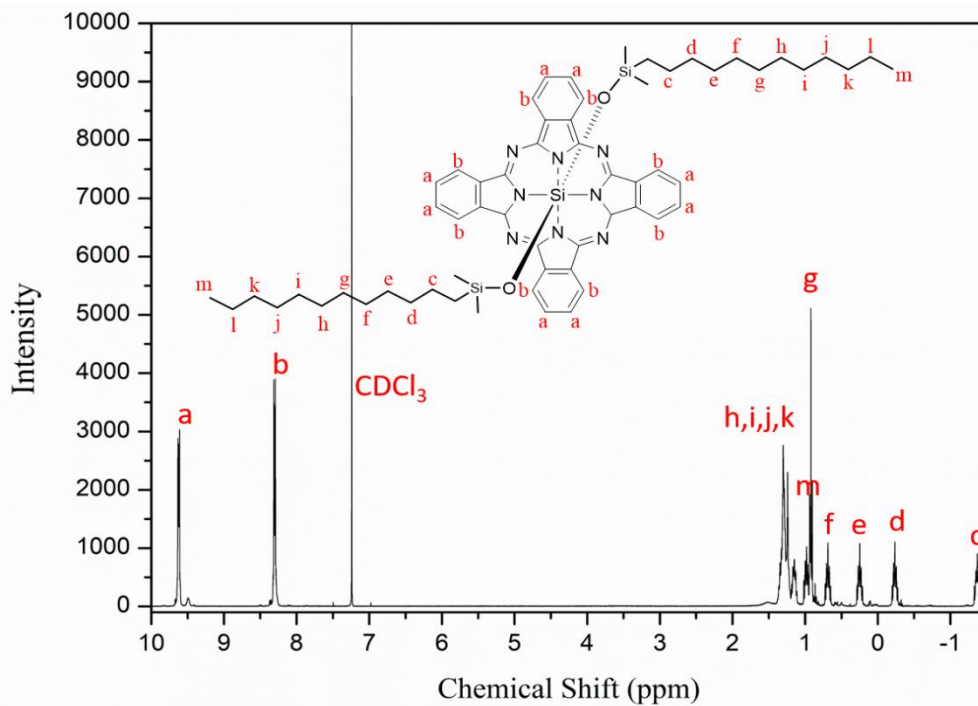


Figure A3. ¹H NMR spectrum of compound (2.3) Bis(n-dodecyldimethylsilyl oxide) silicon phthalocyanine in CDCl₃.

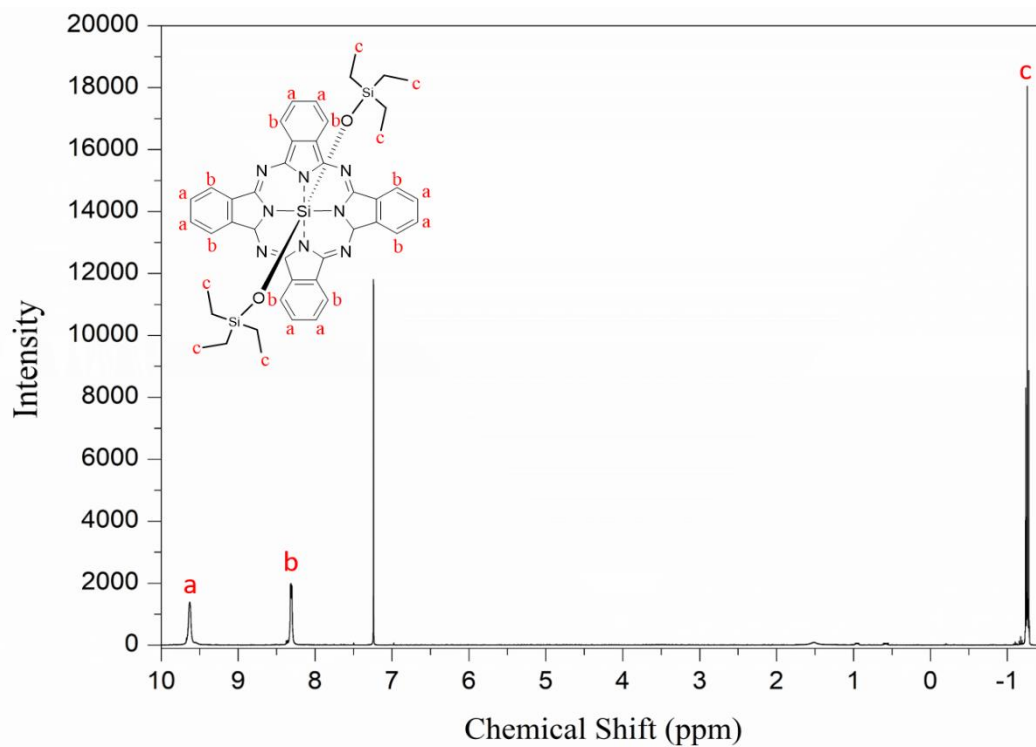


Figure A4. ¹H NMR spectrum of compound (2.4) Bis(tri-n-ethyl oxide) silicon phthalocyanine in CDCl₃.

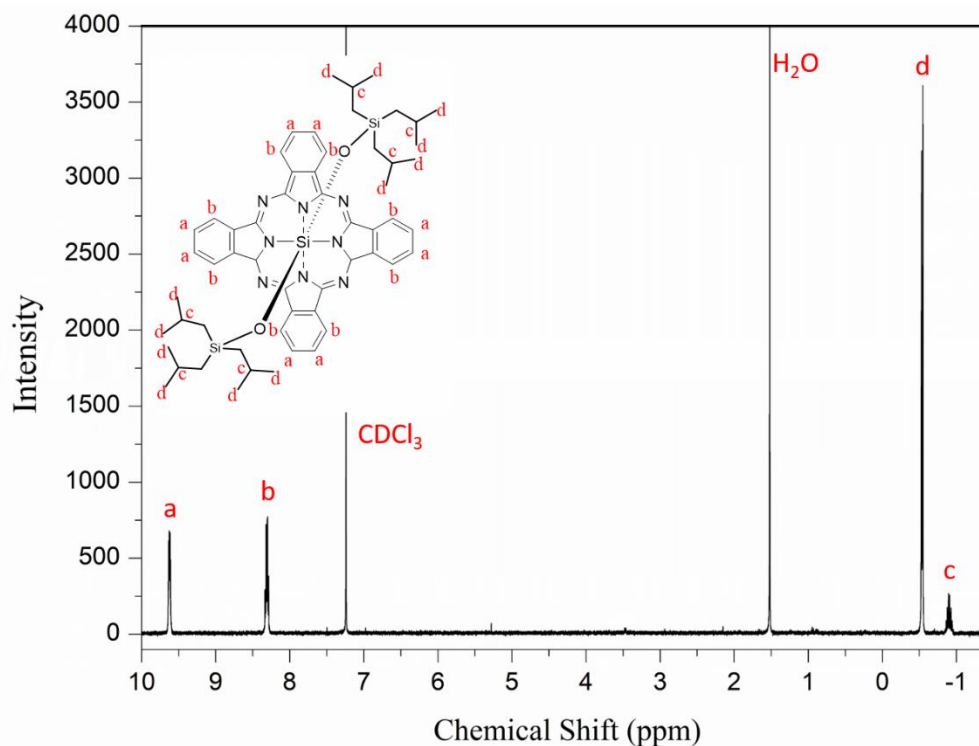


Figure A5. ¹H NMR spectrum of compound (2.5) Bis(triisobutylsilyl oxide) silicon phthalocyanine in CDCl₃.

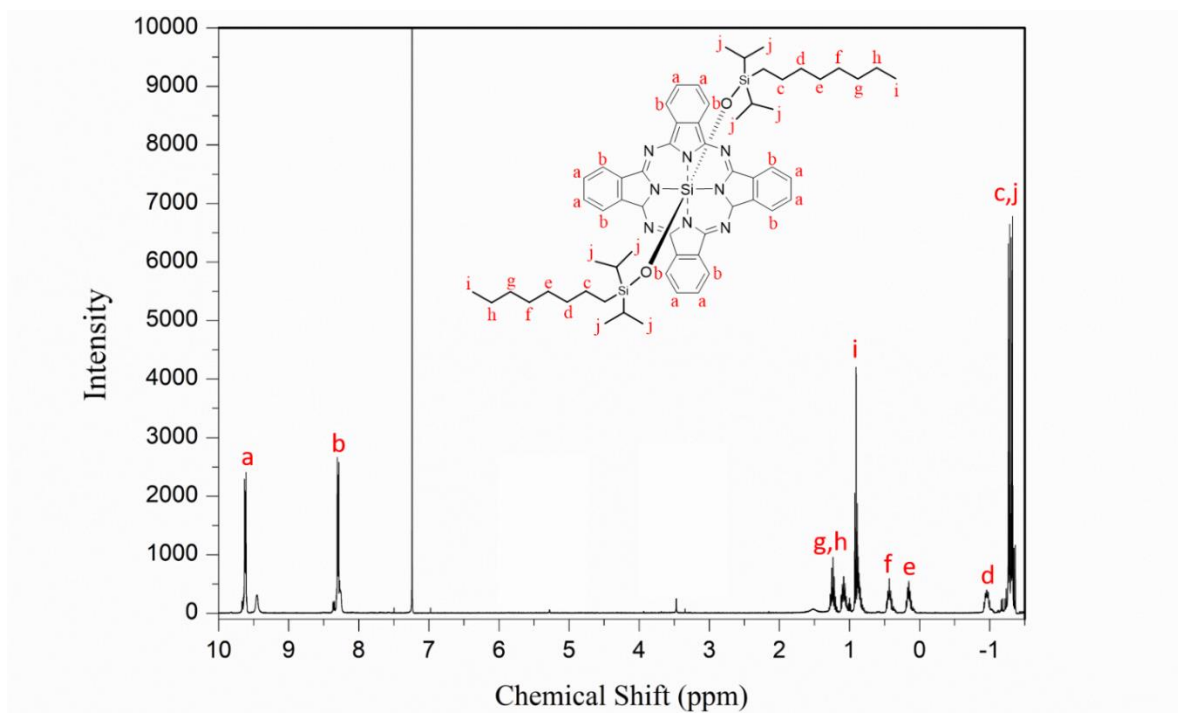


Figure A6. ^1H NMR spectrum of compound (2.8) Bis(diisopropyloctylsilyl oxide) silicon phthalocyanine in CDCl_3 .

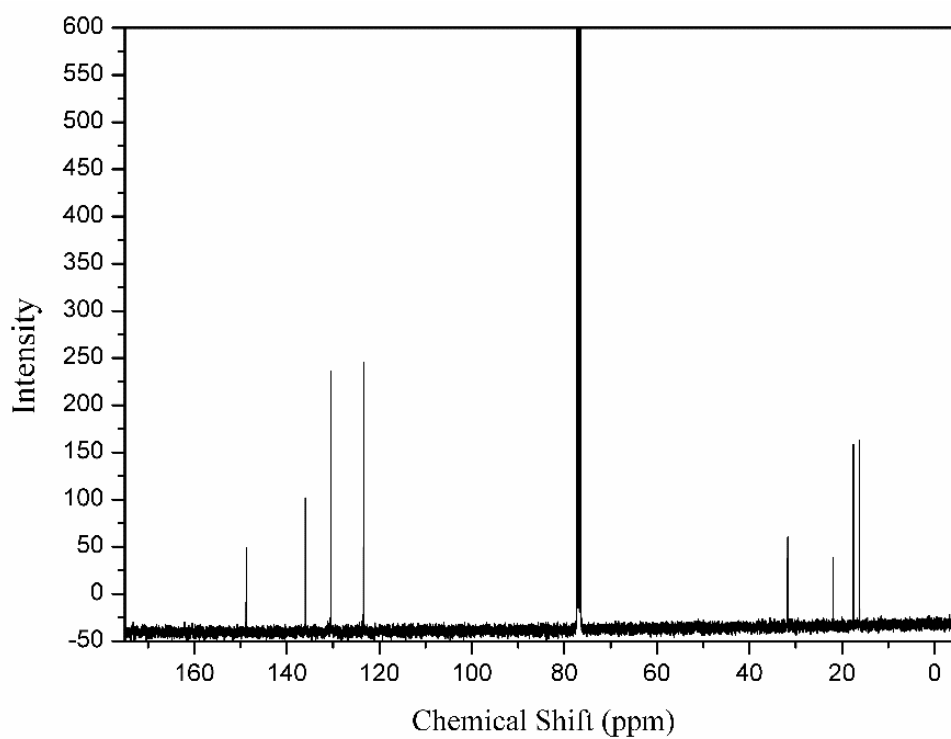


Figure A7. ^{13}C NMR spectrum of compound (2.1) Bis(thexyldimethylsilyl oxide) silicon phthalocyanine in CDCl_3 .

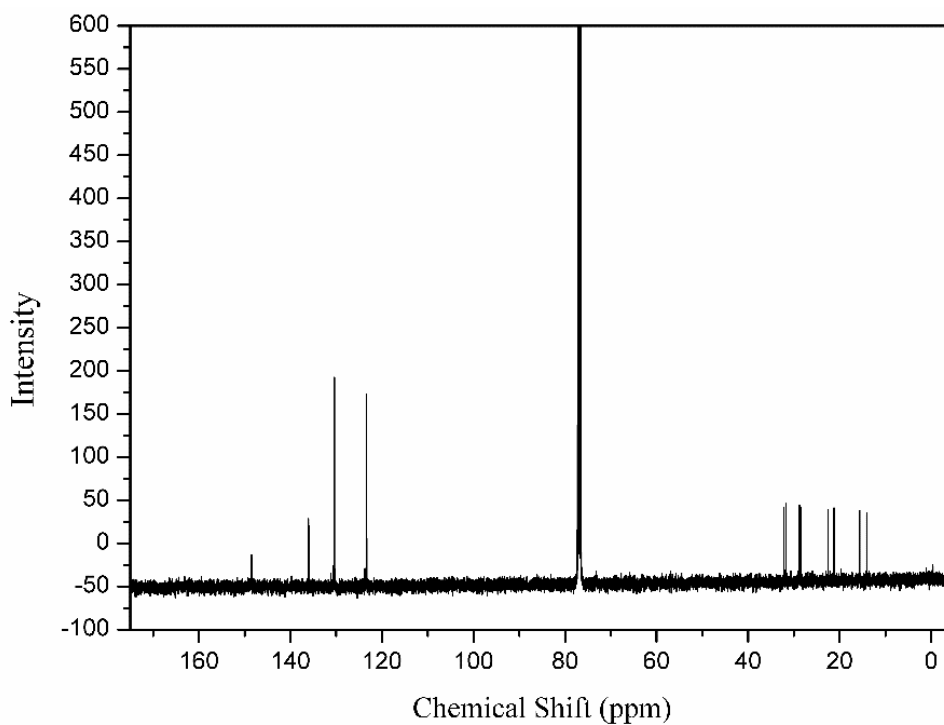


Figure A8. ^{13}C NMR spectrum of compound (2.2) Bis(n-octyldimethylsilyl oxide) silicon phthalocyanine in CDCl_3 .

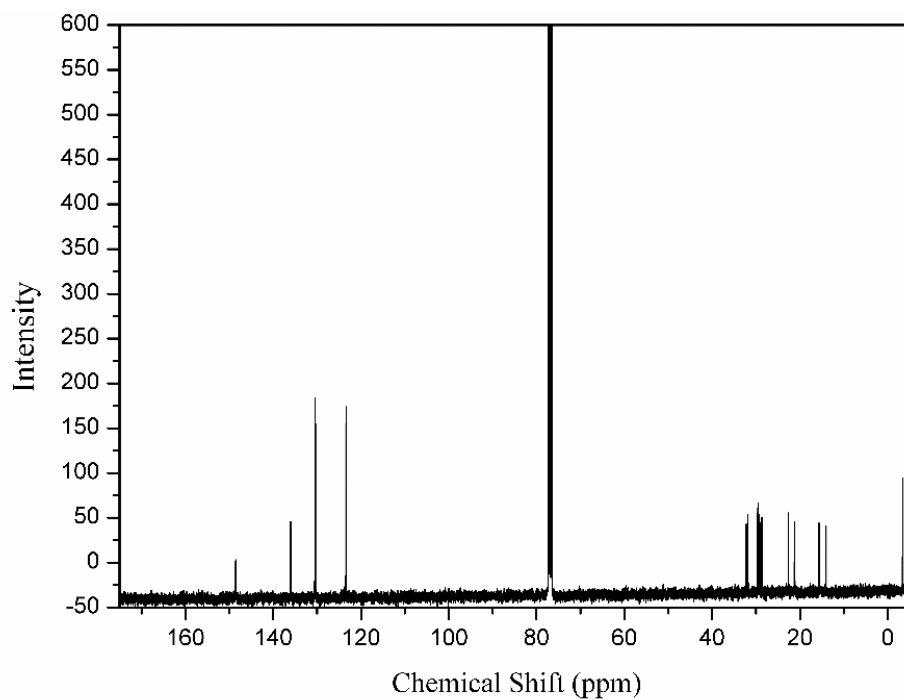


Figure A9. ^{13}C NMR spectrum of compound (2.3) Bis(n-dodecyldimethylsilyl oxide) silicon phthalocyanine in CDCl_3 .

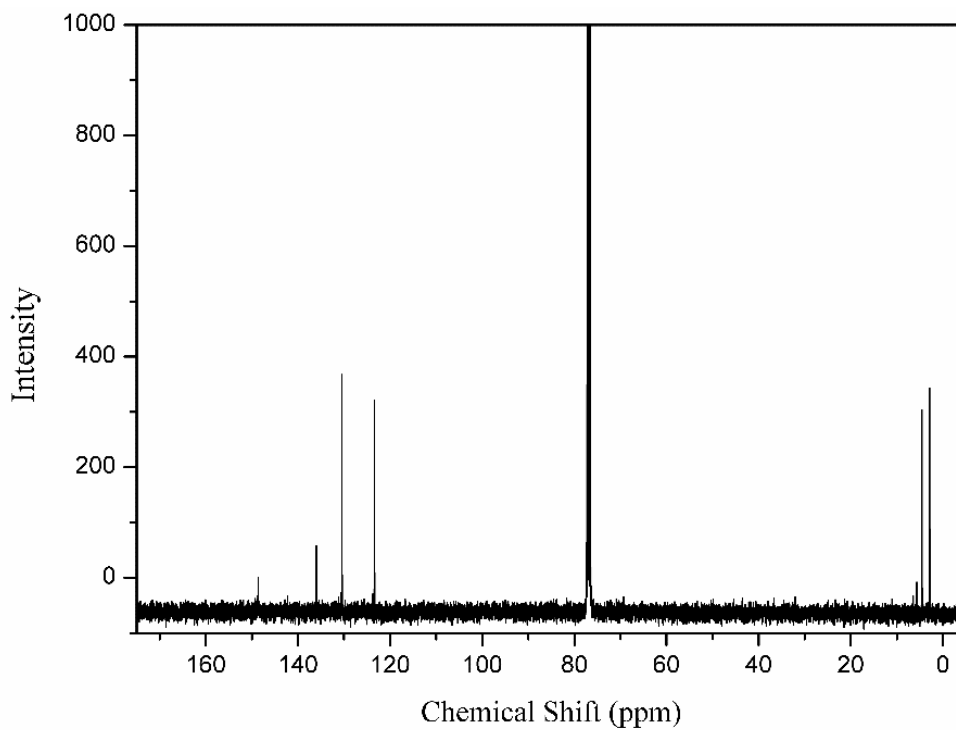


Figure A10. ^{13}C NMR spectrum of compound (2.4) Bis(tri-n-ethyl oxide) silicon phthalocyanine in CDCl_3 .

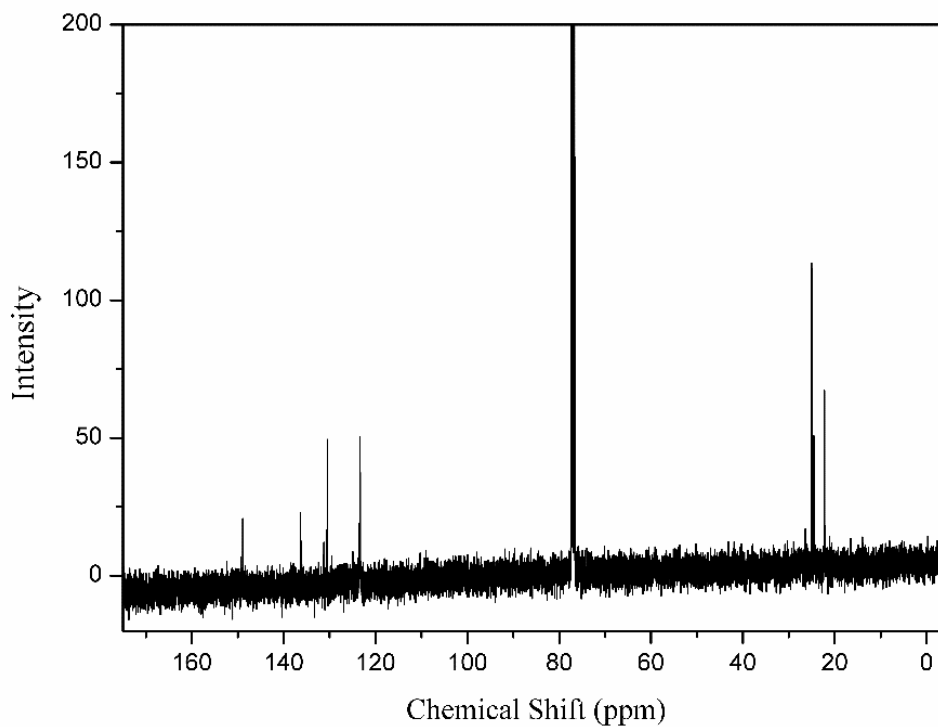


Figure A11. ^{13}C NMR spectrum of compound (2.5) Bis(triisobutylsilyl oxide) silicon phthalocyanine in CDCl_3 .

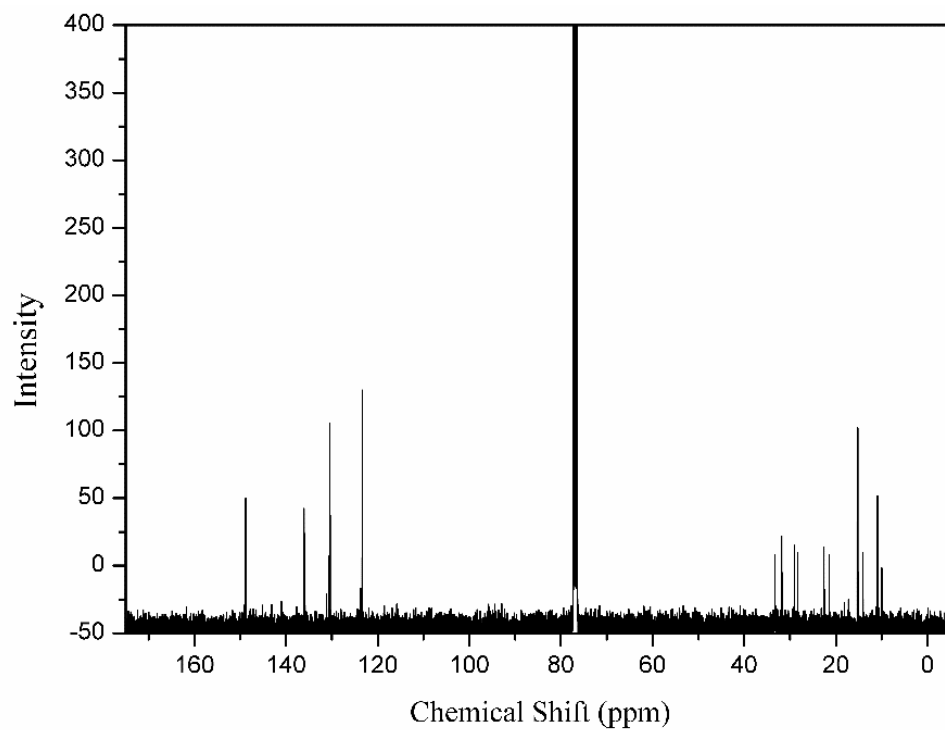


Figure A12. ^{13}C NMR spectrum of compound (2.8) Bis(diisopropyloctylsilyl oxide) silicon phthalocyanine in CDCl_3 .

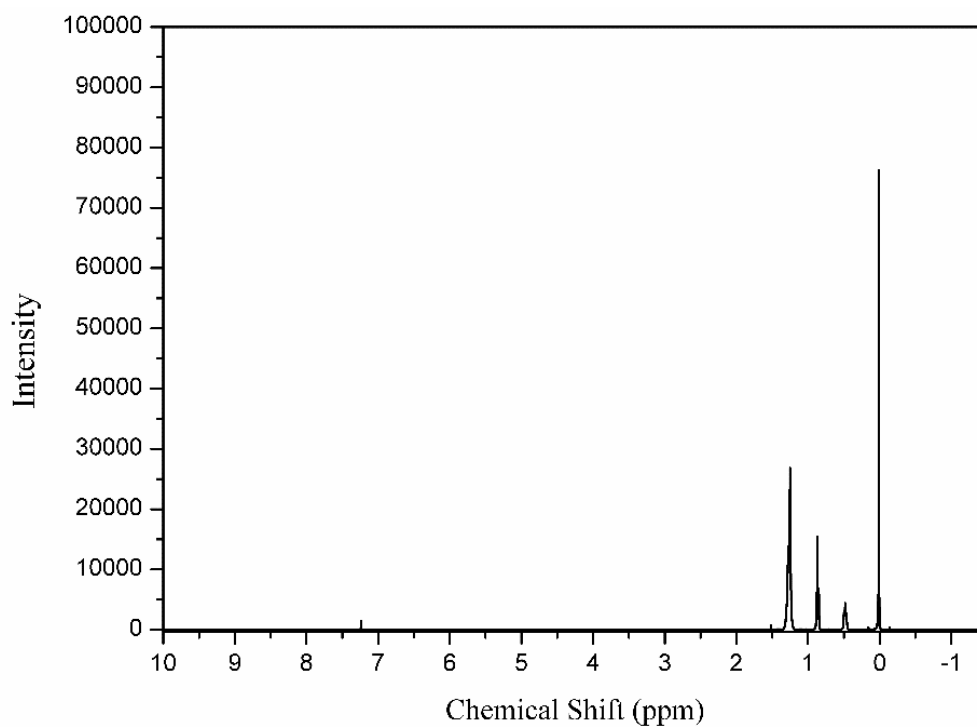
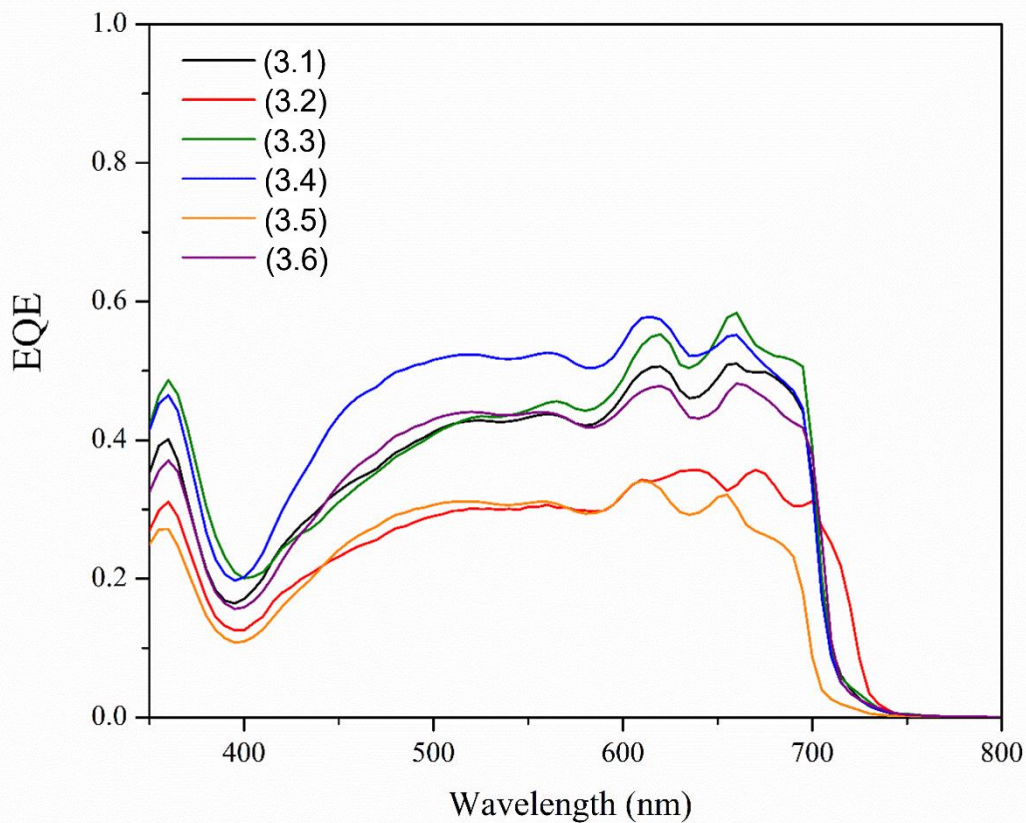


Figure A13. ^1H NMR spectrum of bis(hexyldimethyl)siloxane impurity in CDCl_3 , synthesized from blank reaction; hexyldimethyl chlorosilane + sodium hydroxide in chlorobenzene.

APPENDIX B – Supporting information for Chapter 3.

Thermodynamic Property-Performance Relationships in Silicon Phthalocyanine-based Organic Photovoltaics.**Figure B1.** External quantum efficiency spectra of the P3HT/(R₃SiO)₂-SiPc devices.

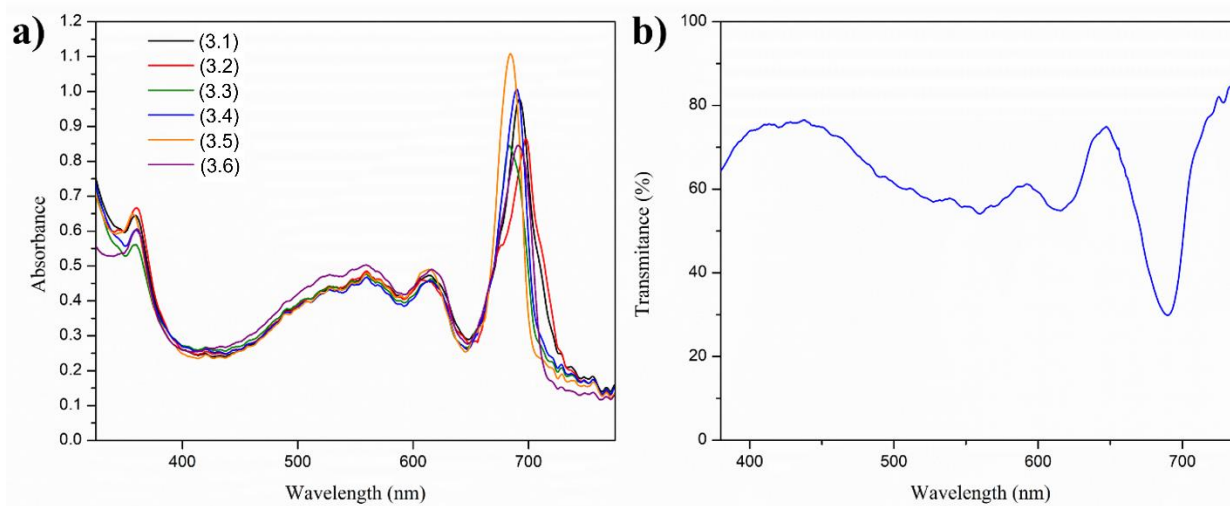


Figure B2. a) UV-Vis spectrum of P3HT/ $(R_3SiO)_2$ -SiPc devices and b) transmittance of device (4).

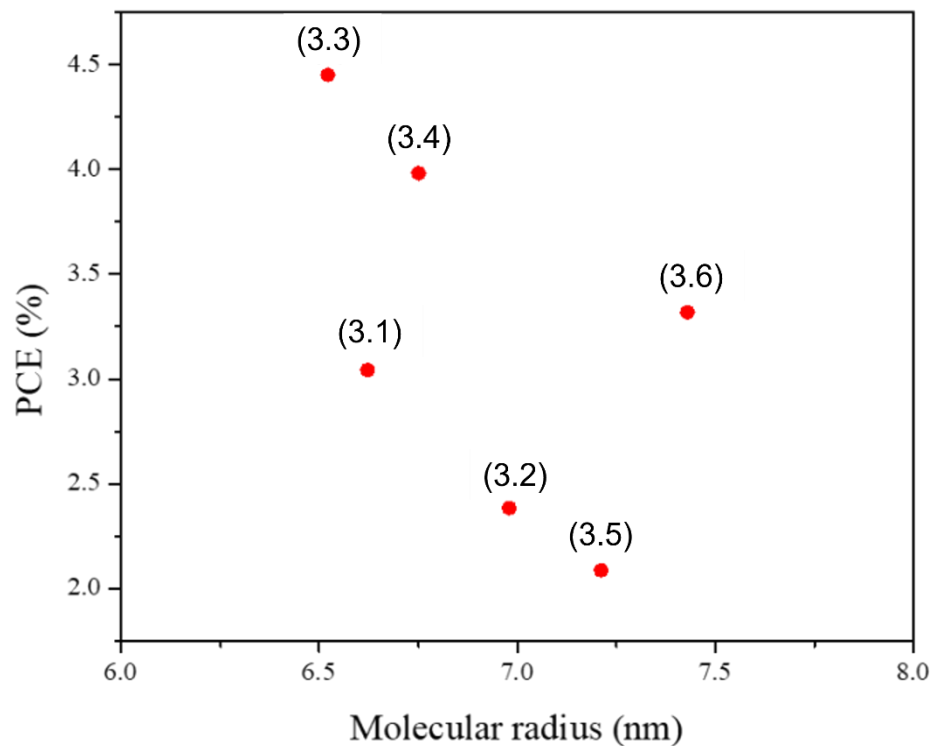


Figure B3. PCE of OPV devices as a function of the molecular radius of $(R_3SiO)_2$ -SiPcs.

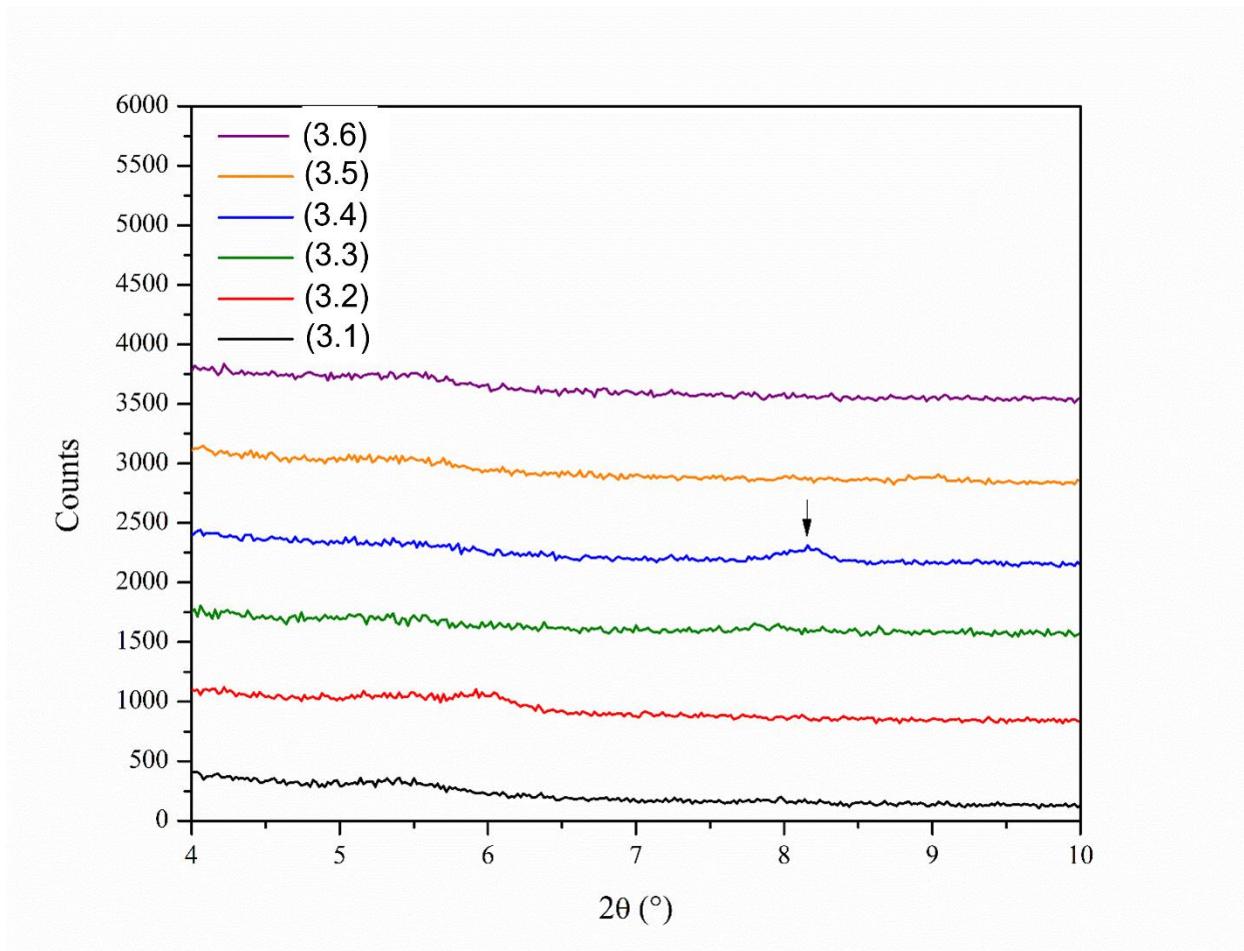


Figure B4. X-ray diffractograms of the P3HT/(R₃SiO)₂-SiPc thin films.

APPENDIX C – Supporting information for Chapter 5.**From P-type to N-type: peripheral fluorination of axially substituted silicon phthalocyanines enables fine tuning of charge transport.****Table C1.** Synthetic yield of F₂-F₁₆SiPc for reactions carried out at different conditions.

Strategy		Yield
As reported		9%
Solvent	Quinoline	No product
	Dichlorobenzene	No product
Silicon Source	SiBr ₄	9%
	Phthalonitrile + SiBr ₄ / no solvent	No product
Reaction time	Increase step i to 24h	8%
	Increase step ii to 48h	7%
	Decrease step ii to 4 h	2%
Reaction temperature	Decrease step ii to 160C	4%
	Decrease temperature of step i to 0C	9%
External fluoride source	CsF	8 %
	CsF + Crown ether	No product
	Tetrabutylammonium fluoride	No product
Phthalonitrile to LiHDMS ratio	1:1	17%
	1: 0.6	23%

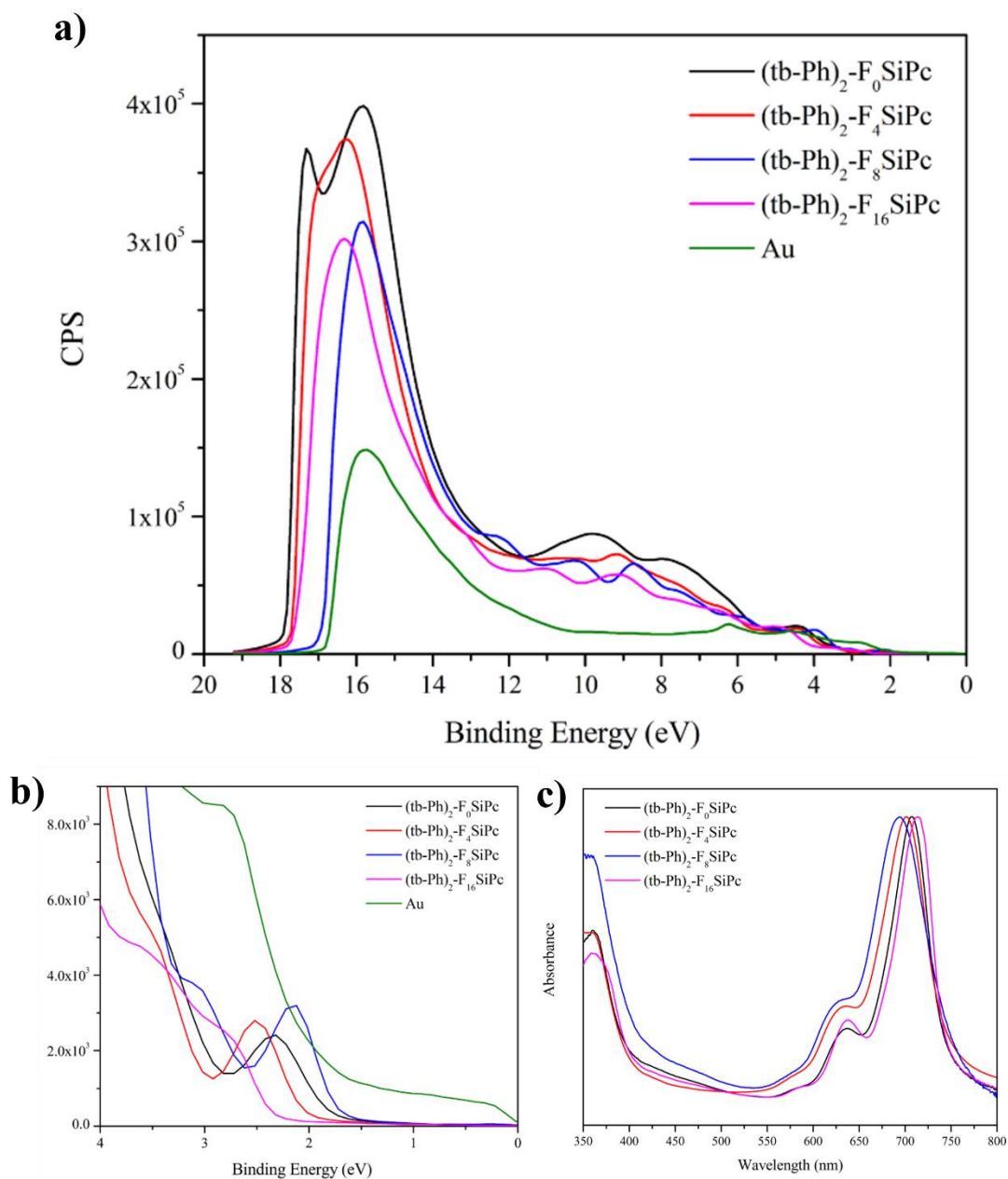


Figure C1. a) UPS spectra, b) zoom of the trailing edge of the UPS spectra, and c) solid-state UV-Vis of functionalized (tb-Ph)₂-F_xSiPcs.

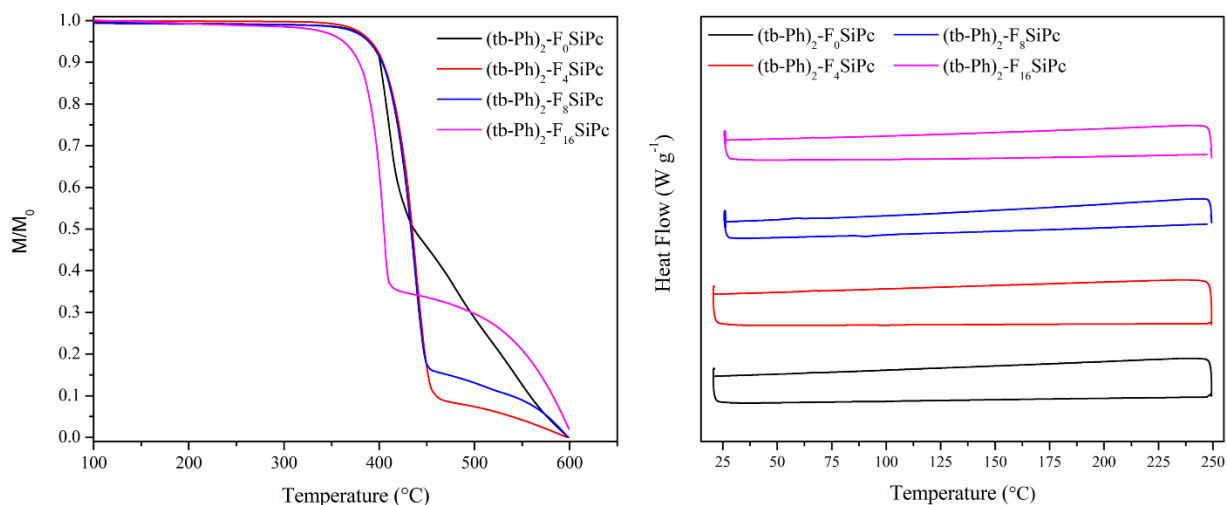


Figure C2. a) TGA and b) DSC curves for $(\text{tb-Ph})_2\text{-F}_x\text{SiPc}$ compounds.

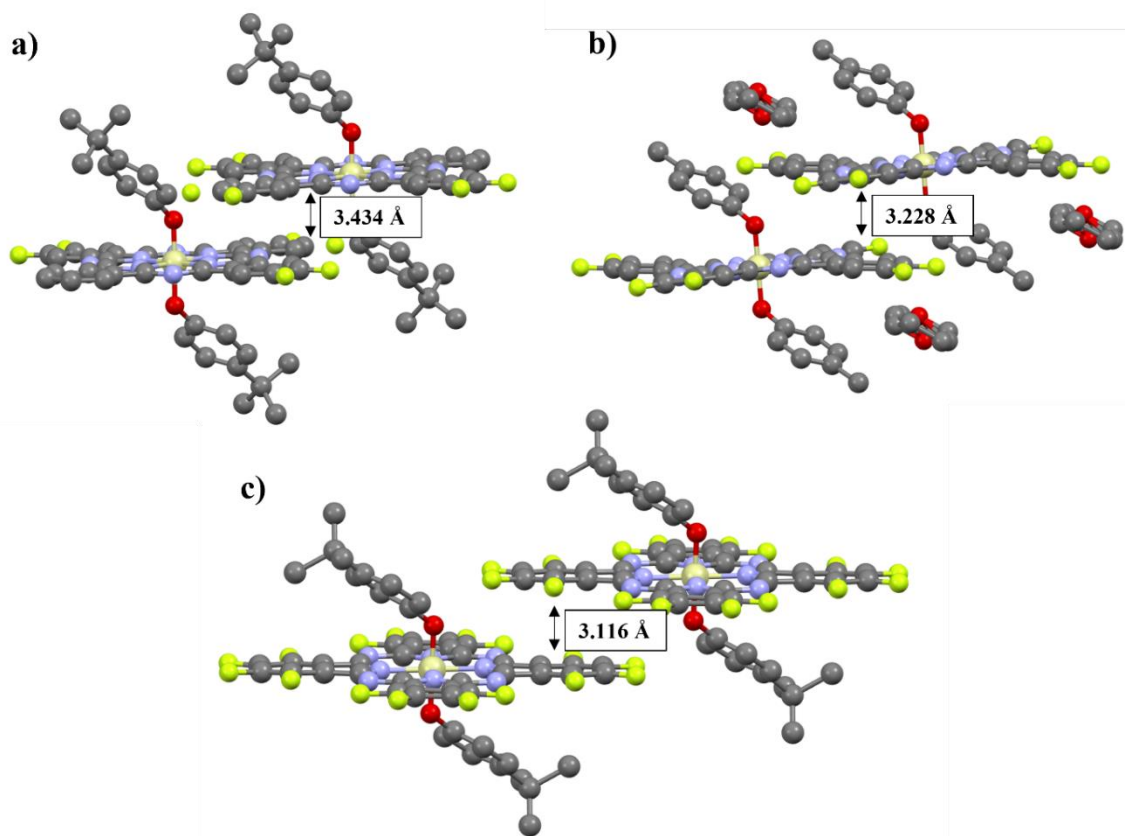


Figure C3. Solid-state packing and interplanar distance of a) $(\text{tb-Ph})_2\text{-F}_4\text{SiPc}$, b) $(\text{tb-Ph})_2\text{-F}_8\text{SiPc}$ (contains significant distortions in the tertbutyl groups, which are not displayed here for that reason. Solvent in structure is THF, from crystal-growth procedure), and c) $(\text{tb-Ph})_2\text{-F}_{16}\text{SiPc}$, obtained from single-crystal X-ray diffraction. Structure factors can be found in in Figures S26-S28.

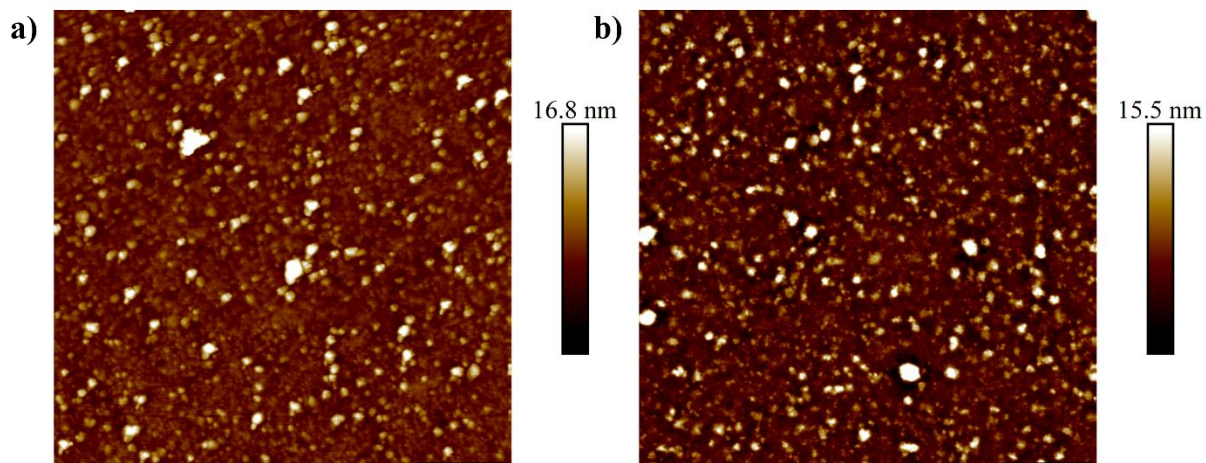


Figure C4. Atomic force microscopy images of bulk heterojunctions composed of PTQ10 and a) $(tb-Ph)_2-F0SiPc$ and b) $(tb-Ph)_2-F4SiPc$.

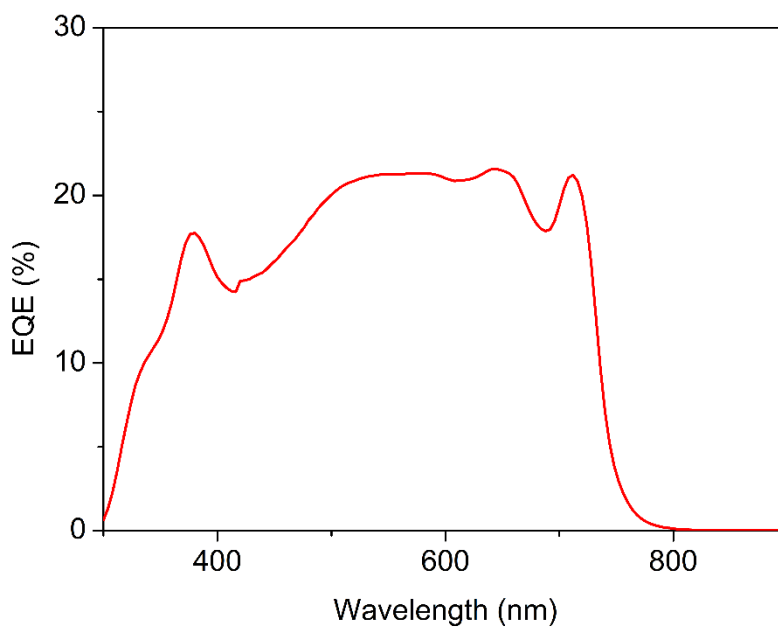


Figure C5. External quantum efficiency of PTQ10/ $(tb-Ph)_2-F4SiPc$ organic photodetectors.

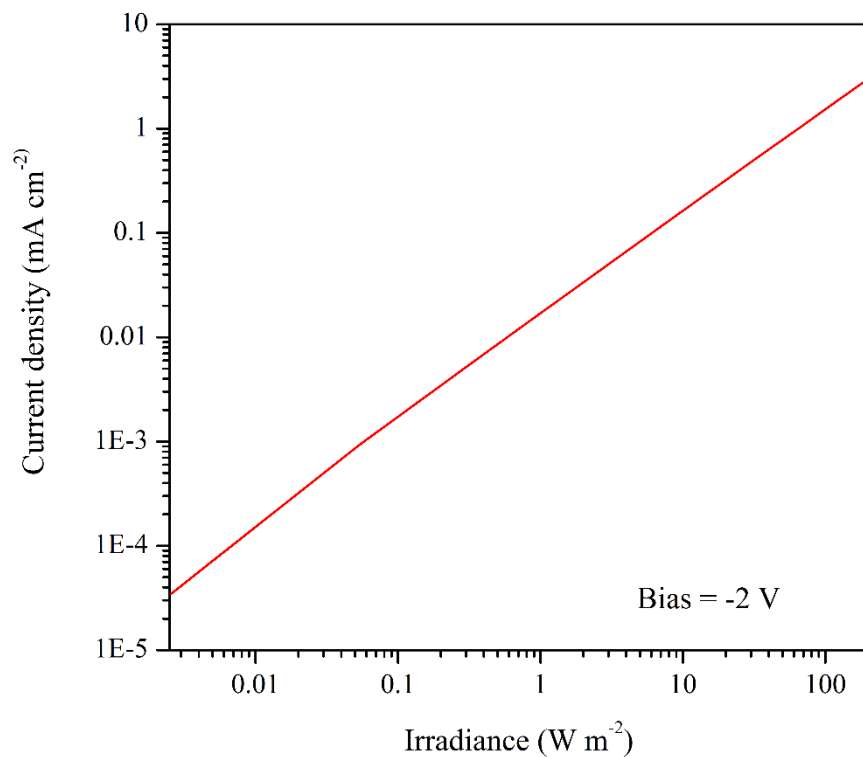


Figure C6. Linearity of PTQ10/(tb-Ph)₂-F₄SiPc organic photodetectors as a function of irradiance power.

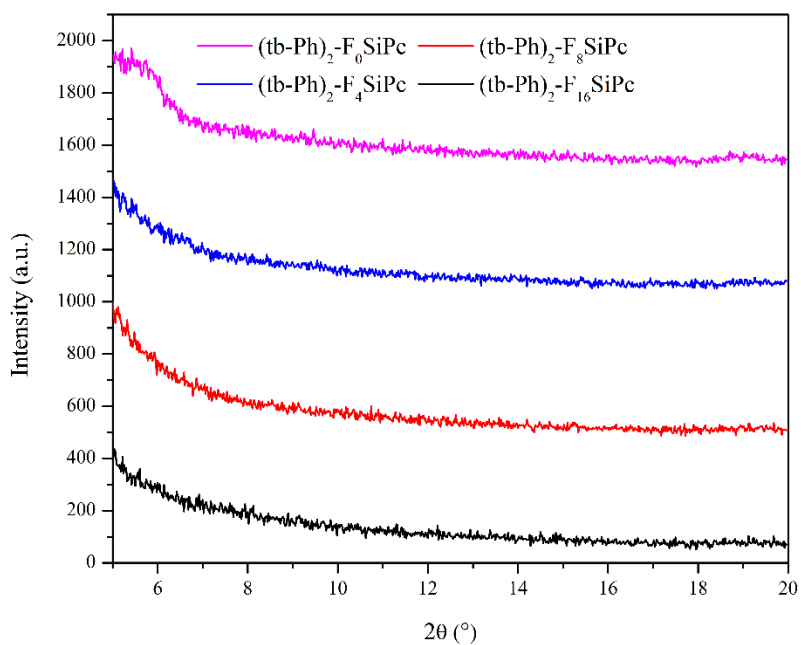


Figure C7. X-Ray diffractograms of (tb-Ph)₂-F_xSiPcs films evaporated on Si/SiO₂ substrates.

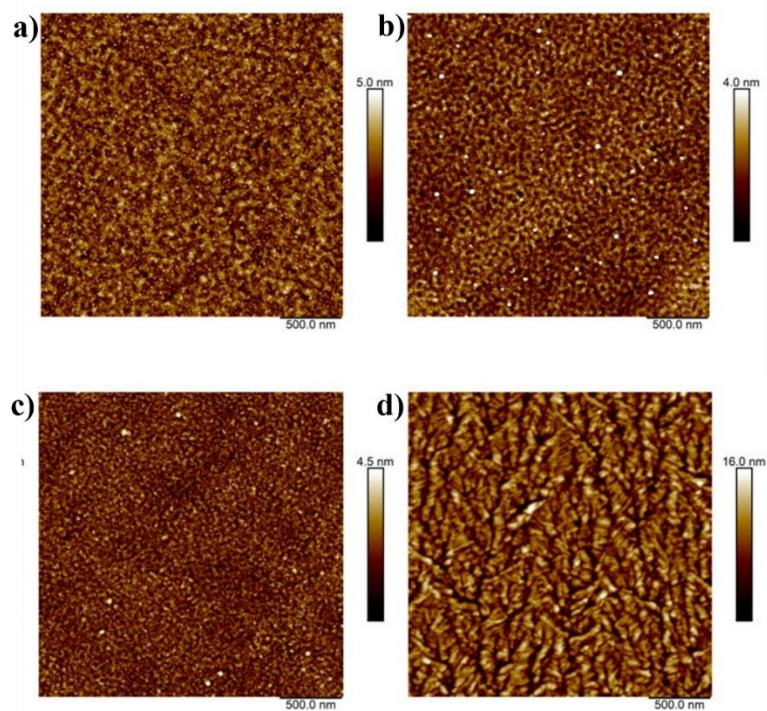


Figure C8. Atomic force microscopy images of a) $(tb-Ph)_2-F_0SiPc$, b) $(tb-Ph)_2-F_4SiPc$, c) $(tb-Ph)_2-F_8SiPc$ and d) $(tb-Ph)_2-F_{16}SiPc$ films evaporated on Si/SiO₂ substrates.

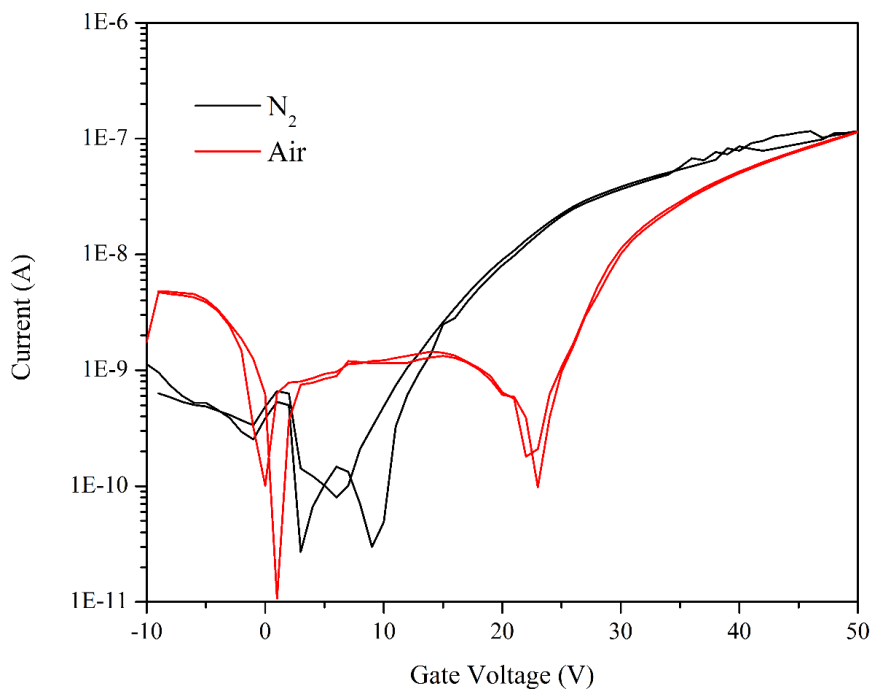


Figure C9. Transfer curves ($V_{DS} = +50V$) of evaporated $(tb-Ph)_2-F_{16}SiPcs$ transistors characterized in N₂ and in air.

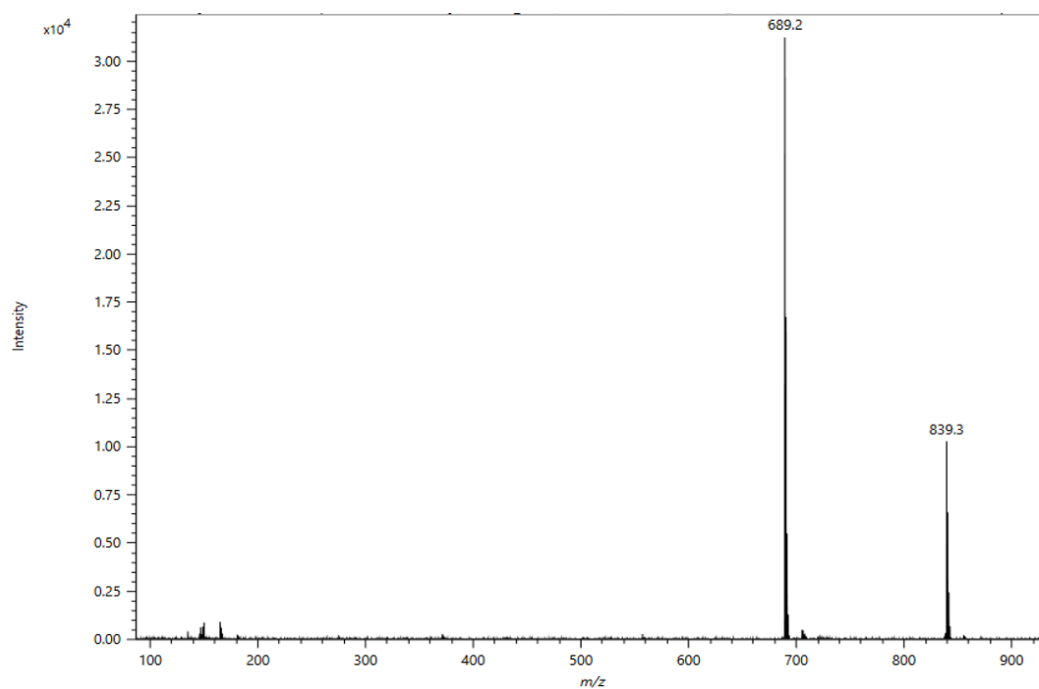


Figure C10. DART-MS spectrum of $(\text{tb-Ph})_2\text{-F}_0\text{SiPc}$.

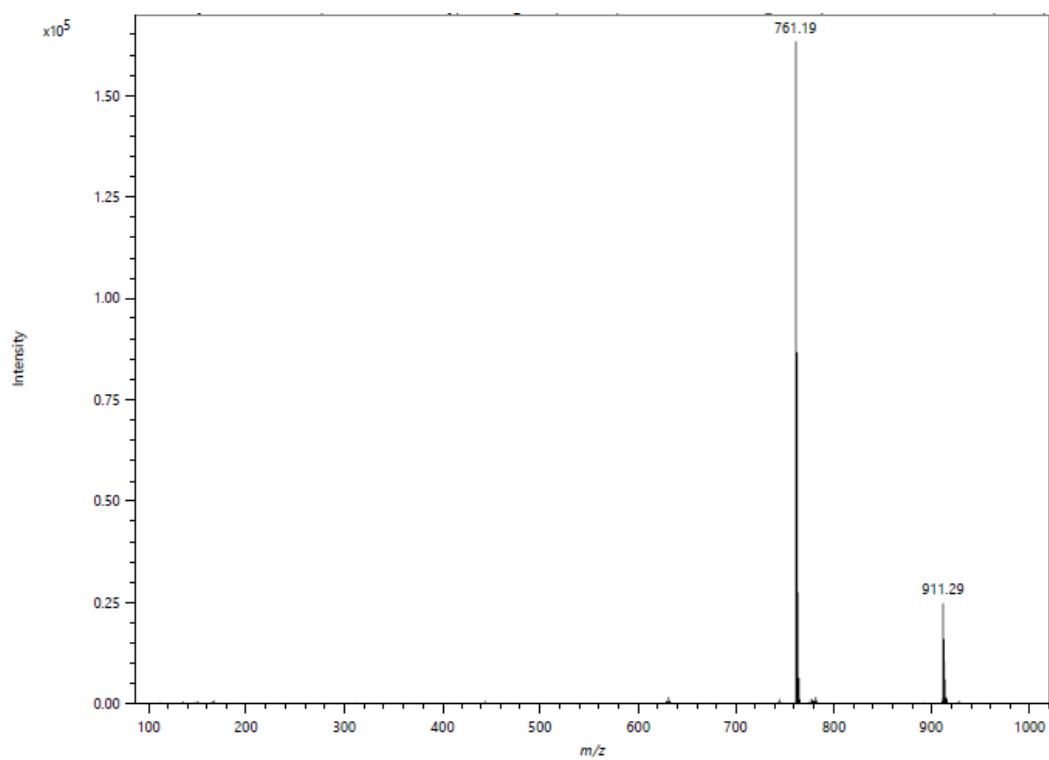


Figure C11. DART-MS spectrum of $(\text{tb-Ph})_2\text{-F}_4\text{SiPc}$.

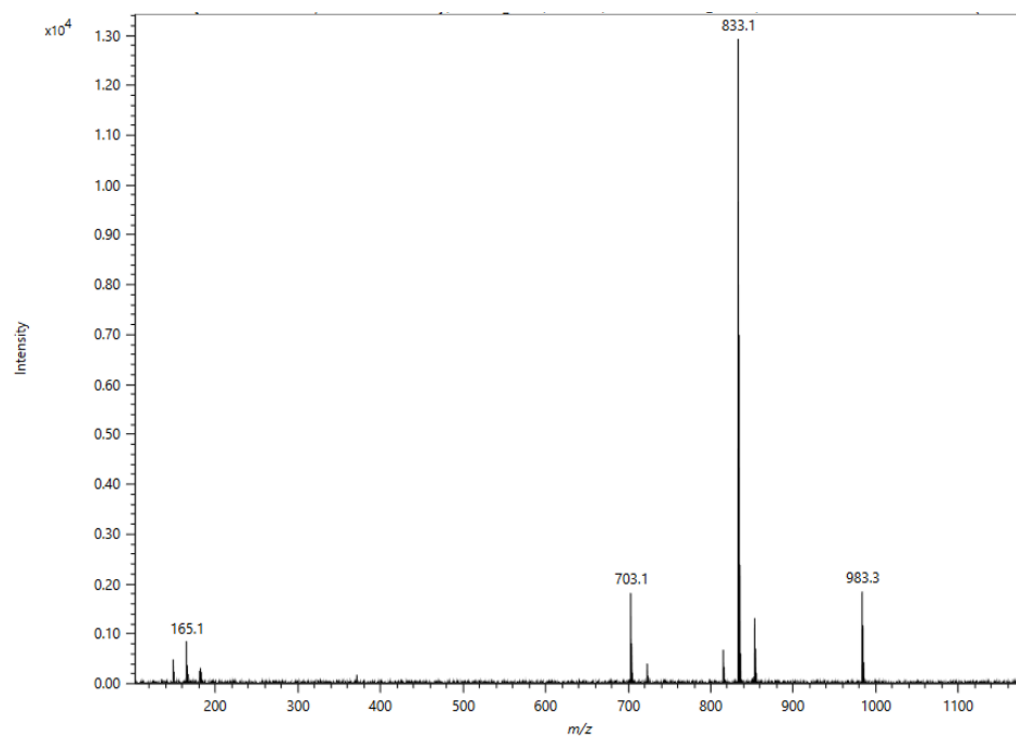


Figure C12. DART-MS spectrum of (tb-Ph)₂-F₈SiPc.

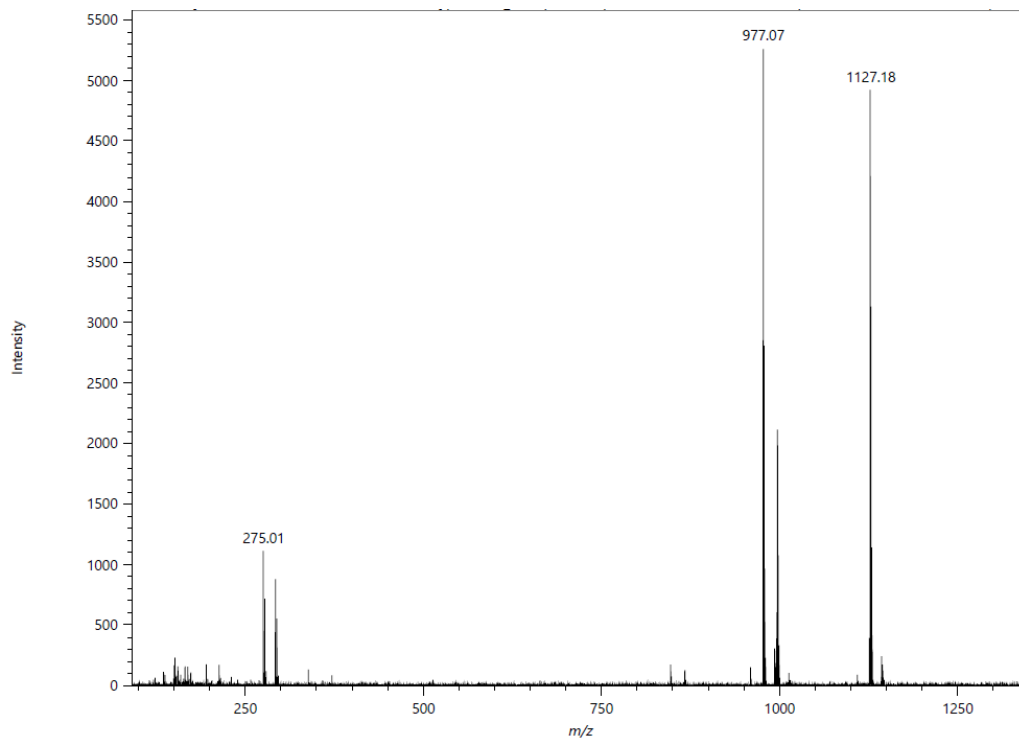


Figure C13. DART-MS spectrum of (tb-Ph)₂-F₁₆SiPc.

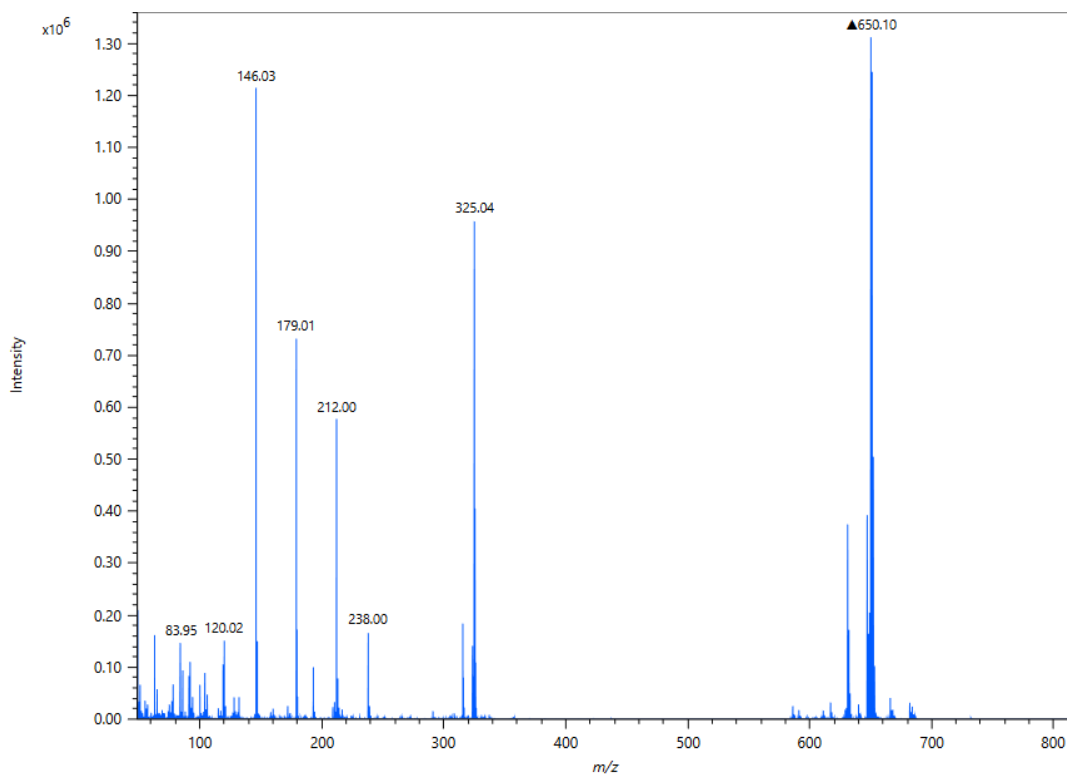


Figure C14. EI-MS spectrum of crude F₄SiPc.

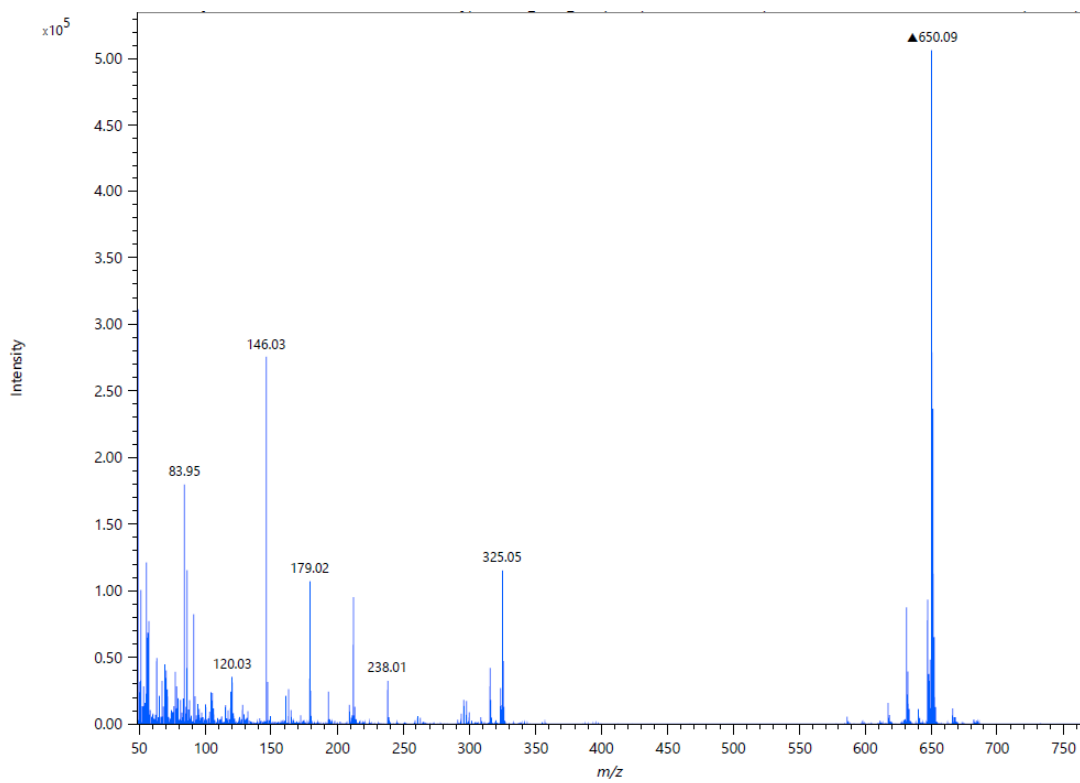


Figure C15. EI-MS spectrum of F₄SiPc after treatment with BCl₃.

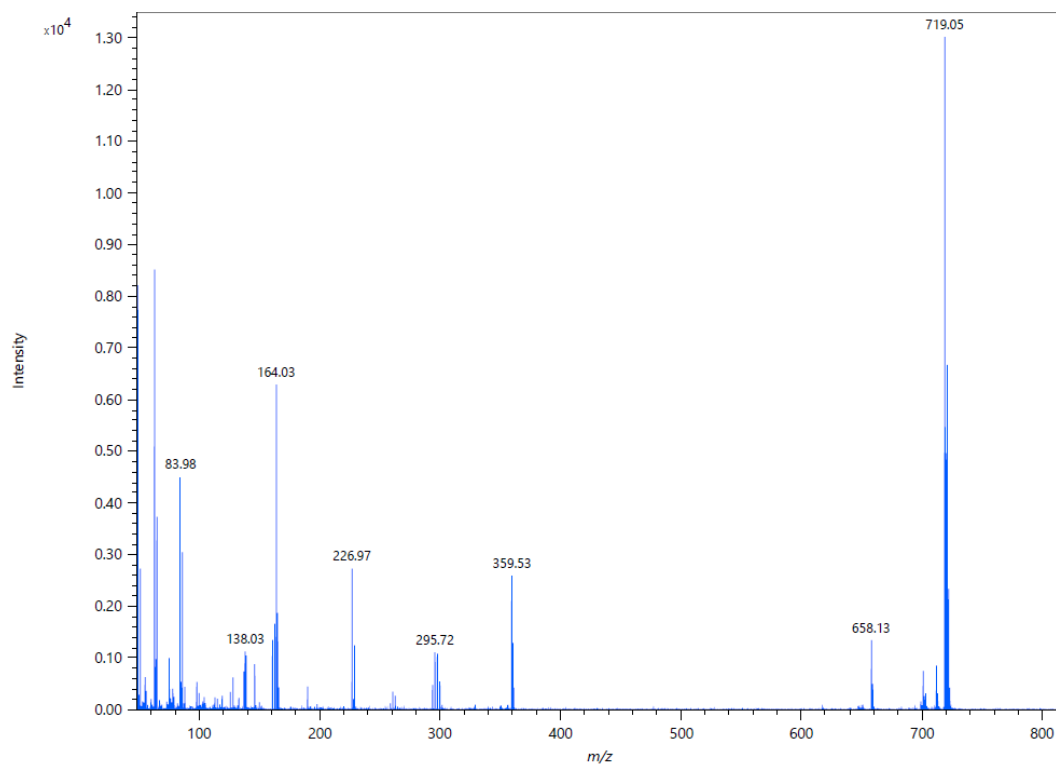


Figure C16. EI-MS spectrum of crude F_8SiPc .

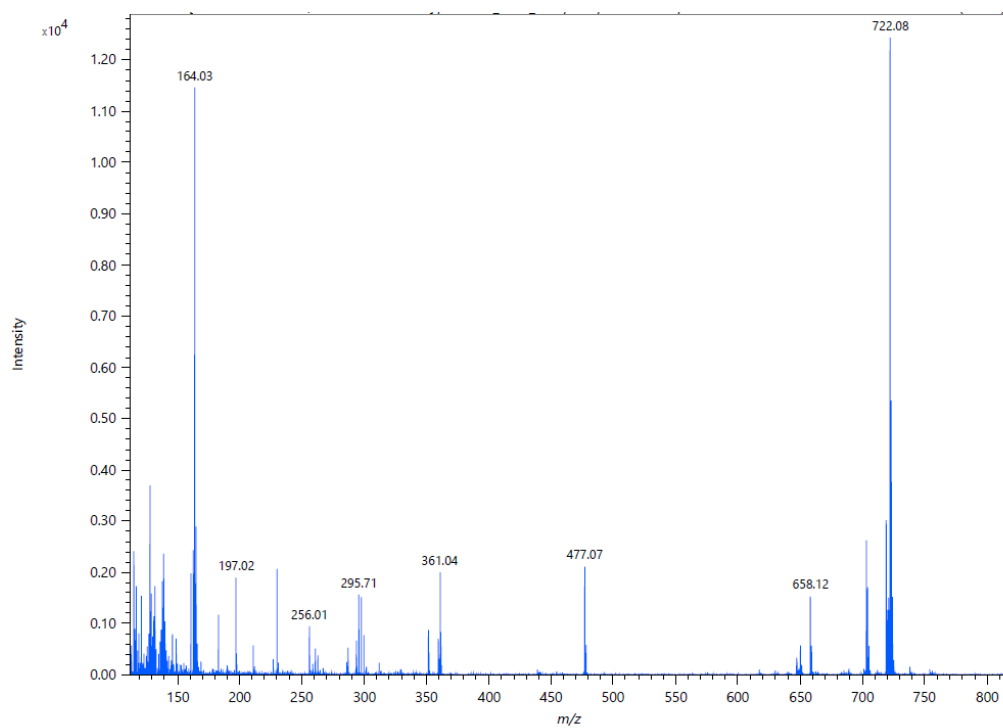


Figure C17. EI-MS spectrum of F_8SiPc after treatment with BCl_3 .

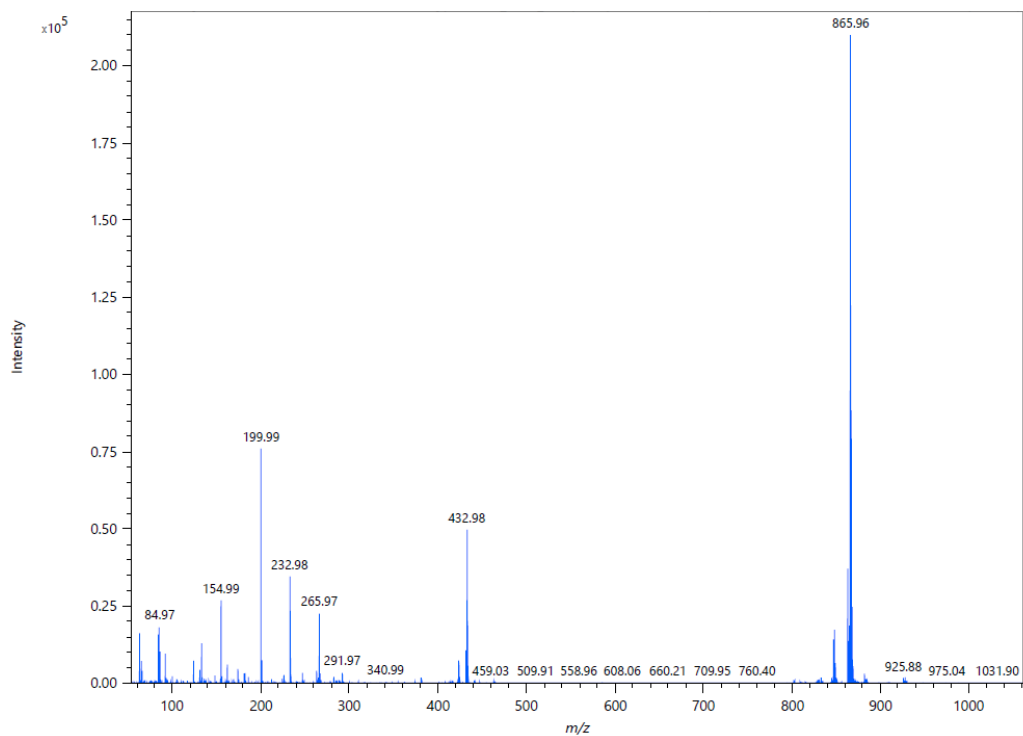


Figure C18. EI-MS spectrum of crude F₁₆SiPc.

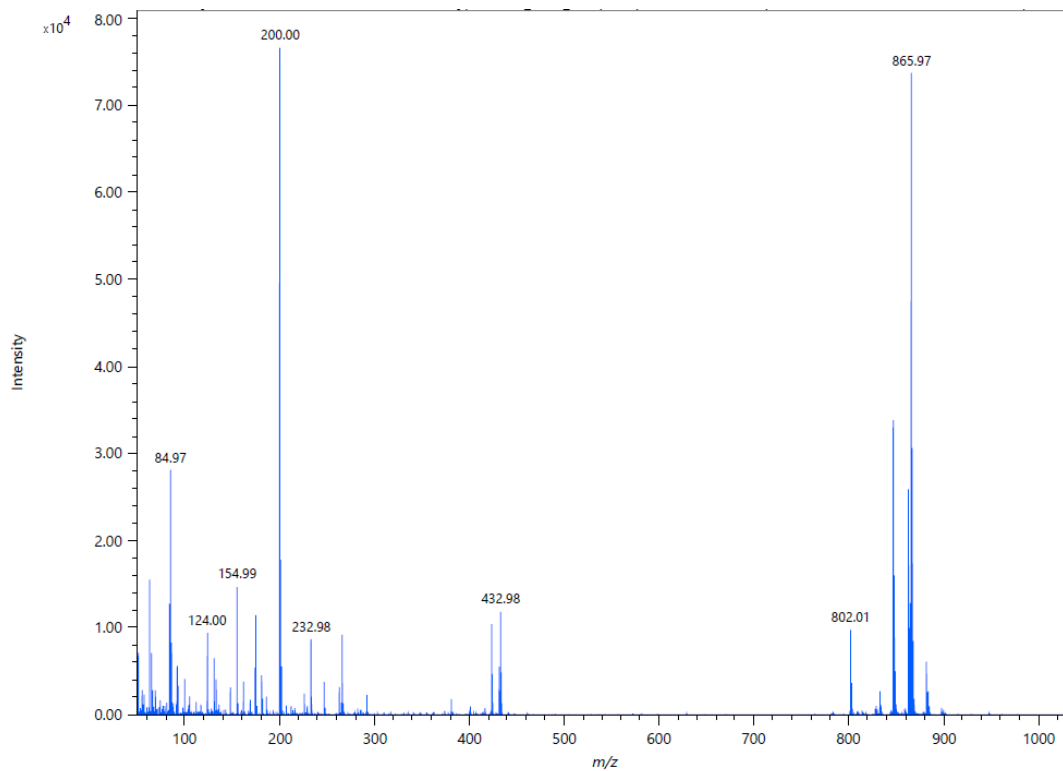


Figure C19. EI-MS spectrum of F₁₆SiPc after treatment with BCl₃.

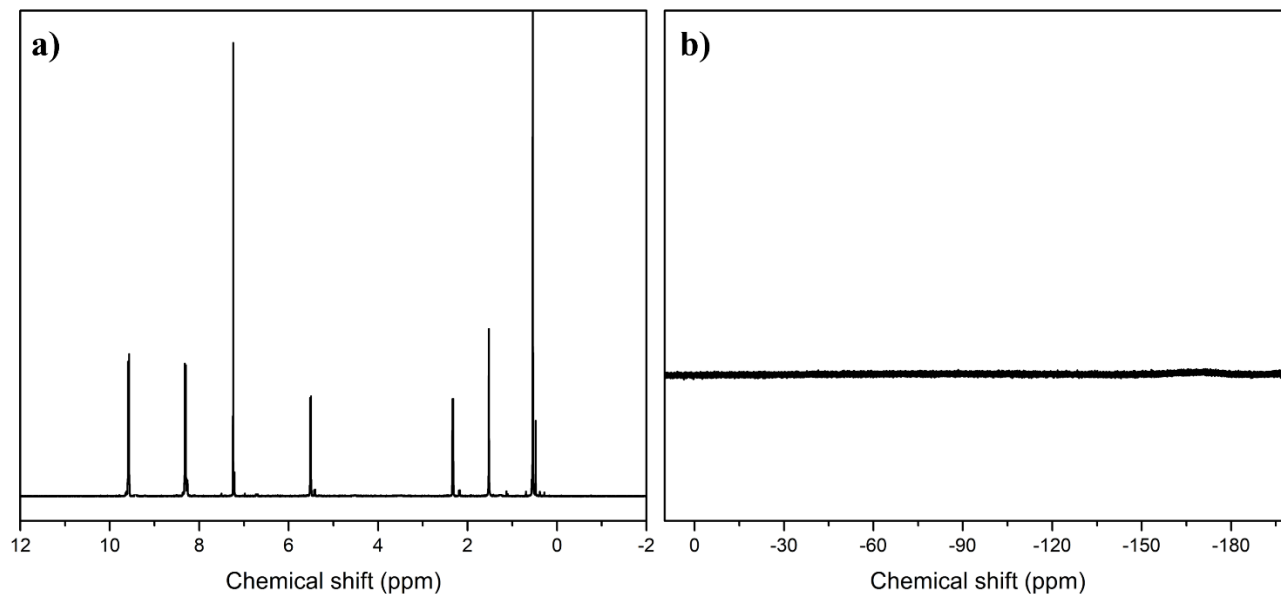


Figure C20. a) ^1H NMR and b) ^{19}F NMR spectra of $(\text{tb-Ph})_2\text{-F}_0\text{SiPc}$ in deuterated chloroform.

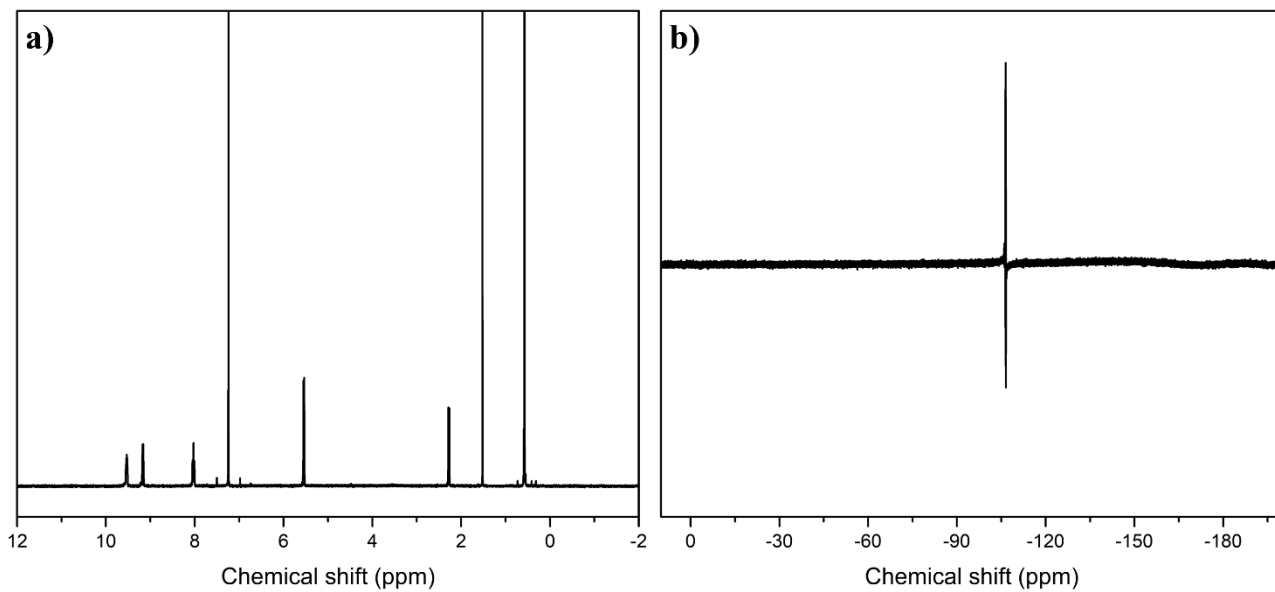


Figure C21. a) ^1H NMR and b) ^{19}F NMR spectra of $(\text{tb-Ph})_2\text{-F}_4\text{SiPc}$ in deuterated chloroform.

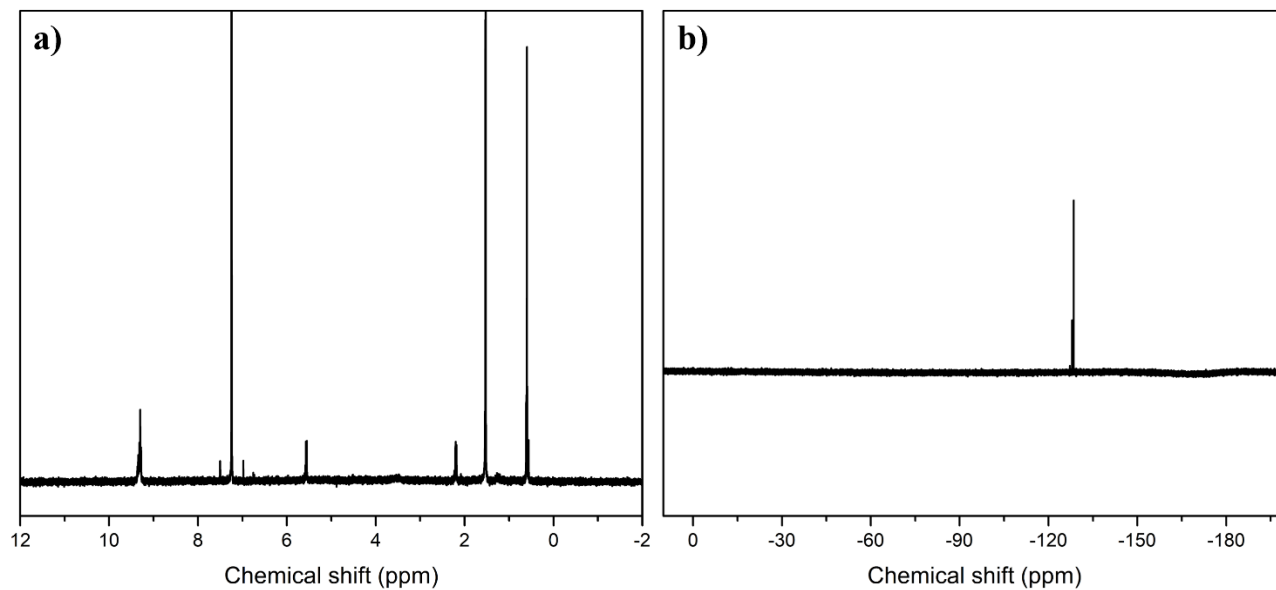


Figure C22. a) ^1H NMR and b) ^{19}F NMR spectra of $(\text{tb-Ph})_2\text{-F}_8\text{SiPc}$ in deuterated chloroform.

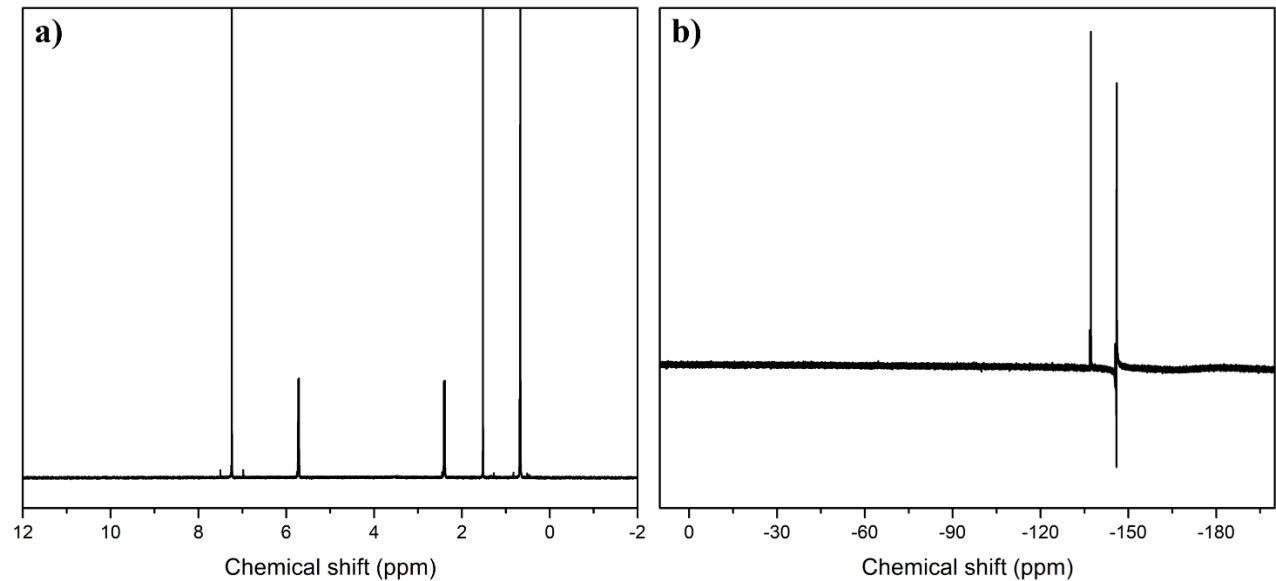


Figure C23. a) ^1H NMR and b) ^{19}F NMR spectra of $(\text{tb-Ph})_2\text{-F}_{16}\text{SiPc}$ in deuterated chloroform.

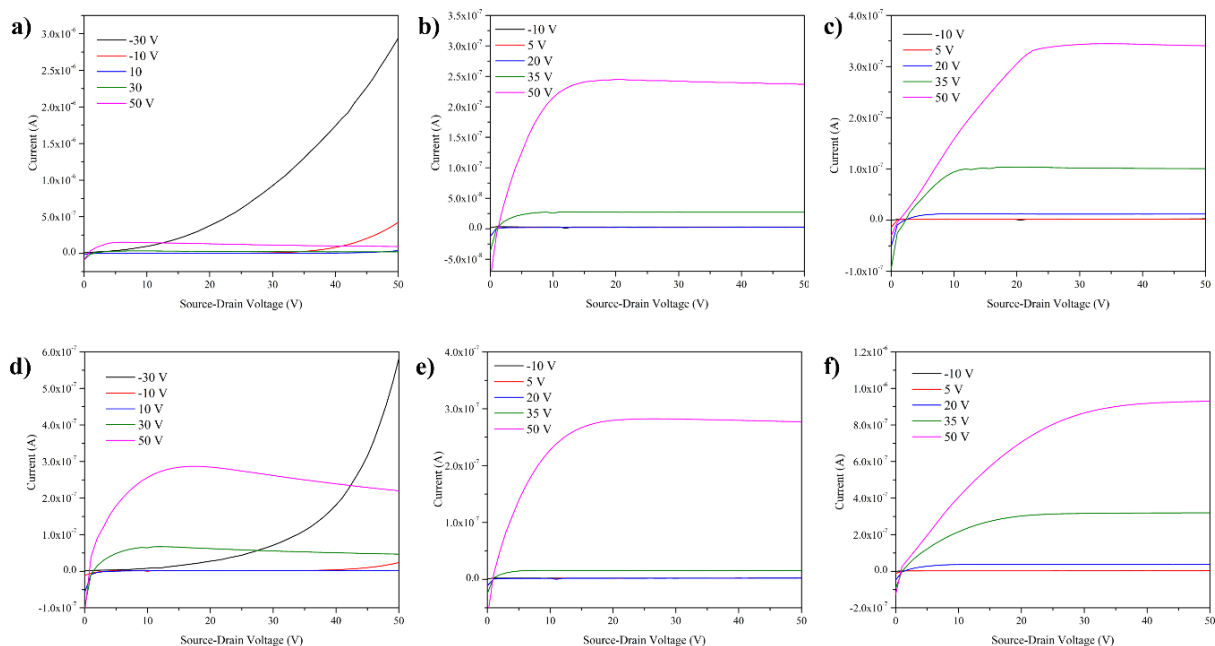


Figure C24. Output curves of working evaporated n-type transistors characterized in N_2 , with Ag electrodes a) $(tb-Ph)_2-F_4SiPcs$, b) $(tb-Ph)_2-F_8SiPcs$, c) $(tb-Ph)_2-F_{16}SiPcs$; and Ag/Mn electrodes d) $(tb-Ph)_2-F_4SiPcs$, e) $(tb-Ph)_2-F_8SiPcs$, f) $(tb-Ph)_2-F_{16}SiPcs$.

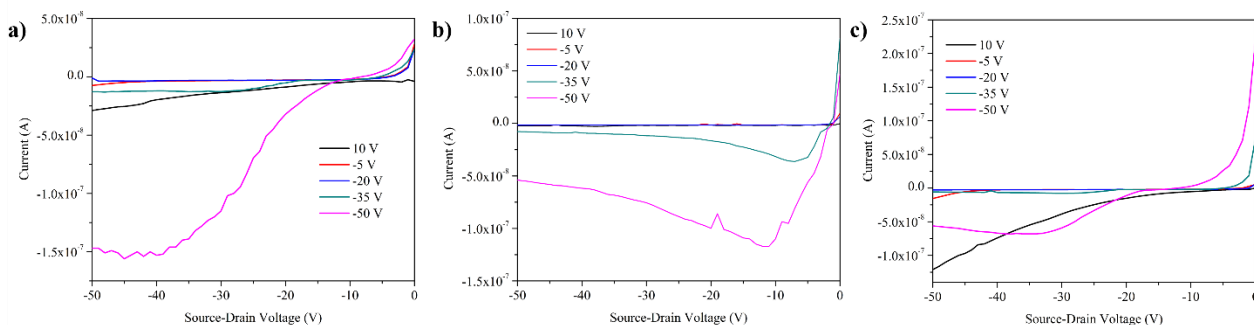


Figure C25. Output curves of working evaporated p-type transistors characterized in N_2 , with Ag electrodes a) $(tb-Ph)_2-F_0SiPcs$, b) $(tb-Ph)_2-F_4SiPcs$; and Ag/Mn electrodes c) $(tb-Ph)_2-F_0SiPcs$.

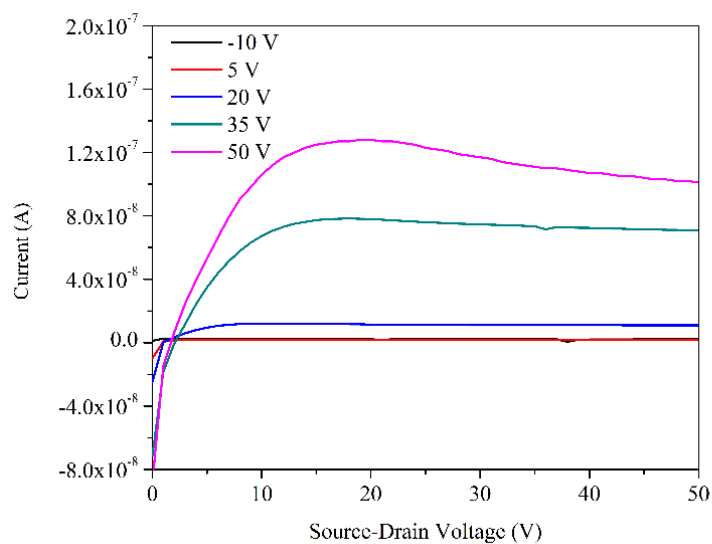


Figure C26. Output curves of working evaporated n-type $(tb\text{-Ph})_2\text{-F}_{16}\text{SiPcs}$ transistor characterized in Air, with Ag electrodes.

Bond precision: C-C = 0.0059 Å Wavelength=0.71073
 Cell: a=18.700(3) b=23.366(3) c=10.1118(16)
 alpha=90 beta=92.206(5) gamma=90
 Temperature: 200 K

	Calculated	Reported
Volume	4415.0(11)	4415.1(12)
Space group	C 2/c	C 2/c
Hall group	-C 2yc	-C 2yc
Moiety formula	C52 H38 F4 N8 O2 S1	C52 H38 F4 N8 O2 S1
Sum formula	C52 H38 F4 N8 O2 S1	C52 H38 F4 N8 O2 S1
Mr	910.99	910.99
Dx, g cm ⁻³	1.371	1.371
Z	4	4
Mu (mm ⁻¹)	0.123	0.123
F000	1888.0	1888.0
F000'	1889.19	
h, k, lmax	20, 26, 11	20, 26, 11
Nref	3262	3203
Tmin, Tmax	0.975, 0.987	0.597, 0.745
Tmin'	0.930	

Correction method= # Reported T Limits: Tmin=0.597 Tmax=0.745
 AbsCorr = MULTI-SCAN

Data completeness= 0.982 Theta(max)= 23.465

R(reflections)= 0.0558(1788) WR2(reflections)= 0.1747(3203)
 S = 1.010 Npar= 326

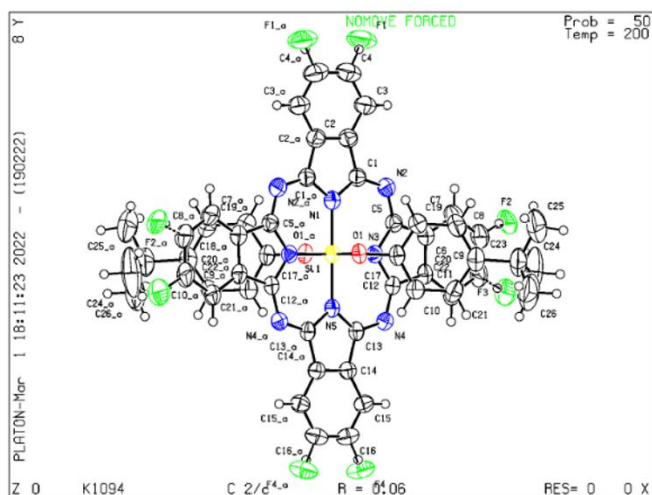


Figure C27. Structure factors from $(tb\text{-Ph})_2\text{-F}_4\text{SiPc}$ Single-crystal XRD analysis.

Bond precision: C-C = 0.0071 Å Wavelength=0.71073

Cell: a=8.5247(12) b=11.3932(17) c=12.6389(19)
 alpha=87.550(4) beta=79.949(4) gamma=82.937(4)
 Temperature: 200 K

	Calculated	Reported
Volume	1199.2(3)	1199.2(3)
Space group	P -1	P -1
Hall group	-P 1	-P 1
Moiety formula	C52 H34 F8 N8 O2 S1, C4 H8	C52 H34 F8 N8 O2 S1, C4 H8
Sum formula	O	O
Sum formula	C56 H42 F8 N8 O3 S1	C56 H42 F8 N8 O3 S1
Mr	1055.07	1055.06
Dx, g cm-3	1.461	1.461
Z	1	1
Mu (mm-1)	0.137	0.137
F000	544.0	544.0
F000'	544.38	
h, k, lmax	9, 12, 14	9, 12, 14
Nref	3490	3361
Tmin, Tmax	0.972, 0.992	0.655, 0.745
Tmin'	0.930	

Correction method= # Reported T Limits: Tmin=0.655 Tmax=0.745
 AbsCorr = MULTI-SCAN

Data completeness= 0.963 Theta(max)= 23.347

R(reflections)= 0.0722(2281) wR2(reflections)=
 S = 1.103 Npar= 401 0.1704(3361)

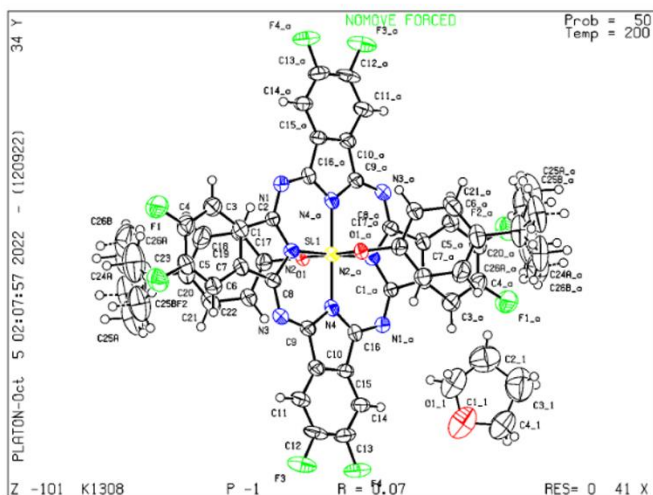


Figure C28. Structure factors from (tb-Ph)₂-F₈SiPc Single-crystal XRD analysis.

Bond precision: C-C = 0.0519 Å Wavelength=0.71073

Cell: a=9.956(6) b=10.800(6) c=11.310(7)
 alpha=88.227(12) beta=87.324(13) gamma=66.824(11)
 Temperature: 213 K

	Calculated	Reported
Volume	1116.6(12)	1116.6(11)
Space group	P -1	P -1
Hall group	-P 1	-P 1
Moiety formula	C52 F16 N8 O2 S1	?
Sum formula	C52 F16 N8 O2 S1	C H F N O S1
Mr	1100.69	90.12
Dx, g cm-3	1.637	1.608
Z	1	12
Mu (mm-1)	0.175	0.458
F000	542.0	540.0
F000'	542.50	
h, k, lmax	9, 9, 10	9, 9, 10
Nref	1770	1487
Tmin, Tmax	0.920, 0.976	
Tmin'	0.853	

Correction method= Not given

Data completeness= 0.840 Theta(max)= 18.894

R(reflections)= 0.2443(870) wR2(reflections)=
 S = 2.689 Npar= 158 0.4946(1487)

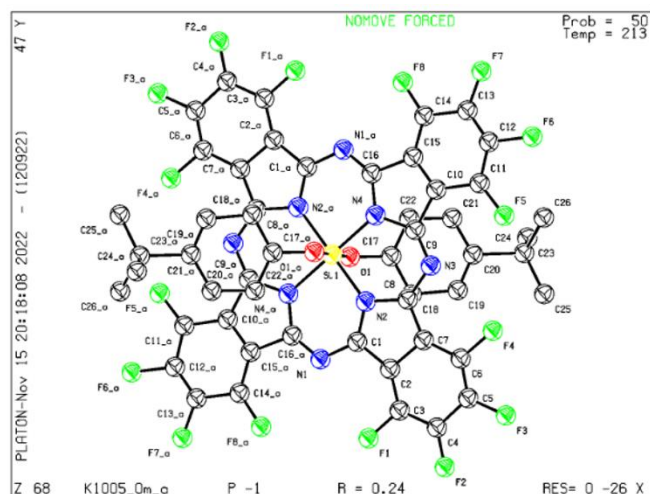



Figure C29. Structure factors from (tb-Ph)₂-F₁₆SiPc Single-crystal XRD analysis.

APPENDIX D – Permissions to reproduce work.


Rightslink® by Copyright Clearance Center

<https://s100.copyright.com/AppDispatchService>



RightsLink

[Home](#)
[Help](#)
[Live Chat](#)
[Sign In](#)
[Create Account](#)



Bis(trialkylsilyl oxide) Silicon Phthalocyanines: Understanding the Role of Solubility in Device Performance as Ternary Additives in Organic Photovoltaics

Author: Mário C. Vebber, Trevor M. Grant, Jaclyn L. Brusso, et al

Publication: Langmuir

Publisher: American Chemical Society

Date: Mar 1, 2020

Copyright © 2020, American Chemical Society

PERMISSION/LICENSE IS GRANTED FOR YOUR ORDER AT NO CHARGE

This type of permission/license, instead of the standard Terms and Conditions, is sent to you because no fee is being charged for your order. Please note the following:

- Permission is granted for your request in both print and electronic formats, and translations.
- If figures and/or tables were requested, they may be adapted or used in part.
- Please print this page for your records and send a copy of it to your publisher/graduate school.
- Appropriate credit for the requested material should be given as follows: "Reprinted (adapted) with permission from (COMPLETE REFERENCE CITATION). Copyright (YEAR) American Chemical Society." Insert appropriate information in place of the capitalized words.
- One-time permission is granted only for the use specified in your RightsLink request. No additional uses are granted (such as derivative works or other editions). For any uses, please submit a new request.

If credit is given to another source for the material you requested from RightsLink, permission must be obtained from that source.

BACK
CLOSE WINDOW



Home



Help ▾



Live Chat



Sign In



Create Account



Thermodynamic Property-Performance Relationships in Silicon Phthalocyanine-Based Organic Photovoltaics

Author: Mario C. Vebber, Nicole A. Rice, Jacyln L. Brusso, et al

Publication: ACS Applied Energy Materials

Publisher: American Chemical Society

Date: Mar 1, 2022

Copyright © 2022, American Chemical Society

PERMISSION/LICENSE IS GRANTED FOR YOUR ORDER AT NO CHARGE

This type of permission/license, instead of the standard Terms and Conditions, is sent to you because no fee is being charged for your order. Please note the following:

- Permission is granted for your request in both print and electronic formats, and translations.
- If figures and/or tables were requested, they may be adapted or used in part.
- Please print this page for your records and send a copy of it to your publisher/graduate school.
- Appropriate credit for the requested material should be given as follows: "Reprinted (adapted) with permission from (COMPLETE REFERENCE CITATION). Copyright (YEAR) American Chemical Society." Insert appropriate information in place of the capitalized words.
- One-time permission is granted only for the use specified in your RightsLink request. No additional uses are granted (such as derivative works or other editions). For any uses, please submit a new request.

If credit is given to another source for the material you requested from RightsLink, permission must be obtained from that source.

[BACK](#)[CLOSE WINDOW](#)



?
Help ▾



Live Chat

SPRINGER NATURE

Variance-resistant PTB7 and axially-substituted silicon phthalocyanines as active materials for high-Voc organic photovoltaics

Author: Mario C. Vebber et al
Publication: Scientific Reports
Publisher: Springer Nature
Date: Jul 28, 2021

Copyright © 2021, The Author(s)

Creative Commons

This is an open access article distributed under the terms of the [Creative Commons CC BY](#) license, which permits unrestricted use, distribution, and reproduction in any medium, provided the original work is properly cited.

You are not required to obtain permission to reuse this article.

To request permission for a type of use not listed, please contact [Springer Nature](#)

Firefox

<https://marketplace.copyright.com/rs-ui-web/mp/license/aa998ee3-4bfa..>

This is a License Agreement between Mario Vebber/ University of Ottawa ("User") and Copyright Clearance Center, Inc. ("CCC") on behalf of the Rightsholder identified in the order details below. The license consists of the order details, the Marketplace Order General Terms and Conditions below, and any Rightsholder Terms and Conditions which are included below.

All payments must be made in full to CCC in accordance with the Marketplace Order General Terms and Conditions below.

Order Date	24-Jan-2023	Type of Use	Republish in a thesis/dissertation
Order License ID	1315327-1	Publisher Portion	John Wiley & Sons Chapter/article
ISSN	1939-019X		

LICENSED CONTENT

Publication Title	The Canadian journal of chemical engineering	Country	Canada
Article Title	From P-type to N-type: peripheral fluorination of axially substituted silicon phthalocyanines enables fine tuning of charge transport	Rightsholder	John Wiley & Sons - Books
Author/Editor	Canadian Society for Chemical Engineering.	Publication Type	e-Journal
Date	01/01/1957	URL	http://www3.interscience.wiley.com/cgi-bin/jhome/116330099
Language	English, English, French		

REQUEST DETAILS

Portion Type	Chapter/article	Rights Requested	Main product
Page Range(s)	1-26	Distribution	Worldwide
Total Number of Pages	26	Translation	Original language of publication
Format (select all that apply)	Electronic	Copies for the Disabled?	No
Who Will Republish the Content?	Academic institution	Minor Editing Privileges?	No
Duration of Use	Life of current edition	Incidental Promotional Use?	No
Lifetime Unit Quantity	Up to 499	Currency	CAD

NEW WORK DETAILS

Title	Development of functionalized tetravalent phthalocyanines for low-cost organic photovoltaics	Institution Name	University of Ottawa
Instructor Name	Benoît Lessard	Expected Presentation Date	2023-04-21